RESEARCH AND DEVELOPMENT STUDY FOR RADIO FREQUENCY SIMULATION

FINAL REPORT

ZZK-66-060

November 1966

Prepared for

JET PROPULSION LABORATORY

PASADENA, CALIFORNIA

(PREPARED UNDER CONTRACT NO. 951 548

BY THE

CONVAIR DIVISION OF GENERAL DYNAMICS

CORPORATION OF SAN DIEGO, CALIFORNIA)

GENERAL DYNAMICS
Convair Division

GENERAL DYNAMICS
Convair Division

RESEARCH AND DEVELOPMENT STUDY FOR RADIO FREQUENCY SIMULATION

FINAL REPORT

Prepared for

JET PROPULSION LABORATORY

PASADENA, CALIFORNIA

Prepared by J. C. Lawrence
J. C. Lawrence,
Electronics Engineer,
Electromagnetic Compatibility
Group

Approved by B. Weinbaum
B. Weinbaum, Assistant
Chief Design Engineer,
Electromagnetic Compatibility
Group

Checked by J. H. Schukantz
J. H. Schukantz,
Sr. Electronics Engineer,
Electromagnetic Compatibility
Group

This work was performed for the Jet Propulsion Laboratory, California Institute of Technology, sponsored by the National Aeronautics and Space Administration under Contract NAS7-100.

(PREPARED UNDER CONTRACT NO. 951 548
BY THE
CONVAIR DIVISION OF GENERAL DYNAMICS
CORPORATION OF SAN DIEGO, CALIFORNIA)

PRECEDING PAGE BLANK NOT FILMED.

ABSTRACT

This is the final report of a study concerning the simulation of an RF radiation environment in the test laboratory for the purpose of susceptibility testing. An analysis of the spectral characteristics of a few specific transmitters was performed and suggestions made for the simulation of these spectra in the laboratory. Methods of determining power density levels caused by a finite number of transmitters with known characteristics are presented. An analysis of test margins is undertaken, and the rationale behind the recommended test margin is fully explained and substantiated. A procedure for carrying out a full-blown RF radiated susceptibility systems test, involving the use of a power density detector developed during this study, is presented. Finally, an analysis of the mechanisms of susceptibility is given and a comparison made with RF overstress.

PRECEDING PAGE BLANK NOT FILMED.

TABLE OF CONTENTS

TABLE OF CONTENTS, Contd

LIST OF APPENDICES

LIST OF FIGURES

LIST OF FIGURES, Contd

1. INTRODUCTION

This is the final report on the study of Radio Frequency (RF) Simulation. All work has been concluded and the results are presented herein. The purpose of the study was to analyze the problems inherent in performing an RF radiated susceptibility systems tests in which it is desired that the radiation environment created in such a test is equivalent, insofar as the inducement of susceptibility is concerned, to the radiation that will exist in the worst probable actual environment. Susceptibility will be defined as that property of a system or part thereof which allows for undesired response caused by undesired stimuli. "Worst" has the meaning of inducing the largest amount of susceptibilities, i.e., undesired responses. In order that the actual environment may be simulated, a knowledge of the factors influencing this environment and their effects as well as a knowledge of the conditions that surround the environment in which the testing takes place becomes imperative. It was for the purpose of contributing to that knowledge that this study was undertaken.

It is assumed herein that the actual environment is created by a finite number of transmitters with known characteristics such as transmitted power, antenna gain and beamwidth, location and modulation. The first problem is to determine the characteristics such as power density and frequency of the resultant composite signal at a particular location. The second problem is to determine the extent to which these characteristics must be simulated. The third problem is to recreate the desired set of characteristics in the test laboratory.

The following are some of the pertinent factors which were considered:

1. Spectra of waveforms with known modulation characteristics.
2. Simulation of spectra of known modulation characteristics by signals with different modulation characteristics.
3. The nature of susceptibility and susceptibility-producing mechanisms.
4. Calculations of power density levels produced by known sources.

5. A device for measuring power density.
6. Uncertainties, test margins, safety factors.
7. Test procedures and equipment.
8. The nature of RF overstress.

Results, substantiations, conclusions and recommendations are included in the report.

2. MODULATION EFFECTS

2.1 FM Signal Analysis. In order to determine the necessary degree of simulation required for different types of signals, the spectra of the signals, themselves, must be known. Phase information about the signals will be considered unimportant for RF simulation since phase is associated with intelligibility of the signal and should not be an important consideration insofar as the signal's effects on a susceptible device are concerned. As adequate simulation of any modulated signal should be provided by a signal which covers essentially the same bandwidth and the same relative amplitudes as the signal that is being simulated. The parameters of a pulse modulated signal can be varied to obtain practically any desired roll-off. The pulse repetition frequency can be varied to provide a relatively small or large number of frequency components in order to simulate a relatively narrowband or broadband spectrum, respectively. In addition, the phase relationships present in a pulse modulated signal should be sufficient to simulate both angle and amplitude types of modulation. Nevertheless, experimental verification of the adequacy of using pulse modulation to simulate any arbitrary type of modulation should be performed.

Various types of intentional and unintentional demodulators as well as a number of types of modulation should be considered. The response of the various demodulators when a signal of each modulation type is applied can be compared to the response when pulsed modulated RF is applied. Future analytical work should also be done on the phase relationships of different types of modulation schemes and how important their role is in the process of demodulation.

An analysis of the spectral characteristics of the Azusa Mark II ground transmitter was performed. The Azusa is used for precision tracking of missiles, and the type of signal it transmits is simple, single side-tone, FM modulation. The single side-tone modulating signal is one of three frequencies which are associated with different degrees of tracking accuracy in the phase-locked system. However, only one frequency is used at any particular time. The following are the three modulating frequencies and their uses:

Modulating Frequency	Tracking Accuracy
98.36 Kc	Fine and Coherence
3.93 Kc	Intermediate
157 cps	Coarse

Other data pertaining to the Azusa Mark II are the following:

Carrier Frequency: 5060.2 ± 0.75 Mc

Power: 2000 W

One other bit of information is required to completely determine the Azusa Mark II spectrum: namely, the deviation schedule. The deviation schedule is an important design characteristic for any type of FM modulation. It is a statement of the deviation of the carrier by each of the modulating frequencies acting individually. In single side-tone FM modulation, total carrier deviation is simply proportional to the amplitude of whichever side-tone is being used at a given time.

There are two modes of operation for the Azusa Mark II with two different corresponding deviation schedules.

DEVIATION SCHEDULE FOR AZUSA MARK II

	Mode 1			Mode 2	
f_m	Δf	D	f_m	Δf	D
98.36 Kc	98.36 Kc	1	98.36 Kc	98.36 Kc	1
3.93 Kc	3.93 Kc	1	3.93 Kc	20 Kc	5.1
157 cps	157 cps	1	157 cps	20 Kc	118

f_m = modulating frequency

Δf = peak deviation

D = deviation ratio = $\frac{\Delta f}{f_m}$

Calculation of the spectra associated with the Azusa Mark II can now be made. The general expression for an FM modulated signal as a function of time is:

(1) $$a(t) = A \sin \left[2\pi f_c t + \frac{\Delta f}{f_m} \sin 2\pi f_m t + \theta_0 \right]$$

A = carrier amplitude

f_c = carrier frequency

θ_0 = arbitrary phase factor (omitted hereafter)

To determine a as a function of f, the procedure is as follows[1]:

(2) $$a = A \left[\sin (2\pi f_c t) \cos \left(\frac{\Delta f}{f_m} \sin 2\pi f_m t \right) + \cos (2\pi f_c t) \sin \left(\frac{\Delta f}{f_m} \sin 2\pi f_m t \right) \right]$$

(3) $$\cos \left(\frac{\Delta f}{f_m} \sin 2\pi f_m t \right) = J_0 \left(\frac{\Delta f}{f_m} \right) + 2 \left[J_2 \left(\frac{\Delta f}{f_m} \right) \cos 4\pi f_m t + J_4 \left(\frac{\Delta f}{f_m} \right) \cos 8\pi f_m t + \cdots \right]$$

(4) $$\sin \left(\frac{\Delta f}{f_m} \sin 2\pi f_m t \right) = 2 \left[J_1 \left(\frac{\Delta f}{f_m} \right) \sin 2\pi f_m t + J_3 \left(\frac{\Delta f}{f_m} \right) \sin 6\pi f_m t + \cdots \right]$$

where $J_n \left(\frac{\Delta f}{f_m} \right)$ are Bessel functions of the first kind.

(5) $$\sin (2\pi f_c t) \cos (2\pi n f_m t) = \frac{1}{2} \left\{ \sin [2\pi (f_c + n f_m) t] + \sin [2\pi (f_c - n f_m) t] \right\}$$

(6) $$\cos (2\pi f_c t) \sin (2\pi n f_m t) = \frac{1}{2} \left\{ \sin [2\pi (f_c + n f_m) t] - \sin [2\pi (f_c - n f_m) t] \right\}$$

$$(7)\qquad a(f) = A\left\{J_0\left(\frac{\Delta f}{f_m}\right)\sin\left[2\pi f_c t\right] + J_1\left(\frac{\Delta f}{f_m}\right)\sin\left[2\pi (f_c + f_m)t\right]\right.$$
$$- J_1\left(\frac{\Delta f}{f_m}\right)\sin\left[2\pi (f_c - f_m)t\right] + J_2\left(\frac{\Delta f}{f_m}\right)\sin\left[2\pi (f_c + 2f_m)t\right]$$
$$+ J_2\left(\frac{\Delta f}{f_m}\right)\sin\left[2\pi (f_c - 2f_m)t\right] + J_3\left(\frac{\Delta f}{f_m}\right)\sin\left[2\pi (f_c + 3f_m)t\right]$$
$$- J_3\left(\frac{\Delta f}{f_m}\right)\sin\left[2\pi (f_c - 3f_m)t\right] + J_4\left(\frac{\Delta f}{f_m}\right)\sin\left[2\pi (f_c + 4f_m)t\right]$$
$$\left. + J_4\left(\frac{\Delta f}{f_m}\right)\sin\left[2\pi (f_c - 4f_m)t\right] + \cdots\right\}$$

As can be seen from the above equations, the FM spectrum consists of a series of components spaced symmetrically about the carrier frequency at intervals of f_m. The amplitude of the n^{th} component is $J_n(D)$ and its frequency is f_c plus nf_m where f_c is the zeroeth component. It can be seen from the deviation schedule that there are three values of D under consideration. Since an FM spectrum can be specified as a function of D and n, the plots will be normalized with the ordinate representing decibels below the unmodulated carrier amplitude and the abscissa, $n = f - f_c/f_m$.

Only half of the spectrum will be plotted since it is symmetrical about the carrier frequency. The $J_n(D)$ can be found in tables[2]. Figures 1 and 2 are spectral plots for D = 1 and D = 5.1, respectively. Figure 1 can be used as the spectrum of any of the modulating signals in Mode 1 of the deviation schedule and for the 98.36 Kc modulating signal of Mode 2. Figure 2 can be used for the 3.93 Kc modulating signal of Mode 2. For any particular case the abscissa must be multiplied by the modulating signal's frequency to obtain the actual spectral distribution.

For the purposes of RF simulation there are two aspects of the spectral distribution that are of interest: (1) the relative amplitudes of the spectral components; (2) the bandwidth of the spectrum. The IRIG Telemetry Standards[3] defines transmitter bandwidth as that region of the transmitted spectrum with spectral components greater than

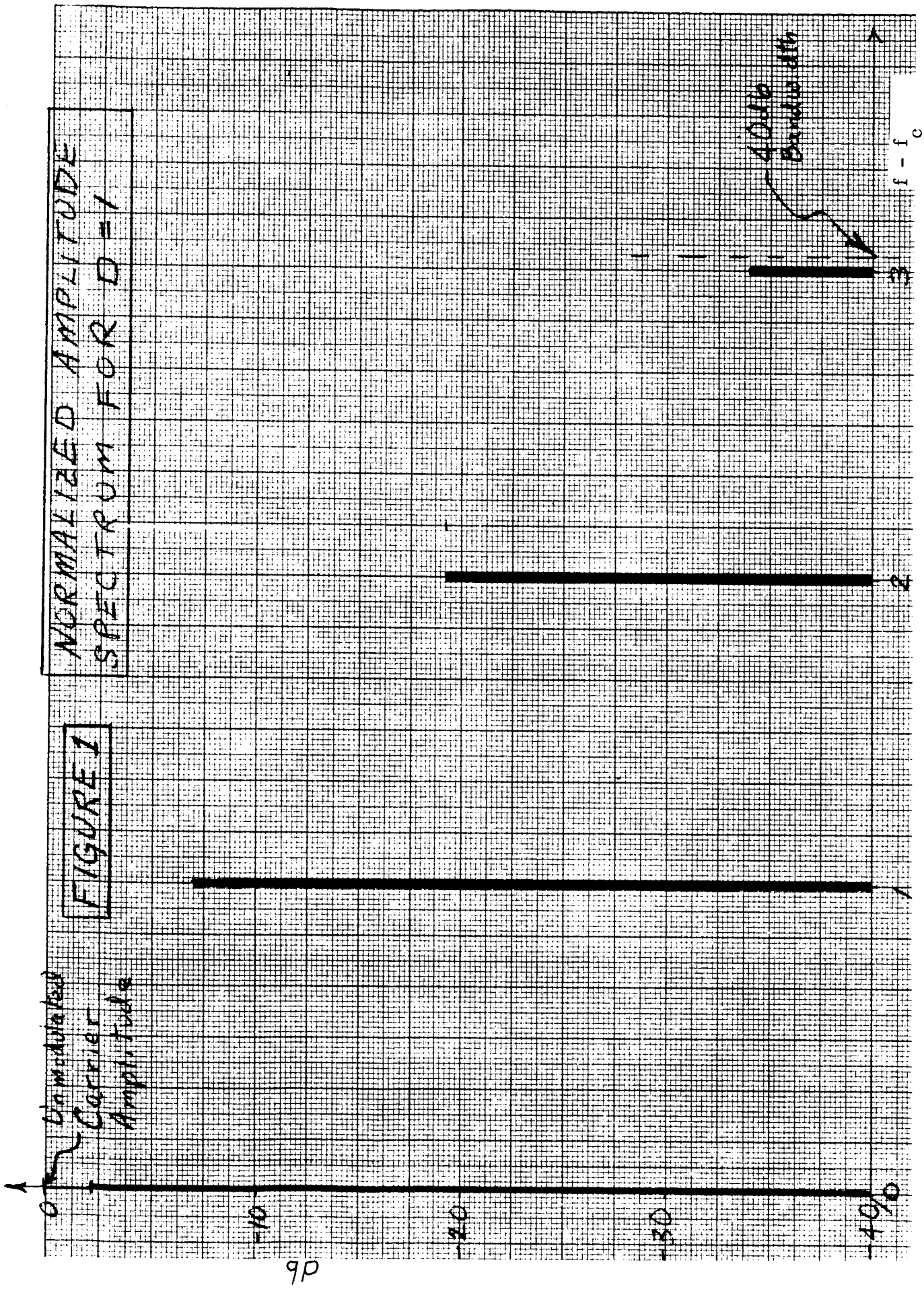
FIGURE 1
NORMALIZED AMPLITUDE
SPECTRUM FOR D = 1
Unmodulated Carrier Amplitude
0 dB
-10
-20
-30
-40
90
1
2
3
4 Side Bandwidth
$\frac{f - f_c}{f_m} = n$

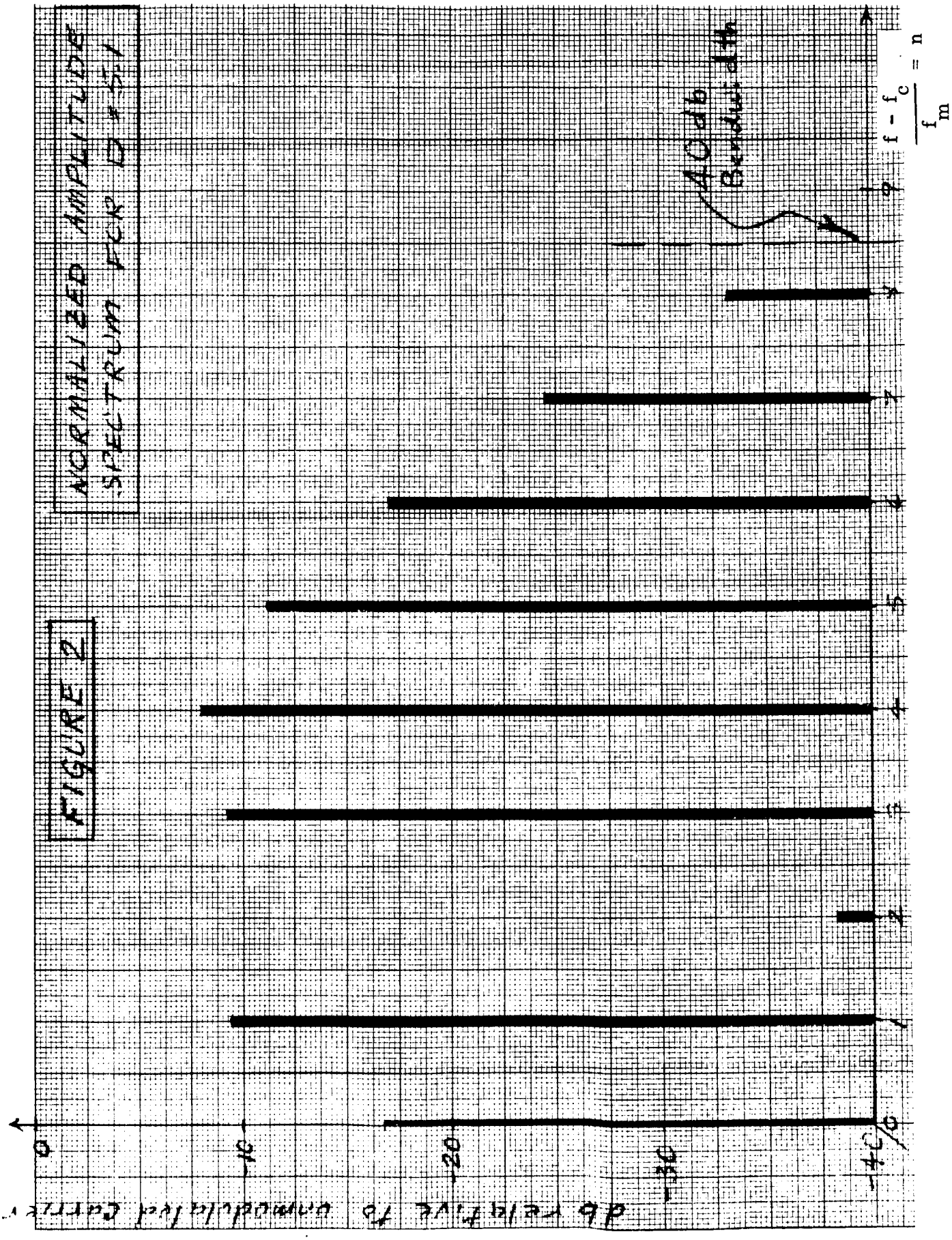
NORMALIZED AMPLITUDE
SPECTRUM FOR D = 2.1
FIGURE 2
40 db Bandwidth
$\frac{f - f_c}{f_m} = n$
0
-15
-20
-30
-40 db
db relative to unmodulated level Center v

-40 db referred to the unmodulated carrier. The 40 db bandwidth will be taken as an adequate representation for simulation purposes of the FM spectrum.

The FM spectrum is rapidly attenuated for frequencies greater than $f_c \pm \Delta f$. In order to determine the 40 db bandwidth the Bessel function is found such that $J_p(D) = .01$. The p^{th} component of the spectrum will then represent the bandedge. If the 40 db bandwidth is related to the peak deviation in accordance with the formula, 40 db bandwidth = $\beta \Delta f$, a plot can be constructed which relates deviation ration, D, to β. For any particular D and f_m the 40 db bandwidth is

$$40 \text{ db B.W.} = \beta D f_m$$

If $f^+_{40\text{ db}}$ = the upper bandedge frequency, then

$$f_c + \frac{\beta}{2} \Delta f = f^+_{40\text{ db}}$$

$$\frac{f^+_{40\text{ db}} - f_c}{f_m} = \frac{\beta}{2} \frac{\Delta f}{f_m} = \frac{\beta}{2} D$$

The bandedge criterion becomes

$$p = \frac{\beta D}{2}$$

$$J_{\beta D/2}(D) = \frac{1}{100} \quad (\beta/2 > 1)$$

Since $\beta D/2$ may not be an integer, the actual bandwidth will be terminated by the smallest component that is greater than .01. Therefore, the actual 40 db bandwidth will be such that $n = (\beta D/2)_n$ where $(\beta D/2)_n$ represents $\beta D/2$ truncated to the largest integer less than $\beta D/2$.

Figure 3 is a plot of β versus D.

There is one remaining FM spectrum to be plotted for the Azusa Mark II. When f_m = 157 cps and Δf = 20 Kc, the deviation ratio is 127.4. This spectrum will consist of more than 127 spectral components on either side of the carrier. A computer program was constructed to calculate the Bessel functions, since the Bessel functions are not tabulated for orders and arguments of the magnitude under consideration. This computer

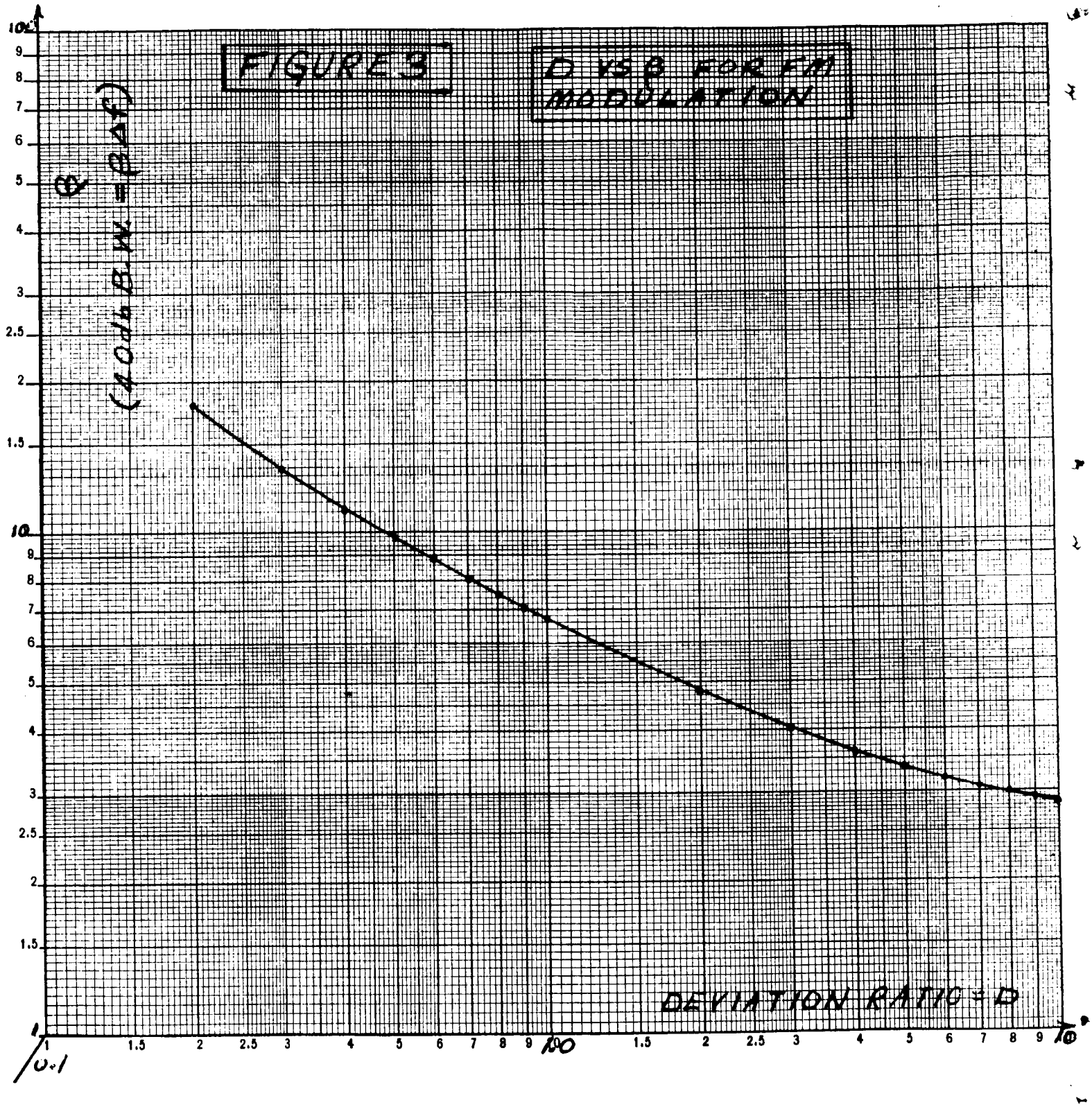
FIGURE 3
D VS β FOR FM MODULATION
(4 db BW = β+2)
DEVIATION RATIO = D
0.1
1
1.5
2
2.5
3
4
5
6
7
8
9
10
100

program is presented in Appendix I. $J_0(127.4)$ and $J_1(127.4)$ were obtained from the large argument approximations for low order Bessel functions.

$$J_V(x) \xrightarrow[x \to \infty]{} \sqrt{\frac{2}{\pi x}} \cos\left(x - \frac{\pi}{4} - \frac{V\pi}{2}\right)$$

The recursion formula was then employed to calculate successive values for $J_n(127.4)$:

$$J_{n+1}(127.4) = \frac{2n}{127.4} J_n(127.4) - J_{n-1}(127.4)$$

The spectrum for D = 127.4 is shown in Figure 4. Since the relative amplitudes of the spectral components do not differ greatly, a linear rather than a decibel scale was used. The 40 db bandwidth occurs for n = p = 138, $\beta = 2.16$ and $f^{+}_{40\,db} - f_c = 21.7$ Kc. The largest spectral component is 17.7 db down from the unmodulated carrier.

To illustrate the application of the spectral plots, the following examples are considered.

Given:

carrier frequency = 5060.2 ± 0.75 Mc

carrier power = 2000 watts

modulating frequency = $f_m = 98.36$ Kc

peak deviation = $\Delta f = 98.36$ Kc

deviation ratio = $D = \frac{\Delta f}{f_m} = 1$

Find:

1. Unmodulated carrier amplitude = A
2. carrier spectrum
3. amplitude and frequency of greatest spectral component
4. 40 db bandwidth
5. 40 db bandedge frequencies

Solution: (assuming a 50 ohm system)

1. $\frac{A}{\sqrt{2}} = \sqrt{(2000\,W)\,(50\Omega)}$

   $A = 447$ volts peak

FIGURE 4

NORMALIZED AMPLITUDE SPECTRUM FOR D=1.18

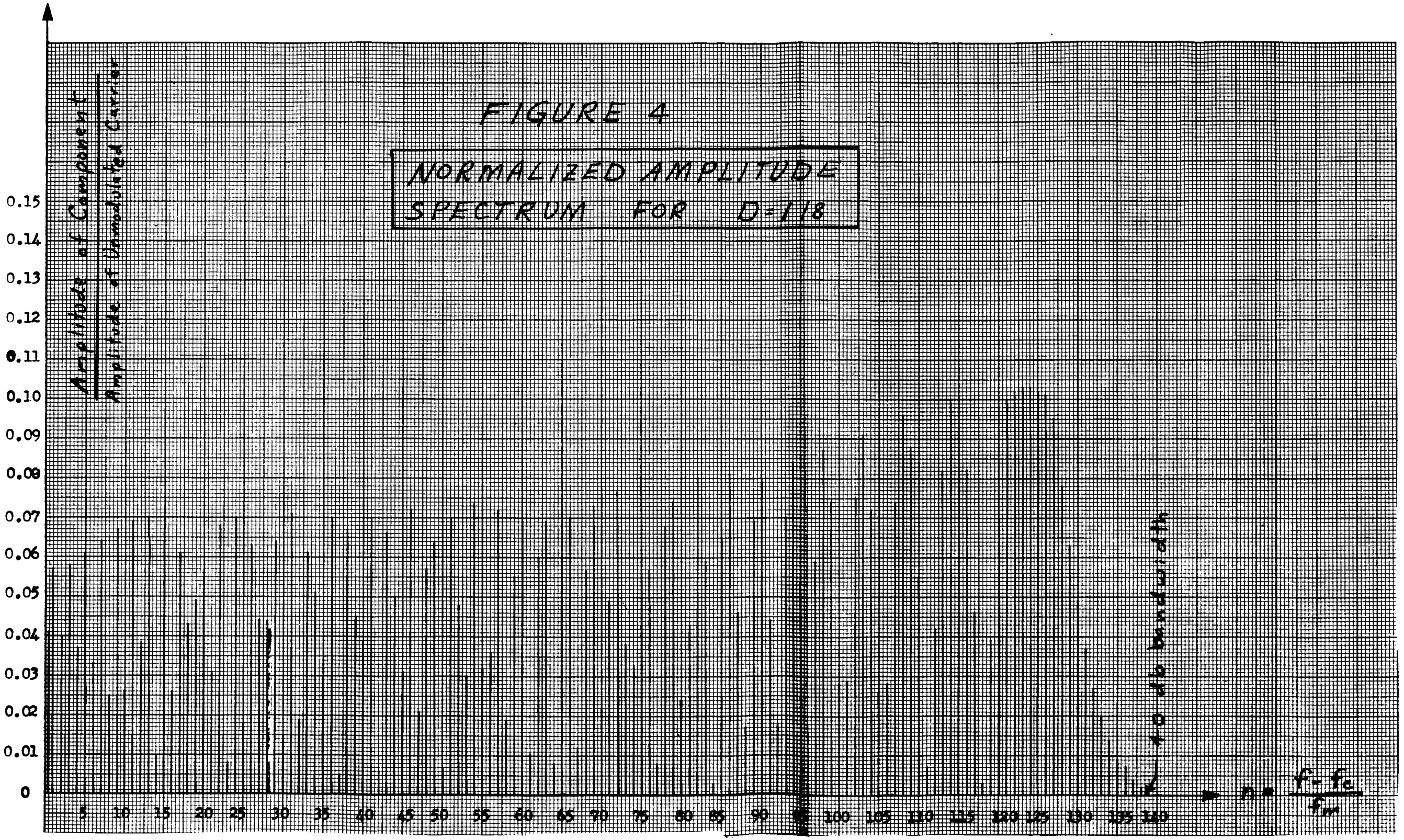

2. Using Figure 1 and the parameters

$A = 447$ volts

$f_m = 98.36$ Kc

$D = 1$

$(\beta D/2)_n = 3$

$f_c = 5060.2 \pm .75$ Mc

It is apparent that there will be seven components in the spectrum spaced 98.36 Kc apart and centered around the carrier. The amplitudes were found as follows:

Amplitude of 5060.2 Mc modulated component = -2.3 db

$$= \log^{-1}\left\{447 - \frac{2.3}{20}\right\} = 344 \text{ volts peak}$$

Similarly, the following table is constructed:

F(Mc)	Amplitude (volts peak)
5060.2	344
5060.298 and 5060.102	198
5060.397 and 5060.003	49
5060.495 and 5059.905	9

3. The largest component is at the carrier frequency, 5060.2 Mc, and equals 344 volts peak.

4. 40 db bandwidth $= 2(\beta D/2)_n f_m = 2(3)(98.36 \text{ Kc}) = 590$ Kc

5. 40 db bandedge frequencies $= f_c \pm (\beta D/2)_n f_m = 5060.2 \pm (3)(98.36 \text{ Kc})$
   $= 5060.495$ Mc and 5059.905 Mc.

There is one other consideration. The ± .75 Mc tolerance on the carrier frequency makes possible an excursion in the frequency domain which requires a 40 db carrier channel of 1.56 Mc. The question of whether the RF simulation must cover this bandwidth can be answered as follows. The modulation characteristics of the signal will be the same even if the carrier frequency is displaced from its nominal value. For a device which is susceptible to the demodulated signal, the displacement of the carrier frequency

makes no difference in the susceptibility so long as the bandwidth of the susceptible device is greater than 1.5 Mc. For a device that is susceptible to the modulated signal, i.e., a spectral component in the range 5060.2 ± .78 Mc, the circuit would have to have a bandwidth less than 1.5 Mc to be selective enough to fail at one frequency in the transmission channel and not at another. In both cases the Q of the susceptible device would have to be greater than 3200 for this particular example. It is highly improbable that susceptible circuits with Q's of this order of magnitude will exist. Therefore, the tolerance on the carrier frequency will be considered of no consequence for the purposes of RF simulation and the signal may be simulated at the nominal carrier frequency.

The spectrum of the preceding example has been plotted in Figure 5.

2.2 Launch Vehicle Telemetry Systems. There are four basic types of telemetry systems in common use today: FM-FM, PAM-FM, PCM-FM and PDM-FM which stand for Frequency Modulation-FM, Pulse-Amplitude Modulation-FM, Pulse-Code Modulation-FM and Pulse Duration Modulation-FM, respectively. Multiplex-multiplex systems, such as PAM-FM-FM are also used. In fact, it is this type of modulation that has been employed on all Atlas and Centaur vehicles to date. For all practical purposes, the PAM-FM-FM carrier spectrum is essentially the same as the FM-FM spectrum. The FM-FM system will be discussed in considerable detail and the other systems will be mentioned briefly.

FM-FM

According to the Telemetry Standards, Document 106-65, there are designated 19 subcarrier channels for an FM-FM multiplex telemetry system. A nominal deviation ratio of 5 is specified for the subcarrier channels. As the center frequency of the subcarrier channels increases so also does the allowable subcarrier deviation and, consequently, the allowable baseband frequency response. The deviation of the carrier by each subcarrier is specified in accordance with a deviation schedule. The total peak carrier deviation is the sum of the carrier deviations by each of the channels acting individually. However, this peak deviation is very seldom approached because of the randomness of phase of the subcarriers. A more useful quantity is rms deviation which is defined as follows:

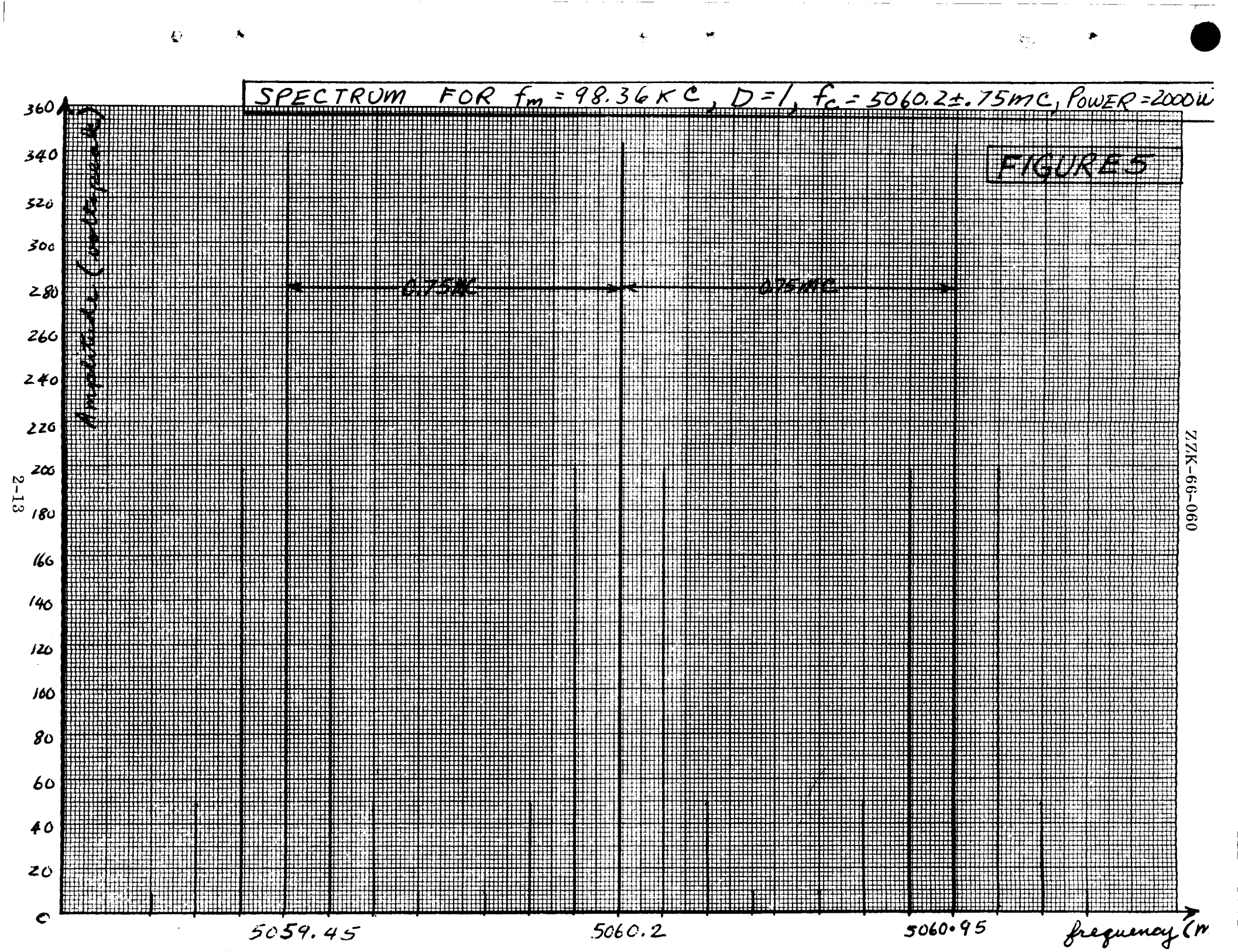
SPECTRUM FOR f_m = 98.36 KC, D = 1, f_c = 5060.2 ± .75MC, POWER = 2000W
FIGURE 5
360
340
320
300
280
260
240
220
200
180
160
140
120
100
80
60
40
20
0
0.75MC
0.75MC
5059.45
5060.2
5060.95
frequency (M
ZZK-66-060
2-13

$$\text{r.m.s deviation } \triangleq f_D = \frac{1}{\sqrt{2}}\sqrt{(\Delta f_1)^2 + (\Delta f_2)^2 + \cdots + (\Delta f_n)^2}$$

where Δf_n is the peak deviation of the carrier by the n^{th} subcarrier. A total of n subcarriers is assumed. In theory, the same type of derivation as was used to obtain the spectrum of an FM signal can be used in deriving the spectrum of the FM-FM signal. Starting with the time-domain signal

$$(8) \qquad a(t) = A \sin \left[2\pi f_c t + \frac{\Delta f_1}{f_{m1}} \sin 2\pi f_1 t + \frac{\Delta f_2}{f_{m2}} \sin 2\pi f_2 t + \cdots + \frac{\Delta f_n}{f_{mn}} \sin 2\pi f_{mn} t \right]$$

This expression can be expanded into a sum of terms of the form

$$\sin (2\pi f_c t) \sin\left(\frac{\Delta f_1}{f_{m1}} \sin 2\pi f_1 t\right) \sin\left(\frac{\Delta f_2}{f_{m2}} \sin 2\pi f_2 t\right) \cdots \sin\left(\frac{\Delta f_n}{f_{mn}} \sin 2\pi f_n t\right)$$

Each of these terms can be broken down to a term of the form

$$\sin \left[2\pi (f_c + a f_{m1} + b f_{m2} + \cdots + z f_{mn}) t\right] ; (a, b \cdots z, \text{ integers}),$$

after expanding the $\sin (\Delta f_n / f_{mn} \sin 2\pi f_n t)$ terms as series of Bessel functions. This process becomes very complicated for more than two or three modulating frequencies. Instead of using this method, a technique is used in which the auto-correlation function of the signal is related to the normalized power spectrum by the Wiener-Khintchine theorem:

$$(9) \qquad G_{xx}(\omega) = \frac{2}{\pi} \int_0^\infty \Gamma_{xx}(\zeta) \cos \omega\zeta \, d\zeta$$

where

$G_{xx}(\omega)$ = power spectral density

$\Gamma_{xx}(\zeta)$ = auto correlation function

The following steps are performed:

(1) Obtain the normalized auto-correlation function of the modulating signal.

(2) Using Wiener-Khintchine theorem, obtain normalized power spectrum of modulating signal.

(3) Substitute expression for normalized spectrum of modulating signal into expression for the normalized auto-correlation function of the modulated signal.

(4) Find normalized power spectrum of modulated signal, $H(\omega)$, again using the Wiener-Khintchine theorem.

McGaughan[4] shows that the normalized average power spectrum for a frequency modulated wave with a normally distributed modulating signal is

$$H(\omega) = \frac{1}{\pi} \int_0^{\infty} \cos(\omega - \omega_c)\,\zeta \cdot \exp\left\{ -\omega_D^2 \int_{-\infty}^{+\infty} \frac{S(x)}{x^2} (1 - \cos \zeta x)\, dx \right\} d\zeta \tag{10}$$

where

$H(\omega)$ = normalized power spectrum of modulated signal

ω_c = 2π (carrier frequency)

ω_D = 2π (r.m.s. deviation)

$S(\omega)$ = normalized power spectrum of modulating signal.

The similarity between the spectrum of randomly phased subcarriers and that of pre-emphasized, band-limited "white" noise has been demonstrated[5] (see Appendix II) so that $S(\omega)$ will be simplified to the expression for "white" noise.

Two modulating signal normalized power spectra will be considered[6]

$$S_1(\omega) = \begin{cases} \frac{1}{2}\,\omega_m, \text{ for } |\omega| \le \omega_m \\ 0, \text{ for } |\omega| > \omega_m \end{cases}$$

$$S_2(\omega) = \begin{cases} \dfrac{3\omega^2}{2\omega_m^2}, & \text{for } |\omega| \leq \omega_m \\ 0, & \text{for } |\omega| > \omega_m \end{cases}$$

where

ω_m = 2π (highest frequency present in modulating signal -- for FM-FM, highest subcarrier frequency)

$S_1(\omega)$ = spectrum of "white" noise which has been passed through a low-pass filter with cut-off at $2\pi\ \omega_m$

$S_2(\omega)$ = spectrum derived by passing $S_1(\omega)$ through a pre-emphasis filter and renormalizing.

It can be shown[7] that the FM carrier spectrum resulting from a modulating signal of $S_1(\omega)$ is

$$(11) \qquad H_1(\omega) = \frac{1}{2\pi\ \omega_D^2} \exp\left[\frac{-(\omega-\omega_c)^2}{2\omega_D^2}\right]$$

as long as $\dfrac{\omega_D}{\omega_m} \geq 1.13$

ω_D = 2π (r.m.s. frequency deviation of carrier)

$\dfrac{\omega_D}{\omega_m}$ = deviation ratio

The FM carrier spectrum resulting from a modulating signal, $S_2(\omega)$, is[8]

$$(12) \qquad H_2(\omega) = \frac{e^{-a}}{2\pi\ \omega_m} \int_{-\infty}^{+\infty} e^{(a \sin x/y)} \cdot e^{ixy}\, dy$$

$$(13) \qquad H_2(\omega) = \frac{e^{-a}}{2\pi\ \omega_m} \sum_{r=0}^{\infty} \frac{a^r}{r!} f_r(X)$$

$$a = 3D^2$$

$$D = \frac{f_D}{f_m}$$

$$X = \frac{\omega - \omega_c}{\omega_m} = \frac{f - f_c}{f_m}$$

For $\frac{f_d}{f_m} \geq 1.52$,

$$(14) \qquad H_2(\omega) \approx \frac{1}{\sqrt{2\pi\,\omega_D^2}} \exp\left\{\frac{-(\omega-\omega_c)^2}{2\omega_D^2}\right\}$$

Equation (14) is the same as equation (11). This fact points out that for deviation ratios greater than 1.5, a band-limited "white" noise spectrum is sufficient to simulate the baseband subcarrier spectrum. For deviations less than 1.5 a pre-emphasized, band-limited, "white" noise modulating signal must be used. The shape of the carrier spectrum envelope is Gaussian for $D > 1.5$, and ω_D corresponds to the standard deviation of the Gaussian curve. For small deviation ratios (<1.5) equation (12) must be solved to obtain an accurate representation of the carrier spectrum. A computer program was constructed to solve equation (12) as a function of the parameters D and X. D was varied from 0.2 to 1.2 in 0.2 increments; X was varied from 0 to 5 in 0.1 increments.

The series

$$\sum_{r=0}^{\infty} \frac{a^r}{r!} f_r(X)$$

was truncated after ten terms.

The computer was used to solve for the r = 1 to 9 terms. The zeroeth term was computed by hand since it represents a CW component. The zeroeth term is

$$e^{-a}\,\delta(X)$$

where

$$\delta(X) = \begin{cases} \infty, & x = 0 \\ 0, & x \neq 0 \end{cases}$$

The following are the values plotted:

D	a	$e^{-a} = [H(0)]\ r = 0$
.2	.12	.887
.4	.48	.619
.6	1.08	.340
.8	1.92	.147
1.0	3.0	.050
1.2	4.32	.013

This approximation yields accurate curves for $D \leq 1$ and $f - f_c/f_m \leq 4$. For $f - f_c/f_m > 4$ Equation 12 asymptotically approaches zero, but the truncated series approximation does not approach this asymptote.

The computer program is given in Appendix III.

Equation (14) can be rewritten as follows:

(14) $$H_2(\omega) \approx \frac{1}{\sqrt{2\pi\ \omega_D^2}} \exp\left\{\frac{-(\omega - \omega_c)^2}{2\omega_D^2}\right\}$$

(15) $$\omega_D H_2(f) \approx \frac{1}{\sqrt{2\pi}} \exp\left\{\frac{-(f - f_c)^2}{2f_D^2}\right\}$$

$$\omega_D = D\omega_m$$

$$\omega_m H_2(X) \approx \frac{1}{\sqrt{2\pi D}} \exp\left\{-\frac{1}{2}\left(\frac{f - f_c}{f_m D}\right)^2\right\}$$

(16) $$\omega_m H_2(X) \approx \frac{1}{\sqrt{2\pi D}} \exp\left\{-\frac{1}{2}\left(\frac{X}{D}\right)^2\right\}$$

$$X = \frac{f - f_c}{f_m}$$

Equation (15) is plotted in Figure 6. This curve which is valid for $D > 1.5$ relates the power spectral density to the r.m.s. deviation, f_D. It is plotted in normalized form enabling the determination of the carrier spectrum for any value of f_D so long as $D \geq 1.5$.

Equation (16) is expressed in a form which shows the dependence of the power spectral density on the deviation ratio D. It is written in essentially the same form as equation (13) which makes a comparison of the plots of the two equations feasible. The following forms of the two equations were plotted.

$$(13) \qquad 2\pi f_m H(X) = \frac{e^{-(3D^2)}}{2\pi} \sum_{r=1}^{9} \frac{(3D^2)^r}{r!} f_r(X)$$

$$(16) \qquad 2\pi f_m H(X) = \frac{1}{\sqrt{2\pi D}} \exp\left\{-\frac{1}{2}\left(\frac{X}{D}\right)^2\right\}$$

The normalized ordinate, $2\pi f_m H(X)$ was plotted versus the normalized abscissa, $X = f - f_c/f_m$, as a function of the parameter D.

For $D \leq 1$ equation (13) is accurate and is plotted in Figure 7. For $D > 1.5$, the Gaussian approximation, equation (15), is accurate and is plotted in Figure 8. Although the region between D = 1 and D = 1.5 is not strictly accurately specified either by the Gaussian approximation, Equation (16), or the truncated series solution, Equation (13), a comparison of equations (13) and (16) for D = 1.2 shows close agreement.

Figures 7 and 8 constitute a basis for examining the nature of the FM-FM carrier spectrum as the parameter D is varied. For $0.2 \lesssim D \lesssim .9$, the spectrum consists of a CW component at the carrier frequency and a rectangular broadband distribution limited to the band $f_c \pm f_m$. As D increases, the power in the CW component decreases while the power in the broadband spectrum increases. Most of this power is in the band $f_c \pm f_m$, but a Gaussian tail starting at $f_c \pm f_m$ and decaying asymptotically toward zero begins to form. At the frequencies $f_c \pm f_m$ there is a discontinuity in the broadband spectrum

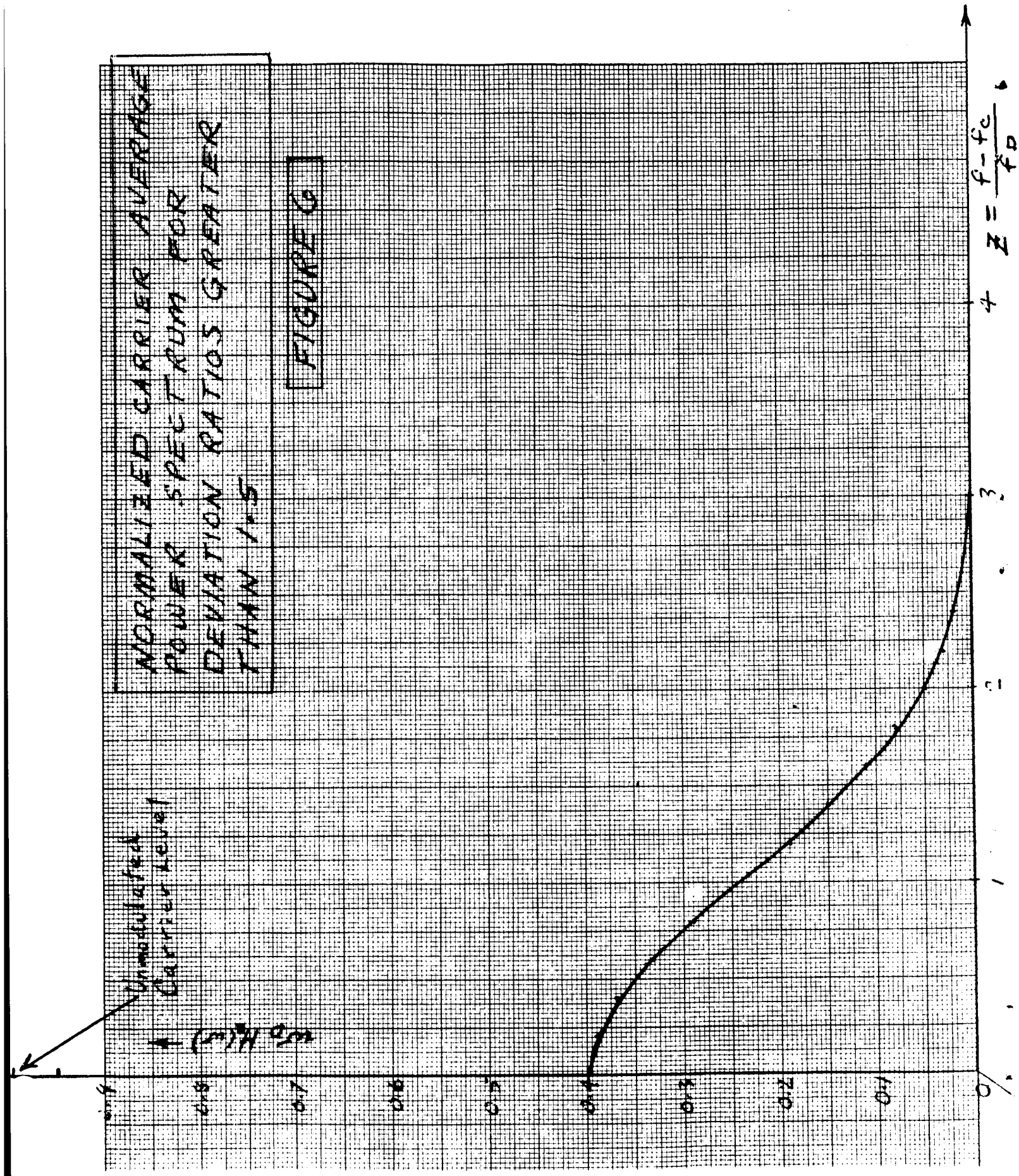
NORMALIZED CARRIER AVERAGE POWER SPECTRUM FOR DEVIATION RATIOS GREATER THAN 1.5
FIGURE 6
Unmodulated Carrier Level
(P)W cm
Z = f - fc / fD
0
1
2
3
4
0.1
0.2
0.3
0.4
0.5
0.6
0.7
0.8
0.9

FIGURE 7

NORMALIZED CARRIER POWER SPECTRA FOR FM-FM TELEMETRY SYSTEMS

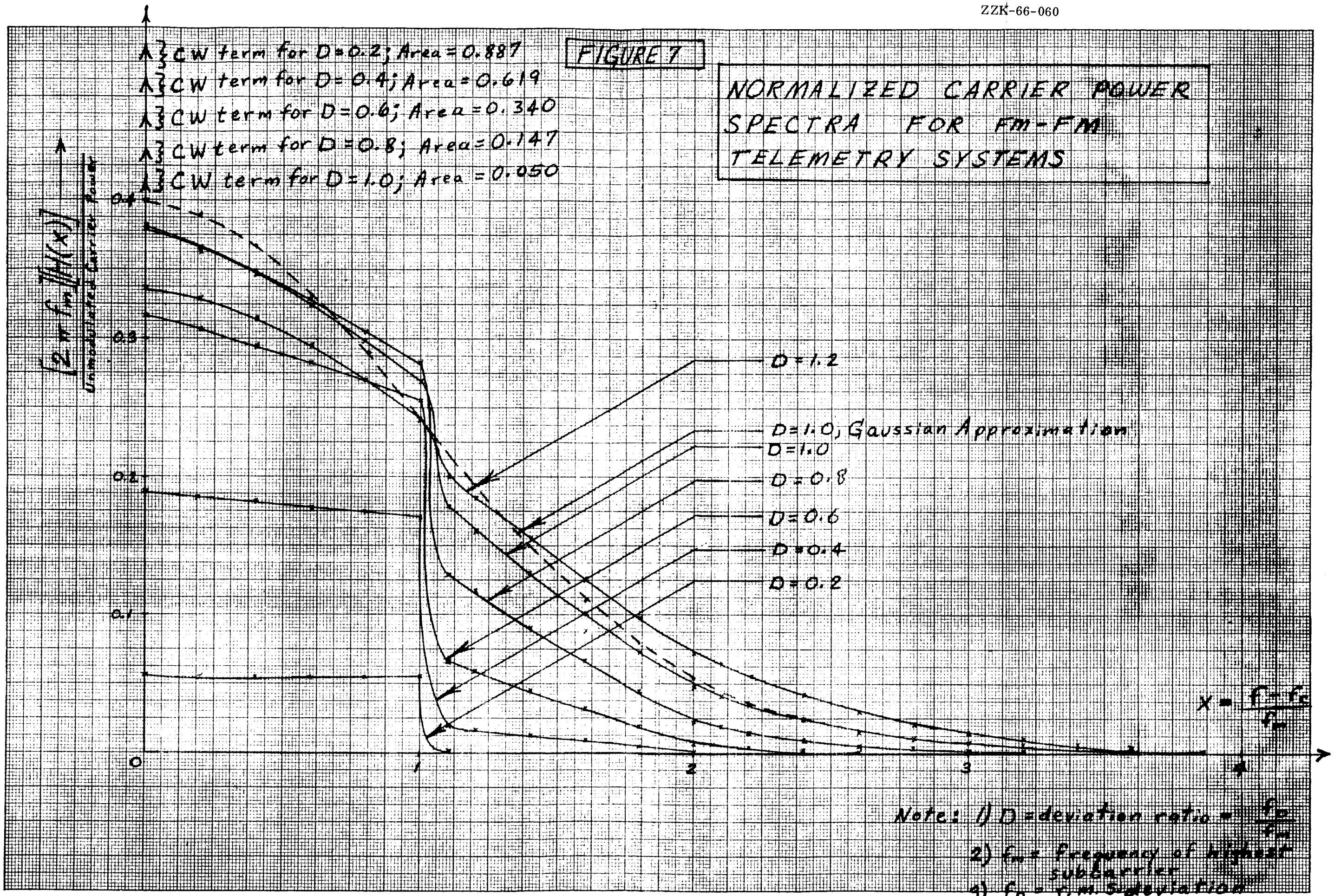

Note: 1) D = deviation ratio = $\frac{f_D}{f_m}$

2) f_m = frequency of highest subcarrier

3) f_D = r.m.s. deviation

4) f_c = carrier frequency

FIGURE 8

GAUSSIAN APPROXIMATION FOR CARRIER POWER SPECTRA OF FM-FM TELEMETRY SYSTEMS

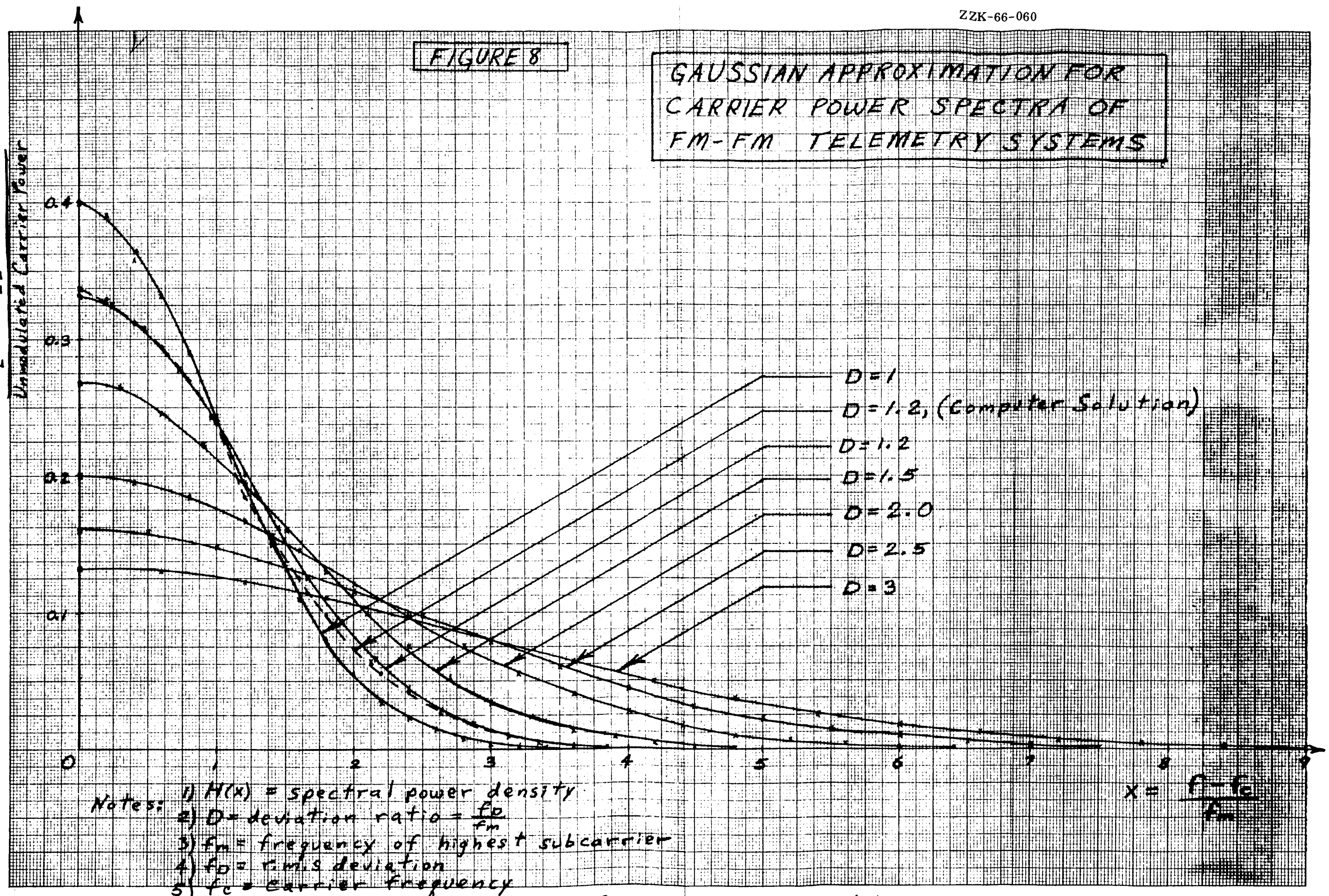

Notes:
1) $H(x)$ = spectral power density
2) D = deviation ratio = $\frac{f_D}{f_m}$
3) f_m = frequency of highest subcarrier
4) f_D = r.m.s deviation
5) f_c = carrier frequency
6) Gaussian approximation valid for $D > 1.5$; approximately correct for $D > 1$.

which becomes less as D increases. The amplitude of the rectangular distribution in the band $f_c \pm f_m$ increases and begins to slope downward as f varies from f_c with the maximum at the carrier frequency. At approximately D = .9 the CW component becomes negligible and power in the band $f_c \pm f_m$ becomes a maximum. For D > .9, the power in the band $(f_c \pm f_m)$ decreases, the maximum at f_c decreases, the discontinuity at $f_c \pm f_m$ starts to disappear and the spectrum becomes wholly broadband and Gaussian shaped.

For D = 1 both the exact solution and the Gaussian approximation are plotted. The Gaussian approximation over-estimates the power spectral density at $f = f_c$ and averages the power spectral density at the discontinuity at $f = f_c \pm f_m$. There is a maximum error of about 20% at the discontinuity in the Gaussian approximation. In an actual system a sharp discontinuity would not be seen and the spectral distribution at $f = f_c \pm f_m$ would be averaged much as it is by the Gaussian approximation for D = 1. Also for D > 1 the agreement between the Gaussian approximation and the exact solution becomes better and better. It can be concluded then that for the purposes of RF simulation, the FM-FM spectrum can be considered Gaussian for D > 1.

Although neither the computer solution nor the Gaussian approximation are exactly correct in the region, $1 < D < 1.5$, a comparison of the plots for D = 1.2, as shown in Figure 8, demonstrates close agreement between the two solutions.

The 40 db bandwidth criterion used for the Azusa Mark II FM spectrum will have to be re-examined since for the FM-FM case a broadband spectrum is being dealt with. For a broadband spectrum, the amplitude of any component is strictly a function of the bandwidth it is referred to since the units of the ordinate are in

$$\frac{AP}{(n)(cps)}$$

where

AP = voltage or power

cps = cycles per second,

n is commonly 1, 10^3, 10^6

If the units of the ordinate are chosen to be volts/Kc, for example, and the units of the abscissa are in Kc then any particular component of the spectrum will be referenced to a 1 Kc bandwidth, i.e., if the bandwidth of the receiver is 1 Kc and the transmitted spectrum changes very little in a 1 Kc increment, then the voltage a receiver will measure at any particular frequency is the amplitude of the spectral distribution at that frequency.

Figures 7 and 8 are normalized such that the ordinate and abscissa are unitless, but for any particular case the appropriate curve can be replotted in an unnormalized manner. In telemetry systems f_m will usually be in units of Kc so that the abscissa can be plotted in Kc and the ordinate in db below unmodulated carrier/Kc. If this is done the 40 db bandwidth criterion becomes 40 db/Kc. However, this criterion is not suitable for an FM-FM system as reference to Figure 6 will demonstrate. Carrier r.m.s. deviations for FM-FM systems are commonly in the range 75 Kc $< f_D <$ 125 Kc. Therefore, the maximum spectral component will be (from Figure 6) less than $\frac{.4}{470} = 8.5 \times 10^{-4}$ times the unmodulated carrier level in watts/Kc. A 40 db/Kc bandwidth criterion would only include components down to 10^{-4} of the unmodulated carrier. This would not be a restrictive enough criterion so far as simulating a spectrum is concerned. As Figure 6 shows, most of the spectrum is contained in a bandwidth of $f_c \pm 3 f_D$. Therefore, a more suitable bandwidth criterion for FM-FM will be chosen as

$$BW\Big|_{FM\text{-}FM} = 6 f_D \quad (D > 1.5)$$

Since $f_D = Df_m$, the bandwidth criterion can also be written

$$BW\Big|_{FM\text{-}FM} = 6 Df_m$$

For the normalized plots of Figures 7 and 8 the bandedge frequencies become

$$f_{BE} = f_c \pm 3 Df_m$$

$$\frac{f_{BE} - f_c}{f_m} = X_{BE} = 3D$$

It can be seen that for values of $D < 1$, as D gets smaller, the bandwidth includes proportionally less and less of the total spectrum. $X_{BE} = 3D$ is still a suitable criterion except for $3D < 1$. The criterion then will be modified to

$$X_{BE} = \begin{cases} 3D, & D > \frac{1}{3} \\ 1, & D < \frac{1}{3} \end{cases}$$

As an example of the application of the preceding material, the spectra of two telemetry systems which are planned for use in future missile systems will be worked out.

The first example is the RF-1 telemeter which will be used on Atlas-Centaur 9 and 10. In general, Centaur systems are designed such that $3f_D \approx 150$ Kc. The carrier frequency will be 225.7 Mc. The detailed deviation schedule for RF-1 follows:

Deviation Schedule Calculations

Taper: Constant 3 Kc for Channels 1, 2 and 3; parabolic from Channel 4 to Channel 13; linear with frequency from Channel 14 to Channel 18.

Receiver bandwidth: 300 Kc

Total Peak Deviation: 225 Kc

Deviation Equation (in peak form)

$$\Delta f(KC) = \sum_{1}^{3} 3\ KC + 0.1017 \left[\sum_{4}^{13} f_i^{1/2} + 0.0675 \sum_{14}^{18} f_i \right]$$

where

f_i = Subcarrier frequency (cps)

From this deviation schedule the following information is extracted.

$f_D = 53.2$ Kc

$f_m = 70$ Kc

$$D = \frac{f_D}{f_m} = 0.76$$

DEVIATION SCHEDULE

Channel	F_i (cps)	Peak Deviation (Kc)	RMS Deviation	$(\text{RMS Dev})^2$
1	400	3.0	2.12 Kc	4.49
2	560	3.0	2.12 Kc	4.49
3	730	3.0	2.12 Kc	4.49
4	960	3.2	2.26 Kc	5.11
5	1,300	3.6	2.54 Kc	6.45
6	1,700	4.2	2.96 Kc	8.76
7	2,300	4.9	3.46 Kc	11.97
8	3,000	5.6	3.95 Kc	15.60
9	3,400	6.4	4.52 Kc	20.43
10	5,400	7.5	5.30 Kc	28.09
11	7,350	8.8	6.21 Kc	38.56
12	10,500	10.5	7.41 Kc	54.91
13	14,500	12.4	8.75 Kc	76.56
14	22,000	15.3	10.41 Kc	108.4
15	30,000	20.8	14.65 Kc	210.0
16	40,000	27.7	19.60 Kc	384.1
17	52,500	36.4	25.70 Kc	660.5
18	70,000	48.6	34.40 Kc	1,187.4
		$\Sigma = 224.9$		$\Sigma = 2,830.3$

$$\sqrt{\Sigma(\text{RMS dev})^2} = 53.2 \text{ Kc}$$

Since D is less than 1, a computer solution was performed for D = 0.76. From the deviation equation it can be seen that the pre-emphasis of the higher subcarriers was not the same as that assumed in solving the equation for the power spectral density ($S_2(\omega) = 3\omega^2/\omega_m^2$). However, the exact pre-emphasis as given by the deviation equation will be close to that assumed for practically any FM-FM telemetry system since

the reasons for the pre-emphasis remain the same. Consequently, the spectra will be approximately identical in the two cases. Appendix II shows graphical proof of this statement.

The spectrum for the RF-1 telemeter is plotted in Figure 9.

As another example, the telemeter for the SLV PRIME Program will be considered.

The deviation schedule for the PRIME telemeter is as follows:

SLV (PRIME) TELEMETER

Subcarrier	Channel	Dev volts	Peak dev. in Kc Nominal
1	400	.0559	3
2	560	.0559	3
3	730	.0559	3
4	960	.0559	3
5	1,300	.0559	3
6	1,700	.0559	3
7	2,300	.0657	3.53
8	3,000	.0751	4.03
9	3,900	.0855	4.59
10	5,400	.100	5.40
11	7,350	.117	6.30
12	10,000	.139	7.50
13	14,500	.164	8.82
14	22,000	.203	10.9
15	30,000	.277	14.9
16	40,000	.369	19.8
17	52,000	.484	26.0
18	70,000	.645	34.6
19	93,000	.801	46.0
			f_D = 50 Kc

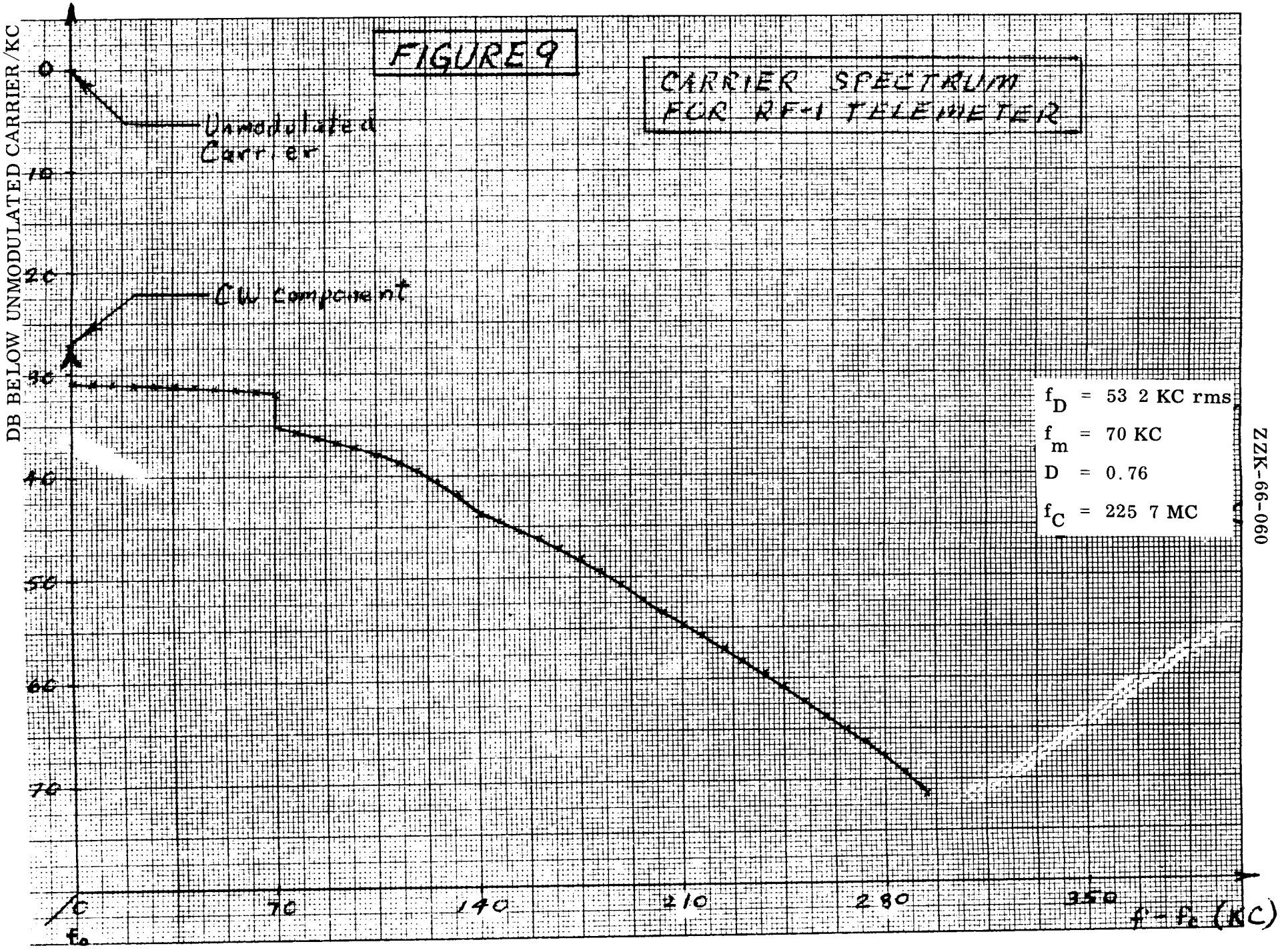
FIGURE 9
CARRIER SPECTRUM
FOR RF-1 TELEMETER
DB BELOW UNMODULATED CARRIER/KC
0
10
20
30
40
50
60
70
Unmodulated Carrier
CW Component
f_D = 53 2 KC rms
f_m = 70 KC
D = 0.76
f_C = 225 7 MC
70
140
210
280
350
$f - f_c$ (KC)
f_o

ZZK-66-060

From this deviation schedule the r.m.s. deviation is calculated to be

$$f_D = 50 \text{ Kc}$$

also

$$f_m = 93 \text{ Kc}$$

$$D = 0.54$$

The spectrum is plotted in Figure 10.

In order to compare the calculated spectrum to an actual spectrum, spectral measurements of the PRIME telemeter were made. All 19 subcarriers set up according to the above deviation schedule were used to FM Modulate a carrier provided by a Boonton Type 202-G FM-AM signal generator. The spectrum was viewed on a Model SPA-1 Panoramic Spectrum Analyzer. Because of the limitations and nature of the equipment, precise measurements were not possible, but the measurements taken conform to the shape predicted by the analytical results.

The procedure for making the measurements was as follows: The unmodulated carrier was adjusted to .01 volts. The gain of the spectrum analyzer was adjusted until the peak of the unmodulated carrier spectrum was at full scale. Modulation was applied and it was noted that the output at the carrier frequency dropped 4.4 db. If the spectrum analyzer had zero bandwidth at the carrier frequency it would be expected that the unmodulated carrier spectrum would be an infinite spike at the carrier frequency with area equal to .01 volt. However, because of the finite bandwidth of the spectrum analyzer, the peak of the unmodulated carrier spectrum will be finite and is related to the input voltage and the bandwidth of the spectrum analyzer as follows[9]:

$$E_{peak} = \frac{E_{in}}{IBW} \text{ (unmodulated carrier)}$$

$$E_{in} = 0.1 \text{ volt}$$

$$IBW = \text{impulse bandwidth} \approx 3 \text{ db BW}$$

FIGURE 10
CARRIER SPECTRUM FOR
PRIME TELEMETER
Double Tone
Carrier
Sub-Carrier
Measured
Calculated
DB BELOW UNMODULATED CARRIER/KC

The 3 db bandwidth was estimated to be 12 Kc from the display on the spectrum analyzer. Therfore,

$$E_{peak} = \frac{.01 \text{ volt}}{12 \text{ Kc}} = 21.6 \text{ db down from unmodulated carrier}$$

Therefore, the peak of the modulated spectrum was

$$21.6 + 4.4 = 26 \text{ db below unmodulated carrier}$$

This measured spectrum was plotted on Figure 10. It should not be concluded that the calculated spectrum underestimates the actual spectrum since the error in measuring the bandwidth of the spectrum analyzer could be as great as 5 Kc. Rather, the fact that the general shape of the measured curve resembles the analytical curve (the spectral power density peaks near the carrier, decreases rapidly near $f_c \pm f_m$ and falls off in a Gaussian manner on the skirts) generates confidence in the analytical results.

In Appendix IV[10] the experimentally measured spectrum of an FM-FM system with D = 1.1 is shown.

The other common types of telemeters, PCM/FM, PAM/FM and PDM/FM were considered in less detail due to time limitations. They may be treated similarly to obtain spectral plots.

PCM-FM

The baseband spectrum for non-return-to-zero PCM is

$$H(\omega) = \frac{T}{6}\left(\frac{\sin\frac{T}{2}\omega}{\frac{T}{2}\omega}\right)^2 \left[1 + \frac{3}{T}\delta(\omega)\right]$$

T = period (sec)

$$\delta(\omega) = \begin{cases} \infty, & \omega = 0 \\ 0, & \omega \neq 0 \end{cases}$$

If a two level system with a uniform probability distribution is assumed with the voltage level of the modulating signal varying between $\pm 1/2$ volt, then the following diagram represents the modulating signal.

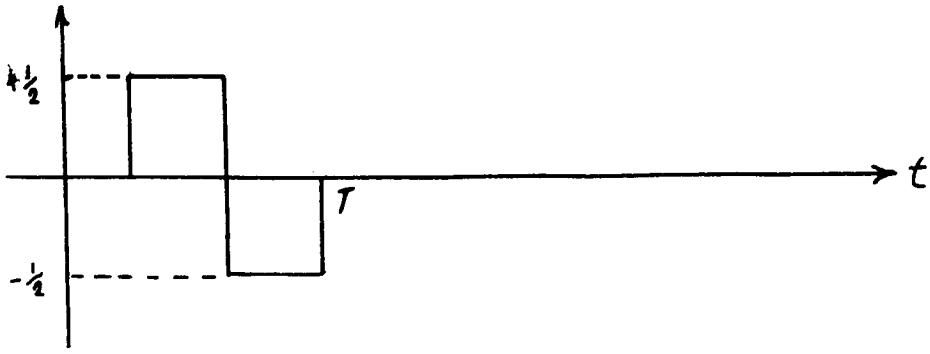

The carrier power spectrum then becomes[11]

$$H(\omega) = \frac{\frac{\omega_D T}{2} \sin\left(\frac{\omega_D T}{8} - \frac{T(\omega - \omega_c)}{4}\right)}{\left(\frac{\omega_D T}{4}\right)^2 - \left[\frac{T(\omega - \omega_c)}{2}\right]^2}$$

If a premodulation filter of one half the bit rate is used, then the baseband spectrum is approximately that of band-limited "white" noise and[12]

$$H(\omega) = \frac{1}{\sqrt{2\pi\,\omega_D^2}} \exp\left[\frac{-(\omega - \omega_c)^2}{2\,\omega_D^2}\right]$$

$f_D = \frac{\omega_D}{2\pi}$ = RMS carrier deviation

$f_c = \frac{\omega_c}{2\pi}$ = Carrier center frequency

f_m = highest modulating frequency

$= \frac{1}{2} f_B = \frac{1}{2}$ (bit rate)

$\frac{f_D}{f_m} \simeq 1.13$

$T = \frac{1}{f_B}$

IRIG Telemetry Standards recommend a premodulation filter with cut-off frequency equal to the nominal bit rate.

In order for carrier and subcarrier thresholds to be reached at the same time D = 0.6 and $\beta = 3.4$[13].

PAM-FM

The IRIG Standards state that the bandwidth of the transmitted signal is not to exceed the IF bandwidth of the receiver. Premodulation filtering is used to limit bandwidth. The bandwidth varies between three and eight times the sampling rate depending on the desired total error in the system. For a 2% (of full data range) total RMS error, the sampling rate should equal 5 times the desired IF bandwidth.

The baseband power spectrum for 100% duty cycle PAM with a uniform probability distribution for the amplitudes is

$$H(\omega) = \frac{T}{6}\left(\frac{\sin\frac{T}{2}\omega}{\frac{T}{2}\omega}\right)^2\left[1+\frac{3}{T}\delta(\omega)\right]$$

The baseband power spectrum for 50% duty cycle PAM is

$$H(\omega) = \frac{T}{2}\left(\frac{\sin\frac{T}{4}\omega}{\frac{T}{4}\omega}\right)^2\left[\frac{1}{12}+\frac{1}{4T}\sum_{n=-\infty}^{+\infty}\delta\left(\omega-\frac{n}{T}\right)\right]$$

$$\delta(X) = \begin{cases}\infty, & x=0\\ 0, & x\neq 0\end{cases}$$

PDM-FM

The PDM-FM carrier power spectrum is given by

$$H(\omega) \cong \frac{T}{8}\left[\left(\frac{\sin\frac{\omega_1 T}{2}}{\frac{\omega_1 T}{2}}\right)^2+\left(\frac{\sin\frac{\omega_2 T}{2}}{\frac{\omega_2 T}{2}}\right)^2\right]$$

where

$$T = \frac{1}{2f_s}$$

$f_s = f_m$ = pulse repetition frequency

$\omega_1 = \omega - \omega_c - \omega_D$

$\omega_2 = \omega - \omega_c + \omega_D$

$f_D = \frac{\omega_D}{2\pi}$ = RMS subcarrier deviation

$f_c = \frac{\omega_c}{2\pi}$ = Carrier center frequency

$f_D \geq 1.36\, f_s$

The spectrum peaks at the deviation frequency. The tails of the spectrum decay as $1/f^2$.

The parameter values found optimum experimentally[14] are

$$\frac{IFBW}{f_s} = 8\,, \quad \frac{f_D}{f_s} \cong 4$$

For both carrier and modulating signal thresholds to be reached simultaneously, $D = 0.6$[15].

The following data refer to Appendix V[18] which shows PAM-FM, PCM-FM, PDM-FM, and FM-FM spectra plotted for equal information BW and equal carrier power.

The following parameters apply to the diagram and were determined to be optimum for 2% rms total system error.

System	B/f_s	B_P/f_s	$f_{DP}/1/2B$
PAM-FM	5	2.5	0.7
PDM-FM	7	5	1.0
PCM-FM	6	3	0.75

System	B	B_i	f_{mh} (Highest modulating freq.)	$f_D/f_{mh} = D$
FM-FM	4.75 Kc/s	4.75 Kc/s	68.5 Kc/s	0.85

B = Receiver BW

B_p = Premodulation video BW

f_{Dp} = peak frequency deviation of carrier

f_s = sampling rate equivalent to pulse repetition frequency for PAM and PDM

$f_s = f_B$ = bit rate for PCM-FM

B_i = info BW = $1/2\, f_B$ for PCM-FM
= $1/2\, f_s$ for PDM-FM
= $1/2\, f_s$ for PAM-FM

The bandwidths of the PCM-FM, PDM-FM and PAM-FM systems extend from the carrier out to the respective bandedges as shown in the diagram. The FM-FM spectrum extends $\pm B/2$ on either side of the carrier.

2.3 RF Pulse Modulation Analysis. The basic system of analysis used for examining the spectrum of a pulse modulated RF signal is the Fourier analysis. By definition in general terms this is given by

$$F(\omega) = \int_{-\infty}^{+\infty} f(t)\, e^{-jwt}\, dt \tag{17}$$

where f(t) in this equation is the time versus amplitude representation of the signal under consideration. For well defined waveshapes, these spectra have been worked out in terms of defining parameters in such a way as to make analysis and prediction a relatively simple task. It is instructive, however, at the outset, to bring the concept of bandwidth into the picture so that the effects of modulating a carrier can be viewed in terms of any receptor.

Using as an example the square pulse of Figure 11 the solution of Equation 17 when f(t) is a square pulse is given by

$$F(\omega) = e = Ad\, \frac{\sin \pi fd}{\pi fd} \tag{18}$$

FIGURE 11

INTERFERENCE LEVEL FOR A 1 VOLT 1 μSEC RECTANGULAR PULSE

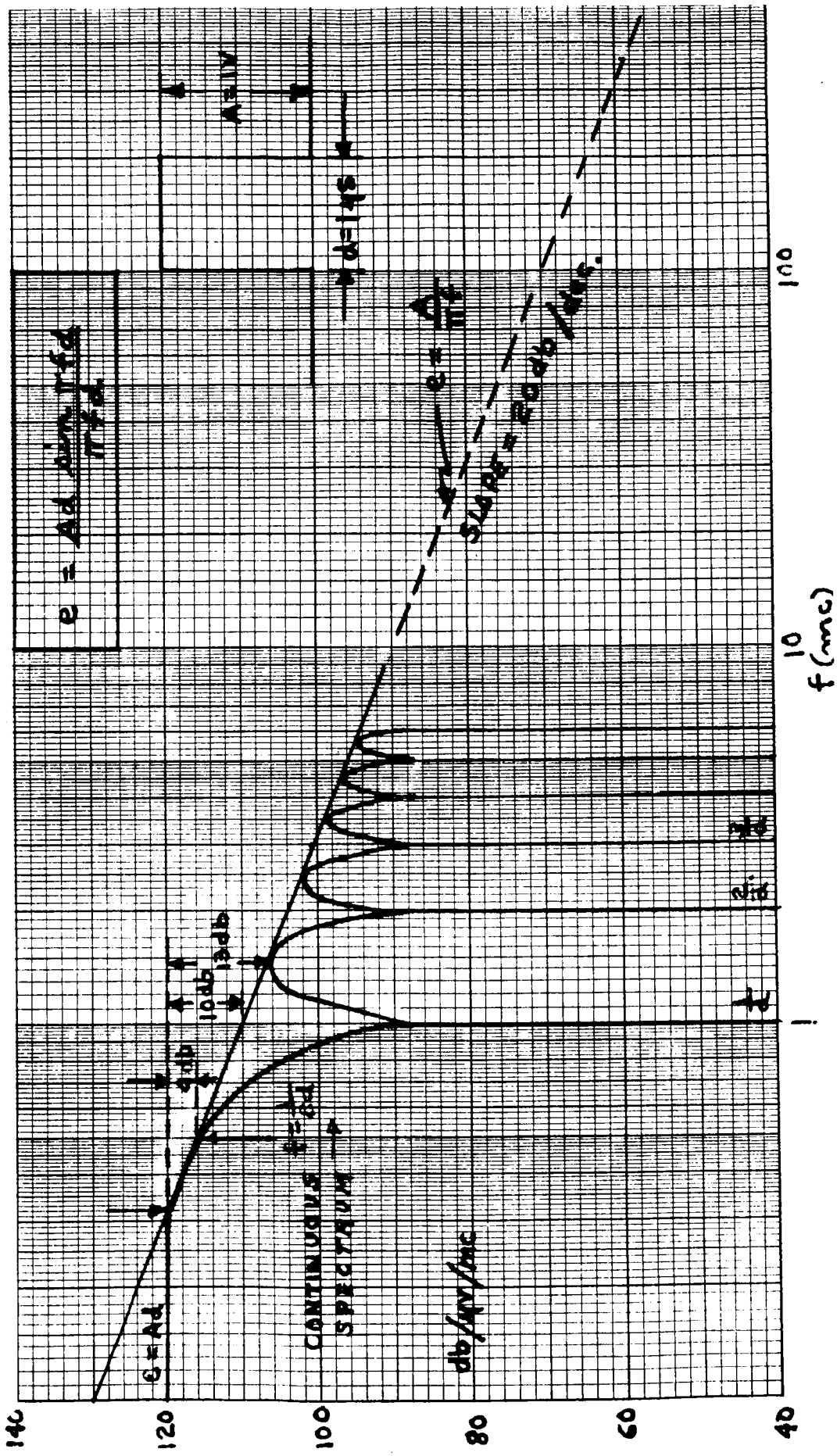

As can be seen, the units in the solution of Equation (18) are A (volts) d (seconds), or in the particular case of a 1 volt, 1 μ second pulse, 1 volt μ second. Since t = 1/f this can quickly be translated to 1 volt/Mc which is a system of units long familiar to the EMC engineer. What should be noted here is the fact that units used are intimately connected with the concept of bandwidth. If the 1 volt, 1 μ second square pulse was viewed through a 1 Mc bandwidth (DC to 1 Mc), the level of the measured signal would be approximately 1 volt. That this is so can be verified by referring to Figure 11 and noting that 95% of the power in this pulse is contained within the first lobe from DC to 1 Mc as shown below. The waveshape at the output has changed a little because 5% of the power at the higher frequencies has been rejected.

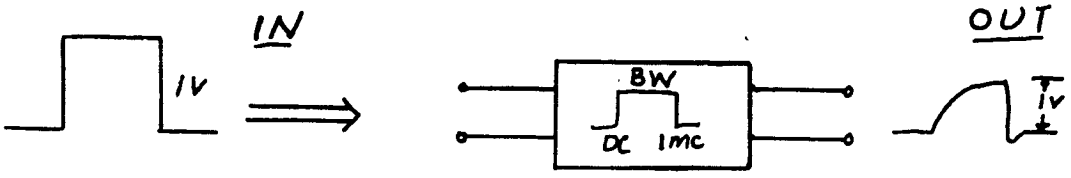

If the bandwidth of the device viewing this spectrum was 1 Kc (DC to 1 Kc) it can be seen that the peak amplitude of the signal at the output would be 1 V/Mc x 1 Kc = 1 x 10^{-3} volts.

Next, the effect on the spectrum of a pulse repetition frequency will be considered. If the same square pulse of Figure 11 is considered assuming a repetition rate of 100 Kc, the spectrum produced is shown in Figure 12. The solution to Equation (17) for this f(t) is

$$F(\omega) = C_0 + \sum_{n=1}^{\infty} \frac{2Ad}{T_1} \left(\frac{\sin \frac{\pi nd}{T_1}}{\frac{\pi nd}{T_1}} \right) \cos \frac{2\pi nt}{T_1} \tag{19}$$

where

$$C_0 = \text{DC component} = \frac{Ad}{T_1}$$

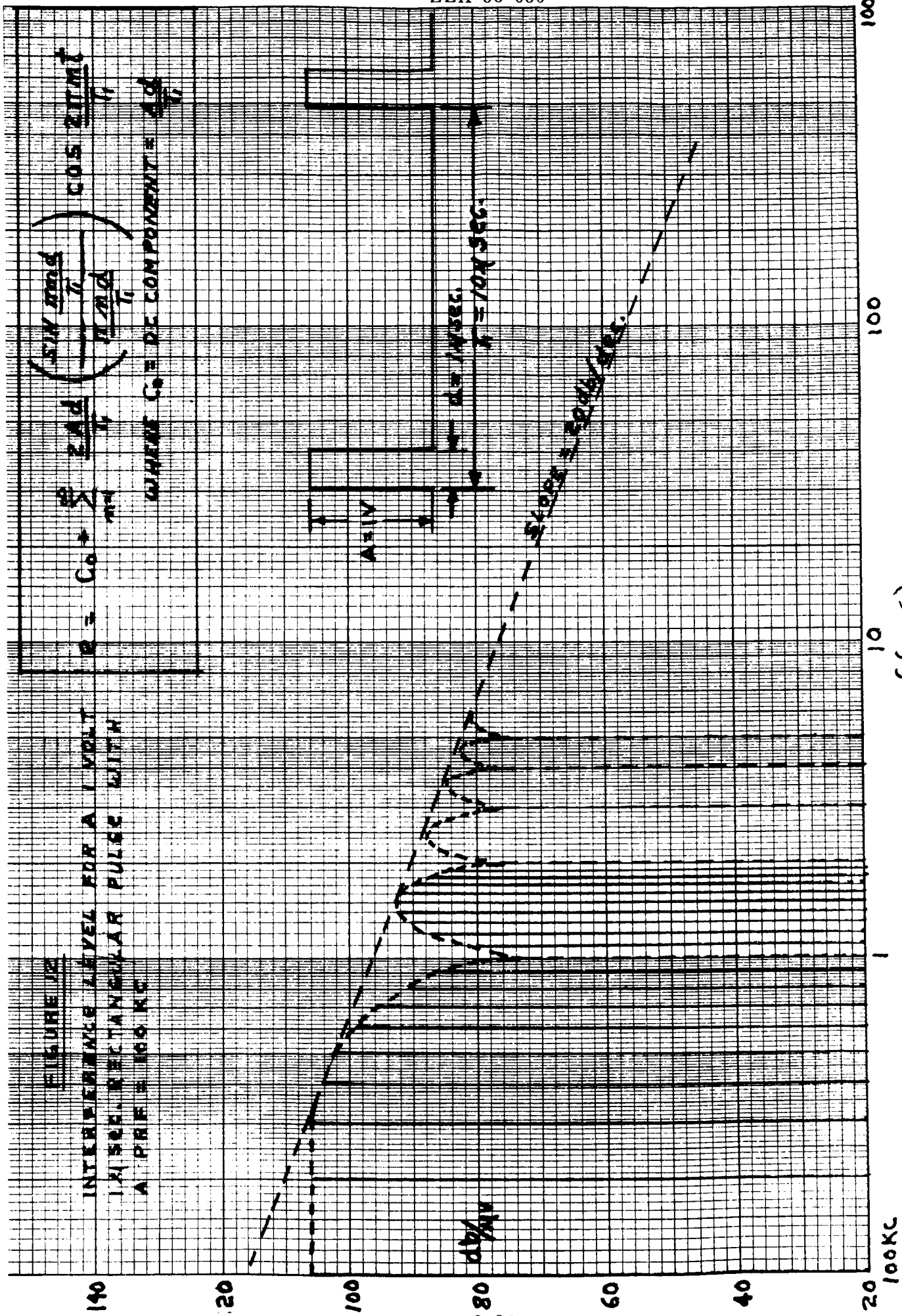

FIGURE 12
INTERFERENCE LEVEL FOR A 1 VOLT
1 USEC. RECTANGULAR PULSE WITH
A PRF OF 100 KC

The spectrum is described by the envelope function which can be seen to be the same as that for the single pulse except for the factor of two. The cos function describes the location of frequency components at n/T_1 where n = 1, 2, 3 ---. It should be noted that the DC component cannot be shown on this presentation but appears in Equation (19). It can also be seen by reference to the spectrum of Figure 12 that the effect of this signal on any device would be dependent on the location and width of the passband of the device. The discrete frequency components shown in this spectrum would approximately add in phase at their peak values in any band limited device. Using the example of the 1 Mc bandwidth mentioned previously, it can be seen that the addition of the frequency components shown in the first lobe of Figure 12 would add to reproduce the square pulse if this spectrum were to be viewed through such a band limited device.

The discussion above has been limited to the square pulse, both single and repetitive, but the same procedure holds for pulses of any shape, such as clipped sawtooth, trapazoidal, critically damped exponential, triangular, cosine, cosine squared and gaussian. The envelope structure for these pulses (minus the fine detail) is shown in Figure 13 along with relationships which can be used to work out spectrums of any amplitude and pulse widths.

The next point of interest is that of modulating an RF carrier with one of the pulse shapes mentioned above. The easiest shape to deal with and the one which can be produced most simply is the square pulse modulated RF carrier. This can be produced by turning the RF carrier on and off, producing the waveform of Figure 14. This function substituted in Equation (17) produces a spectrum described by the following equation:

$$(20) \qquad F(\omega) = e = \frac{Ad}{2}\left[\frac{\sin(\omega - \omega_0)\, d/2}{(\omega - \omega_0)\, d/2} + \frac{\sin(\omega + \omega_0)\, d/2}{(\omega + \omega_0)\, d/2}\right]$$

This equation is shown in graphical form in Figure 14. For pulse widths on the order of microseconds and greater and high frequencies (above 10 Mc) the second term of Equation (20) can be ignored and the equation for the spectrum in Figure 14 can be represented by

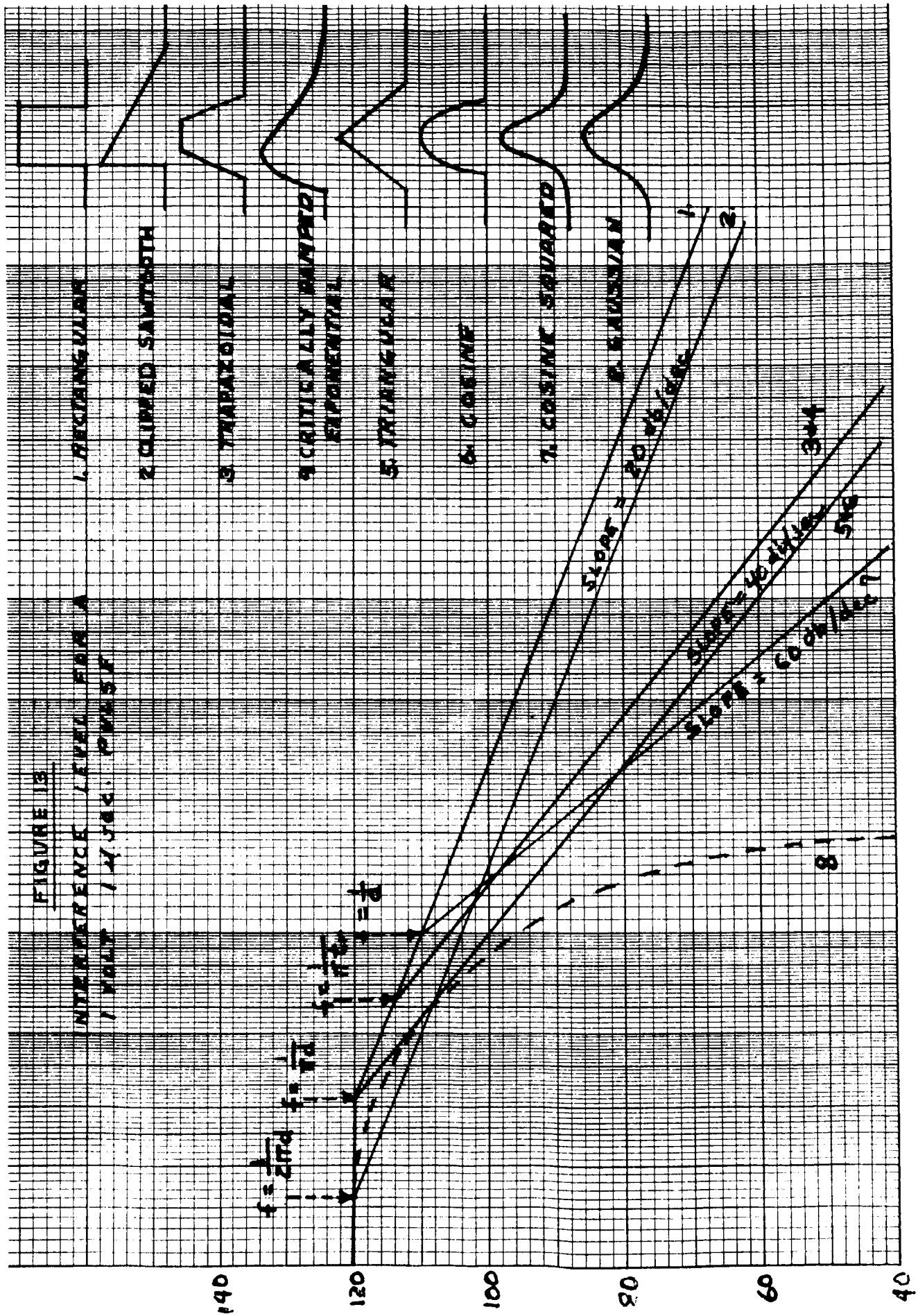

FIGURE 13
INTERFERENCE LEVEL FOR A 1 WATT 1 MEV. GAMMA

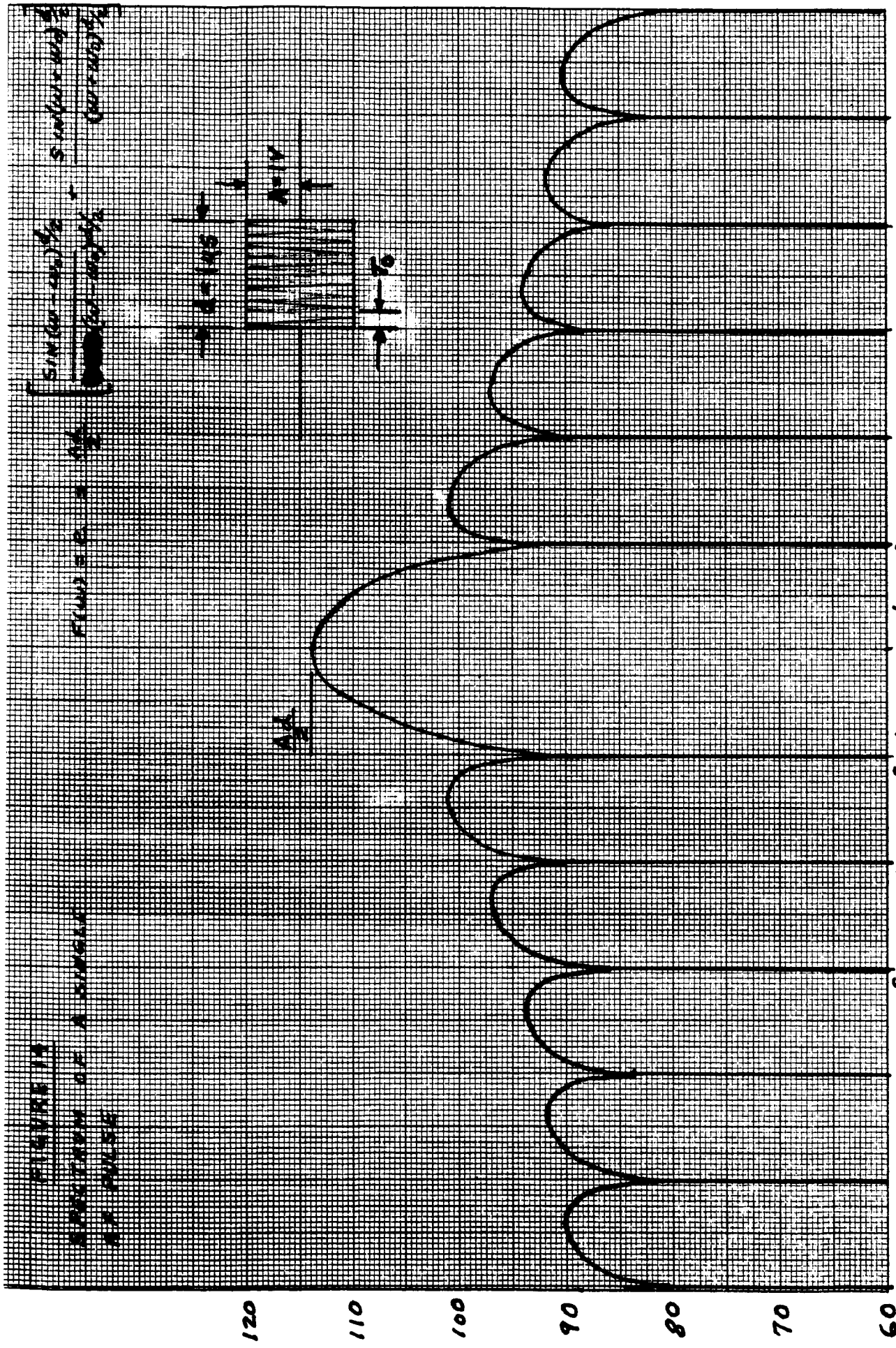
FIGURE 11
SPECTRUM OF A SINUSOIDALLY
AM PULSE
f0-3mc f0-2mc f0-1mc f0=1/τ f0+1mc f0+2mc f0+3mc
120
110
100
90
80
70
60

$$(21) \qquad F(\omega) = e = \frac{Ad}{2}\left(\sin \frac{[\omega - \omega_0]\, d/2}{[\omega - \omega_0]\, d/2}\right)$$

This is nothing more than the spectrum of the square pulse of Figure 11 displaced symmetrically about the RF carrier frequency f_0, with an amplitude reduction of 1/2. This is the spectrum pictured in Figure 14. If the RF carrier is turned on and off at a given repetition rate the spectrum changes to that shown in Figure 15. This spectrum is given by

$$(22) \qquad F(\omega) = \frac{Ad}{T_1} \sum_{n=0}^{\infty} (2 - \delta_{n,0}) \frac{\sin\left(\pi n \frac{d}{T_1}\right)}{\pi n \frac{d}{T_1}} \left[\sin\left(\omega_0 + \frac{2\pi n}{T_1}\right) + \sin\left(\omega_0 - \frac{2\pi n}{T_1}\right)\right]$$

$$\delta_{n,0} = \begin{cases} 1, & n=0 \\ 0, & n \neq 0 \end{cases}$$

As can be seen, this now represents a discrete spectrum symmetrical about the RF carrier frequency f_0, with frequency components located at n/T_1 where n = 1, 2, 3, etc., and an amplitude of $A\, d/T_1$ at f_0 dropping off at a sin X/X rate symmetrically about this point. Figure 15 is the spectrum of a 1 V, 1 μ sec pulse modulated with a duty cycle of 10%. Figure 16 is a graph of a general spectrum which shows how the waveform parameters are related to the spectrum. As can be seen, this is a rather detailed spectrum. Usually the pulse modulated RF spectrum would be shown on a log frequency scale to indicate the nature of the spectrum far removed from the carrier. Using Figure 15 the spectrum of the FPS 16 radar could be worked out assuming that the pulses of the RF carrier have a zero rise time. Given:

f_0 = 5480 Mc
peak power = 1.1 megawatt
pulse rate = 160 pps, T_1 = 1/160 = 6.25 msec
pulse width = 1 μsec
rise time = 0

Under these conditions the steps necessary to obtain the frequency versus amplitude spectrum shown in Figure 16 are:

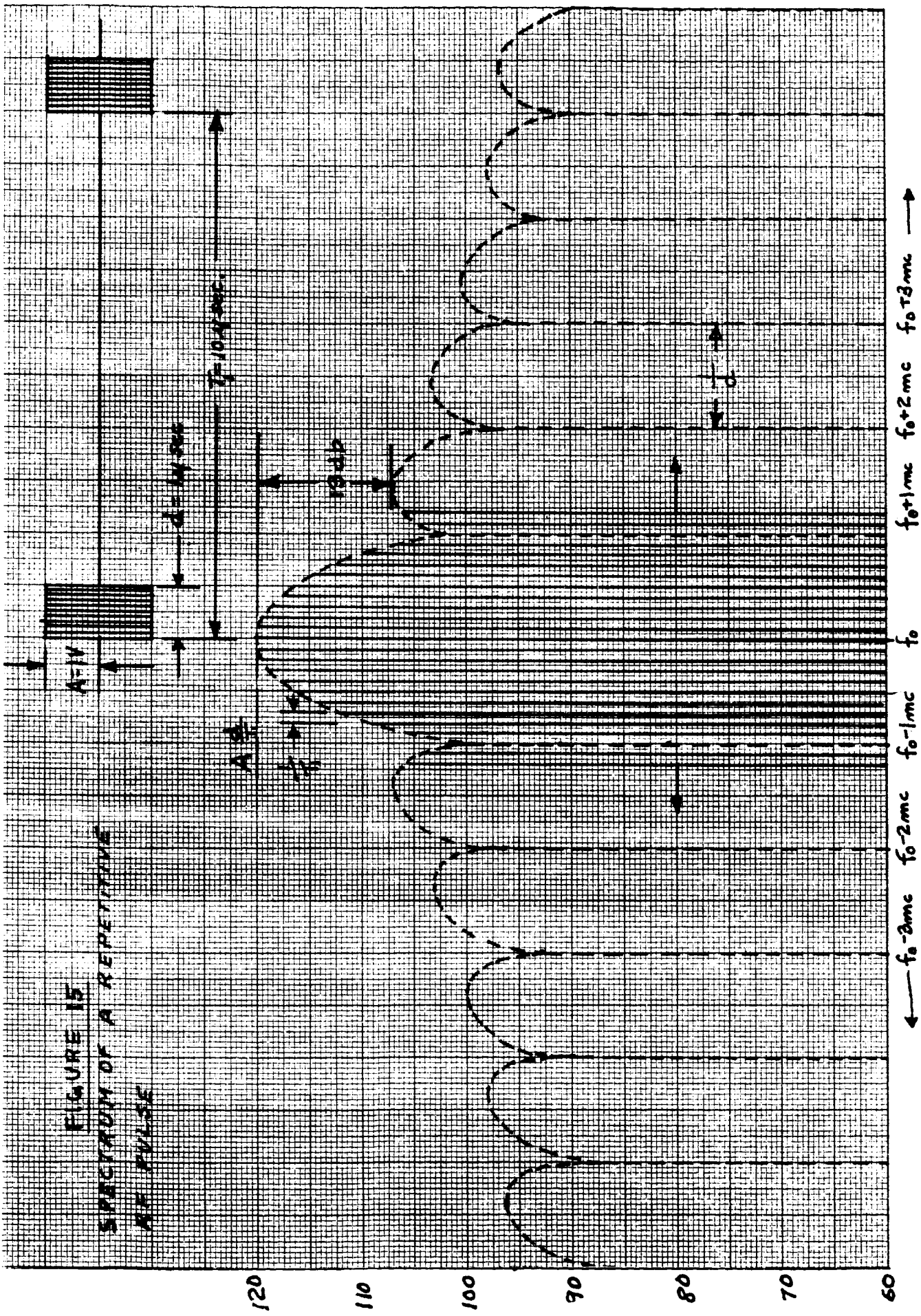

FIGURE 15
SPECTRUM OF A REPETITIVE RF PULSE

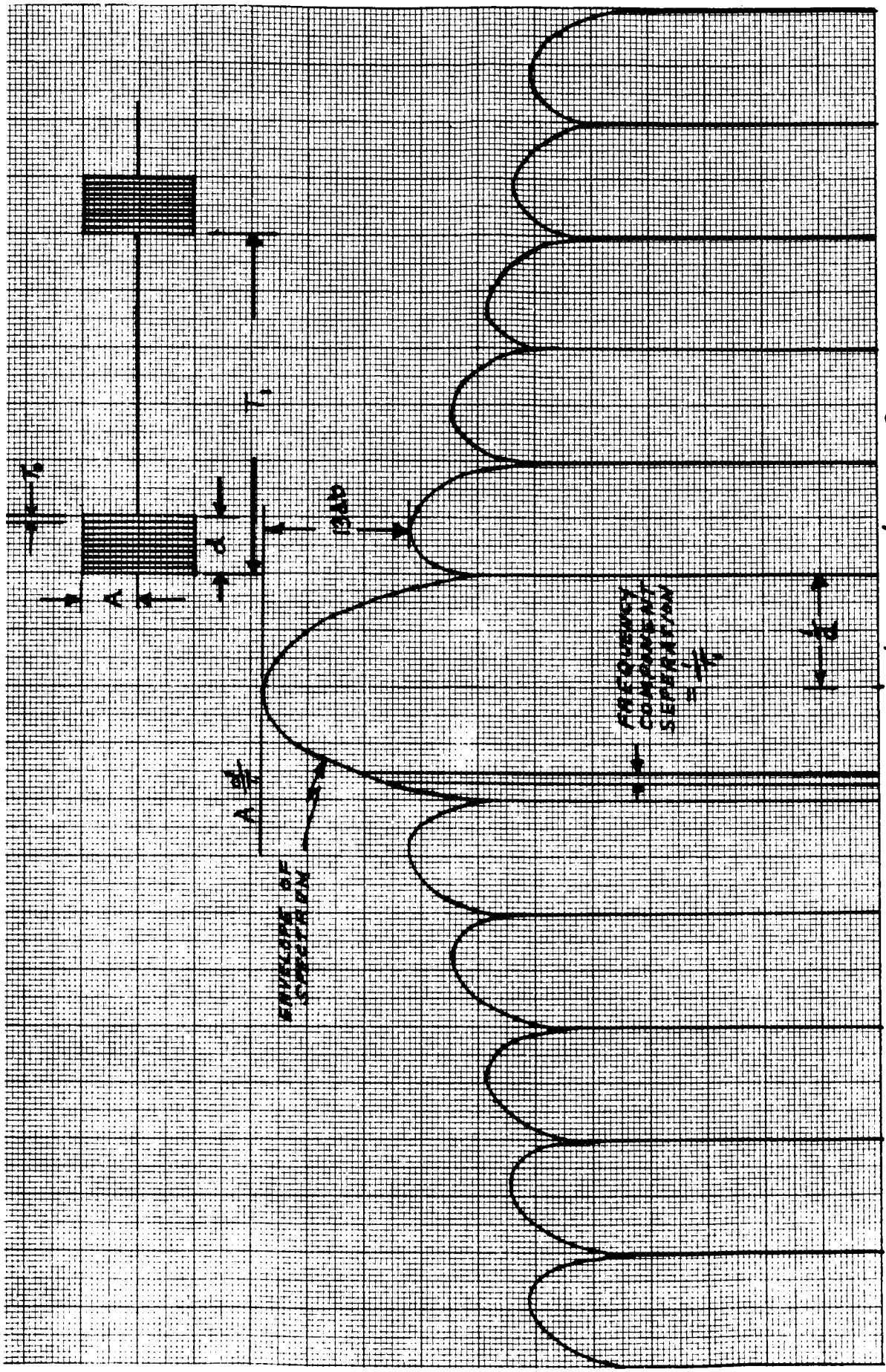

FIGURE 16
SPECTRUM OF A REPETITIVE RF PULSE (GENERAL)

1. Convert peak power to voltage (assuming that this power is into a matched broadband antenna).

$$A = \sqrt{1.1 \times 10^6 \times 50} = \sqrt{55 \times 10^6} = 7.4 \times 10^3 \text{V} = 197 \text{ db}/\mu\text{V}$$

2. Find amplitude at f_0 = 5480 Mc.

$$e(f_0) = A\frac{d}{T} = \frac{7.4 \times 10^3 \times 10^{-6}}{6.25 \times 10^{-3}} = 1.18 \times 10^6 \text{ V/Mc}$$

3. The frequency component separation $1/T_1$ is 160 cps so that there are frequency components distributed about f_0 every n/T_1 where n = 1, 2, 3---.

NOTE: This is a true and complete representation of the spectrum of the FPS-16 radar, but clarification must be added concerning the practicality of representing the spectrum in this way. A frequency separation between components of 160 cps cannot be easily represented on a linear graph such as Figure 15. Under these circumstances, the relationship of the spectrum to a device with a finite bandwidth will again be considered. It is reasonable to assume that any device tuned at 5480 Mc will have at least a 2 Mc bandwidth. If this bandwidth were centered at f_0 most of the signal shown in Figure 16 would pass as shown below.

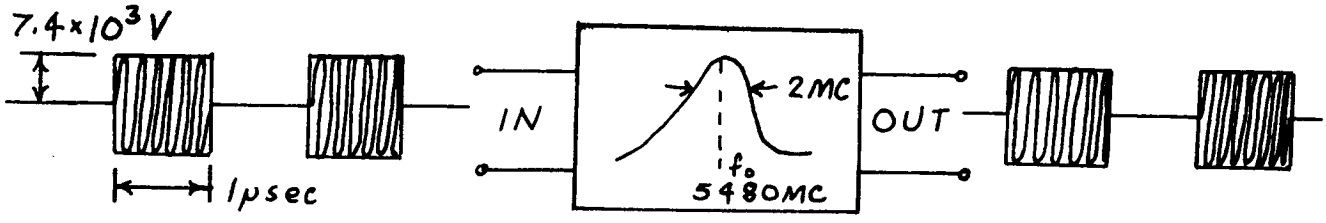

If this bandwidth were used to sweep the entire signal, the peak value seen at 5480 Mc would be that given in step (1) above, 197 db/μV. The envelope about f_0 would drop off at 6 db per octave as shown in Figure 15. If Figure 15 is expanded to a log representation the entire signal spectrum as seen by a swept 2 Mc bandwidth would be that shown in Figure 19 (curve 1). The skirts of this signal have a substantial value far from f_0.

If this type of signal were practically obtainable (zero rise time pulse), it would be modified by the antenna tuning characteristics. This would limit the signal to a much narrower bandwidth.

If must be remembered that the analysis above was made with reference to a zero rise time pulse modulated RF carrier. Actually, a practical rise time would be in the order of 0.1 μsec. The peak envelope for a 1 volt, 1 μsec rise time trapazoidal pulse is shown in Figure 17. It should be noted that the effect of the rise time is to cause the envelope to fall off at 12 db per octave above $f = 1/\pi_r$. If the FPS 16 radar were considered to have this rise time, the spectrum could be worked out using the steps previously mentioned and Figure 18. The peak value at f_0 would not change and the spectrum would roll off at 6 db per octave until $f = f_0 \pm 1\pi t_r$ and then would proceed to roll off at 12 db per octave for the remainder of the spectrum. This spectrum is shown in Figure 19 (curve 2). It should be noted that this spectrum would also be modified by the antenna characteristics.

In order to more accurately ascertain the actual spectral characteristics of a real transmitting system, more information than was given for the FPS 16 radar would be necessary.

It would be helpful to know the rise time and the antenna bandwidth characteristics so that a true transmitted spectrum can be obtained. The degree to which these modulation effects would have to be simulated would be dependent upon bandwidth and location in the spectrum of any intentional or non-intentional receiving device. Referring again to Figure 19, it can be seen that the bandwidth of any transmitted modulated RF carrier in the GC frequency range would not be great enough to warrant simulation unless there are devices in the system under consideration that are susceptible to the demodulated signal. An important consideration, therefore, is information concerning the susceptibility characteristics of the devices in any particular system.

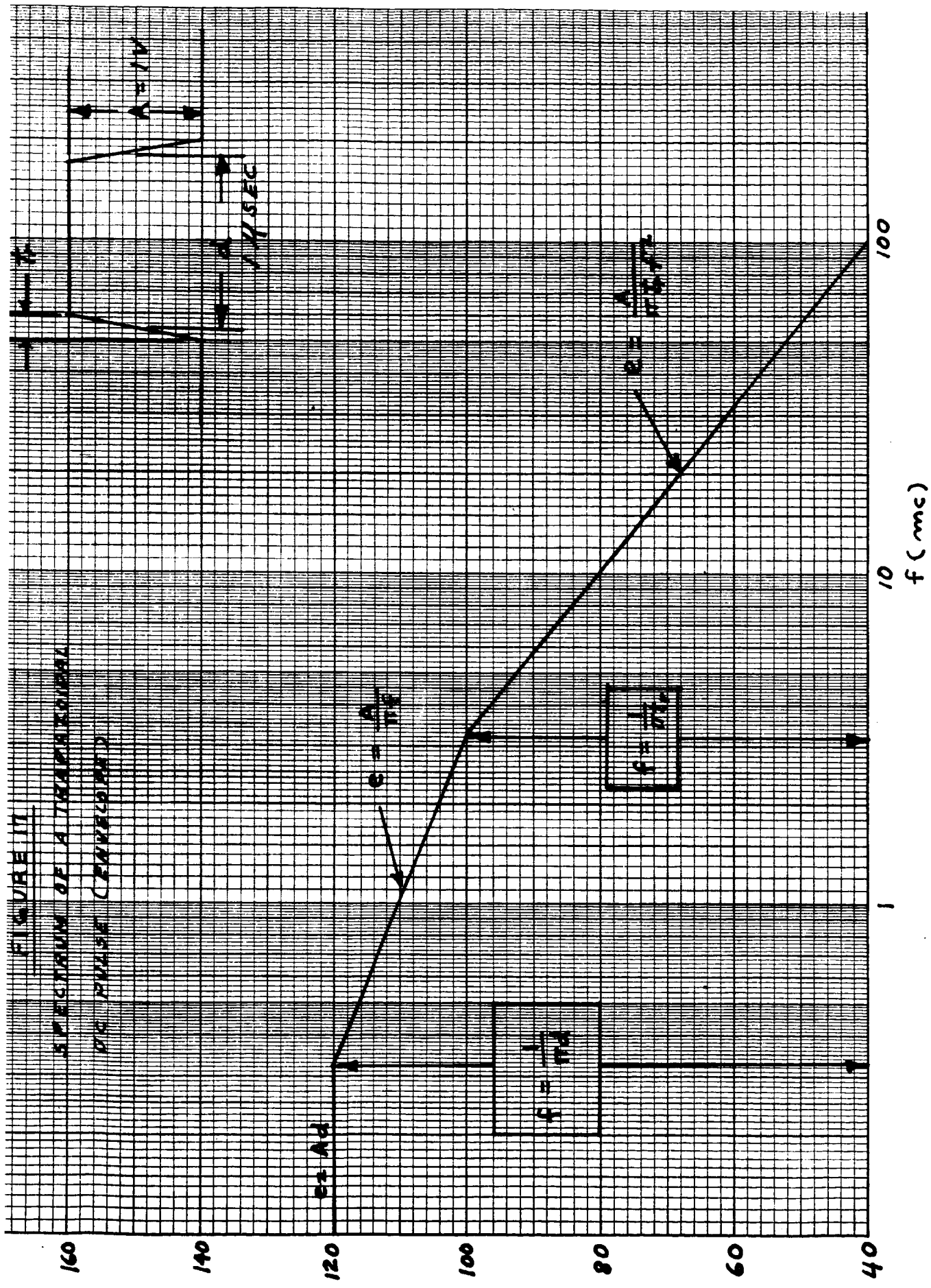

FIGURE III
SPECTRUM OF A TRAPEZOIDAL
DR PULSE (ENVELOPE)

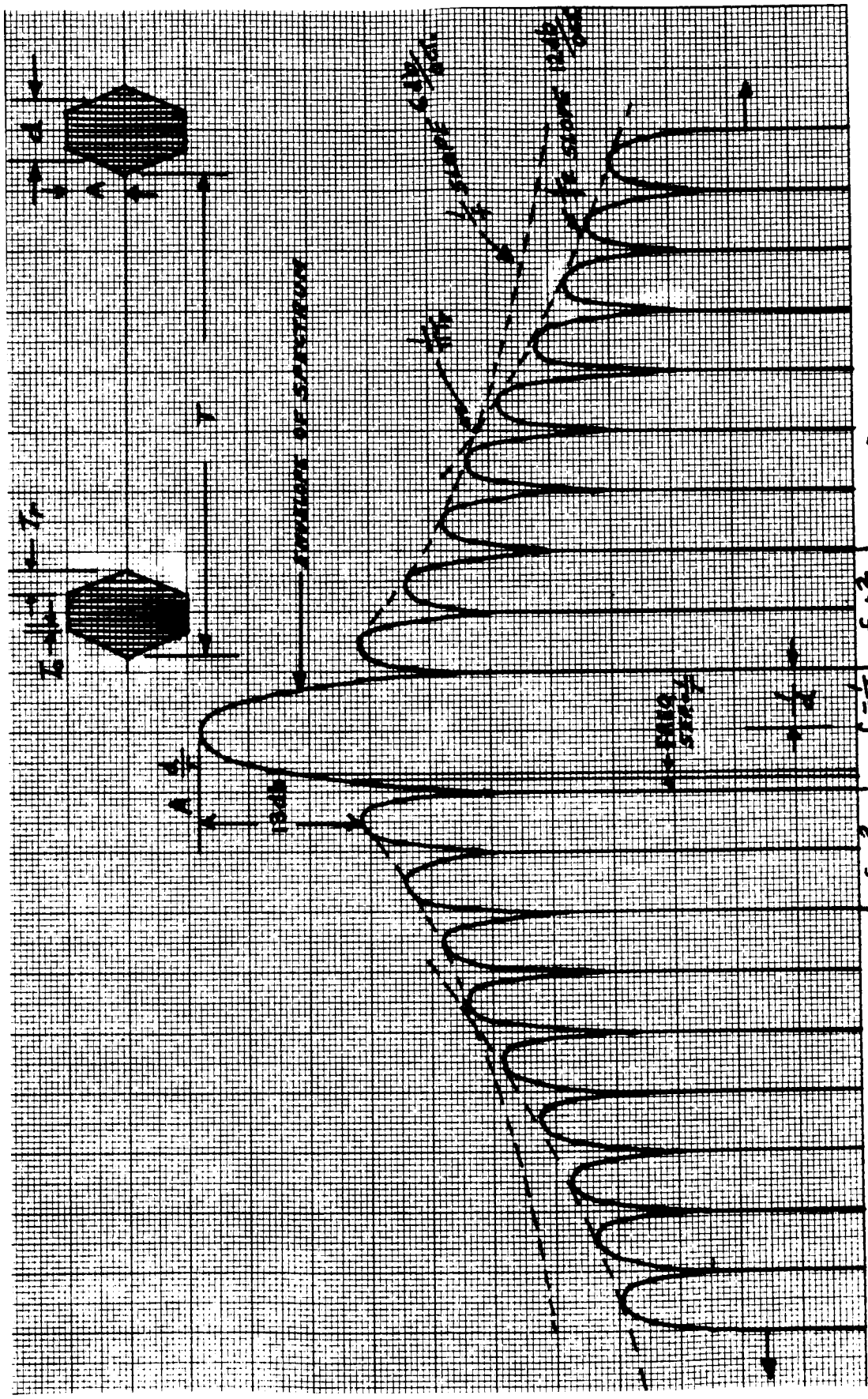

FIGURE 18

SPECTRUM OF AN RF TRAPEZOIDAL MODULATED PULSE

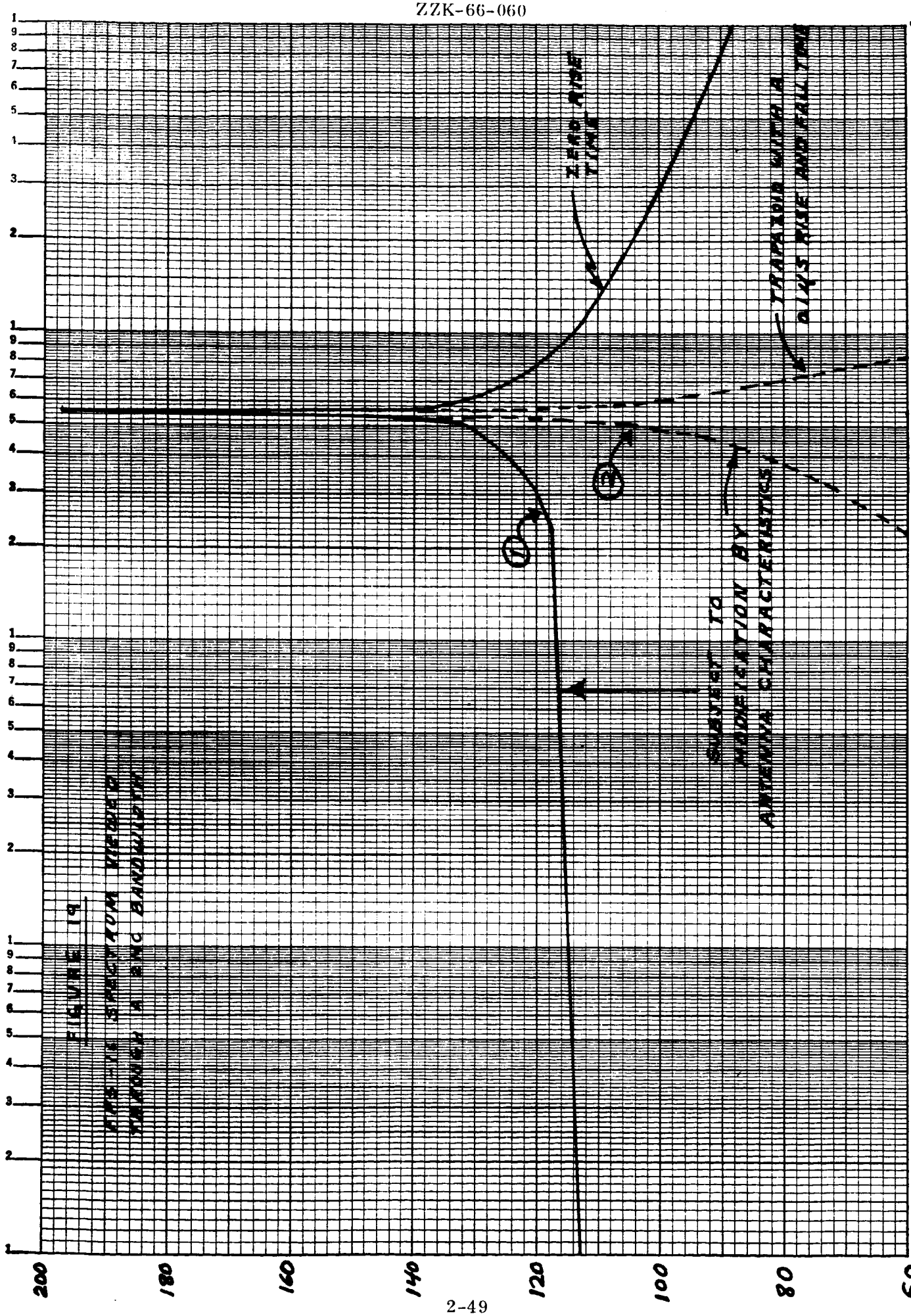
ZERO RISE TIME
THYRATRON WITH A 0.1 μS RISE AND FALL TIME
SWEEP AT 1Q MODULATION BY ANTENNA CHARACTERISTICS
1 KMC SPECTRUM WIDTH
KLYSTRON X-BAND AMPLIFIER
1 KMC
10 MC
100 MC
1 GC
10 GC
200
180
160
140
120
100
80
60

FIGURE 19

3. MODULATION SIMULATION

The main purpose of the previous presentation has been to provide enough background material in modulation characteristics so that simulation in any given test situation can be greatly simplified. This is especially true of telemetry signals which are inherently complex in nature. The chief similarity between telemetry and pulsed signals is their broadband nature. It can be shown that a pulsed RF signal can produce a frequency coverage very similar to that of an FM or FM-FM signal. To do this the example of Figure 10 will be used and some steps outlined so that such a simulation will have adequate technical background.

The spectrum of Figure 10 has been reproduced in Figure 20. The steps required to obtain a pulsed RF spectrum which has the same band coverage and amplitude characteristics are as follows:

1. Construct a pulsed spectrum (using the data of Figure 11 and 15) such that the pulse width and amplitude at least encompass the telemetry spectrum of interest. (In this case, a 9.1 μsec pulse width was chosen and the roll off of the spectrum is then dictated by $f = 1/\pi d$, where $d = 9.1\,\mu$sec.

2. According to the simulation level given, or obtained by calculation, find the power needed into the test antenna necessary to produce the power density required by calculation of on or off-board radiators.

3. The power from (2) will be the zero db level in Figure 20. Subtract from this amount the number of db to obtain the simulation level of the pulse spectrum in Figure 20.

4. Calculate the voltage spectrum using the level in (3) as follows:

$$E_0 = \sqrt{p_0 R}$$

where p_0 = power of unmodulated carrier from (2)
R = 50 ohms

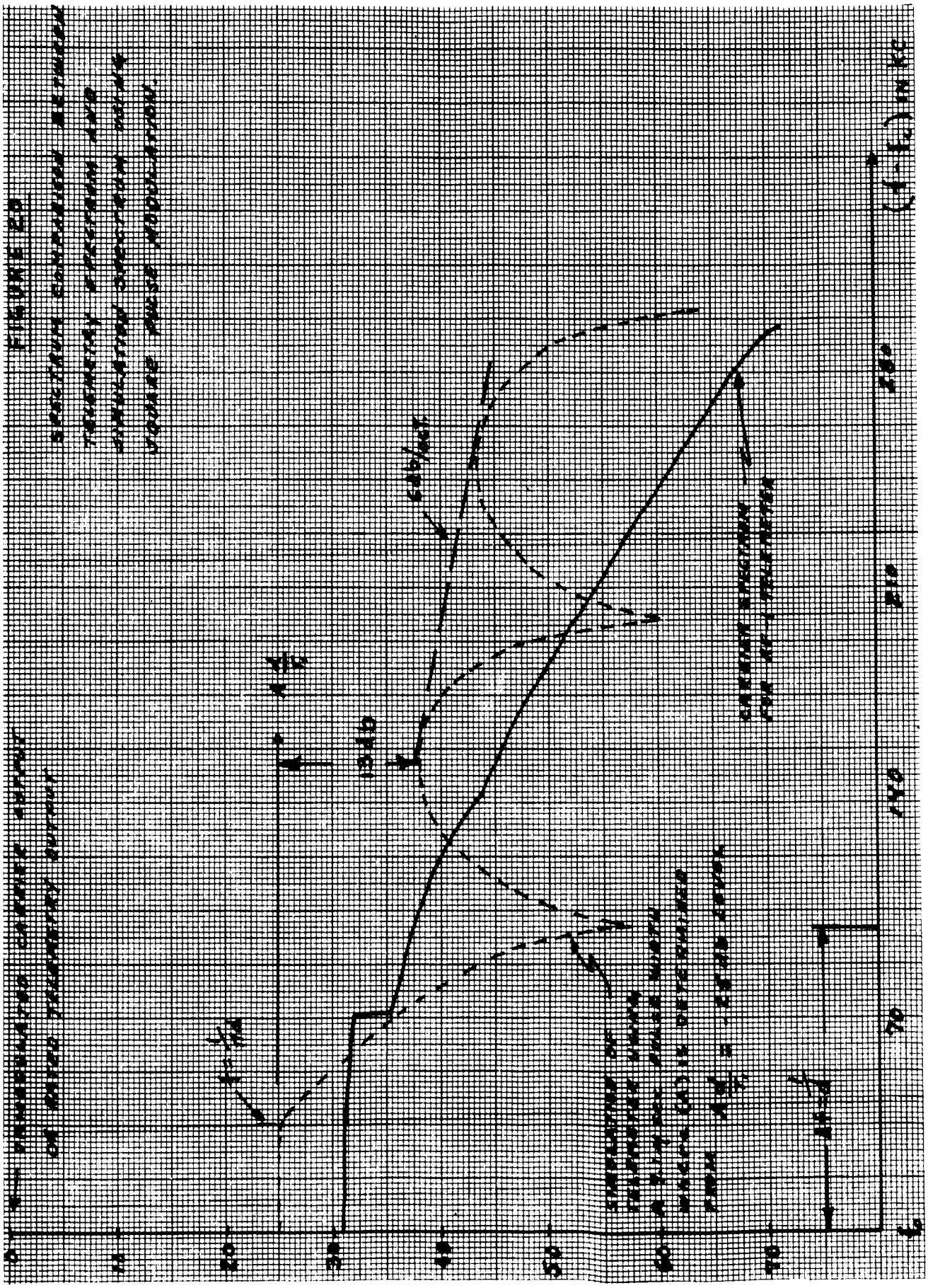

$E_s = E_0$ - (db down from p_0) where $E_s = \frac{\text{volts}}{\text{Kc BW}}$

$\frac{Ad}{T_1} = E_s$ where $d = 9.1 \times 10^{-6}$ sec

$A = \frac{E_s T_1}{d}$ where $T_1 = 1\ K_c$

A = RF pulse amplitude for simulation

The following are examples using the above procedure. The information given on JPL inter-office memo 2946-24 shows a simulation level for an Atlas telemeter of 37.2 mw. This would be the zero db level given in Figure 20, since the 37.2 mw was derived from a 5 watt power out of the telemetry transmitter. Therefore, 25 db has to be subtracted from the figure of 37.2 mw to obtain the simulating level shown in Figure 20.

$\frac{E_0^2}{R} = 37.2 \times 10^{-3}$ W

$E_0^2 = 1.86$

$E_0 = 1.365$

E_0 - 25 db = 0.076 V

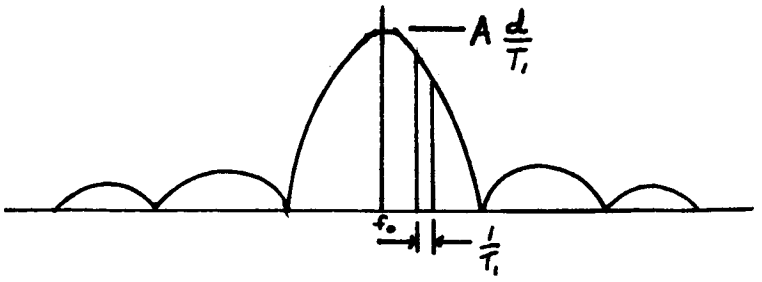

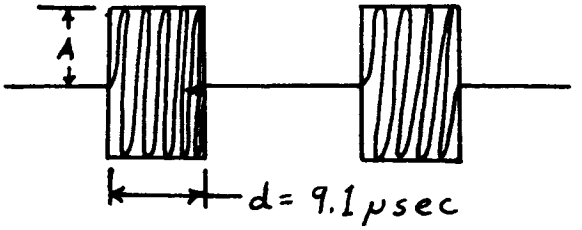

The level shown at -25 db in Figure 20 is referenced to a 1 Kc bandwidth. Therefore, the level of A in the pulse modulated signal would be A d/T_1 = 0.076 V.

The base frequency component at f_0 is assumed to have a value of .076 V for a repetition frequency of $f = 1/T_1$ = 1 Kc, therefore:

$$A = \frac{0.076\ T_1}{d} = \frac{0.076 \times 10^{-3}}{9.1 \times 10^{-6}} = 8.35\ V$$

The simulation could then be accomplished with a 9.1 μsec pulse modulated RF signal 8.35 volts in amplitude.

Another example given in the JPL document mentioned above is the Agena telemetry. The minus db level for the simulation is given at 2.2 watts. Referencing again Figure 20, the -25 db point can be obtained as follows:

$$\frac{E_0^2}{R} = 2.2\ W$$

$$E_0^2 = 110\ V^2$$

$$E_0 = 10.9\ V$$

$$E_0 - 25\ db = .615\ volts$$

The -25 db level is given in Figure 20 in a 1 Kc bandwidth, therefore the level of A can be calculated as follows:

$$A\frac{d}{T_1} = 0.615$$

$$A = \frac{0.615 \times 10^{-3}}{9.1 \times 10^{-6}} = 68\ volts$$

The pulse width of 9.1 μsec was chosen for the best fit of the FM spectrum shown in Figure 23.

The base repetition rate was chosen at 1 Kc, but this does not limit the decrease of the repetition rate down to a 60 cps or 400 cps repetition rate with the same pulse parameters. For instance, if the repetition rate were lowered to 500 cps there would be twice the number of frequency components as there were at a 1 Kc repetition rate, but these amplitudes would be one-half of the 1 Kc case yielding the same total amplitude as seen in a 1 Kc bandwidth. By using similar techniques discrete spectra such as those

of the Azusa ground transmitter can also be simulated. The pulse repetition frequency would be adjusted so that the spacing of components in the simulating signal would coincide with that of the simulated signal.

4. SUSCEPTIBLE CIRCUIT EVALUATION

4.1 Analysis of Reported Susceptibility. At the outset of this study a unit described as a high level switch was reported to have experienced a susceptibility to modulation effects. Based on this report a study was made of the device and the schematic to determine the possible causes of such a susceptibility.

There is at least one necessary combination of electrical networks (as shown in Figure 21) such that there will be a response at the output to AM, FM or pulsed CW applied at the input; but there will be no response at the output with a pulsed DC or CW signal applied at the input. Typical examples of arrangements of circuit elements that represent each of the three networks are also shown in Figure 21. Some of these potentially susceptible combinations are apparent in the schematic for the test circuit, Figure 22. The dotted lines outline the possible routes a modulated RF carrier could follow to cause a residual DC offset across pins 10-13. One possible route is through the ground lead pickup (this depends on where pin 9 finds its ground). This possibility could easily be eliminated by proper installation practices. The power line (+6 V) might also be a pick up location since from both of these locations there are routes which enter a transformer circuit which might be tuned at some f_0. The output of the transformer passes through a diode and the output of the diode has a capacitor tied to ground. This fulfills the three basic elements in the proper sequence needed to allow coupling to the output circuitry (bandpass filter, non-linear device, low-pass filter). Two other possible coupling points are indicated at the output (pins 10-13) of the test unit. These points could be considered to couple CW, pulsed CW, FM, or whatever happens to excite the output leads to the output transmitters. In this case, the transistors could act as rectifiers of the coupled energy causing the DC offset at the output.

4.2 Evaluation and Analysis of Actual Test Circuit. The foregoing section covered modulation effects and an analysis of the test circuit based on previous tests run at JPL which indicated that the test unit showed a susceptibility to changes in frequency or amplitude (interpreted as FM or AM modulation of an RF carrier) of an

FIGURE 21

COMBINATION OF ELEMENTS REQUIRED FOR SUSCEPTIBILITY TO MODULATED SIGNALS

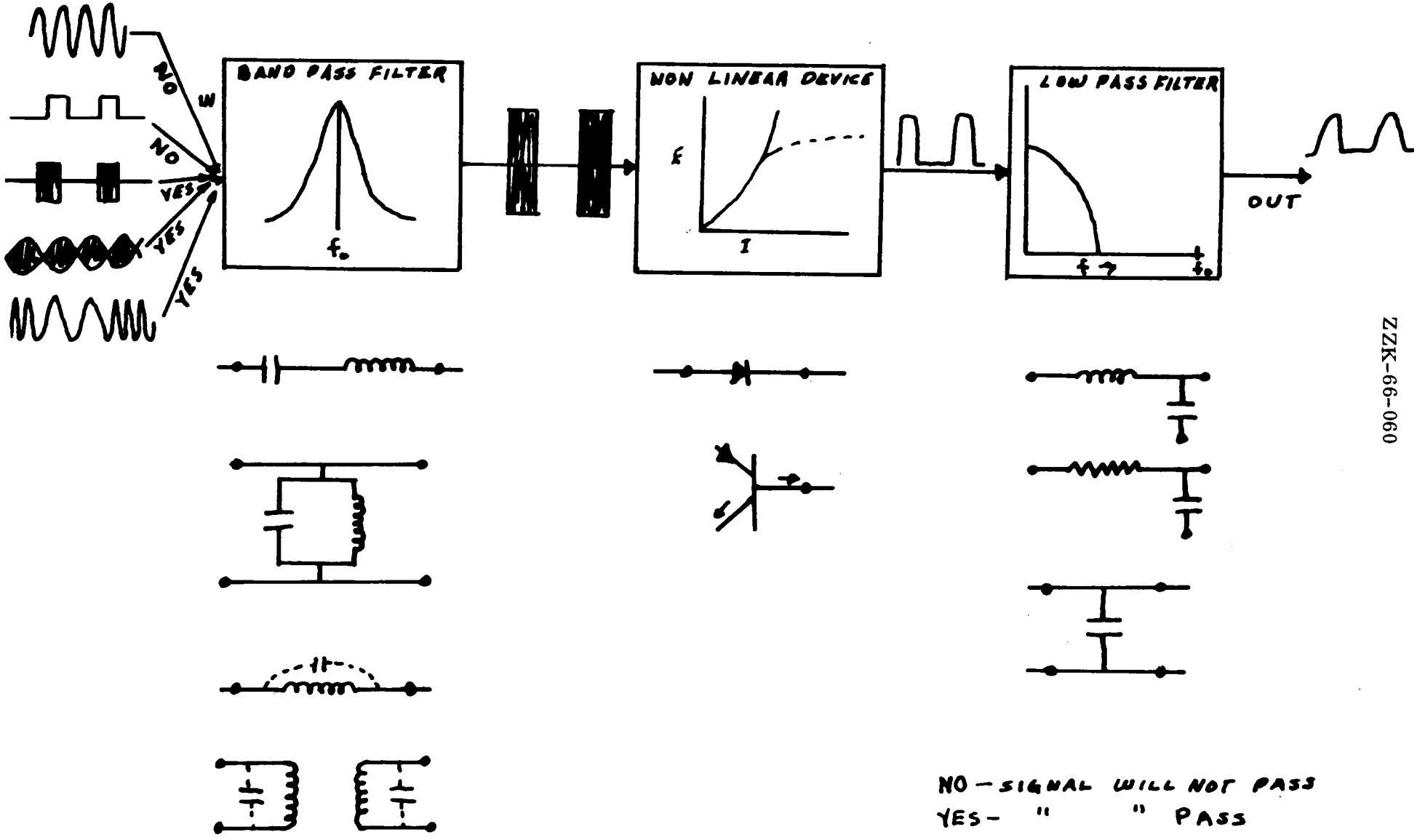

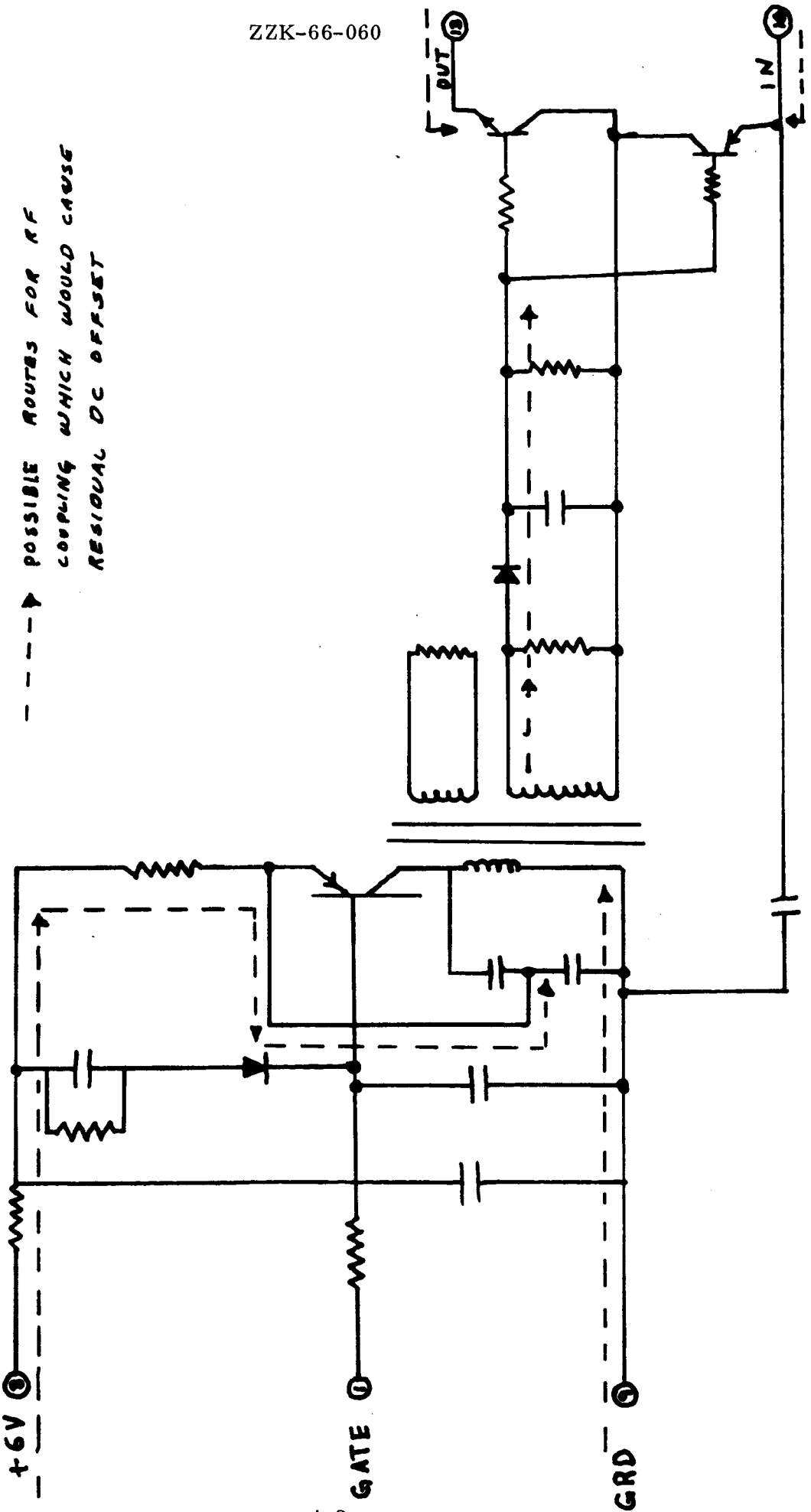

FIGURE 22

SCHEMATIC OF TEST CIRCUIT

injected test function. During this period of study a test was run on a similar unit to check this previous data.

The test set up used is shown in Figure 23. Since radiation simulation was the object, no direct coupling to the test circuit was used. The test frequencies used were confined to approximately the telemetry frequency band 210 to 280 Mc since this is where previous susceptibilities were noticed. The power level used was 10 watts into a tuned dipole. The procedure was to turn up the power on the transmitter while watching the DC shift level at the output of the test circuit (pins 10 and 13 on Figure 22).

The result of this test was that the test circuit responded strictly to average power at CW or pulsed CW in certain fixed bands, depending on the test configuration. FM modulation over a frequency range comparable to the telemetry band was accomplished by FM modulation of a T. I. telemetry transmitter, and, since this type of modulation is restricted to a band fairly close to the carrier, power level changes or changes in the test circuit response were not noted.

It was found that the main point of coupling in the test circuit was via the gate lead or ground when the test circuit was operated with the gate grounded. This can be shown by referring to Tables I and II. Table I shows the response of the test circuit with the gate grounded through a 1 ft. test lead, and Table II shows the results with the gate grounded through a 1 inch lead length. It can be seen that in the first case the main susceptibility of the unit was around 230 to 240 Mc. Amplitude changes of the radiated signal, due to vicinity effects in the screen room, proved to be extensive but this range of susceptibility was found to be greatest. When the gate-ground lead was changed to 1 inch, the susceptibility changed to 210 Mc. No susceptibilities in this mode of operation of the test circuit were noted outside of the frequency range shown in Tables I and II.

When both the gate lead and the test circuit were shielded, the susceptibilities shown in Tables I and II disappeared indicating that this was a solution to the problem of the DC offsets.

FIGURE 23
TEST SET-UP

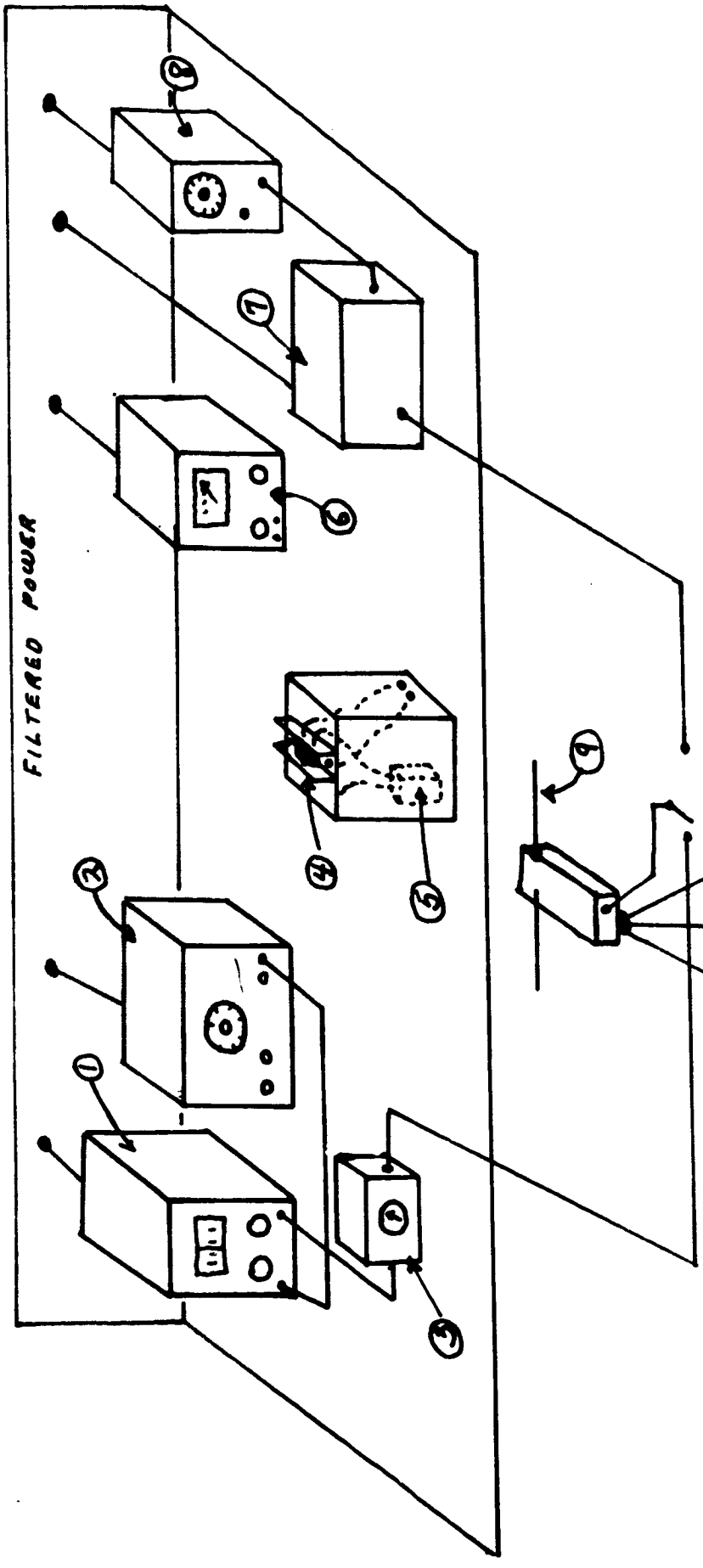

TABLE I

Gate Grounded Through One Foot Lead

Frequency	CW Level	1 Kc Sq. Pulse	DC Shift
210 Mc	10 w	10 w	400 mv
			400 mv
220 Mc	10 w	10 w	3 mv
			3 mv
230 Mc	10 w	10 w	* 1 mv
			* 1 mv
240 Mc	10 w	10 w	* 3 mv
			* 3 mv

*erratic

TABLE II

210 Mc	10 w	10 w	3 mv
			3 mv
220 Mc	10 w	10 w	800 μv
			800 μv
230 Mc	10 w	10 w	200 μv
			200 μv
240 Mc	10 w	10 w	---

At this point it would be informative to specify the power density that the test unit was exposed to during the tests outlined above. This is done by using Figure 24. The test sample was in the near field of the dipole used in the test set up. The point P in Figure 24 specifies the point in the near field at which the transmitting antenna was located. The formula for obtaining the electric field intensity at this point is (from ordinate of curves in Figure 24)

$$\frac{E\lambda^2}{I_0 f(\lambda_n)^2} = 1.3 \times 10^{-5}$$

where

E = electric field intensity at point P

I_0 = peak feed point current of a half wave dipole

FIGURE 24

THEORETICAL VARIATION OF NORMALIZED ELECTRIC FIELD INTENSITY AT $\theta = 90°$ OF WAVE EMANATING FROM DIPOLE ANTENNA OF HALF-HEIGHT H AS A FUNCTION OF DISTANCE TIMES FREQUENCY

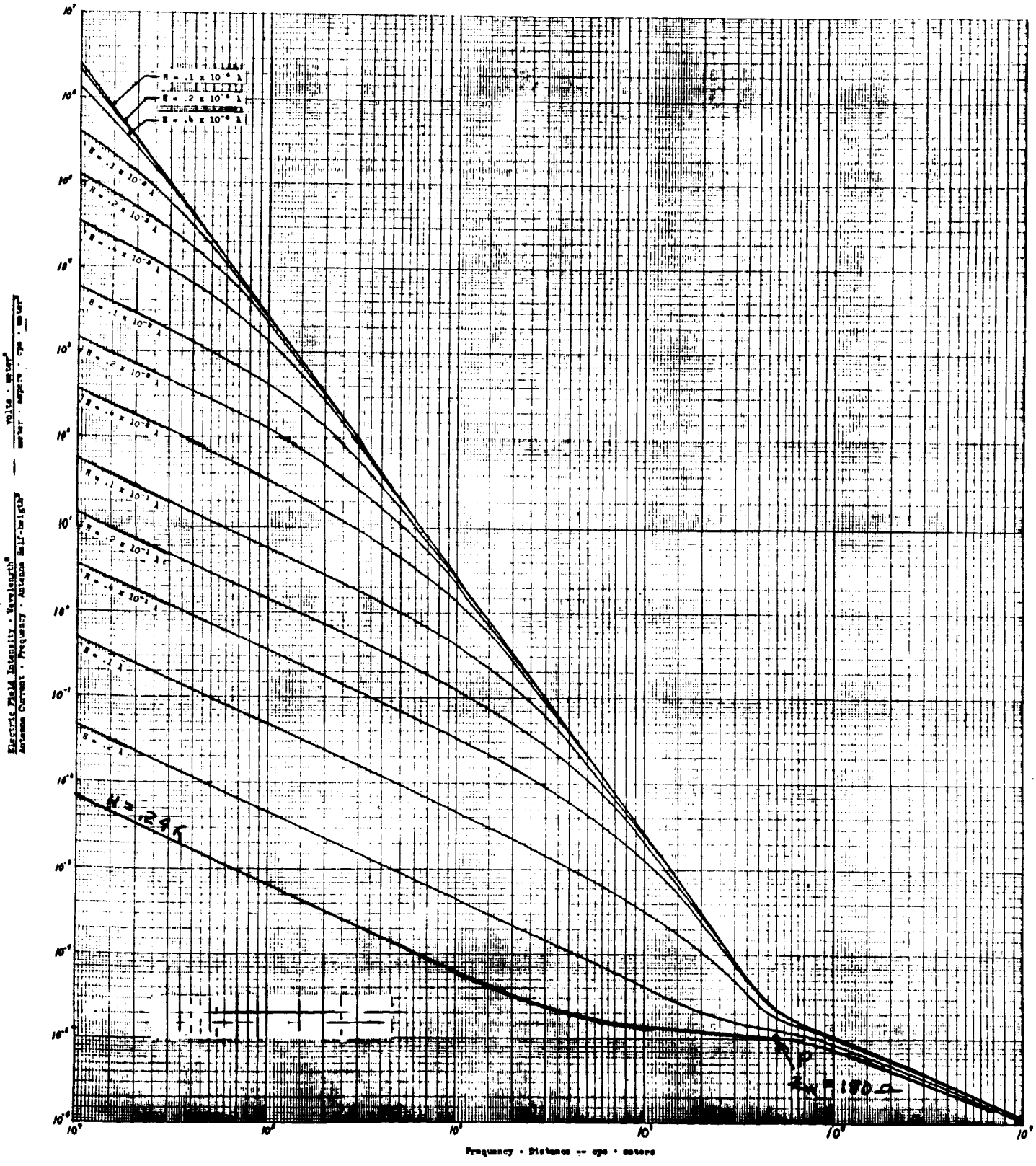

f = frequency

λ_h = antenna half height in wavelengths = $\lambda/4$

V_d = (at dipole feed point) = $\sqrt{R P_0}$

where

R = dipole resistance

P_0 = power into dipole = 10 watts

$$V_d = \sqrt{72.10} \cong 27 \text{ volts}$$

$$I_0 = \frac{27}{72} = 0.376 \text{ amps}$$

$$\frac{E\lambda^2}{\frac{27}{72}\ 250 \times 10^6\ \frac{\lambda^2}{16}} = 1.3 \times 10^{-5}$$

$$E = 76 \text{ V/m}$$

$$\text{Power density} = Pd = \frac{E^2}{Z_W} = \frac{(76)^2}{180} = 32 \text{ W/m}^2$$

where

Z_W = wave impedance at point P in the near field of the dipole.

This power density may seem high but its magnitude is an indication of the poor coupling factors involved between the radiated field and the test sample. Since it was found that the test unit was not particularly susceptible to modulation effects it could not be used to confirm that FM or FM-FM modulation could be adequately simulated by pulsed CW for the purposes of RF radiated susceptibility tests.

5. EQUIPMENT LIST FOR SIMULATION

It is proposed that the simulation of FM spectra be handled with an RF pulse generator for several reasons. The most important of these is that pulse generators are available at power outputs up to 50 watts over a frequency range from 10 Mc to 1000 Mc while there is a scarcity of FM signal generators with adequate power outputs for even the telemetry band. In the C-band frequency range, RF signal generators and traveling wave tubes are the only present means of obtaining the levels necessary for simulations.

One possible technique for strict FM simulations (or telemetry simulations) could be to use a low level signal source and an expensive traveling wave tube to obtain the bare minimum necessary for simulations. If FM simulation is ever deemed necessary these equipments could be used. Also, the possibility of noise modulation, as pointed out in the FM signal analysis, could be used for accurate telemetry band modulation simulation since the spectra generated using a noise source have been shown to be a good simulation. In many cases amplified, band limited white noise may be used as an adequate simulation. The equipment list shown in Figure 25 is what would be needed to simulate the sources studied in the analysis shown previously. If any other simulations are required between the present telemetry bands and S-band, it should be pointed out that the Microdot line of power oscillators cover a frequency range from 10 Mc to 3000 Mc with power outputs ranging up to 50 watts. From a review of catalog files, it appears that any simulation requirements above 3000 Mc will require the use of signal generators and traveling wave tubes. Appendix VI contains a list of high power signal sources prepared by the Systems Engineering Group at Wright-Patterson AFB for use in MIL-STD-826 Tests.

FIGURE 25

EQUIPMENT DIAGRAM

AZUSA MARK II AND FPS-16 RADAR

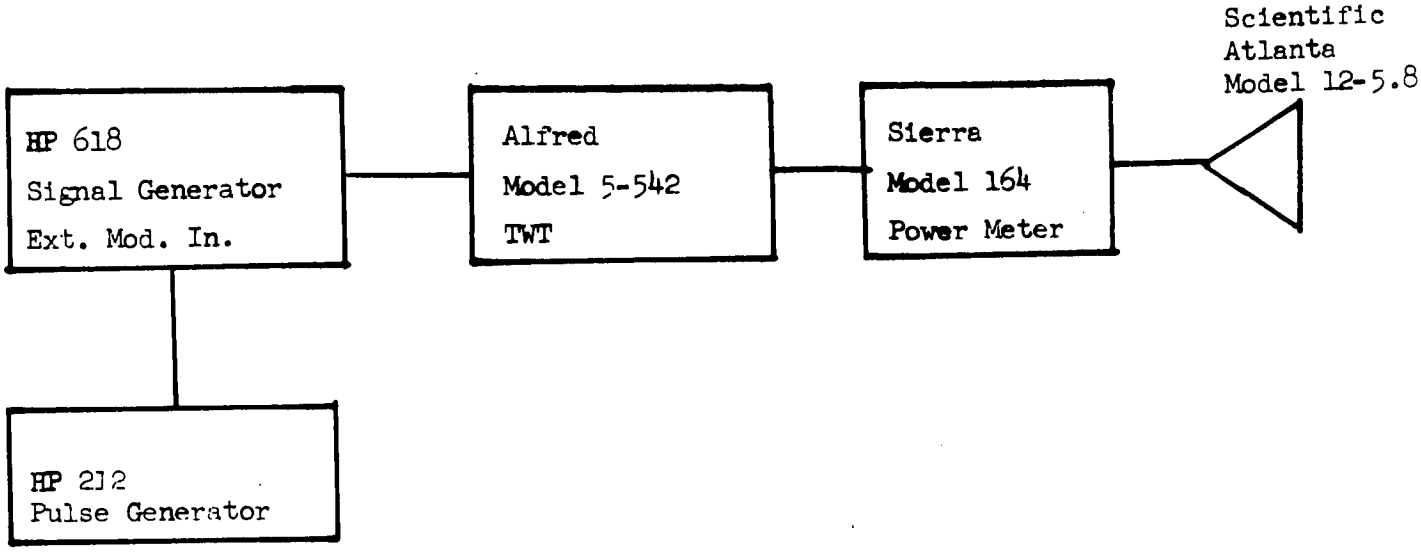

TELEMETRY - ATLAS AND CENTAUR (PULSE SIMULATION)

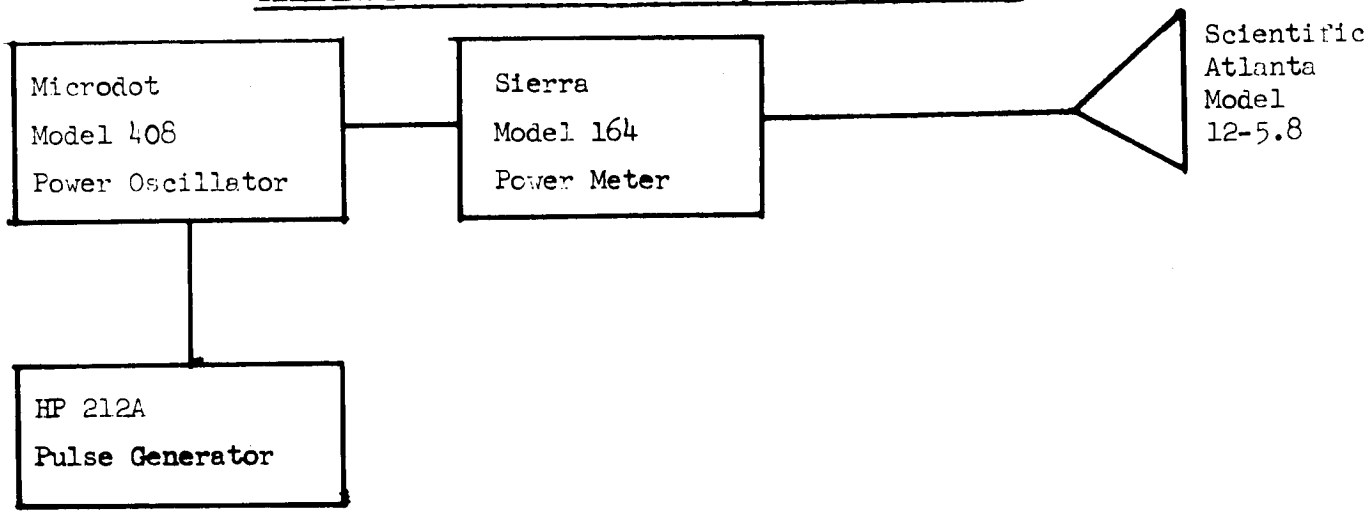

TELEMETRY - ATLAS AND CENTAUR (FM SIMULATION)

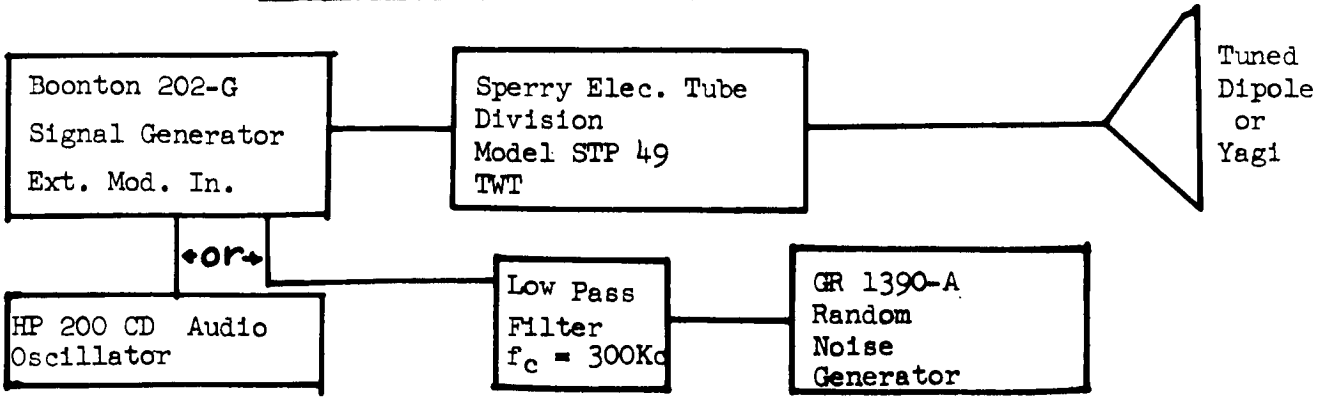

6. CALCULATION OF RF POWER DENSITY LEVELS

6.1 Power Density Levels Caused By Off-Board Radiators. Calculations of power density at the spacecraft due to off-board radiators have previously been made using the range formula:

$$P_R = \frac{P_T G_T}{4\pi R^2} \tag{23}$$

where

R = distance between transmitter and point of interest

P_T = antenna transmitted power

G_T = gain of transmitting antenna

P_R = power density at distance R.

The usage of this formula is only justified under free space conditions, i.e., no reflecting surfaces in the vicinity of transmitting antenna and region intervening with point of interest.

In an actual situation a particular off-board radiator will be located a certain height above the earth and the point at which the power density is to be calculated will also be at a particular height. The intervening region may be called the interference region since it is possible for waves launched by the transmitting antenna to arrive at the point of interest (spacecraft) via two different routes, the direct and the ground-reflected, with consequent interference between the two waves.

Figure 26 illustrates the situation.

In order to determine to what extent the ground-reflected (TGR) wave is canceling or reinforcing the direct wave (TR), three things must be taken into consideration: the free-space attenuation of the direct and reflected waves, the electrical path length difference (θ) between the two and the reflection coefficient (magnitude and phase angle) at the surface of earth. (In the following discussion specular reflection and flat earth

FIGURE 26

GEOMETRY OF OFF-BOARD RADIATOR AND SPACECRAFT

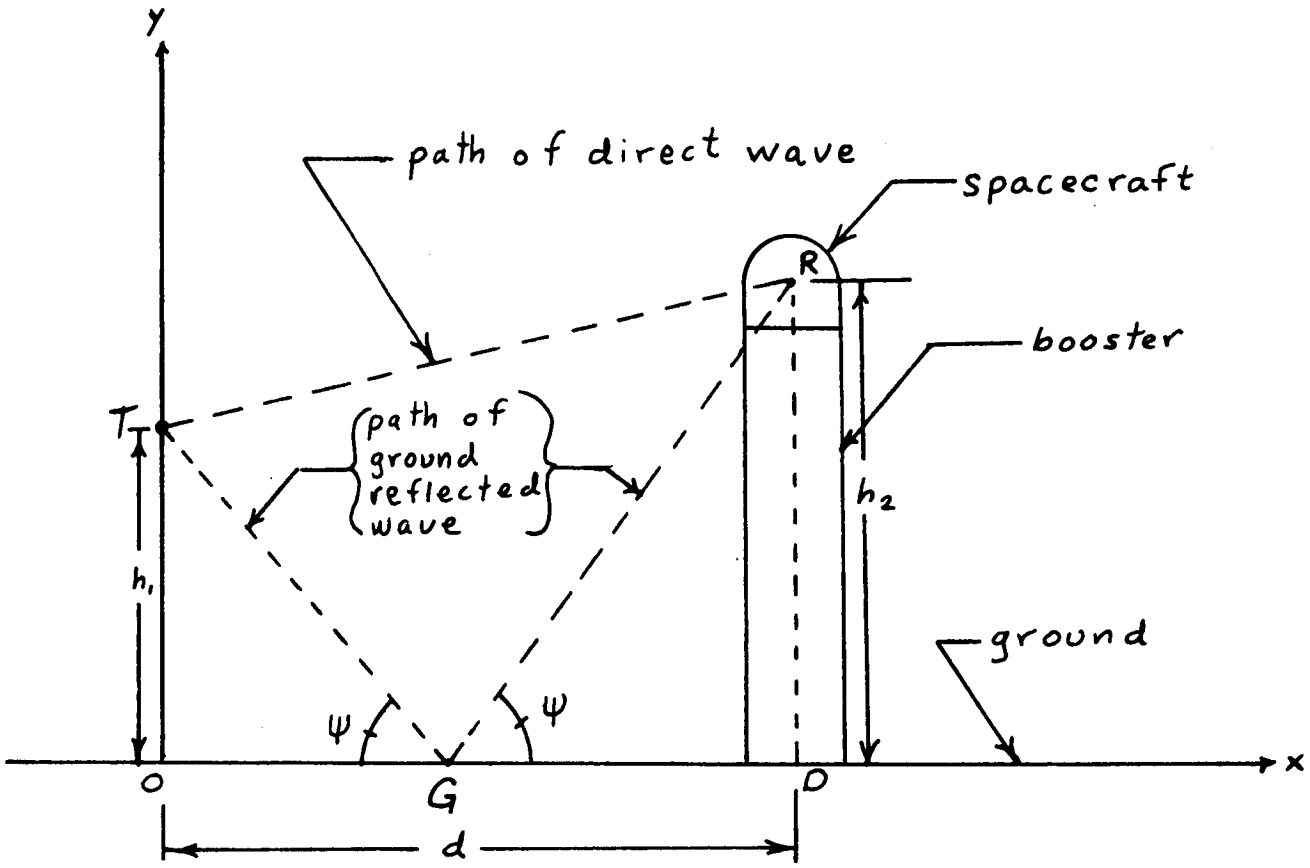

d = distance from transmitter to reception location

O = origin

T = location of transmitter

R = point at which power density calculation is made

G = point of reflection

ψ = grazing angle

h_1 = height of transmitter above ground

h_2 = height of point of calculation

$\angle TGO = \angle RGD$

are assumed. Also G_T for both the direct and ground-reflected waves is assumed to be the same.)

Referring to Figure 26

(24) $$r_1 = TR = \sqrt{(h_2 - h_1)^2 + d^2}$$

$$r_2 = TGR = \sqrt{(h_1 + h_2)^2 + d^2}$$

According to the range formula for free space,

$$P_R = \frac{|\vec{E}|^2}{377} = \frac{P_T G_T}{4\pi R^2}$$

$$|\vec{E}| = \frac{1}{R}\sqrt{\frac{377}{4\pi} P_T G_T} = \frac{5.45}{R}\sqrt{P_T G_T}$$

Let

E_{Rd} = field intensity due to direct wave

E_{Rgr} = field intensity due to ground-reflected wave

θ = electrical path length difference between r_1 and r_2

$\gamma = |\gamma| \angle \phi$ = reflection coefficient at surface of earth

(25) $$E_R = E_{Rd} + E_{Rgr} = |E_R| \angle \alpha$$

$$E_{Rd} = \frac{5.45}{r_1}\sqrt{P_T G_T}$$

$$E_{Rgr} = \frac{5.45}{r_2} |\gamma| \sqrt{P_T G_T} \angle \theta - \phi$$

where

(26) $$\theta = \frac{2\pi}{\lambda} [r_2 - r_1] \text{ radians}$$

The following is a vector diagram interrelating E_R, E_{Rd} and E_{Rgr}.

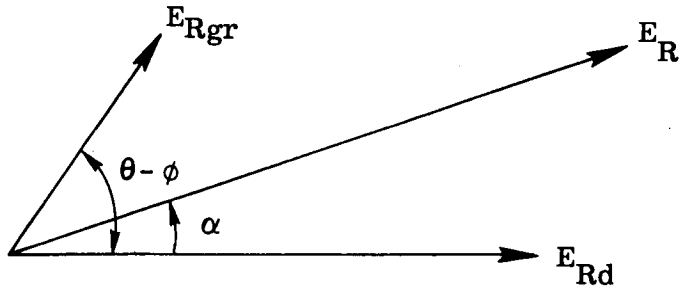

Solving for E_R in terms of E_{Rd} and E_{Rgr}, the following steps are taken.

$$E_R = \sqrt{|E_{Rd}|^2 + |E_{Rgr}|^2 + 2|E_{Rgr}||E_{Rd}| \cos(\theta - \phi)}$$

$$|E_R| = \sqrt{(5.45)^2 P_T G_T \left[\frac{1}{r_1^2} + \frac{|\gamma|^2}{r_2^2} + \frac{2|\gamma|}{r_1 r_2} \cos(\theta - \phi)\right]}$$

$$= \frac{5.45\sqrt{P_T G_T}}{r_1 r_2} \left[r_2^2 + |\gamma|^2 r_1^2 + 2|\gamma| r_1 r_2 \cos(\theta - \phi)\right]^{1/2}$$

$$(27) \qquad P_R = \frac{|E_R|^2}{377} = \frac{P_T G_T}{4\pi r_1^2 r_2^2} \left[|\gamma|^2 r_1^2 + r_2^2 + 2|\gamma| r_1 r_2 \cos(\theta - \phi)\right]$$

An examination of Equation 27 will be undertaken for a few special cases to elucidate its implications. First, however, a few comments about the reflection coefficient γ are in order. When a wave strikes a reflecting surface, the magnitude and angle of the reflection coefficient are dependent upon the grazing angle and polarization of the incident radiation. A phase lag of 180° is introduced by the reflecting surface for a horizontally polarized wave. A vertically polarized wave has a lagging phase angle that varies from 180° at 0° grazing angle to 0° at 90° grazing angle.

The assumption of specular reflection means that the incident ray is reflected in one direction, and the angle of reflection equals the angle of incidence. There is no scattering or diffraction. In order for this assumption to hold, the reflecting surface must be large compared to a wavelength and be relatively smooth compared to a wavelength.

Let us examine Equation 27 for the following cases:

Case 1: $\cos(\theta - \phi) = 0; |\gamma| = 1$

$$P_R = \frac{P_T G_T}{4\pi r_1^2 r_2^2}\left(r_1^2 + r_2^2\right)$$

Case 2: $\cos(\theta - \phi) = 1; |\gamma| = 1$

$$P_R = \frac{P_T G_T}{4\pi}\left(\frac{r_1 + r_2}{r_1 r_2}\right)^2$$

Case 3: $\cos(\theta - \phi) = -1; |\gamma| = 1$

$$P_R = \frac{P_T G_T}{4\pi}\left(\frac{r_1 - r_2}{r_1 r_2}\right)^2$$

Case 4: $r_2 \approx r_1; r_2 - r_1 \approx 0$; horizontal polarization

$\phi = -180°, \theta \approx 0$

$\therefore \cos(\theta - \phi) = -1$ and $P_R \approx 0$

Case 5: $r_2 \approx r_1; r_2 - r_1 \approx 0$; vertical polarization $\rightarrow \phi \approx -180°; \theta = 0; P_R \approx 0$

Case 6: $r_2 \approx r_1 \gg \lambda; r_2 - r_1 \stackrel{\circ}{=} \lambda$ ($\stackrel{\circ}{=}$ means "of the order of"); $|\gamma| = 1$

$$P_R = \frac{P_T G_T}{2\pi r^2}\left[1 + \cos(\theta - \phi)\right]$$

Case 7: P_R a maximum

$\cos(\theta - \phi) = 1; \theta - \phi = 2n\pi$ $\qquad n = 0, 1, 2, \ldots$

$r_2 \approx r_1 \gg \lambda$

$|\gamma| = 1$

It can be seen that if

$\theta - \phi = 2\pi$ and $\phi = -90°$	$\theta - \phi = 2\pi$ and $\phi = -180°$	$\theta - \phi = 0$ and $\phi = 0$
$\theta = 90°$	$\theta = 180°$	$\theta = 0$
$r_2 - r_1 = \frac{3\lambda}{4}$	$r_2 - r_1 = \frac{\lambda}{4}$	$r_2 = r_1$

The maximum value of $(r_2 - r_1)$ is

$$r_2 - r_1 = \lambda$$

If $r_1 \approx r_2 >> \lambda$ and also $r_2 - r_1 = \lambda$, then P_R is a maximum:

$$(28) \qquad P_R = \frac{P_T G_T}{\pi r^2}$$

Equation 28 represents the maximum or worst case power density at a point due to the effects of the ground reflected and direct waves. This formula is 6 db greater than the corresponding free space range formula.

In an actual situation the reflection coefficient at the surface of the earth, the heights of transmitter and receiver, the polarization of the transmitter, and the distance from transmitter to receiver would have to be known. Values of the reflection coefficient as a function of grazing angle for horizontal and vertical polarization can be found in the literature.[17]

A practical example will now be worked out. A diagram showing the pertinent information is found on the next page.

$$\lambda = \frac{3 \times 10^8}{4 \times 10^8} = \frac{3}{4} \text{ m}$$

$$RD = 45\text{m} = h_2$$

$$R'D = 40\text{m} = h'_2$$

$$OT = 30\text{m} = h_1$$

$$OD = d = 100\text{m}$$

$$r_1 = \sqrt{(h_2 - h_1)^2 + d^2} = 101\text{m}$$

$$r'_1 = \sqrt{(h'_2 - h_1)^2 + d^2} = 100\text{m}$$

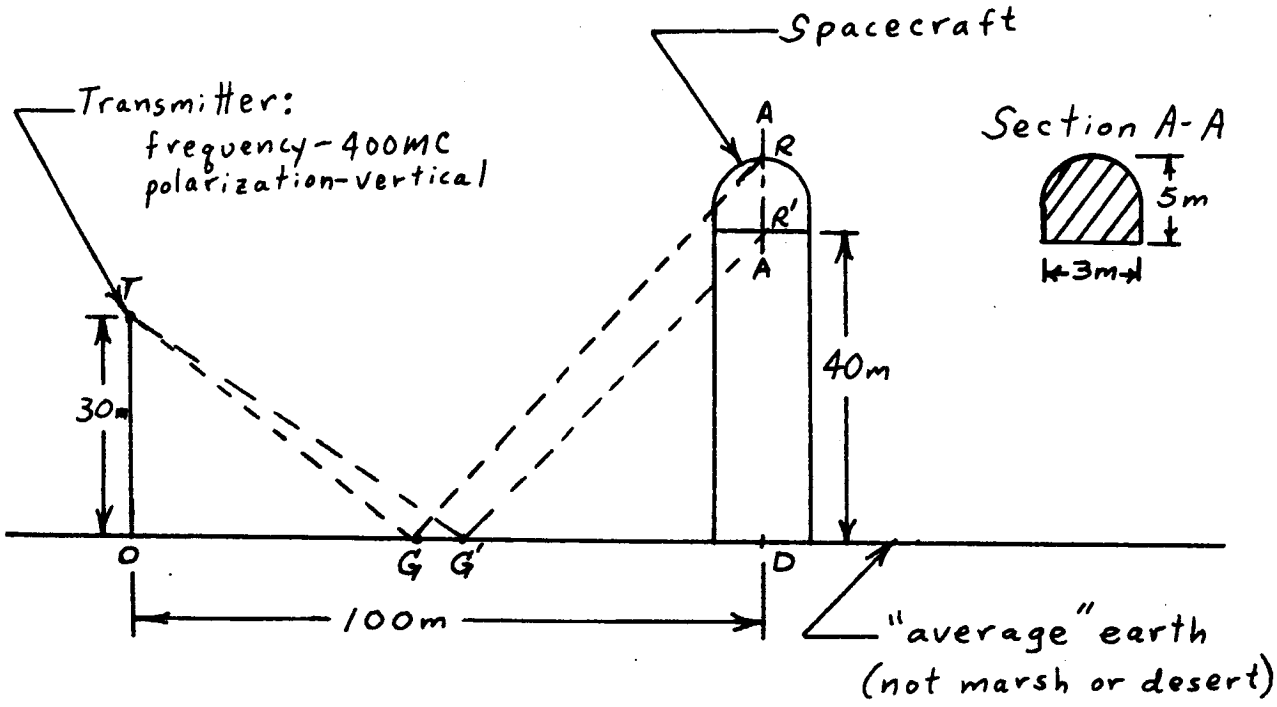

$$r_2 = \sqrt{(h_1 + h_2)^2 + d^2} = 125\text{m}$$

$$r_2' = \sqrt{(h_1 + h_2')^2 + d^2} = 122\text{m}$$

$$\theta = \frac{2\pi}{\lambda}(r_2 - r_1) = 200 = (62\pi + 5.32)\ \text{rad}$$

$$\theta' = \frac{2\pi}{\lambda}(r_2' - r_1') = (58\pi + 1.88)\ \text{rad}$$

$$\tan\psi = \frac{OT}{OG} = \frac{RD}{GD}$$

$$\tan\psi' = \frac{OT}{OG'} = \frac{R'D}{G'D}$$

$$OG = 100\text{m} - GD$$

$$OG' = 100\text{m} - G'D$$

$$\frac{OT}{100 - GD} = \frac{RD}{GD}$$

$$\frac{100 - GD}{GD} = \frac{OT}{RD}$$

$$\frac{100}{GD} - 1 = \frac{OT}{RD}$$

$$\frac{100}{GD} = \frac{OT + RD}{RD}$$

$$GD = \frac{100\ RD}{OT + RD} = 60m$$

$$G'D = \frac{100\ R'D}{OT + R'D} = 57m$$

$$OG = 40m$$

$$OG' = 43m$$

$$\tan\psi = \frac{30}{40};\ \psi = 37°$$

$$\tan\psi' = \frac{30}{43};\ \psi' = 35°$$

From page 96 of Reed and Russell for f = 400 Mc, vertical polarization, and "average" land, the following holds:

ψ	$\lvert\gamma\rvert$	ϕ
37°	0.41	0
35°	0.40	0

Everything that is needed for a calculation of power density at the spacecraft has now been found. It can be seen from the expressions for θ and θ' and the fact that $\phi = 0$ that the power density will be a maximum on the axis A-A′ at two points, namely, the points corresponding to $\theta = 60\pi$ and $\theta = 62\pi$. For these values $\cos(\theta - \phi) = 1$ and assuming

$$r_1 = 100m,\ r_2 = 125m \text{ and } \gamma = .4,$$

$$P_R = \frac{P_T G_T}{4\pi}\left[\frac{(.16)(10,000) + 15,800 + (.8)(12,500)}{(12,500)^2}\right]$$

$$= \frac{P_T G_T}{4\pi}\left[\frac{27,400}{(12,500)^2}\right] = \frac{P_T G_T}{4\pi}\left[1.73 \times 10^{-4}\right]$$

The power density as calculated using the range equation would be

$$P_d = \frac{P_T G_T}{4\pi d^2} = \frac{P_T G_T}{4\pi} [10^{-4}]$$

It can be seen that for this particular example the calculated result for power density using the range equation will under estimate the power density, taking into account the effect of ground reflections, by a factor of 1.73 or 2.4 db.

6.2 Power Density Levels Caused By On-Board Radiators. Before considering the RF power densities in the vicinity of the spacecraft contributed by on-board launch vehicle sources, it is important to distinguish exactly what is meant by "spacecraft", "on-board radiator", etc. "Spacecraft" or "payload" refers to the uppermost stage of the missile system. The "on-board radiators" refer to sources in the booster or sustainer stages only and not to any source on the "spacecraft". Sources on the spacecraft need not be simulated since they are part of the unit that will be undergoing testing and will be available in any test involving the whole unit. These sources are not a part of the environmental compatibility problem but of the self-compatibility problem. The germane consideration concerning on-board radiators is whether or not the spacecraft will be in the near field of the radiator. The problem becomes how to determine the boundary between the near or induction field and the far or radiation field. The electric field components which comprise the near field fall off with either the square or cube of distance, whereas those that comprise the far field fall off with the first power of distance. At some distance from the source the near field components will be negligible compared to the far field components. Let us take as our point of demarcation between near and far fields the point at which the far-field, range equation is in error by 10 percent, i.e.,

$$P_R = \frac{P_T G_T}{4\pi R^2} \qquad \text{in error by 10 percent}$$

Using curves obtained in GDC Report No. ZZK-65-062, Development of Probes and Measurement Techniques for Automated Interference Measurements in Shielded

Chambers - 3 to 300 Megacycles, for electric field intensity and wave impedance in the near field and boundary region, the point is picked such that

$$\Delta P_R = 0.1$$

is the difference in power density between that calculated using the range equation and that actually present according to the above report. From the curves it is found that

$$\Delta P_R \approx 0.1 \text{ when } f \cdot D = 10^8 \text{ or } D = \lambda/3$$

f = frequency (cps)

D = distance from source (meters)

Since for the purposes of this study f > 200 Mc, $D < \frac{10^8}{2 \times 10^8} = 1/2$ meter $\approx$ 20 inches.

It is improbable that a package on the spacecraft will be located closer than 20 inches to a 200 Mc on-board radiator. In the event a package was located closer than $\lambda/3$ to a radiator, the only adequate simulation would be to locate the test antenna so that the package would be in the near field in the simulating test setup. The configuration of most missile systems does not lend itself to reinforcing reflections in the vicinity of the spacecraft. On the contrary the ground planes of on-board antennas would, in most cases, be located such as to reflect waves away from the spacecraft. Even if the on-board radiator was located as close to the spacecraft as possible, there would still be the separation provided by the fairing between the spacecraft and launch vehicle which would be at least 20 inches. Therefore, a worst case formula for calculation of power density caused by on-board radiators would be

$$P_d = \frac{P_T G_T(\theta, \phi)}{4\pi d^2}$$

where

P_T = on-board antenna transmitted power

$G_T(\theta, \phi)$ = on-board antenna gain in direction of spacecraft

d = distance between source and spacecraft.

It is important to use the gain in the direction of the point of interest, $G_T(\theta, \phi)$, since the main beam of an on-board radiator will generally be pointed away from the spacecraft. If the gain in the direction of the beam were used, a large degree of overtest might result.

If the on-board launch vehicle radiator is flush with the skin of the launch vehicle, and the diameter of the spacecraft is less than or equal to the diameter of the launch vehicle, then the power density in the vicinity or the spacecraft contributed by the on-board radiator can be neglected providing there are no nearby off-board reflecting surfaces. Reference to the following diagram will make this point clear.

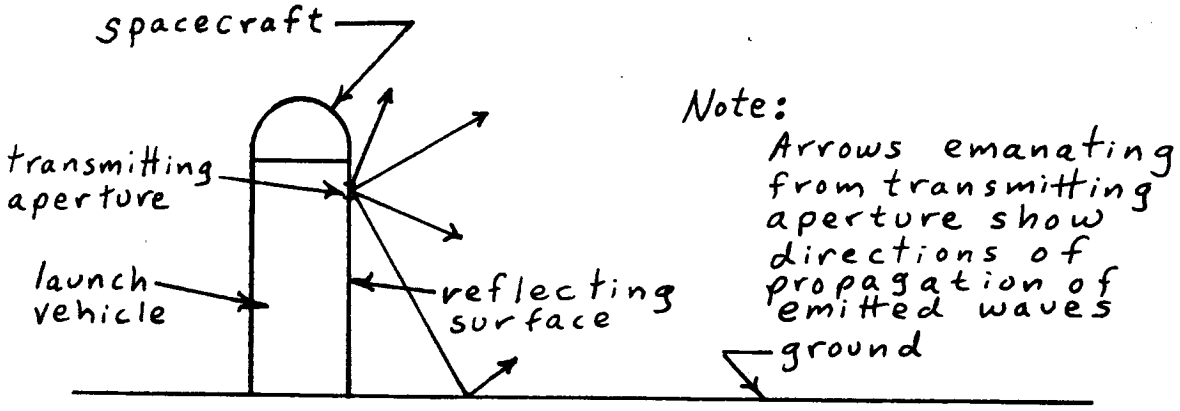

As can be seen from the above diagram, none of the waves from the on-board radiator will impinge on the spacecraft. Insofar as we are dealing with an electromagnetic phenomenon that has wave structure and directional properties, it can fairly be said, then, that the on-board radiators will not be able to couple energy into the spacecraft. If the spacecraft has antennas which extend outward, energy transfer is possible and the power densities at the antennas should be calculated using the above formula.

Considering briefly the near-field situation, little is known concerning the directional and polarization characteristics of near-field radiation. In general, the ratio of $\vec{E}$ to $\vec{H}$ is not constant; H field usually plays a larger role than E field and far-field shielding is useless. The near field coupling is inductive or capacitive and similar to the coupling that exists between wires and circuit elements that are located close together. Reference is made to literature concerning wire to wire coupling.[37, 38]

Future work should be carried out with regard to measuring antenna to wire coupling characteristics in the near field with consideration given to direction, polarization, shielding and type of antenna.

7. NEW TECHNIQUES FOR MEASURING FIELDS ABOUT AND WITHIN A SPACECRAFT IN A FORMAL TEST

7.1 Explanation. During the study period a device was developed for the purpose of measuring power densities about and within a spacecraft in a formal test. This device will be termed a power density detector and the description is accurate when measuring radiation which is far-field or radiative in a relatively open region.

Consideration will first be given to the characteristics of a device required for power density measurements. The device must possess the following attributes.

1. It must be small so that it will not perturb the EM fields in the region in which the measurement is to be made.
2. It must be sensitive to EM fields in one small region and that region only in order to obtain an accurate calibrated reading of power density in the region of concern.
3. It should be sensitive to fields polarized in any direction and which are propagated from any direction.

How these problems were solved in the development of the power density detector will be explained subsequently. Requirement (1) can be further subdivided into two parts:

a. The device should be small compared to a wavelength.
b. It must not be used to make measurements in a confined area of dimensions comparable to the dimensions of the device.

Requirement (2) must be provided for with adequate shielding so that measurements do not depend on the arrangement of the test equipment, and leakage of radiation into the system at undesired points is kept to a minimum. Only if this requirement is met can the device be accurately calibrated. Requirement (3) is necessary in order that the device respond to the total electromagnetic environment in the region of measurement.

The basic element in the power density detector is a radio frequency energy converter manufactured by Rafec Electronics, Model Number 307. This device is frequency sensitive and will respond to frequencies in the range from 0.15 Mc to at least 1 Gc. When its input is subjected to an RF field (either by radiated link or by direct conduction), its output will be a DC voltage. This characteristic of a DC output for an RF input is advantageous since it reduces susceptibility to an RF field for those components of the power density detector in back of the RF energy converter, i.e., cable and DC voltmeter. A determination of the transfer characteristics of the Rayfec RF energy converter as well as other basic work has been reported previously.[20]

The main problem that had to be solved in adapting the Rayfec RF converter to a power density measuring device was that of proper shielding to insure energy pickup at only one point. In order to do this the shield must not be part of the pickup circuit. In a monopole arrangement, the capacitance to ground is responsible for energy pickup. Therefore, the nature of the ground, itself, influences energy pickup and cannot be integrated with the shielding system. If the shielding is left ungrounded or floating, it will not be effective in keeping extraneous energy pickup to a minimum. Therefore, a balanced pickup device was decided upon: specifically, a short dipole element. Since the pickup device is balanced with respect to ground, a device had to be incorporated that would unbalance the RF energy. Consequently, a balun was employed to convert the double-ended input to a single-wire system. The particular balun employed was produced by CGS Laboratories, Inc., Model No. BPC-200/50. The output of the balun was applied to the Rayfec RF energy converter. The output of the Rayfec RF converter consists of two leads. One was grounded and one fed through a 30 foot length of RG-58 shielded coaxial cable to a DC voltmeter. The purpose of the cable is to provide for the remote location of the readout equipment so as to perturb the fields in the region of measurement as little as possible. The power density detector, then, consists of the elements mentioned above which are, concisely,

1. Short dipole element
2. Balun

3. RF energy converter
4. Shielded coaxial cable
5. DC voltmeter

The case of the DC voltmeter was the ground reference of the system. The shield of the cable was grounded at the voltmeter. The RF energy converter was completely enclosed in a 360° shield which provided continuity with the cable shield. The balun also is shielded except in the region where the dipole elements are located. This lack of shielding will not hamper calibrated measurements, however, since, if any energy is entering and being picked up by the system in this unshielded region, it will be relatively the same in any situation. The RF energy converter and the balun were located in two separate enclosures connected by BNC coaxial connectors. If the system were to be produced, the entire unit could be packaged in one small enclosure with dimensions of the order of 2" × 2" × 1". Throughout the entire system RF shielding integrity was maintained in order to eliminate field pickup at any point in the system except at the short dipole elements. The following is a diagram of the system and a table of data concerning the components.

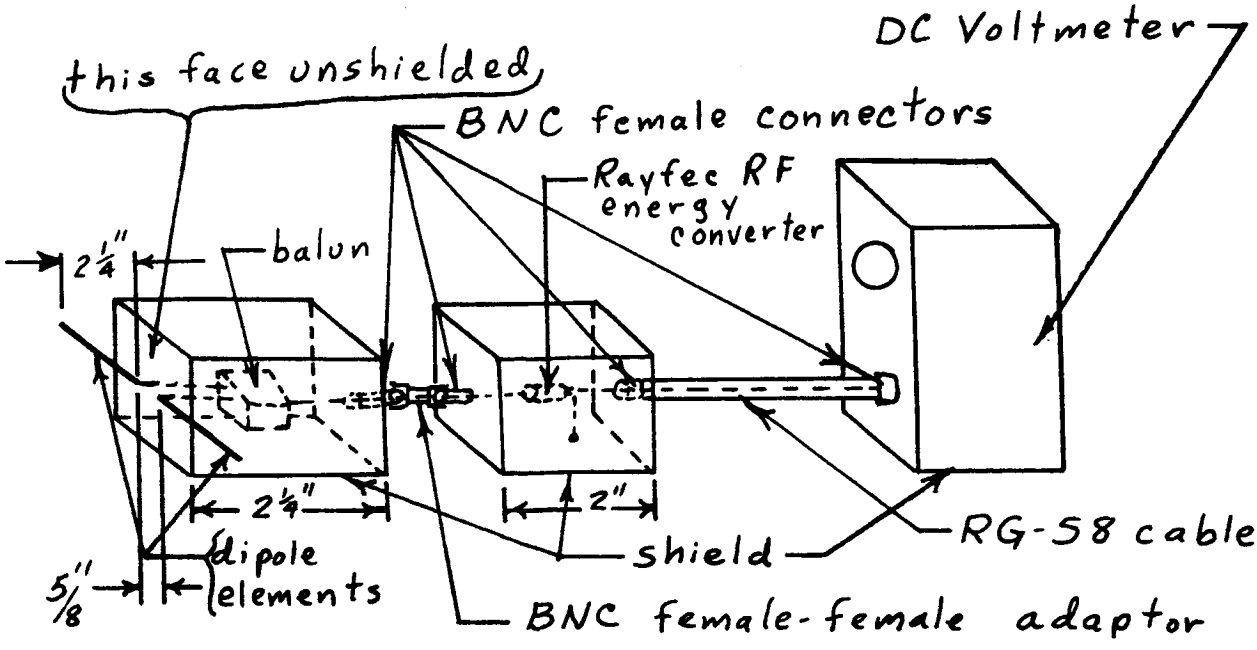

COMPONENT DATA

Component	Manufacturer	Model Number	Serial Number	Range	Dimensions
Dipole Elements					2-1/4" (each)
Balun & Shield	CGS Laboratories	BPC-200/50	26795	Wideband 50Ω balanced to 200Ω unbalanced	2-1/4" x 1-7/8" x 1-1/8"
RF Energy Converter	Rafec Electronics	307		150 Kc to > 1 Gc	(Size of a 2 watt carbon resistor)
Shield for RF Energy Converter					2" x 1" x 3/4"
Shielded Cable		RG-58			30 ft.
DC Microvolt-Ammeter	Kintel	203		100 microvolt, 1000 V	

The three attributes mentioned earlier which were ascribed to an optimum power density detecting device can be considered in light of the power density detector's characteristics which were just described. It has been shown that the developed device is small. With slight modification, the device could be packaged in a box with dimensions of the order of an $(\text{inch})^3$. Since the wavelength of EM radiation does not approach an inch except for frequencies greater than 10 Gc, it seems possible for a device of this sort to be useful at least to frequencies of the order of 10 Gc. For higher frequencies a device which produces a known amount of heat when placed in a field of known power density should be used. It has been explained how the device has been made sensitive only to fields in the region of measurement and has been shielded against stray field pickup. Since the sensing element is a short dipole, the power density detector is polarization sensitive. This presents no essential problem, however, since measurements of the total power density at a point can be made in three orthogonal planes and the results combined to give the total. This method of measurement will be outlined in a later section. The short dipole has a 90° beamwidth and

this must also be taken into account when making power density measurements as will be explained later. With a slight modification, the power density detector can be made frequency selective by installing a bandpass filter ahead of the RF energy converter. This was not done in this study and it will be assumed in the report that the power density due to only one frequency at a time is being considered. Finally, this device is only a power density detector when making measurements in the far field where the ratio of $\vec{E}$ to $\vec{H}$ is a known constant, and, strictly speaking, in the situation where only travelling waves exist. It is important to distinguish the definition of power density which is in terms of power flowing into an aperture from the definition of energy in a field which can exist with no net flow of power as in the case of an incident wave perpendicular to a reflecting surface. In this case, standing waves are set up, and there are points where the $\vec{E}$ vector is very large, but there is no power density since $\vec{E} \times \vec{H} = 0$. There is a constant energy density though which equals $\varepsilon |\vec{E}|^2 + \mu |\vec{B}|^2$. Since the developed device is primarily sensitive to $\vec{E}$ field, it would respond even in the case where there was no net power density or change in $\vec{E}$ with space so long as there was a standing wave in which $\vec{E}$ varies with time. In this case, the appellation, "power density detector," is not accurate and the term, "$\vec{E}$ field detector," would be more appropriate. However, in a radiated susceptibility systems test, standing waves would not be expected to be substantially characteristic of the overall electromagnetic environment because of the randomness of the characteristics of the reflecting structure and the divergence of the radiation incident thereon.

Once it was demonstrated that the power density detector configuration decided upon was capable of making bonafide measurements without being susceptible to "stray" fields, the problem of calibration was next considered.

Extensive calibration measurements were conducted. Certain elements of these measurements were common to all of them:

1) power source
2) wattmeter

3) transmitting antenna

4) 30 feet of RG 58 shielded cable between power source and transmitting antenna.

The equipment used to establish the field was the following:

1) Microdat Power Oscillator; Model No. 408-1; ESL No. 341369; range - 200 - 400 Mc.

2) Thruline Wattmeter; Bird Electronic Corp.; Model No. 43; Serial No. 8551; range - 10 W and 200 - 500 Mc.

3) Dipole antenna - NF-105 kit; Empire Devices.

4) 30 feet RG-58 shielded cable.

In order to assure accurate calibration, all reflecting surfaces should be removed from the calibration site, and a known power density, created (according to the formula, $P_d = P_T G_T / 4\pi R^2$).

In an accurate calibration, one reflecting surface, the ground plane, cannot be removed although height above it can be varied. In all calibration measurements the receiving and transmitting elements were placed at equal (but not necessarily the same) heights above the ground plane. A diagram of the calibration setup is found on the next page.

In the first series of measurements R was varied from 1/2 meter to 10 meters. h was adjusted to 58" or ~ 1.5 meters. For each R the power generated by the source was varied between 0 and 10 watts and the reading on the DC voltmeter recorded. The frequency was adjusted to 300 Mc. The transmitting and receiving elements were adjusted for horizontal polarization and aligned perpendicular to the direction of propagation. P_T, antenna radiated power, was found from the following formula,

$P_T = P_f - P_r - 2$ (cable attenuation)

P_f = forward power at wattmeter

P_r = reverse power at wattmeter

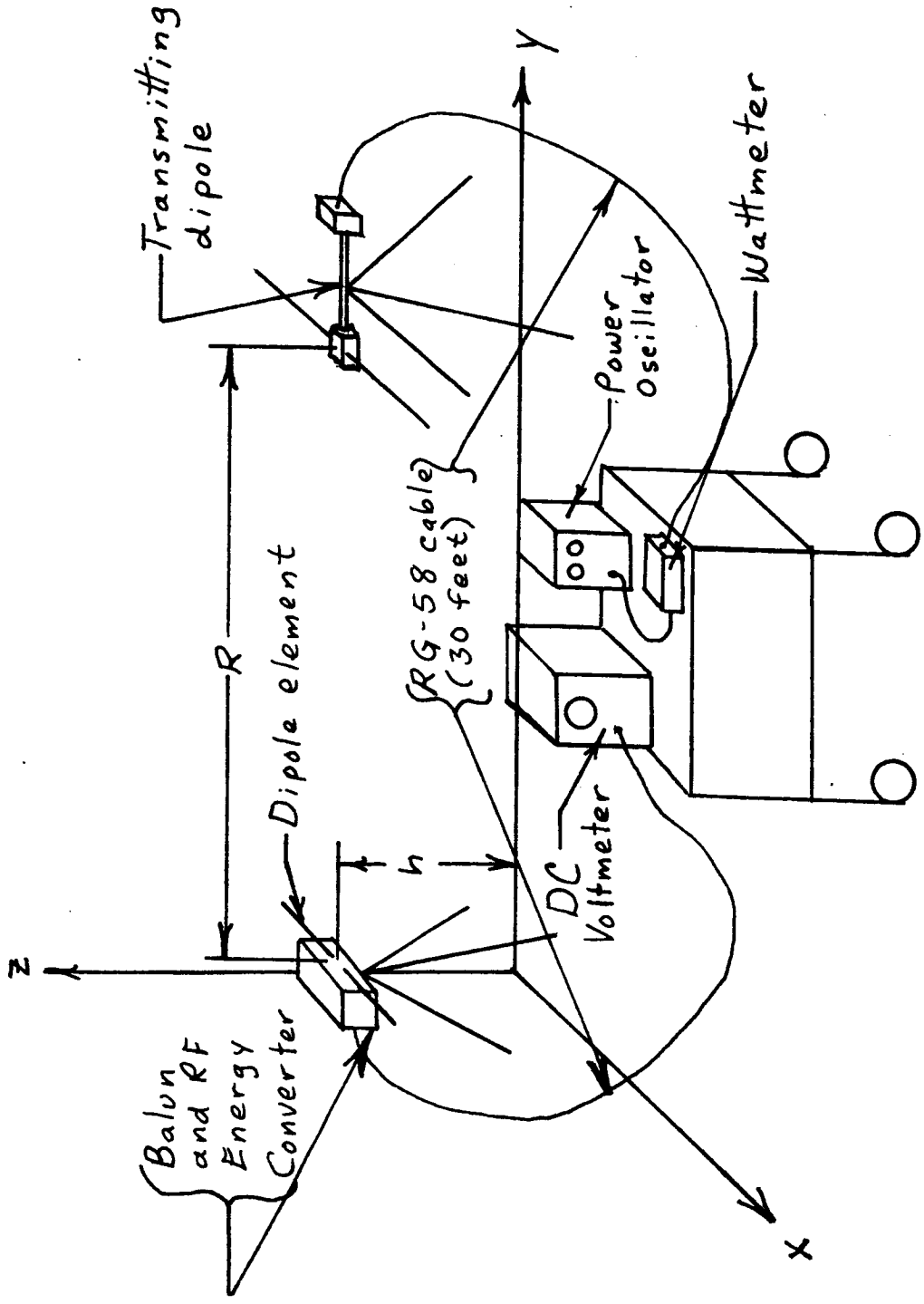

Diagram of Calibration Setup

P_f and P_r were measured by adjusting the wattmeter to read power in each direction, respectively. The 30 foot length of cable was tested and found to have 2 db of attenuation at frequencies between 200-300 Mc. G_T for the transmitting dipole is 1.6. Power density was then calculated from the following formula and plotted versus the DC voltmeter reading as shown in Figure 27.

$$P_d = \frac{P_T G_T}{4\pi R^2}$$

If the calibration procedure just outlined were adequate, it would be expected that the curves plotted for the different R s would all lie along the same curve. Reference to Figure 27 shows that this is not the case. It can be seen that all curves have the same slope and that the transfer function is linear, but there is a spread in the abscissas for a given ordinate. It is concluded from Figure 27 that the ground reflected wave from the transmitting dipole has been detected by the power density detector in addition to the direct wave and that for each value of R these two waves have tended to either cancel or reinforce producing the dispersion in meter readings for the same calculated power density. This corroborates the results presented earlier concerning an improvement in the calculation of power density taking into account ground reflected waves. This conclusion indicates that the power density detector has not been adequately calibrated and that the true calibration curve lies somewhere between the uppermost and lowermost curves of Figure 27.

At this point it was decided to try two independent calibration procedures in order to corroborate the results. One approach was to increase the height above the ground plane of the transmitting dipole and the receiving element of the power density detector. This would increase the path length of the ground reflected wave providing greater free space attenuation (due to dispersion) than the direct wave would experience. Thus, the reflected wave could not interfere at the receiving element to the extent that it had in the first series of experiments. The second approach was to measure power density at a point with an already calibrated (although unwieldy) device and make a substitution measurement with the power density detector.

CALCULATED POWER DENSITY LEVELS FOR KNOWN TRANSMITTED POWER VERSUS INDICATED METER READING WITH POWER DENSITY DETECTOR AS PICKUP DEVICE (FREQUENCY=300MC)

FIGURE 27

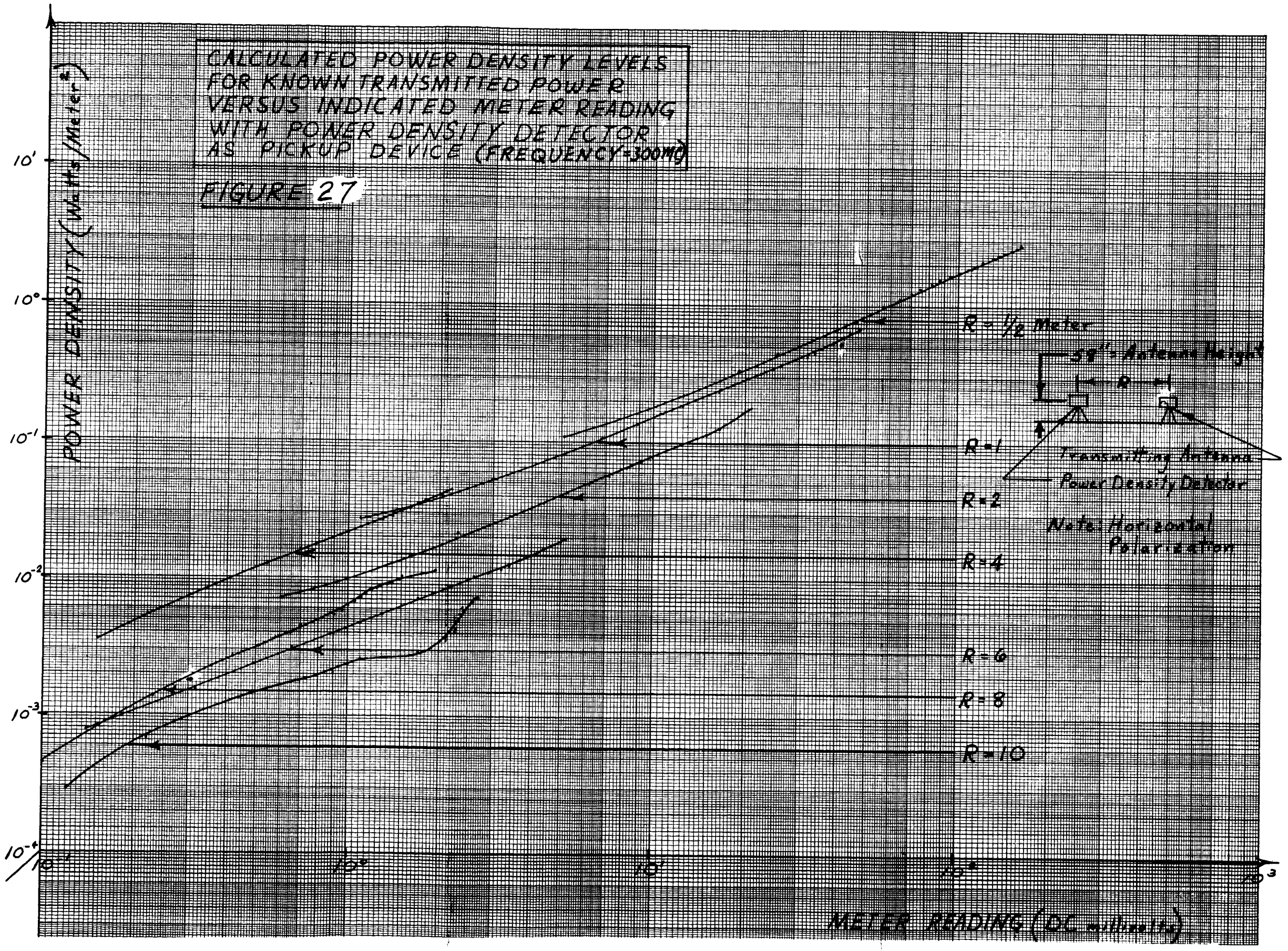

The former approach will be discussed first. An adjustable boom was used to place the receiving element of the power density detector a height of 20.5 feet above the ground plane. The transmitting antenna was also placed at this height by positioning it on top of a van. The experiment was conducted in exactly the same way as the one described previously. The results for a frequency of 300 Mc are shown in Figure 28. This experiment was also performed at five other frequencies between 200 and 300 Mc in order to obtain calibration data versus frequency in this range. The results are shown in Appendix VII. Also shown in Appendix VII is a set of curves for R = 1/2 meter, the data for which was taken at three different times over a two day period. This plot demonstrates consistency and repeatability of measurements made with the power density detector. It can be concluded from the results that the calibration curve for the device will be the same for any frequency in the 200-300 Mc range since there is no trend in the nature or position of the curves with respect to the axes. No attempt was made to calibrate the device outside this range which covers telemetry assignments. If it is desired at any future time to use the device to measure power densities at a frequency other than one between 200 and 300 Mc, the device will have to be calibrated for the particular frequency. After this set of experiments was performed, all subsequent measurements were performed at a frequency of 300 Mc. Reference to Figure 28 shows that the curves plotted for different values of R lie very nearly along a straight line and a calibration curve could be taken as the median of the plotted curves.

The second approach will now be discussed. Instead of calculating power density at the receiving point due to a known antenna transmitted power, P_T, power density was measured at the receiving point using an Empire Devices NF-105 noise and field intensity meter. The pickup device was a dipole. Field intensity, $\vec{E}$, was obtained by applying the calibrated correction factor to the NF-105 meter reading. Power density was then obtained from the following formula

$$P_d = \frac{|\vec{E}|^2}{377}$$

After a power density measurement was obtained, the power density detector was substituted for the receiving dipole and NF-105 arrangement. The response of the DC volt-

CALCULATED POWER DENSITY LEVELS FOR KNOWN TRANSMITTED POWER VERSUS INDICATED METER READING WITH POWER DENSITY DETECTOR AS PICKUP DEVICE (FREQUENCY=300MC)

FIGURE 28

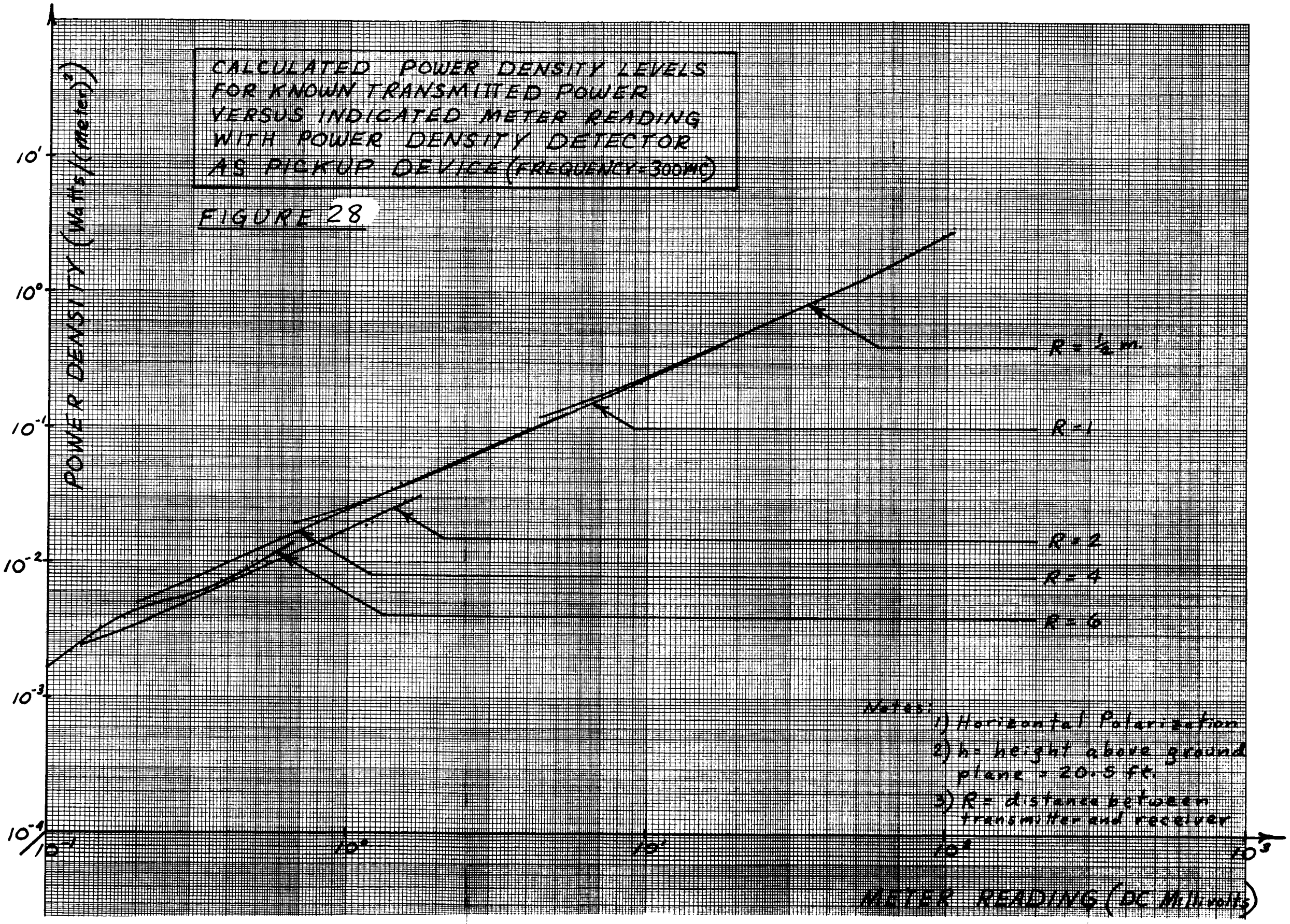

meter was then recorded. This response was plotted as the abscissa and the measured power density as the ordinate. The results are plotted in Figures 29 and 30 for horizontal and vertical polarization, respectively. These curves point out the inadequacy of the NF-105 for making power density measurements because of fluctuations in the readings. It is suggested that these fluctuations are caused by cable pickup of "stray" fields. This clearly indicates the unsuitability of using the NF-105 or similar instruments with an RF output for RF input in an RF environment unless the circuitry after the receiving element can somehow be isolated from the RF field. Nevertheless, the usefulness of the measurements made in this way is connected with the fact that ground reflections don t affect the calibration procedure since the total effect of both ground reflected and direct waves has been measured both by the power density dector and the precalibrated NF-105 dipole arrangement. It would be expected that the resultant plots for different values of R would be bunched closely together with a lack of linearity of each individual plot due to the "stray" or random pickup of the NF-105 dipole arrangement. This is indeed the case as reference to Figures 29 and 30 will show. The true calibration curve is most probably represented by a curve drawn so that the sum of the mean square distances to measured points lying close to the curve is a minimum for R's of closely separated values. It is possible that there is some systematic error which either increases or decreases as R increases or decreases. The plots of Figures 28, 29 and 30 were each mentally integrated to find the curve with the most representative slope and intercepts. These three resultant curves then were used to determine the mean calibration curve for the power density detector and the calibration accuracy. The results are shown in Figure 31. The mean of the three curves which is the same as the median is taken as the calibration curve. The other two curves represent upper and lower bounds on the calibration accuracy. This calibration curve represents the results of many independent measurements and, while the statistical accuracy obtained was not explicitly calculated, it stands to reason that the accuracy of and confidence in any measurement is increased the more corroborating results are produced.

MEASURED POWER DENSITY LEVELS FOR KNOWN TRANSMITTED POWER VS METER READING OF POWER DENSITY DETECTOR FOR SAME TRANSMITTED POWER

FIGURE 29

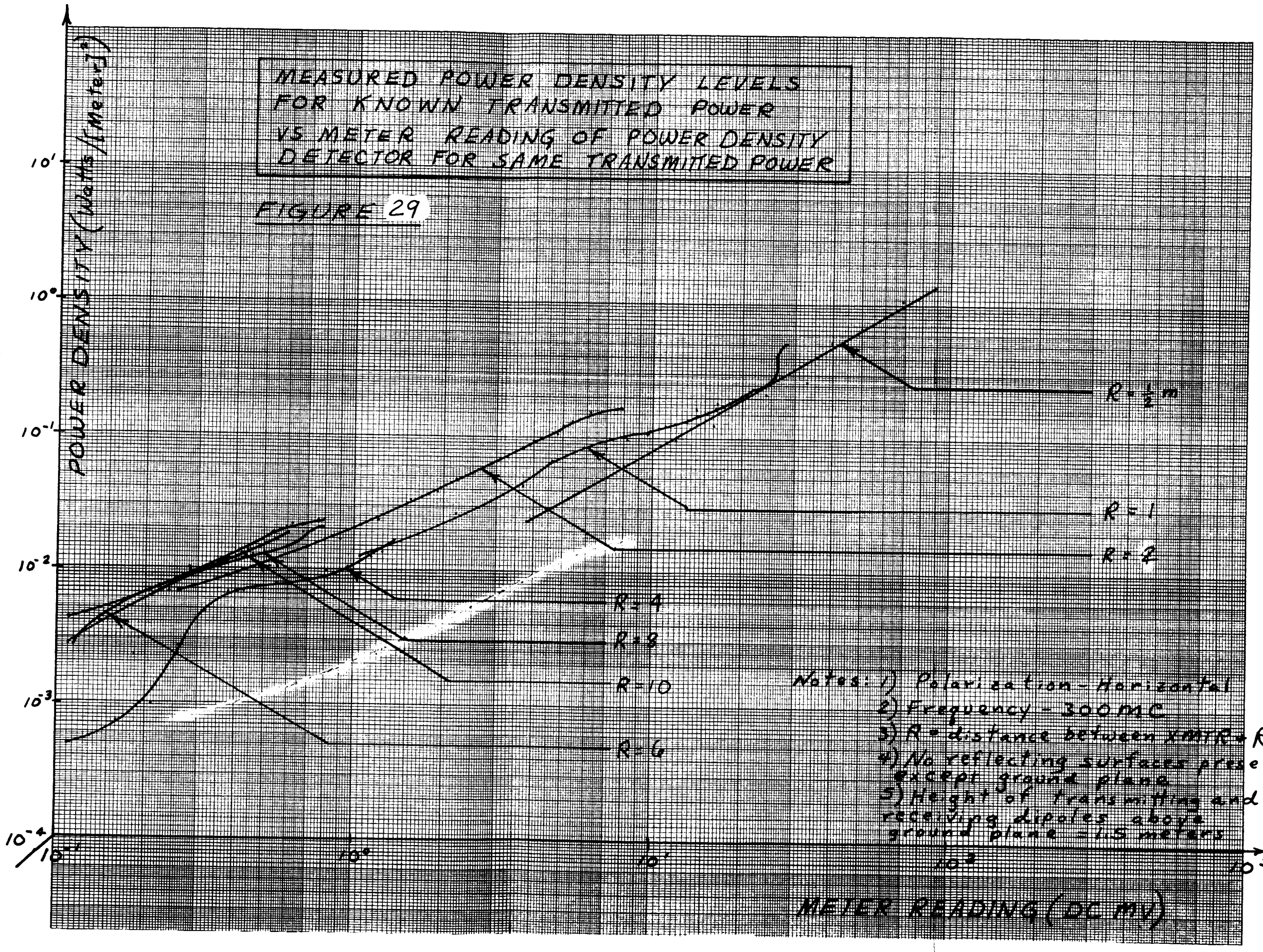

MEASURED POWER DENSITY LEVELS
FOR KNOWN TRANSMITTED POWER
VS METER READING OF POWER DENSITY
DETECTOR FOR SAME TRANSMITTED POWER

FIGURE 30

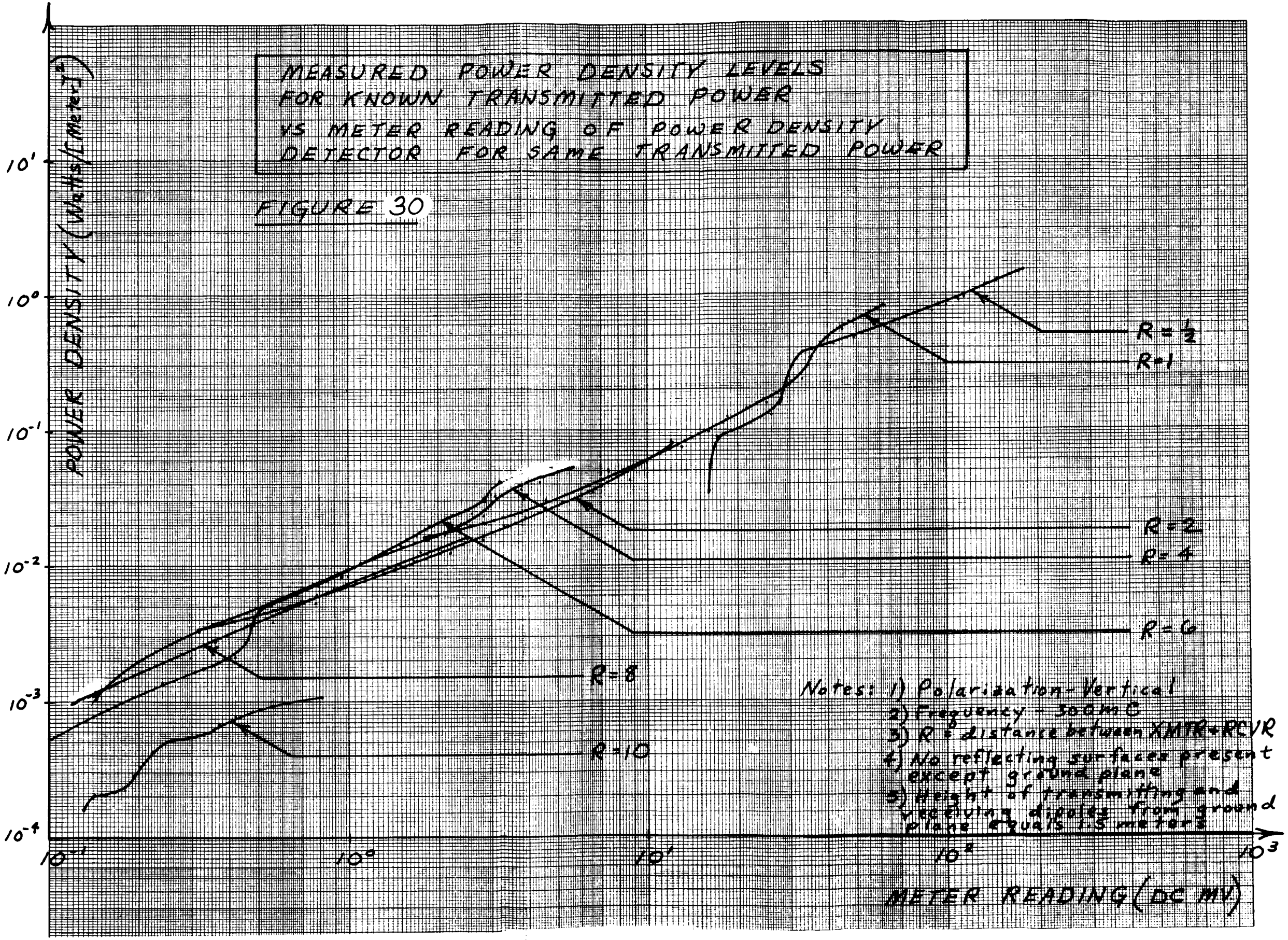

CALIBRATION CURVE FOR POWER DENSITY DETECTOR USED IN CONJUNCTION WITH 30 FEET OF RG-58 CABLE AND KINTEL DC VOLTMETER

FIGURE 31

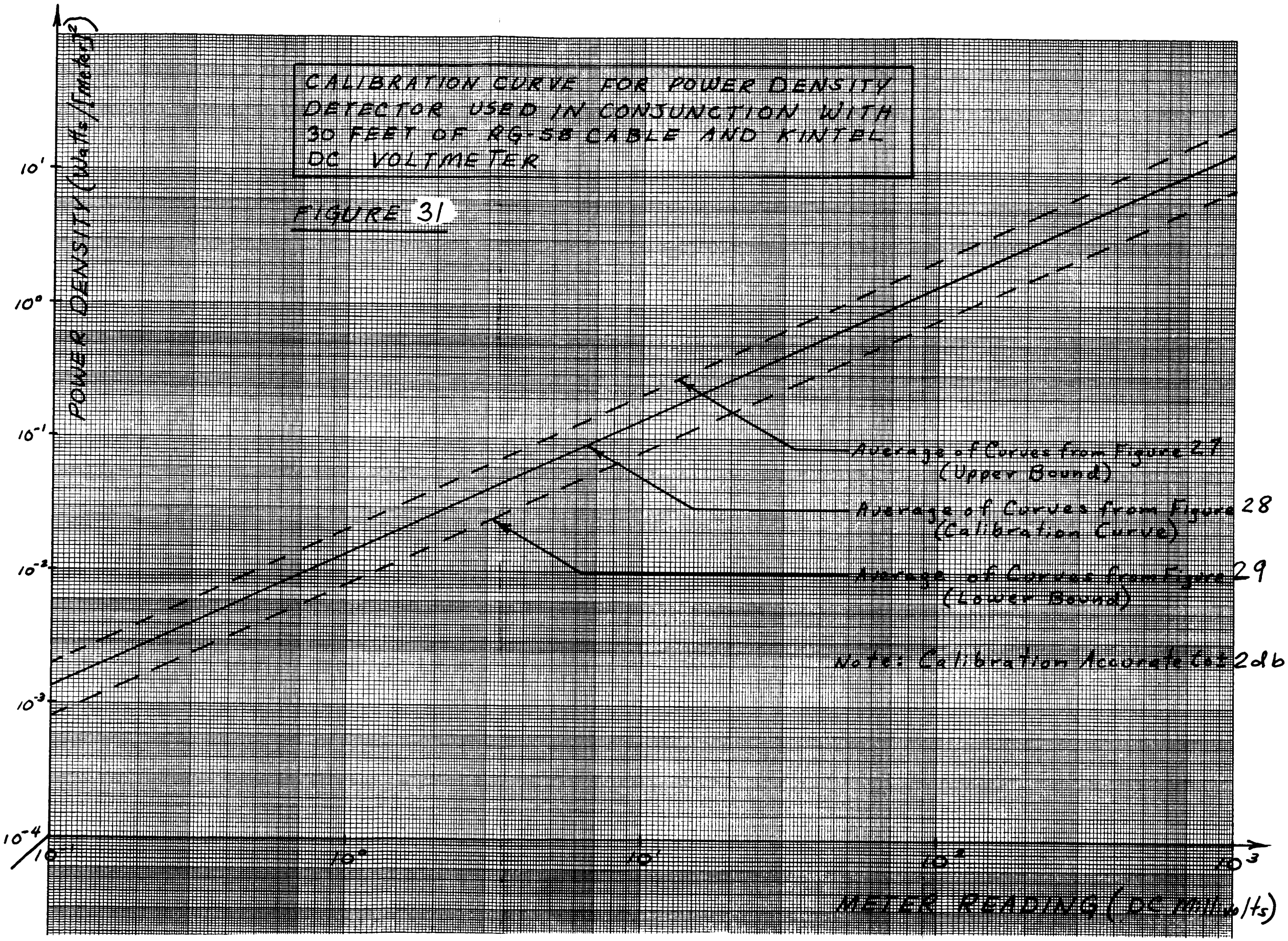

7.2 Procedure. In this section a procedure for conducting a formal RF systems radiated susceptibility test will be presented, a sub-part of which involves useage of the power density detector. The power density detector's use in such a test is envisioned to be threefold:

1) To aid in the establishment of desired power density levels in the vicinity of the test specimen (spacecraft).
2) To verify desired power density levels in the vicinity of the spacecraft.
3) To measure power density levels within and about the spacecraft.

By using the power density detector to establish power densities in the laboratory, it is suggested that factors that contribute to a lack of accuracy in attaining desired power densities in the laboratory can be counteracted by adjustments in the transmitting equipment. The effects of these adjustments will be monitored with the power density detector until the desired RF environment is attained. The factors that contribute to a lack of accuracy in attaining desired power densities in the laboratory will be considered in another section.

The suggested procedure for conducting an RF systems susceptibility test is the following:

1. Accumulate data as to on-board and off-board radiators, which shall include the following.

   a. Antenna radiated power P_T
   b. Effective gain as a function of azimuth and elevation, $G_T(\theta, \phi)$

NOTE: A reference azimuth line will have to be assumed so that radiators may be located relative to each other and to the spacecraft.

   c. Location of radiator
   d. Distance of radiator from spacecraft.
   e. Physical height above ground-plane of radiator.
   f. Polarization, beamwidth and pointing direction of radiator.
   g. Modulation characteristics and bandwidth.

Other pertinent data should include (if possible)

1. Height above ground plane and physical dimensions of spacecraft.
2. Reflection coefficient (magnitude and angle) of ground.

2. Using above data calculate power densities in vicinity of spacecraft due to each radiator.
3. Procure test equipment for use in simulation testing which might include:

a. Signal generators

1. AM
2. FM
3. Pulsed
4. White noise
5. Capable of accepting modulation

b. Amplifiers

1. Traveling wave tubes
2. Audio and video

c. Modulators

1. Capable of providing desired modulation characteristics and modulating signal generators.

d. Monitoring Equipment

1. Wattmeters
2. Frequency counters

e. Antennas

1. Suitable bandwidth and beamwidth characteristics
2. Polarization similar to source to be simulated.

f. Filters

1. Bandpass (to provide band limited white noise)

g. Hookup Equipment

1. Cables, connectors, etc.

NOTE: The signal source equipment should be capable of simulating bandwidth, modulation and power characteristics of the radiator it's being used to simulate. The antennas should be of beamwidth narrow enough so as to illuminate just the spacecraft, but should be of sufficient beamwidth to radiate the spacecraft uniformly.

4. Consider laboratory space and disposition of test specimen and test equipment.

a. Record dimensions of testing area.

b. Determine position of test specimen.

c. Locate ancillary equipment as far away from test specimen as possible so as to perturb fields in the vicinity of the test specimen as little as possible.

d. Locate signal generators, monitoring equipment, etc., as far from test specimen as possible.

e. Connect signal sources to test antennas with appropriate cables.

f. Determine location of test antennas.

1. Locate test antenna so that direction of incident radiation will be the same relative to the spacecraft as it is for the radiator being simulated.

2. Locate test antenna so as to point at spacecraft.

3. Locate test antenna a distance from the spacecraft, d, as determined from the following formula.

$$d = \frac{L}{2} \cot \frac{\theta}{2}$$

where

L = greatest horizontal or vertical dimension of spacecraft in plane perpendicular to incident radiation.

θ = beamwidth in horizontal or vertical direction.

d = distance from spacecraft.

The above formula should be used twice:

1. L and θ in the horizontal dimension.
2. L and θ in the vertical dimension.

Whichever d is the largest, should then be used as the test distance. Figure 32 is a plot of d versus L with θ as parameter as adapted from MIL-I-11748B (sig. C), page 36. In accordance with this document, a minimum test distance of three feet is shown in Figure 32. This is to ensure uniform illumination of the test specimen (spacecraft).

5. Calculate power settings of test equipment that will produce previously calculated power density levels.

   a. Use the following formula.

$$P_T = \frac{4\pi d^2 P_d}{G_T}$$

where

P_T = antenna radiated power (watts)

d = test distance (meters)

G_T = gain of test antenna

P_d = previously calculated power density levels according to Step (2).

   b. The monitored power level should be

$$P_f(\text{dbw}) = 10 \log P_T - 10 \log (1 - |\Gamma|) + 2 L_C$$

where

P_f = power measured by wattmeter in forward direction (decibels above 1 watt)

P_T = antenna radiated power (watts)

$|\Gamma|$ = reflection coefficient at wattmeter

L_C = one-way loss in cable between power source and test antenna db.

FIGURE 32

TEST DISTANCE VS ANTENNA BEAMWIDTH

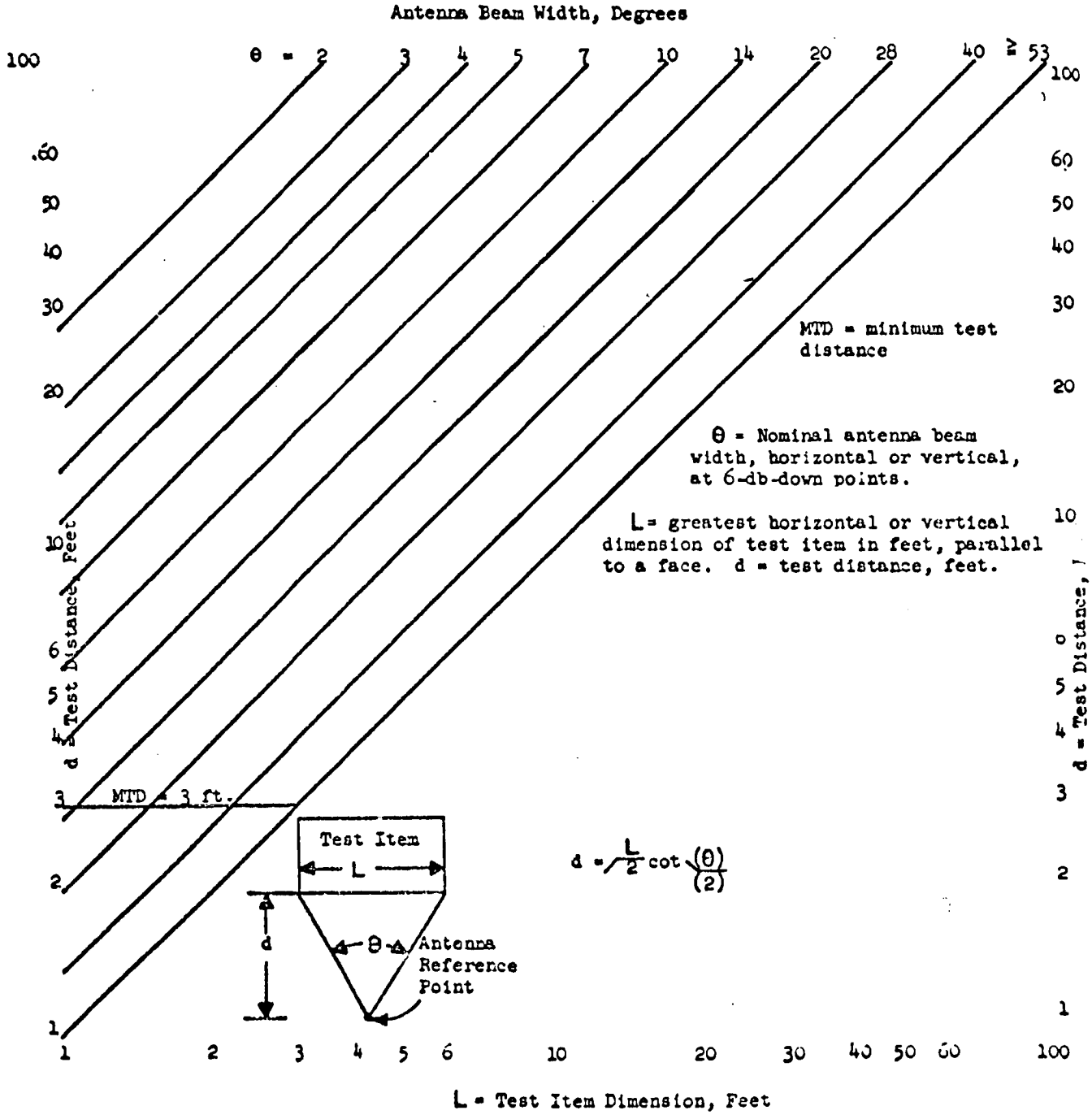

NOTE: This calculation will be only approximately correct due to the neglect of the effects of the ground reflected wave. However, the power density levels will be more accurately set using the power density detector.

6. Set power density levels

   a. Disposition of test equipment, ancillary equipment and room configuration should be the same as during actual test.

   b. This part of procedure should be performed with test specimen (spacecraft) removed from its position in test room to allow a controlled setting of power density levels.

   c. Place power density detector in space in which test specimen (spacecraft) is to be located.

   d. Turn on one power source test antenna combination at a time.

      1. Set at level calculated in 5(b).

   e. Align power density detector with direction of incident radiation and polarization of source or determine power density level in accordance with 9(b)2.

   f. Adjust level of power source until power density level as calculated in Step (2) is attained.

      1. Refer to appropriate calibration curve for frequency under consideration.

   g. Move power density detector throughout volume to be occupied by spacecraft and verify constant power density levels throughout this volume.

   h. Record power level setting of signal source.

   i. Repeat for each simulating power source-test antenna combination.

7. Add safety factor to each power level as found in 6(g) to obtain test power setting for power sources.

8. Place test specimen (spacecraft) in its test position.

9. Conduct test.

   a. Turn on all powers sources simultaneously to provide for the possibility of intermodulation. (See Appendix VIII for computer program that determines potential intermodulation.)

   b. Use power density detector to detect power density levels in vicinity of spacecraft.

      1′. Provides information about positive or negative (energy concentrating) shielding provided by configuration of spacecraft itself.

      2′. Procedure for determining power density using power density detector when polarization and direction of arrival of radiation are unknown.

         a′. This situation prevails when there is a complex disposition of reflecting surfaces which will alter direction of arrival and polarization of radiation at point of measurement.

         b′. It is desired to sum up the power densities contributed by all components which might arrive from any direction. As shown in Appendix IX, six measurements must be made and the power densities measured in each measurement added together. Although below the development is in terms of power density while in Appendix IX, it is in terms of electric field intensity, there should be no confusion since these two quantities are simply related.

$$P_d(\text{total}) = \sum_{n=1}^{6} P_{dn}$$

Where two orthogonal measurements are made in each of three orthogonal spatial planes. If we take the measurements with respect to the X-Y, Y-Z and X-Z planes then

$$P_d(\text{total}) = \sum_{m=x,y} \sum_{n=y,z} P_{dmn} (1 - \delta_{mn}) + \sum_{m'=x',y'} \sum_{n'=y',z'} P_{dm'n'} (1 - \delta_{m'n'})$$

where

$$\delta_{mn} = \begin{matrix} 0 & m = n \\ 1 & m = n \end{matrix}$$

and the primed subscripts refer to measurements made orthogonal to those represented by the unprimed subscripts.

c. Determine RF susceptibility of test specimen (spacecraft) caused by its RF environment.

d. Determine which simulated source or sources caused susceptibility by switching them on or off singly and in combinations.

e. "Fix" susceptibilities or make design recommendations.

f. Conduct any further testing deemed necessary.

In summary, it can be said that a power density detector was developed and calibrated. The advantages of the detector are its compactness and DC output with RF input which allows for isolation between the test apparatus and the RF field. The limitations are that it cannot be used in either a closed or semi-closed region whose dimensions are comparable to the dimensions of the detector itself. Characteristics of the device are that it is polarization sensitive and directional. Techniques for coping with this situation were developed for the case when the direction and polarization of the incident wave are not known. The device was calibrated in the frequency range of 200 to 300 Mc. If frequencies outside this range are to be used, the device must be calibrated for the frequencies of interest. It also is not frequency selective so that it must be used in

conjunction with one transmitter at a time. Further development might involve a bandpass filter on the front end. In the controlled environment of a test lab, none of these limitations or characteristics will hamper the usefulness of the device when it is used for the intended purposes and with the limitations in mind. The intended purposes of the power density detector are to provide a check on the calculation used in setting up power density levels, to verify that the desired power density level has been achieved and to make power density measurements in the vicinity of the spacecraft. A procedure for using the device within the framework of a formal test was developed.

8. TEST MARGIN CONSIDERATIONS

8.1 Uncontrolled Factors in Spacecraft Environment. Ground reflections have been discussed and it has been shown that their effect on power density levels can either be calculated directly if certain information is available or can be assumed worst case if it is not. If the latter condition holds they are to be taken into account by using a test margin. In general, the fact of unknown conditions or environment motivates the use of a test margin, and the worst case assumption is the criterion which determines its magnitude. If the nature of all boundary surfaces and sources in the vicinity of the spacecraft could be specified mathematically, we could compute the exact power density at any given point, but, since they cannot, a test margin will be relied upon. A test margin is tacitly assumed in the calculation of power densities due to specified sources if the gain of the antenna in the direction of the beam is used. If the spacecraft doesn't lie directly in the beam of a radiator, the gain in the direction from the source to the spacecraft should be used in power density calculations. Since we have already considered ground reflections, there remains to be considered the effect on power density levels of random reflections from other surfaces such as the launch vehicle, associated ground equipment, etc. For the purposes of this study, all of these reflections were treated by lumping them together and a worst case experiment was devised to measure the greatest increase in power density likely to occur in a spacecraft due to the focusing effects of adjacent reflecting surfaces.

Let us consider the interaction of the spacecraft with its RF power density environment. For a susceptibility to occur energy must be coupled from the environment into the spacecraft. The mechanism responsible for this coupling is an unintentional antenna or pickup device. One of the principles regarding intentional antennas that also holds for unintentional antennas is the following: the incident waves must be coherent over the aperture dimensions for maximum pickup. This is the case for most designed antenna systems. For instance, it is assumed that for an antenna of height, h, and effective height, h_{eff}, that the impinging waves are coherent (add in phase) along h and the coupled voltage

is E (volts/meter) times h_{eff}. If the waves interfere along the dimension h, the relation

$$V = Eh_{eff}$$

does not hold, and, if the phases of the impinging waves are randomly distributed over the aperture, the voltages that are produced will tend to cancel each other if the randomly phased waves are all of the same relative amplitude level. However, if there is produced a focusing effect at a point within an aperture dimension such that all the waves add constructively there, there will be a net voltage coupled into the circuit. Therefore, a large power density at a point or a coherent power density over an aperture dimension will couple voltage into a circuit. These two modes of coupling are the characteristic modes of radiative or far-field coupling. The properties of the electromagnetic radiation which is coupled in either of these modes are the following:

1. directionality
2. wave structure
3. polarization.

The two modes of radiative coupling are analogous to the two modes of signal reception: CW and broadband. Let us consider Figure 33.

Both Figures 33A and B consist of continuous and discontinuous distributions. In Figure 33A the distance, $X_1 - X_2$, represents an aperture dimension of an antenna. There are two types of radiation incident on the antenna:

1. a focused part, $E' \delta(X - X_0)$, which consists of many waves focused by a uniquely shaped reflecting surface which all add in phase at X_0.
2. a beamed component, E(X), which represents a signal all of whose components add in phase over the aperture dimension $X_1 - X_2$.

In the analogous Figure 33B there are two types of signal at the input to the receiver of bandwidth $f_1 - f_2$:

FIGURE 33

ANALOGY BETWEEN FIELD DISTRIBUTION AND SPECTRUM

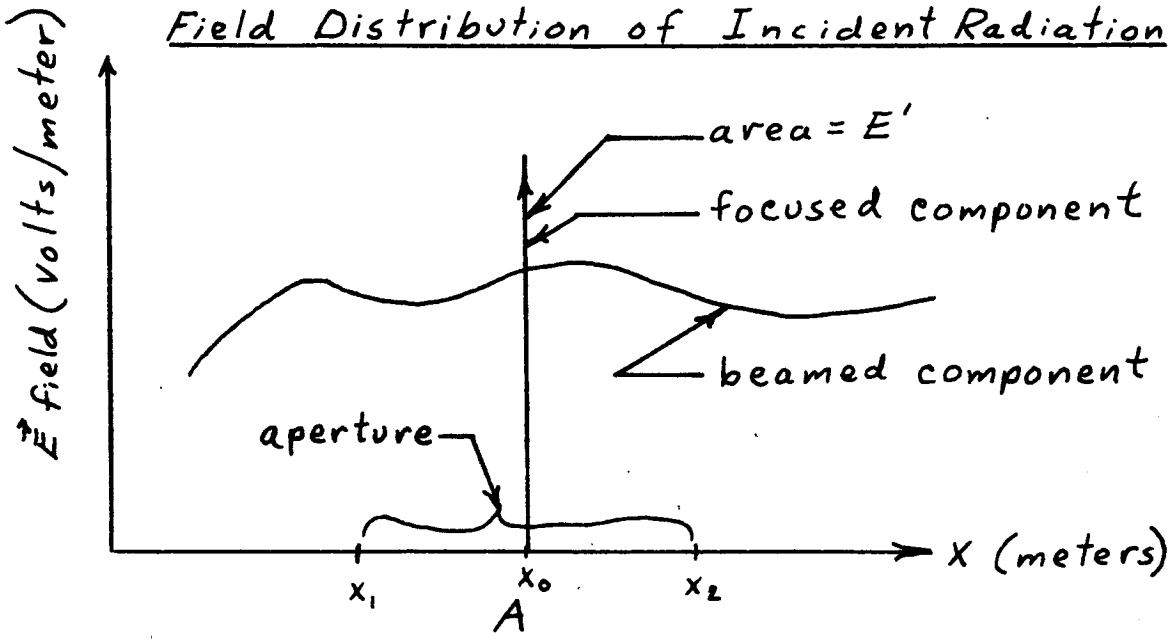

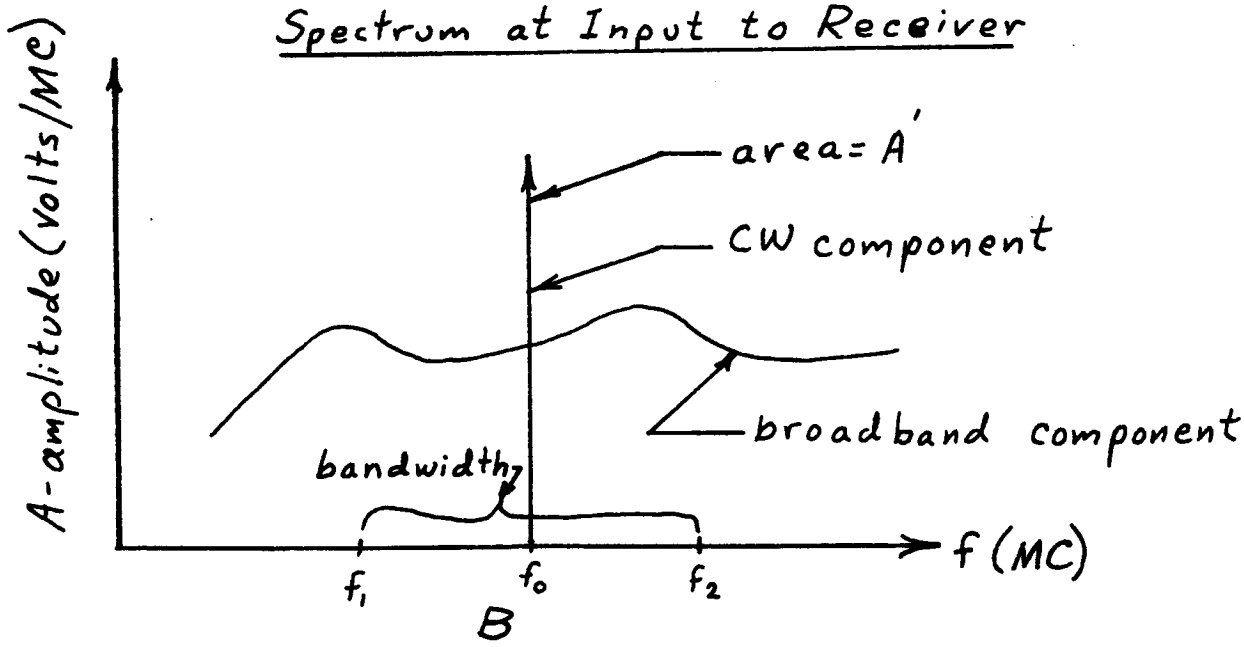

1. A CW part $A'\delta(f-f_0)$ which consists of a signal from a monochromatic CW source.
2. A broadband component, A(f), which consists of an intelligent signal from a single source in which the phase relationship is non-random.

The following items are analogous.

From Figure 33A	From Figure 33B
$E'\delta(X - X_0)$	$A'\delta(f - f_0)$
$X_1 - X_2$	$f_1 - f_2$
E(X)	A(f)
in-phase characteristic of E(X)	non-random phase relationship of A(f)
unique sources for $E'\delta(X - X_0)$ and E(X)	unique sources for $A'\delta(f-f_0)$ and A(f)
total response = integration of $\vec{E}$ from X_1 to X_2 = $\int_{X_1}^{X_2} E(X)\,dX + E'$	total response = integration of A from f_1 to f_2 = $\int_{f_1}^{f_2} A(f)\,df + A'$

A further analogy can be drawn if we consider a random distribution of signals from many sources incident on $X_1 - X_2$ and on $f_1 - f_2$. In the former case the random phases of the signals will cancel or reinforce such that a "white" noise signal is coupled into the aperture. In the latter case the random phases of the signal will produce a "non-intelligent" signal also resembling "white" noise. A source that would produce the signal shown in Figure 33B would be an FM-FM telemetry system, the spectrum of which has been fully discussed in Section 2.2. A reflecting surface that would act as a source for the signal depicted in Figure 33A would form the basis of a worst case experiment involving the focusing and beaming of energy at an unintentional aperture. Since a non-intentional aperture would likely be of a small and linear nature (the least complicated geometry), a reflecting surface that focuses energy at a point and beams energy along a linear dimension was chosen. Such a surface is a parabolic cylinder.

It focuses energy at the focus of the parabola in the parabolic plane and beams energy along the focal line in the cylindrical plane providing that the incident radiation is of wavelength such that

(29) $$L = \frac{n\lambda}{4} ; n = 1, 3, 5 \ldots$$

and the polarization of the radiation is parallel to the cylindrical axis. The incident radiation must also have a plane wavefront. The following diagram illustrates the characteristics of a parabolic cylinder.

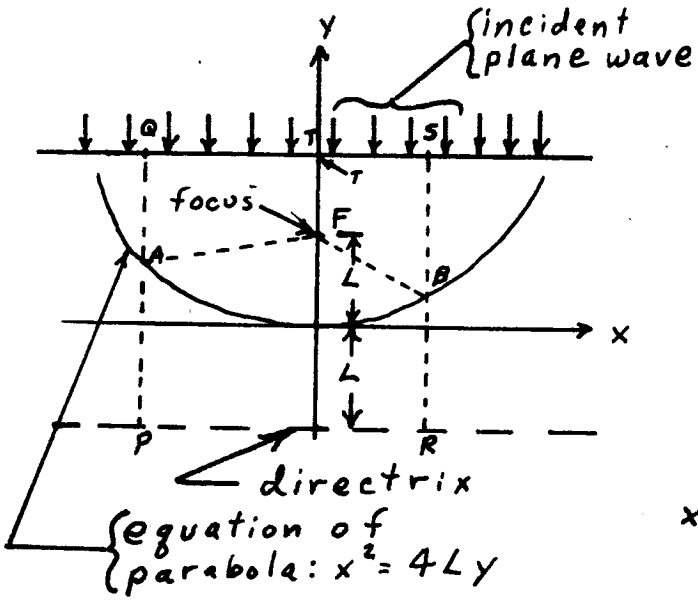

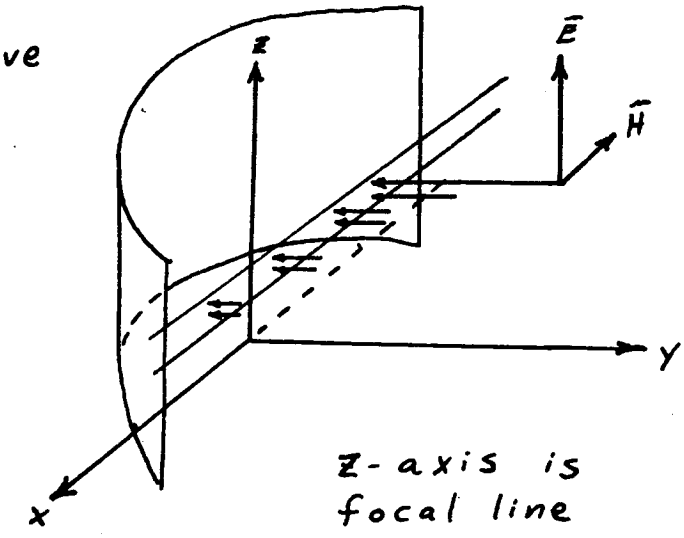

We see that

$$AQ + AF = BS + BF = TF + 2L$$

$$AP = AF$$

$$BR = BF$$

$$AQ + AP = QP$$

$$BS + BR = SR$$

$$SR = QP$$

Now if $L = n\lambda/4$, the direct wave incident in the direction TF will add in phase with reflected waves from all points of the surface in the X-Y plane since there is a 180° phase reversal at the reflecting surface. At this point it can be seen that the amount of energy coupled into the receiving circuit depends on both the reflector's aperture and the aperture of the receiving element. For the purposes of determining the field intensity on the focal line a determination of power density at one point is sufficient. This was accomplished using the calibrated power density detector. This eliminated the need for calculating the aperture of the receiving device since this had been already taken into account in the calibration. The next consideration is to determine the dimensions of the parabolic cylinder to simulate the worst case condition that might be encountered on a spacecraft. Let us first consider what value n should be in the expression $L = n\lambda/4$ (n odd). According to Kraus[21] if the distance from the focus to the reflector (L) is small compared to a wavelength, the exact shape of the reflector is not important. This means that as n is made larger, a more perfectly formed parabola is required to obtain the same relative power density at the focus assuming constant aperture (and the same wavelength). For these purposes $\lambda/4$ is considered small compared to λ but $3\lambda/4$ is not. Therefore, we choose $n = 1$.

Next, the aperture of the reflector and the wavelength of radiation to be used in the worst case experiments were chosen. The important points to bear in mind at this stage are that it is highly unlikely that there will exist in any missile system reflecting surfaces more complex than planes, spheres or circular cylinders. Of the combinations of these surfaces that can be imagined, the circular cylinder is the closest approximation to the worst case parabolic cylinder. Invoking the principle that reflecting surface shape becomes more important as distances greater than a wavelength are considered, it is unlikely that any reflecting surface encountered in a missile system will approximate a parabolic cylinder to such a degree that it will gather incident radiation over an aperture with dimensions large compared to a wavelength such that the waves all add constructively over the focal dimension. Therefore, it is reasonable to choose our aperture as approximately a wavelength. It can be seen from the equation of the parabola and the condition for constructive interference that the parabola will be defined by the following.

$$X^2 = 4L_Y$$

L = distance to focus = $\lambda/4$

$$X^2 = \lambda Y$$

Since we assume

$$2X_{max} = \lambda$$

$$X_{max} = \lambda/2$$

$$Y_{max} = \frac{(X_{max})^2}{\lambda}$$

$$Y_{max} = \lambda/4$$

Therefore, the point on the reflecting surface the greatest distance from the focus is a distance, $\lambda/2$, away.

The parabola becomes the following:

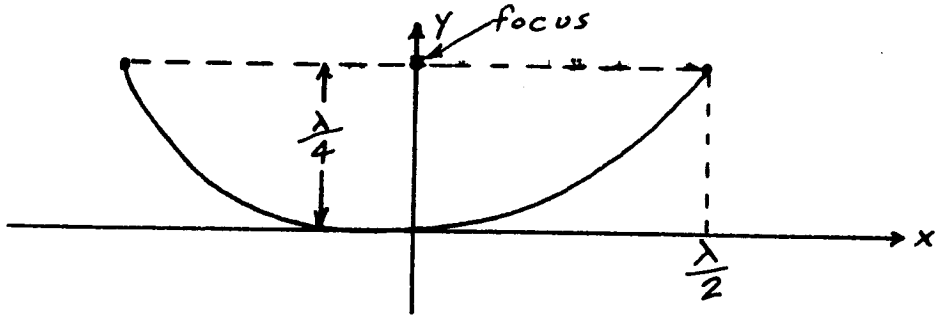

It can be seen that the higher the frequency, the smaller will be the aperture. For a worst case condition we should choose the lowest frequency under consideration as the test frequency. This will determine the aperture dimension which will have a larger power focusing capability than any other possible choice. Since only frequencies greater than 200 Mc are being considered, it stands to reason that a measurement of the power density that can be produced over the focal line of a parabolic cylinder using a frequency of 200 Mc and an aperture with a dimension 1.5 meters in the parabolic

plane will represent the worst case of energy concentration due to reflecting surfaces in a missile system. When this power density level is compared to the level present when the parabolic cylinder is removed, the ratio will represent an adequate test margin for the effects of reflections from random surfaces. Such an experiment was performed. A frequency of 300 Mc instead of 200 Mc was actually used. The results will differ at most by a factor of 1.5 since the length of the aperture in the parabolic dimension at 200 Mc is 1.5 meters (one wavelength) which was scaled down to 1 meter at 300 Mc. Since the amount of gain in power density due to nearby reflecting surfaces is a function of frequency, we can safely be assured that the test margin will result in relatively larger and larger margins of safety at higher frequencies unless a sliding test margin is used. It can safely be said that power density calculations and measurements will become more accurate as frequency increases due to the increase in precision of a reflecting surface necessary to focus or beam energy at higher frequencies. The parabolic cylindrical reflector that was used in the measurements had an aperture of 1 meter by 1/4 meter. The latter dimension (parallel to axis of cylinder) is not critical since the only requirement is that this dimension be equal to or greater than the length of the receiving element of the calibrated power density detector. The experiment was performed in an open area so that random reflections from nearby objects would be eliminated. A Microdot signal generator was the power source. Power was monitored with a wattmeter and transmitted by a dipole. The distance between the transmitting dipole and the receiving power density detector was varied as was the power delivered to the transmitting antenna. In this way an average can be made over either distance or power which tends to "average out" random errors. More will be said about this subject in a later section concerning a statistical approach to establishing a test margin. Thirty foot cables were used between the transmitting dipole and the power source as well as between the receiving part and readout part (DC voltmeter) of the power density detector in order to minimize reflections from test equipment and personnel.

The parabolic cylinder was positioned so that the parabolic plane was parallel to the ground plane and the aperture was aligned with the direction of incident radiation. The power density detector was located at the focus of the parabolic cylinder. Two experiments were performed: (1) measurement of power density using vertical polarization and power density detector dipole element positioned along focal line, and (2) measurement of power density using horizontal polarization and power density detector dipole element perpendicular to focal line.

Experiment (2) was performed for comparison purposes and by no means constitutes a worst case experiment because there will be cancellation among the waves when they arrive at a point on the focal line and the dipole receiving element extends into a non-focused region. In addition to the measurements made using the parabolic cylinder, measurements were also made under identical conditions except that the parabolic cylinder was removed in order that a comparison might be made between the power densities with and without the parabolic cylinder. Figures 34 and 35 show the results for vertical and horizontal polarization, respectively.

The vertical axes represent power density measured in db relative to the antenna radiated power, P_T. This power density was determined from the following equation:

$$P_R = \frac{P_T G_{eff}}{4\pi R^2} \tag{30}$$

Taking the logarithm and rearranging yields

$$-10 \log \left(\frac{4\pi R^2}{G_{eff}} \right) = 10 \log P_R - 10 \log P_T \tag{31}$$

where

G_{eff} = effective power gain = $G_T G_{ref} = G_T G_{refg} G_{refpc}$

R = distance from transmitter (distance from transmitter to power density detector)

G_T = gain of transmitting antenna

G_{ref} = gain due to environmental reflections

G_{refg} = gain due to ground reflection

G_{refpc} = gain due to parabolic cylinder

In this particular experiment $G_T = 1.6$ and G_{eff} was due to the effects of either the ground reflections or both ground reflections and reflections from the parabolic cylinder. The experiment was performed for several values of R. For each R, P_T was varied and power density, P_R, was recorded. The quantity on the left hand side of Equation (31) was determined by substituting the measured values for P_R and P_T in the right hand side. For a particular R this quantity was averaged over the several values of P_T that were used, and the resulting mean value was plotted versus R, represented on the horizontal axes. Three plots each are shown in Figures 34 and 35 corresponding to the following conditions:

1. measured P_R and P_T with parabolic cylindrical reflector
2. measured P_R and P_T without parabolic cylindrical reflector
3. calculated values of the quantity $-10 \log \left(\frac{4\pi R^2}{G_{eff}} \right)$

assuming no reflecting surfaces present, i.e., $G_{eff} = G_T$.

The third condition corresponds to the same assumptions that are made when the range equation, is employed. According to the equation that was used in constructing the plots the power density in db should approach $+\infty$ as R approaches zero. However, the equation is only representative of reality for values of R in the far field ($R \geq 1/3$ m); therefore, the plots are constructed so that power density, P_R, equals zero when R equals zero. The error associated with each plotted point is shown in the figures. It was found by considering the maximum measured values and the minimum measured values of power density for each value of R - $P_{R_{max}}$ and $P_{R_{min}}$, respectively. The error was then taken to be

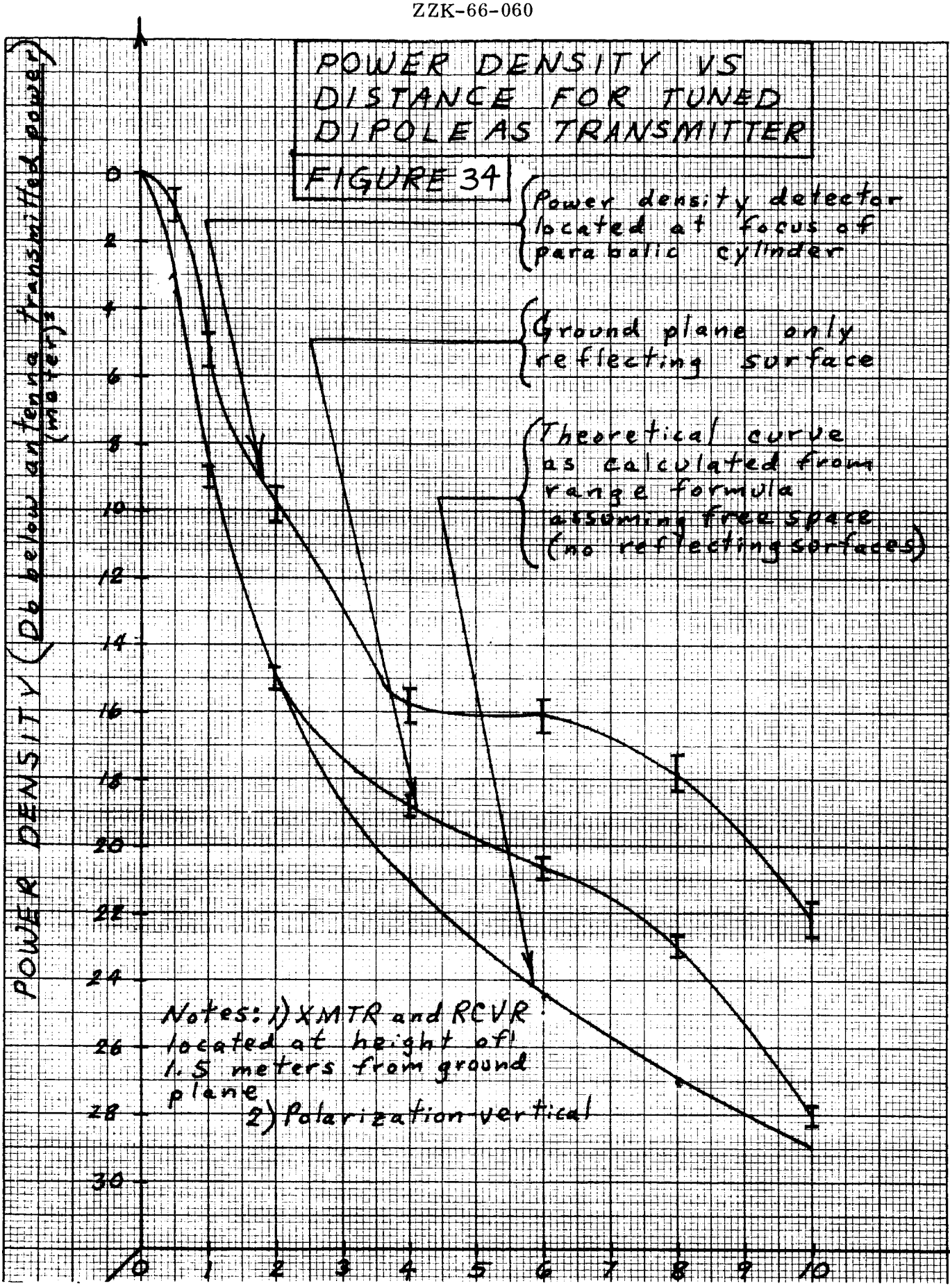

R = distance between transmitting dipole and receiving power density detector (meters)

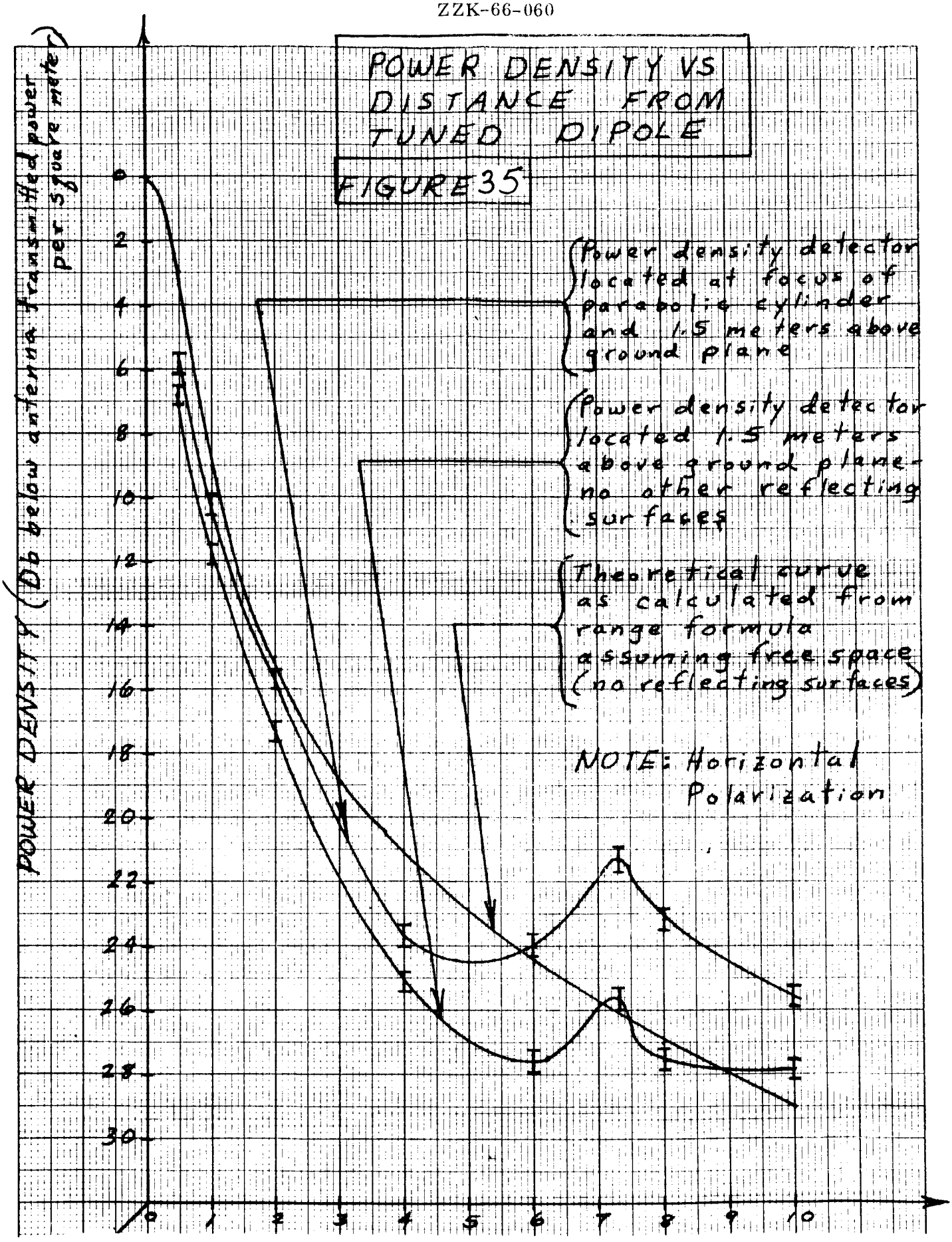

R = distance between transmitting dipole and receiving power density detector (meters)

$$(32) \qquad \text{Error} = \pm \frac{1}{2n} \sum_{k=1}^{n} \left(P_{R_{max}} - P_{R_{min}} \right)_k$$

where n = the number of values of R for which the experiment was performed

$\left(P_{R_{max}} - P_{R_{min}} \right)_k$ = the value at the k^{th} value of R.

Figures 34 and 35 can be generally interpreted as follows. The ground reflected wave will alternately cancel and reinforce the direct wave so that the plotted curve for power density with only a ground plane present should oscillate as R increases with respect to the calculated curve which accounts for only the direct wave. The maximum difference between the measured curve and calculated curve should give the maximum gain in power density due to the ground reflected wave. The curve that was plotted for the case in which both the ground plane and the parabolic cylindrical reflecting surface were present should exhibit a characteristic gain with respect to the curve which was plotted for identical conditions except that the parabolic reflecting surface was absent. Both of the measured curves should oscillate with respect to the calculated curve in the same manner. Reference to Figures 34 and 35 shows that the foregoing is indeed the case.

As predicted, Figure 34 results in greater "worst case" power gains than does Figure 35. The latter Figure will be dismissed in the subsequent discussion. It will be noticed that in Figure 34 the predicted behavior involving constant spacing of the two measured curves and the oscillation of the two measured curves with respect to the calculated curve does not occur except for values of $R \gtrsim 4$. The behavior for small R will now be explained. For small values of R the ground reflected wave's path length is very much larger with respect to the direct wave's path length than it is for large values of R. In other words, the free space attenuation (due to dispersion) of the ground wave is very much greater than that of the direct wave: therefore, the direct wave predominates and the ground reflected wave causes only a small perturbation on the total power density. For instance, when R = 1 meter, the free space attenuation of the ground reflected wave is 10 db greater than that of the direct wave. When R = 3 meters, the comparable

figure is only 3 db. The closer spacing of the two measured curves at small values of R can also be explained. When the distance between the transmitter and receiver is small, the transmitter is not uniformly illuminating the entire aperture of the parabolic cylindrical reflector. Therefore, the reflector's power concentrating capability is effectively reduced for small R. For $R \gtrsim 4$, however, the constant gain due to the "worst case" parabolic cylinder is evident as is the ground reflection's pronounced effect on the total power density level.

Since the gain due to the ground reflected wave was caused by a number of arbitrary factors including polarization, grazing angle and reflection coefficient of the ground at the test site, no general statement can be made about this gain insofar as a safety or test margin is concerned. The theoretical analysis presented earlier will be used as the basis for determining a safety margin due to ground reflections. However, it is mentioned that the maximum measured gain caused by the ground reflection was 4 db. This compares favorably with the 6 db "worst case" figure derived previously. The gain caused by the parabolic cylinder will be taken as a "worst case" gain and consequently, a safety margin due to the effects of energy concentration produced by reflecting surfaces other than the ground plane. For this purpose the average of the differences at the measured points between the two measured curves will be used for $R \geq 4$. The safety margin due to reflecting surfaces other than the ground plane becomes 4.4 db at 300 Mc. Therefore, the "worst case" value is 6.2 db (scaled up by a factor of 1.5 for the "worst case" reference frequency of 200 Mc).

A theoretical derivation of this safety margin will now be presented. Specifically, the power density along the focal line of a parabolic cylinder will be calculated and compared to the power density that would exist if the parabolic cylinder were removed. Let us consider the following diagram.

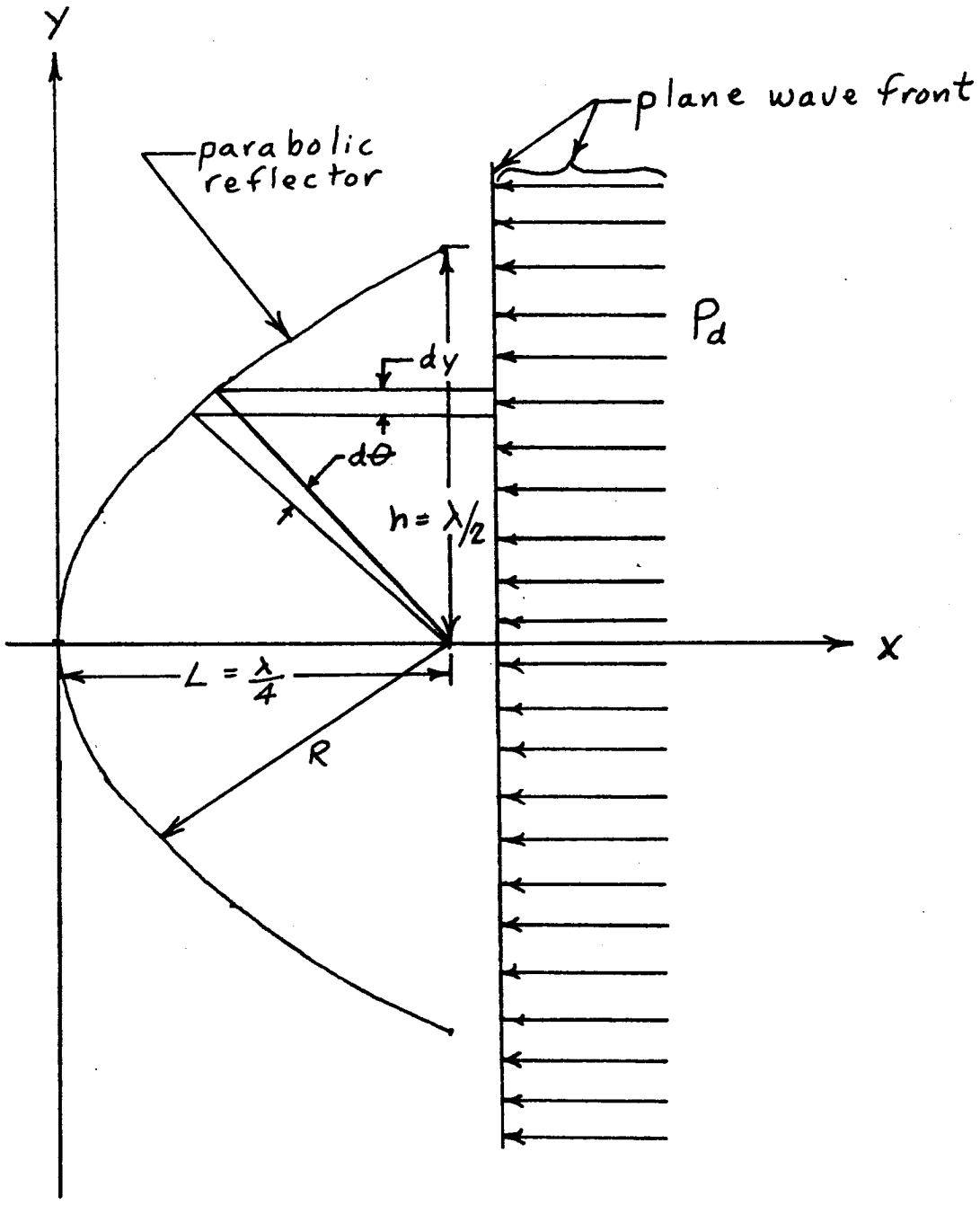

A plane wavefront of power density, P_d, is incident upon a parabolic cylinder of aperture dimension, λ, in the X-Y plane and an arbitrary aperture dimension in the Y-Z plane. The waves are all reflected so that they add in phase along the focal line in the Z-dimension at X = L. The incoming power reflected by an increment of the aperture is

(33) $$W = P_d \, dy \, dz$$

The incident incremental power along X = L can also be expressed as

(34) $W = U\, d\theta\, dz$

where U = power per unit angle per unit length in Z-direction. Now we have

$$P_d\, dy = U\, d\theta$$

(35) $$U = P_d \frac{dy}{d\theta}$$

$$y = R \sin\theta$$

$$R = \frac{2L}{1+\cos\theta}$$

$$\frac{dy}{d\theta} = \frac{2L}{1+\cos\theta}$$

(36) $$U = \frac{2L}{1+\cos\theta}\, P_d$$

Now we sum the power densities contributed from each angle.

Power density along focal line = power density contributed by parabola + power density that would exist in parabola's absence.

(37) $$P_{D\ total} = \int_{\theta=-\pi/2}^{+\pi/2} \frac{2L}{1+\cos\theta}\, P_d\, d\theta + P_d$$

$$= 2L P_d \left[\tan\frac{\theta}{2}\right]_{-\pi/2}^{+\pi/2} + P_d = 2L P_d\,[2] + P_d$$

Since $L = \lambda/4$

(38) $$P_{D\,total} = (\lambda+1)\, P_d$$

The gain provided by the parabolic cylinder is

(39) $$G_{refpc} = \lambda + 1$$

For a frequency of 200 Mc

(40) $G_{refpc} = 2.5$ or 4 db

The measured and calculated gains for both ground reflections and reflections caused by a "worst case" reflecting surface can now be summarized.

Measured	Calculated
$G_{refg} = 4$ db	$G_{refg} = 6$ db
$G_{refpc} = 6.2$ db	$G_{refpc} = 4$ db

The reason why the measured value of G_{refg} is less than the calculated value can be given as the fact that the test conditions were not "worst case" for ground reflections. It is suggested that the reason for the discrepancy between the measured and calculated values of G_{refpc} may have to do with the scattering properties of the parabolic cylinder. Strictly speaking the analysis that has just been performed is only accurate for the condition of specular reflection. Specular reflection only obtains when the dimensions of the reflecting surface are very much greater than a wavelength which is clearly not the case for the parabolic cylinder that has been described. When the dimensions of the reflector are not large compared to a wavelength, there will be scattering from the extremities of the reflecting surfaces, and the additional power density contributed by this scattering may account for the difference in the calculated and measured values of G_{refpc}. As shown in Skolnik[22], there are three regions of scattering.

1. Where the dimensions of the scattering object are very much less than the wavelength (Rayleigh region).
2. Where the dimensions of the scattering object are approximately the same as the wavelength (resonance region).
3. Where the dimensions of the scattering object are very much greater than a wavelength (optical region).

It is the third region to which specular reflection pertains, i.e., angle of incidence equals angle of reflection. In the resonance region it is possible to have scattering

such that the reflected radiation appears to have been scattered by a reflecting surface with area 5.7 db greater than the actual physical area[23].

This phenomenon bears a similarity to the phenomenon pointed out by Kraus and mentioned earlier; namely, that for reflectors with dimensions in the neighborhood of a wavelength, beaming or focusing can occur without the exact shape of the reflector being of great importance. In the experiment performed with the parabolic cylinder, one aperture dimension was exactly a wavelength. Therefore, it is probable that in addition to the power density collection afforded by the parabolic cylinder, there were also observed resonance scattering effects. Consequently, the appropriate safety margin to account for the effects of energy concentration due to focusing, beaming and resonance scattering of radiation is stated as 6 db.

8.2 Uncontrolled Factors in Simulation Environment. The possibility of reflections from test consoles, building stanchions and ancillary equipment located within the testing room was considered. The dimensions of the object compared to the wavelength of the incident radiation determine whether the reflected radiation will be scattered diffusely, or reflected specularly, or beamed in some manner. These three possibilities depend on which scattering region the dimensions of the object under consideration correspond to as discussed in the previous section. Since the resonance region was discussed there, only the two remaining regions will be discussed here. If the dimensions of an object are small compared to a wavelength or its surface is rough where the roughness is of the order of a wavelength, incident radiation will generally be reflected or scattered in all directions. This phenomenon is called diffuse scattering. On the other hand, if the dimensions of an object are large compared to a wavelength, and the surface is smooth compared to a wavelength, incident radiation will be reflected such that the angle of reflection equals the angle of incidence and the dispersion remains the same. This is called specular reflection. When radiation is scattered diffusely, the radiation reflected in any particular direction is greatly reduced in intensity. In particular, for a given incident power level, the maximum reflected radiation in any direction is a minimum when the incident radiation is scattered isotropically. As an illustration of diffuse scattering and specular reflection, let us consider Figure 36.

FIGURE 36

SPECULAR REFLECTION AND DIFFUSE SCATTERING

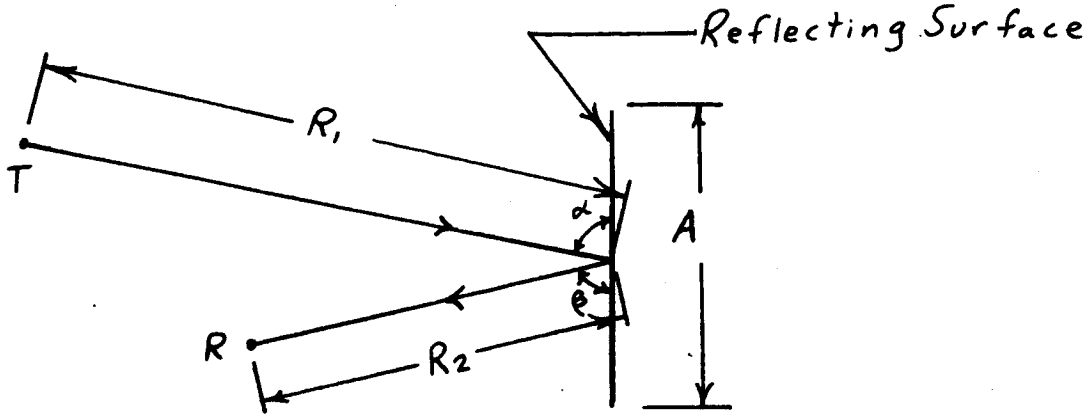

A - Specular Reflection

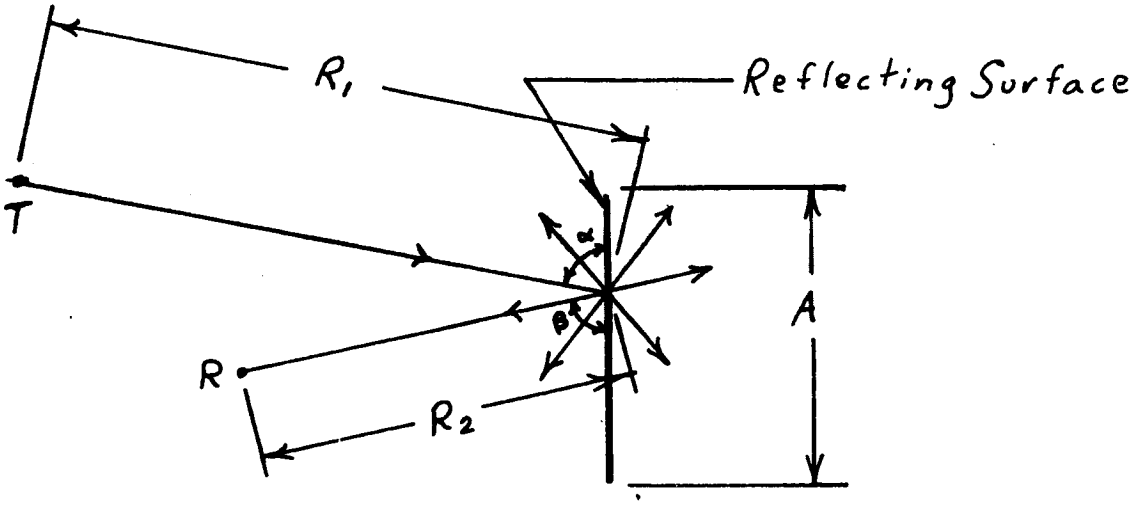

B- Diffuse Scattering (Isotropic)

In Figure 36A the transmitter, receiver and reflecting surface are of exactly the same dimensions and are located in exactly the same position relative to each other as in Figure 36B. Let it be desired to calculate the power density levels at R in Figures 36A and B. The following formulas are applicable.

$$(41) \qquad P_R = \frac{P_T G_T}{4\pi (R_1 + R_2)^2} \qquad \text{(specular reflection)}$$

Diffuse scattering:

$$(42) \qquad P_R = \frac{P_T G_T}{(4\pi R_1 R_2)^2}$$

The justification for the first formula is found in Reed and Russell[24]. The justification for the second formula is as follows.[25] According to formulas well known in the radar field, the power density of an echo signal at the radar is[26]

$$(43) \qquad \frac{P_T G_T \sigma}{(4\pi R^2)^2}$$

R = distance to target

σ = radar cross section.

The similarity between gain and radar cross section has been noted previously. In fact, aside from the consideration of units, they may both be interpreted in the same way.

A reflecting surface may be thought of as a repeater, a combination receiving and retransmitting antenna. It has characteristic reception characteristics including aperture and beamwidth. It also has characteristic transmitting characteristics including gain and direction. In this interpretation the power density at a point after one reflection has units of watts per square meter per square meter of reflecting surface. If the reflecting surface is an isotropic reradiator with an effective aperture of one square meter, $\sigma = 1$ and

$$P_{R_2} = \frac{P_T G_T}{4\pi (R_1)^2 \, 4\pi (R_2)^2} \tag{44}$$

R_1 = distance from transmitter to reflecting surface

R_2 = distance from reflecting surface to point of measurement.

It must be remembered that there is a 1 m^2 factor understood in the numerator of the formula (44). Without this the units would be incorrect. This represents an approximate upper bound on the area which will scatter diffusely in the frequency range under consideration (>200 mc). Consideration of the maximum value of P_{R_2} in this way will facilitate the comparison between specular reflection and diffuse scattering which follows.

The ratio of power densities at a point caused by a specularly reflected wave, P_{Rspec}, and a diffusely scattered wave, P_{Rdif}, which have both traveled the same total distance is

$$\frac{P_{Rspec}}{P_{Rdif}} = 4\pi \left[\frac{R_1 R_2}{R_1 + R_2} \right]^2 \tag{45}$$

or

$$P_{Rspec} = 20 \log \frac{\sqrt{4\pi} R_1 R_2}{R_1 + R_2} \text{ db above } P_{Rdif} \tag{46}$$

where the units of R_1 and R_2 are meters if the power densities are in units of watts per square meter.

It can be seen that P_{Rspec} is a minimum with respect to P_{Rdif} when $R_1 = R_2 = 1/2R$

$$P_{Rspec}(\text{min}) = 20 \log \frac{\sqrt{\pi} R}{2} \tag{47}$$

Let it be assumed that power densities contributed by diffuse scattering can be neglected compared to those contributed by specular reflection if

(48) $P_{Rspec} > 3$ db above P_{Rdif}

When $P_{Rspec} = 3$ db, R = 1.6 meters. Therefore, if $R \gtrsim 2$ meters, diffuse scattering can be neglected compared to specular reflection. Since the minimum distance from the transmitting test antenna to the test specimen has been suggested to be three meters, it stands to reason that power densities due to reflections from objects small compared to a wavelength (diffuse scatterers) can be neglected not only with respect to specular reflections but also with respect to the direct wave. The criterion for determining whether an object has dimensions small compared to a wavelength is Rayleigh's criterion of roughness:

(49) $\ell \sin \theta < \frac{\lambda}{8}$

ℓ = dimension of object in plane of propagation direction and field intensity vector of incident radiation

θ = angle of incident radiation

λ = wavelength.

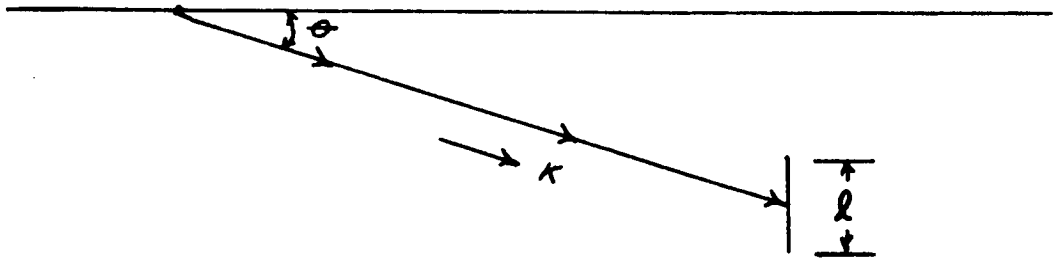

For example, if the frequency in concern is 300 Mc and the angle of incidence is greater than 7.2°, objects in the testing room with dimensions smaller than 1 meter do not have to be considered. This means that any stanchions, consoles, tools, etc. of small dimensions will not affect the power densities in the testing room. Since it is assumed that the source of power in the simulated RF radiation test will be aimed

at the spacecraft, any radiation that does not illuminate the spacecraft (which is assumed to absorb or scatter all radiation incident upon it) will either strike a small object obliquely and be scattered diffusely or will strike the object normally and be reflected normally. In either case the power densities in the region of the spacecraft will not be affected.

In considering reflections from surfaces of dimensions large compared to a wavelength, the ratio of power density levels at a point of the direct wave, P_d, and the reflected wave P_R, respectively is,

$$\frac{P_d}{P_R} = \left(\frac{R_1 + R_2}{d}\right)^2 \tag{50}$$

or

$$P_d = 20 \log \frac{R}{d} \text{ db above } P_R \tag{51}$$

where

d = distance from transmitting antenna to point in concern

R_1 = distance from transmitting antenna to reflecting surface

R_2 = distance from reflecting surface to point in concern

$R = R_1 + R_2$

The criterion that perturbations of total power density will be neglected if $P_d > 3$ db with respect to P_R will now be used. If $P_d > 3$ db, $R > 1.4\ d$. The application of this statement can be visualized by the following. If the distance from the transmitting test antenna to a large object in the testing room such as a wall plus the distance from the object to the test specimen is greater than 1.4 times the distance from the test antenna to the test specimen, then reflections from the object will not perturb the power density level in the vicinity of the test specimen. It must be remembered that the foregoing is applicable for only one reflection. If the testing room is such that there are many reflections with a net concentration of energy in the vicinity of the test specimen, then some other analysis must be made. Specifically, an analysis could be made relating attenuation of the waves by non-perfect reflecting surfaces and the dimensions of the

testing room to the power density levels created at a point by the sum of the reflected waves. The net energy dispersion and concentration characteristics of a particular set of boundary surfaces would be included in the analysis. Reference to the literature can be made for work in this area.[27,28]

One item which wasn't included in the work statement but which is appropriate to be included in this section is the subject of which test antenna is optimum for use in simulating an RF source in the laboratory environment.

The guidelines for choosing an antenna should include the following considerations.

1. The beamwidth of the antenna should be narrow enough so that rays are not propagated in angles at which they will not strike the spacecraft, but may strike reflecting surfaces resulting in interfering rays which might cause a change in power density levels at the spacecraft.

2. The antenna should direct a beam of uniform intensity which diverges as little as possible and whose beamwidth is large enough to fully illuminate the spacecraft so that the waves impinging on the spacecraft are plane and will create as little variation as possible in power density over the dimensions of the spacecraft.

3. Especially if high power densities are required, the beam of the transmitting antenna should be as narrow as the dimensions of the spacecraft permit and as directional as possible so that optimum use of the power delivered to the antenna for the purpose of creating power density levels can be made.

8.3 Review of Test Margins and Recommendations. It was mentioned in the work statement that test margin levels of 10 db and 6 db are being considered for proof test model spacecraft tests and flight spacecraft, respectively. With this in mind, a few words can be said about the philosophy of test margins as they are used in the electromagnetic compatibility field. The basic philosophy is that uncertainties arising from all sources can be treated by assuming the worst possible situation they might

create. A comparison of this worst case situation with the nominal situation due to known causes results in the testing or safety margin. In an RF radiated susceptibility systems test the uncertainties arise from the following sources:

1. Lack of knowledge of the power densities and frequencies that the spacecraft might be subjected to in its actual environment.
2. Lack of knowledge concerning the reflecting surfaces in the spacecraft's environment and how they might reshape, redirect, rebeam and refocus the waves incident upon them.
3. Lack of ability to control the testing environment because of
   a. Inability to simulate frequency conditions,
   b. Inability to simulate power conditions,
   c. Inability to simulate radiation conditions -- beaming, polarization, direction of propagation, and
   d. Inability to control and predict reflecting surfaces in laboratory.

As our knowledge of formerly unknown quantities increases, the more accurately we can predict the total environment and the less we are forced to depend on the testing or safety margin. As our ability to simulate the environment increases, the more we can decrease the test margin resulting from inaccuracies and limitations of our test equipment.

It has been demonstrated analytically that the worst case power density level at a point due to ground-reflected waves is 6 db greater than the free space level. It has also been demonstrated both from theoretical considerations and from actual measurements that there can be as much as a 6 db increase in power density levels due to nearby reflecting surfaces for frequencies greater than 200 Mc. The possibility of beam forming by reflecting surfaces remote from the point under consideration was considered from the standpoint of radiation scattering from a reflecting surface as applied in the radar field. A pertinent reference was quoted in which it was shown that a maximum of 5.7 db gain or increase in the effective cross section of a particular reflecting

surface was possible. From these considerations it seems reasonable to conclude that an adequate safety margin would be 6 db for the effects of ground reflections plus 6 db for the effects of all other reflecting surfaces. These figures represent the maxima of the respective calculated and measured values. It is concluded that a safety margin of 12 db is adequate to allow for fluctuations in the actual environment of the spacecraft. If enough information is known so that the effects of ground reflections can be taken into account explicity, then this figure may possibly be reduced.

Directing our attention toward the simulating environment (test laboratory), a power density detector has been developed and calibrated with an accuracy of 2 db. By using such a device no safety margin has to be assumed for the random reflections in the simulating environment. Adding 1 db for equipment stability and calibration considerations, a total of 3 db will be taken as the safety margin due to effects of the simulating environment.

The total safety margin for a completely adequate test will be the sum of the margins due to each of the factors considered which is 15 db. This margin can be reduced by 6 db if the configuration of the launch site is such that the only possible reflecting surfaces are located a distance large compared to a wavelength from the spacecraft and the effects of beaming from distant reflecting surfaces can be neglected. The former assumption is dependent upon a knowledge of the configuration of the launch site and the latter can be made plausible by the following argument. Since the beaming surface would be located near the ground, it is very probable that self-interference and attenuation effects would be produced by the terrain intervening between the surface and the spacecraft. In order to see in which case the effects of reflections from reflecting surfaces other than the ground plane can be neglected, let us consider the following diagram.

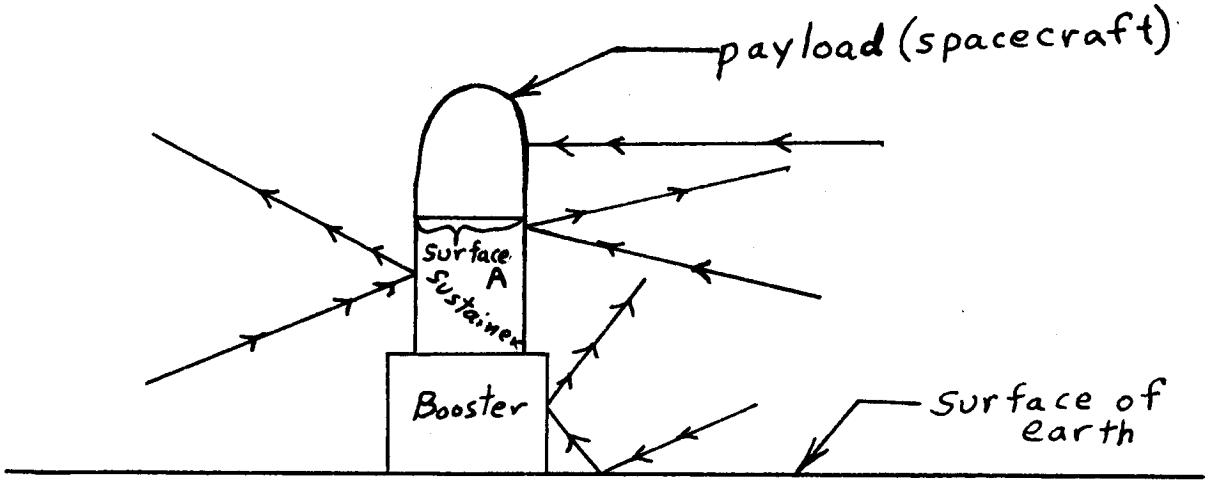

The skin of the booster and sustainer is assumed to be perfectly reflecting. The payload is assumed to be perfectly absorbing. The payload is mounted flush with the adjacent stage. As long as surface A is considered non-reflecting, there is no possible way for reflections from the outside of the sustainer or booster to reach the payload. Only reflections from inside the missile system could reach the payload and since only radiation from external known radiators is being considered in this study, it will be assumed that there are no sources of radiation inside the booster or sustainer. Of course, unintentional inductive radiation from components or wires in the booster or sustainer might very well exist, but these effects are without the scope of the type of test that is being considered here. If there were other equipment surrounding the payload and missile system, such as a gantry or crane, this equipment might conceivably form a worst case reflecting surface resulting in an increase in power density if it were located close enough to the payload. If it were a greater distance than λ max (the largest wavelength in the environment under consideration) away from the payload, it would not be considered likely to be capable of concentrating sufficient power density over a large enough aperture to cause a situation that might result in an RF susceptibility. If the above assumptions and constraints hold the test margin could be taken as 6 db for ground reflections plus 3 db for inaccuracies and errors in calibration of the test equipment. Rounding this figure off to 10 db provides an extra margin of safety to cover any considerations that might have been overlooked.

It is recommended that the 10 db safety margin be used on both proof test model spacecraft and flight spacecraft. The only rationale connected with lowering the safety margin for testing of flight articles is that, assuming the safety margin represents an overtest which results in RF overstressing, the reliability of the flight article can be improved by decreasing the over-all power density levels in the testing environment, thereby reducing the RF overstress. It should be pointed out that RF overtest can only possibly exist when the safety margin is chosen such that the tested article would never experience, even in a worst case environment, the power density level resulting from nominal plus safety margin levels. In this sense a safety margin represents overtest. However, if the safety margin is chosen only to represent worst case conditions that the article might possibly encounter, then the power density level resulting from nominal plus safety margin levels does not represent an overtest and, therefore, should be used in testing all articles. If the safety margin results in RF overstress, then the system is underdesigned for its environment and should be exposed as such during testing. It has been shown that the safety margin suggested in this paper is based strictly on worst case conditions. Both proof test model and flight spacecraft should be subjected to these conditions because the design of the system should be such as to provide for system operation in "worst case" environmental conditions and also unhampered reliability after passing through a normal testing cycle.

A later section will consider the effects on electronic components due to RF overstressing. It will be argued there that there should be no adverse effects on electronic components which are subjected to RF power densities of great intensity compared to nominal operating conditions unless these effects are caused by the movement of electrons which has been caused by the coupling of energy from the field. In this case the cause and usually the effects should be readily identifiable. It should be emphasized, however, that should there by any adverse effects on electronic components resulting from power density levels imposed during testing which represent worst case environmental conditions, these adverse effects should be treated as a susceptibility or failure of the components due to underdesigning. If the time of exposure is critical in producing a failure, then the time of exposure to the worst case environment must be considered.

In this case the system should not be exposed a longer period of time in the test environment than it would be exposed in the actual environment in order that overtesting not result.

8.4 Statistical Approach To Establishing Test Margins. To a certain extent statistics can be employed in dealing with the problems that have been considered in the course of this study. Specifically, statistical techniques were employed in the experimental measurements phase of this study involving calibration of the power density detector (developed during this study) and measurements relating to increase in power density due to reflections from a parabolic cylinder. Statistics were used to improve the accuracy of the measurements by effectively averaging out random errors.

The theoretical considerations are the following. Whenever a quantity is a function of two or more independent variables and there is some uncertainty of a random nature associated with one of the variables, the quantity can be measured as a function of the accurate variables and averaged over the uncertain variables with the result that the inaccuracy is integrated out. Let us consider the following formula.

$$P_R = \frac{P_T G_T}{4\pi R^2}$$

Let there be assumed some random inaccuracy, ΔP_T, associated with the power setting P_T, but that R can be determined as accurately as necessary. We design an experiment for which it is desired to measured P_R as a function of R. If we set P_T at an arbitrary value and perform all the measurements, our results would be accurate within ΔP_T. However, if at each value of R, measurements are made for n values of P_T and P_R is normalized by dividing by P_T, the resulting curves can be averaged together with the result that, as $n \to \infty$, $\Delta(P_R/P_T) \to 0$. The preceding example can also be worked through assuming $\Delta P_T = 0$ and $\Delta R = \varepsilon$.

In calibrating the power density detector, the power density calculated from the formula,

$$P_R = \frac{P_T G_T}{4\pi R^2} ,$$

was plotted against the reading obtained on the readout device for the power density detector, a DC voltmeter. This measurement was performed for different values of P_T and R and for vertical and horizontal polarization. The resulting curves were then averaged to eliminate random errors due to polarization misalignment and random errors in R and/or P_T. By so doing a more accurate calibration was obtained. Another set of measurements was performed in which a field intensity measuring receiver was substituted for the power density detector. In this case, random errors due to fluctuations and inaccuracy of calibration of the receiving equipment were also averaged out.

In the measurements involving the presence and absence of a parabolic cylinder placed such that power density was measured at the focal point, statistical averaging was also used. Several values of P_T were used at each R and the curves averaged over P_T. The final curves were plotted with power density in db below P_T as the ordinate and R as the abscissa. This averaging tends to eliminate errors associated with change of the test conditions with time since the tests were performed at different times and also errors due to settings of P_T. Random errors associated with R can be eliminated to some extent by drawing a smooth curve through the points obtained from the averaging procedure described above. By eliminating random errors associated with the test set-up, we are in a position to more confidently predict the change in power density levels produced by the focusing effect of the parabolic cylinder, itself. To the extent that the parabolic cylinder represents the worst case power density concentrating reflecting surface (which we have considered earlier), it can be said that an accurate test margin has been experimentally determined which holds for the effects caused by reflecting surfaces. In general, statistical approaches can be used to improve the accuracy of experiments and to single out effects due to one particular cause. A somewhat different approach to the problem using statistical techniques is found in the literature[29]. In general, when a certain quantity of interest is a function of several other quantities some of which have completely predictable behavior and others of which exhibit random behavior, a probability distribution for the quantity of interest can be constructed. A decision then has to be made as to what will be considered the value of the quantity of interest based upon the properties of the probability distribution. In the above examples,

it was decided that the mean of the values of the quantity of interest was the best estimation of that quantity. This is a good assumption when the errors are of a completely random or Gaussian nature. An example of a problem that might be of interest is the following. Let us assume it is desired to find the mean gain due to ground reflections over the volume of the spacecraft according to the following equation.

$$P_d = \frac{P_T G_{mean}}{4\pi d^2} \tag{52}$$

According to a formula derived earlier

$$P_R = \frac{P_T G_T}{4\pi r_1^2 r_2^2} \left[|\gamma|^2 r_1^2 + r_2^2 + 2 |\gamma| r_1 r_2 \cos(\theta - \phi) \right] \tag{27}$$

In this formula, P_R is a function of spacecraft height above the ground and lateral distance from the transmitter. It can be seen that

$$E(G) = E\left(\frac{G_T d^2}{r_1^2 r_2^2} \left[|\gamma|^2 r_1^2 + r_2^2 + 2 |\gamma| r_1 r_2 \cos(\theta - \phi) \right] \right) \tag{53}$$

where E(G) is the expectation of G which equals the mean value.

The technique for solving the problem is to find the probability distribution for G - p(G). This is done by assigning to a certain possible value of G, i.e., G_1, a probability, $P(G_1)$, which is the ratio of the volume of space occupied by the spacecraft in which the value of G is G_1 to the total volume of space occupied by the spacecraft. Then the mean value of this probability distribution is taken as the representative gain over the entire volume of the spacecraft and is used in Equation 52.

A computer program using a Monte Carlo technique would be useful in finding p(G). The general procedure would be as follows:

1. Assign numerical values to the points within the dimensions of the spacecraft and determine boundary values.
2. Generate a pseudo-random number.

3. If this number corresponds to a point that lies within the dimensions of the spacecraft, substitute the coordinates of the point (which determine r_1, r_2 and θ) into the expression for G and evaluate G. If the number corresponds to a point outside the dimensions of the spacecraft, go to the next number.
4. Iterate the procedure a large number, N, of times.
5. Record each value of G and keep a running record of the number of times each value is calculated.
6. Assign to each value of G a probability which is the ratio of the number of times that value was calculated to the total number of iterations.
7. Find the mean value of G according to

$$E(G) = \int_{G_{min}}^{G_{max}} G' p(G') \, dG'$$

For the purposes of this report it was considered that the maximum value of G over the volume of the spacecraft rather than a statistical average was more useful in establishing a test margin.

9. RF OVERSTRESS AND ELECTRONIC SUSCEPTIBILITY

9.1 General Remarks. An extensive literature search was conducted to find material on this subject. The search consisted of three parts: (1) a manual search of the literature filed in the catalogs of General Dynamics Convair; (2) a computerized search of NASA International Aerospace and Scientific and Technical Aerospace abstracts and reports; (3) a DDC search conducted at Alexandria, Virginia. The results are compiled in Appendix X. Much of the literature touches on the problem in concern here obliquely or incompletely. The problem can be stated as, 'will there be any degradation of performance or reliability of a system or the components thereof after it has been subjected to RF fields of high power density levels?' If the answer is 'yes', the system is said to have been RF overstressed.

RF overstressing will be defined as an irreversible process which changes the physical nature of the electronic components. Contrasted with this definition is the definition of RF radiated susceptibility: an undesired electronic response to an RF radiated stimulus such that when the stimulus is removed the electronic component or system returns to the state it was in before the stimulus was applied. In general, it can be seen that susceptibility is strictly an electronic phenomenon whereas RF overstress is a more general physical phenomenon.

Before the phenomenon of RF overstress is considered, the subject of electronic susceptibility will be explored in detail.

9.2 Electronic Susceptibility. Without loss of generality it can be assumed that an electronic circuit can be characterized by an n port black box with n-k input ports and K output ports as in the following diagram:

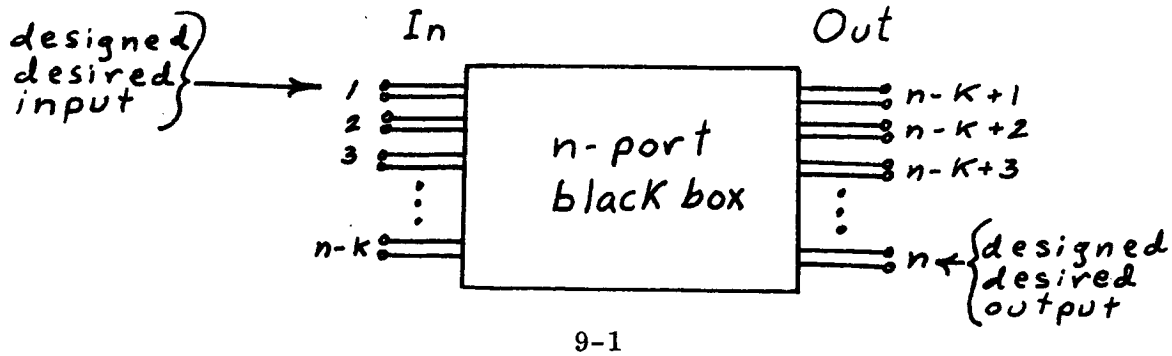

At this point it can be assumed that there is only one designed, desired input and one designed, desired output. This is true for most missile and spacecraft systems. The remaining n-K-1 inputs represent undesired coupling paths and unintentional pickup points in the system, and the remaining K-1 outputs represent interference generated by the circuit. Since we are considering here RF radiated susceptibility, we can restrict our attention to only one output port, the designed, desired one, since a consideration of interference generated by the system is without our scope. For our purposes the n-K-1 undesired inputs represent points in the circuit which transduce the RF radiated field resulting in electrical voltages and currents originating at these points. In general, each of the n-K input ports will be associated with the designed, desired output port by means of a transfer function $H_q(\omega)$ where $q = 1, 2 \cdots n-K$. These transfer functions will not be the same since the unintentional sources and source impedances will not be located at the same point in the circuit as the intentional source and source impedance. It is assumed that a designed, desired load is placed in series with the designed, desired output. In general, this load may be anything from a resistor to a receiver. The load will be treated in a generalized way, and the amplitude limiting characteristics of the circuit will be associated with it. At the same time the frequency limiting effects of the load will be lumped with those of the circuit in $H_q(\omega)$.

The generalized load is designed to respond to a certain class of signals and to give no response to signals outside this class. The class of signals that the load will respond to is limited by the sensitivity of the load to current and voltage amplitude levels. There is also a saturation level associated with the load above which level it will not respond.

The total of the amplitude limiting effects in the circuit will be associated with the functions, V(a) and C(a) which refer to voltage and current, respectively. In order to complete the description of the circuit, the generalized transducer and generalized observer are introduced. The generalized transducer is characterized by the functions α and β which represent response to voltage and current, respectively. The observer

is characterized by a response of "Yes" or "No" to every possible output from the transducer. A diagram of the generalized circuit is the following.

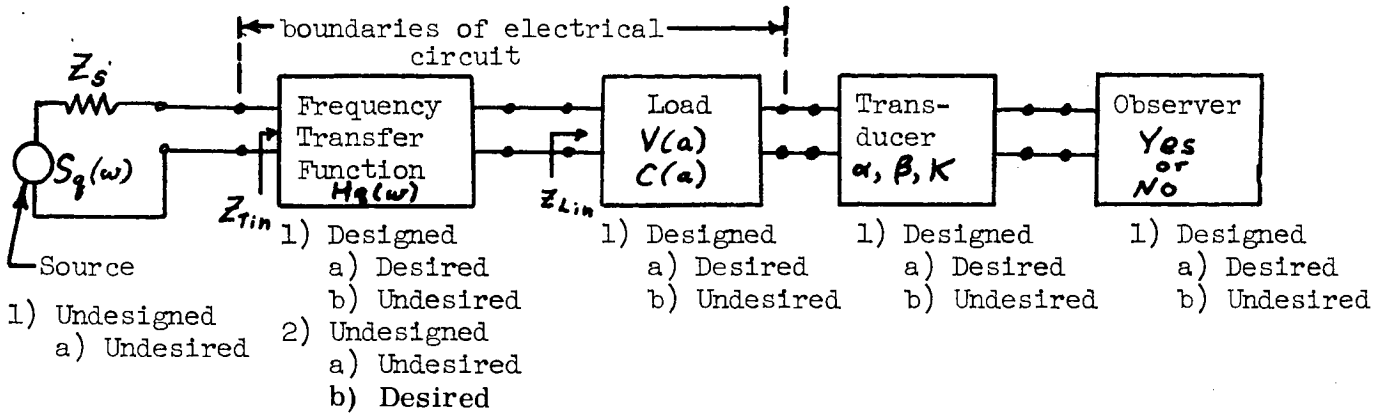

An important distinction can be made between designed and desired characterizations of a circuit. It is entirely conceivable that a designed circuit might have both desirable and undesirable aspects, of which some of each might be known and some unknown. The case of an undesigned circuit which has both desirable and undesirable characteristics is also possible. This might occur in a system where an adjacent piece of ancillary equipment provides natural shielding (desirable) but produces electromagnetic interference (undesirable). For this circuit the ancillary hardware constitutes an undesigned sub-circuit. In general, a circuit has both designed and undesigned characteristics both of which might be desirable or undesirable. If the designed, desired characteristics predominate, the circuit is well-designed. If the designed, undesired characteristics predominate, the circuit is poorly designed. If the undesigned characteristics of a circuit predominate, the circuit is underdesigned and, if these characteristics are desired, it is a fortuitous circumstance. In the above diagram the source and source impedance are considered undesigned and undesired since they are a result of the RF field in the vicinity of the circuit being coupled into it by an undesired path. The transfer function, $H_q(\omega)$ might be either designed or undesigned, depending on whether or not the RF is coupled into the circuit at the designed input or an undesigned input.

The further to the right attention is directed in the above diagram, the more the characteristics become designed as is the case for the load, transducer and observer.

Referring to the previous diagram and assuming far field conditions, we see that the source can be considered a voltage source. The source impedance reflects the coupling between the RF $\vec{E}$ field and the designed circuit. If $H_q(\omega)$ is assumed to be a voltage transfer function, then the input to the load will be

$$INL_V = \left[S_q(\omega) \frac{Z_{Tin}}{Z_{Tin} + Z_s} \right] H_q(\omega) \text{ volts} \tag{54}$$

and

$$INL_I = \left[S_q(\omega) \frac{Z_{Tin}}{Z_{Tin} + Z_s} \right] \frac{H_q(\omega)}{Z_{Lin}} \text{ amperes}$$

Since the previous two expressions are not independent, it is usual to work through a problem retaining only one of them and finding the other at any point by dividing or multiplying by the impedance at that point. For a reason that will become apparent later it is desired to carry along both expressions as we venture toward the final output of the circuit (the observer). We can do this very easily by expressing the input to the load as a column matrix,

$$\text{Input to load} = \begin{bmatrix} INL_V \\ INL_I \end{bmatrix}$$

with the understanding that at any point in our electrical circuit the voltage (current) can be recovered by multiplying the above matrix by the matrix, [10] ([01]). At the load the signal will be acted on by the matrix, $\begin{bmatrix} V(a) & 0 \\ 0 & C(a) \end{bmatrix}$ in the following manner:

$$\text{Output from load: } \begin{bmatrix} OUL_V \\ OUL_I \end{bmatrix} = \begin{bmatrix} INL_V \\ INL_I \end{bmatrix} \begin{bmatrix} V(a) & 0 \\ 0 & C(a) \end{bmatrix} \tag{55}$$

The nature of the functions V(a) and C(a) will now be considered. V(a) and C(a) can be considered as row matrices in which each of the elements is either a one or a zero such that a series of zeros, representing the region below the sensitivity threshold, precede a series of ones, representing the normal operating range. The series of ones is succeeded by a series of zeros representing the saturation range. INL_V and INL_I

are interpreted as n-dimensional column matrices in which all elements are zero except the one corresponding to the actual numerical value calculated for INL_V or INL_I. In general, the n^{th} element in either the one row or one column matrix represents a voltage or current level of n volts or n amperes. In the INL_I and INL_V matrices the actual value of voltage or current is entered as the element corresponding to the value. For example, if

$$INL_V = \left[S_q(\omega) \frac{Z_{Tin}}{Z_{Tin} + Z_s}\right] H_q(\omega) = 5 \text{ volts}$$

$$INL_I = \left[S_q(\omega) \frac{Z_{Tin}}{Z_{Tin} + Z_s}\right] \frac{H_q(\omega)}{Z_{Lin}} = 2 \text{ amperes}$$

then

$$INL_V = \begin{bmatrix} 0 \\ 0 \\ 0 \\ 0 \\ 0 \\ 5 \\ 0 \\ 0 \\ \cdot \\ \cdot \\ \cdot \end{bmatrix} \qquad INL_I = \begin{bmatrix} 0 \\ 0 \\ 2 \\ 0 \\ 0 \\ \cdot \\ \cdot \\ \cdot \end{bmatrix}$$

and if

$$V(a) = [00011100\cdots]$$

$$C(a) = [01111100\cdots]$$

corresponding to a normal voltage operating range of 3 to 5 volts and a normal current operating range of 1 to 5 amperes, then the output from the load will be

$$\begin{bmatrix} 5 \\ 2 \end{bmatrix}$$

It can be seen that a load that is sensitive only to voltage will have a C matrix all of whose elements are zero, and the converse is true for a V matrix all of whose elements are zero. Let us consider another example in which the load is nominally sensitive only

to voltage but has a spurious sensitivity to current without the normal operating range. The V and C matrices might be

$$V = [0011110000]$$

$$C = [00000000011]$$

It can be seen that for a load with these characteristics, the output will only be a function of input voltage until the voltage saturation region is reached. As the input levels are further increased, the output will become a function of input current.

The next block in the circuit diagram corresponds to the transducer. At this point we leave the electrical circuit. The transducer function is characterized by the matrix $[\alpha\ \beta]$ where α and β have the units response/volt and response/ampere, respectively, and response is a generalized unit which could be sound intensity, volts, etc. The output from the transducer, therefore, will be

$$\text{Output from transducer} = \begin{bmatrix} OUL_V \\ OUL_I \end{bmatrix} K\,[\alpha\beta] = K\alpha\,(OUL_V)$$

$$+ K\beta\,(OUL_I) \text{ responses}$$

The reason for carrying along both voltage and current in the development now becomes obvious. The possibility that the transducer may respond to both current and voltage has been allowed for. The generalized transducer might be a test instrument such as an oscilloscope, a built-in monitoring device such as a threshold detector, a loudspeaker, etc. α and β may vary from 0 to ∞ and represent the relative degree to which the transducer responds to voltage and current, respectively. The units of α and β are response per volt and response per amp, respectively. α and β are normalized such that $\alpha\,\beta = 1$. The total response to voltage or current is obtained by multiplying α or β, respectively, by the normalizing factor K. For instance, if the transducer were such that it had the following characteristics,

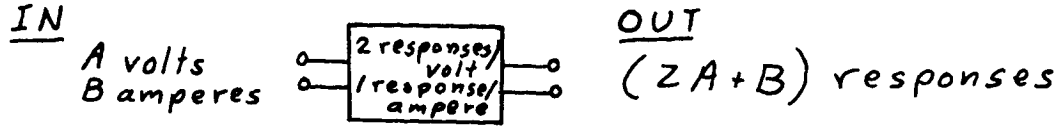

then

$$\frac{\alpha}{\beta} = \frac{2}{1} \qquad \alpha = +\sqrt{2}$$
$$\alpha\beta = 1 \qquad \beta = +\frac{1}{\sqrt{2}}$$
$$\alpha^2 = 2 \qquad K = \sqrt{2}$$

In general, if the transducer is such that there are m responses/volt and n responses/amp, then $K = \sqrt{mn}$ and $\alpha/\beta = m/n$. A few special cases will now be discussed. A piezoelectric transducer responds only to voltage.

$$\therefore \quad \begin{matrix} \alpha = \infty \\ \beta = 0 \end{matrix}$$

such that $K\alpha$ = M volts/volt = transfer characteristic of transducer.

A magnetostrictive transducer responds only to current.

$$\therefore \quad \begin{matrix} \alpha = 0 \\ \beta = \infty \end{matrix}$$

such that $K\beta$ = N amps/amp = transfer characteristic of transducer.

An oscilloscope responds only to voltage

$$\therefore \quad \begin{matrix} \alpha = \infty \\ \beta = 0 \end{matrix} \quad \text{and} \quad K\alpha = \text{M volts/volt}$$

Let us consider a device which responds to power such that the characteristic is

$$A\,\frac{\text{(responses)}}{\text{volt} \cdot \text{amp}}$$

Then

$$\alpha = \beta = 1 \text{ and } K = \frac{A}{2} \left(m = n = \frac{A}{2}\right)$$

It may be remarked that statements such as $K\alpha$ = M volts/volt while $\alpha = \infty$ can be interpreted by assuming that α is a delta function of weight M and the normalizing constant K is an operator which extracts the weight of the delta function.

After the transducer has produced a response, this response must be accurately observed or interpreted in order to say, for instance, that a desired function has occurred or that a susceptibility has or has not occurred. We can consider the actual response from the transducer as an element in an n-dimensional row matrix where all the other elements are possible, but are, in fact, responses which did not occur. The ideal observer then is an n-dimensional matrix such that the elements corresponding to incorrect choices are zero.

For example:

$$\underbrace{\begin{bmatrix} r_1 \\ r_2 \\ r_3 \\ \cdot \\ \cdot \\ \cdot \\ r_n \end{bmatrix}}_{\text{response}} \times \underbrace{[0000100\cdots000]}_{\text{ideal observer}} = \underbrace{r_5}_{\text{read-out}}$$

r_5 represents the actual response or the output of the transducer. There is a possibility for a non-ideal observer that there will be more than one element in the observational matrix that is one or that the element corresponding to the actual event will be zero. If this is so the state of the circuit will have been incorrectly interpreted.

It can now be seen that the analysis of a susceptibility depends on all the elements of the circuit. An example will now be worked out. Let us consider the following circuit.

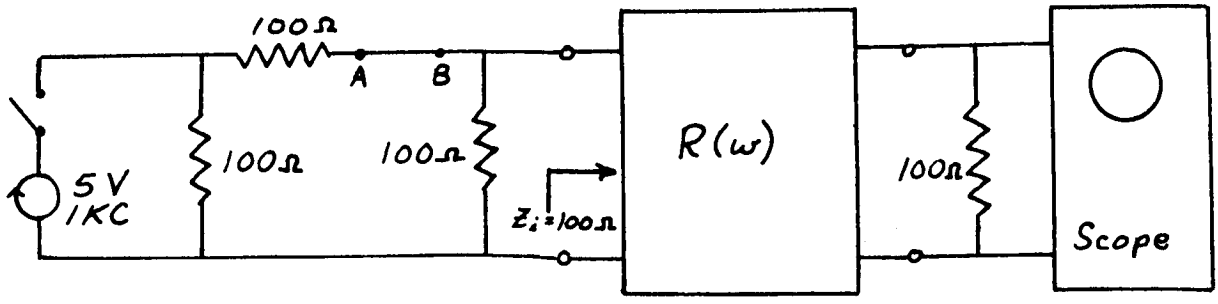

Let us assume that a radiative field with power density of 10 watts/meter at a frequency of 300 Mc impinges on the circuit over the length AB which is assumed to be 2 meters. According to Kraus[30], the power that can be absorbed by the circuit is equal to the effective aperture multiplied by the power density. To find the effective aperture of the length AB would require an analysis of a 2 wavelength end fed dipole involving a derivation of radiation resistance. Rather than perform the analysis, "worst case" assumptions will be used. Maximum power is coupled into the circuit when the radiation resistance of the antenna is equal to the resistance looking back into the circuit from the antenna terminals and the antenna losses are zero. The aperture so described is known as the maximum effective aperture. The maximum effective height of an antenna may be found from the radiation resistance, maximum effective aperture and wave impedance of the medium. The "worst case" maximum effective height would be

$$(h)_{\text{worst case}} = 2 \text{ meters}$$

Since for maximum power transfer the radiation resistance equals the resistance of the circuit as seen from the terminals AB, the radiation resistance is equal to 250 ohms. The circuit diagram can be redrawn as follows:

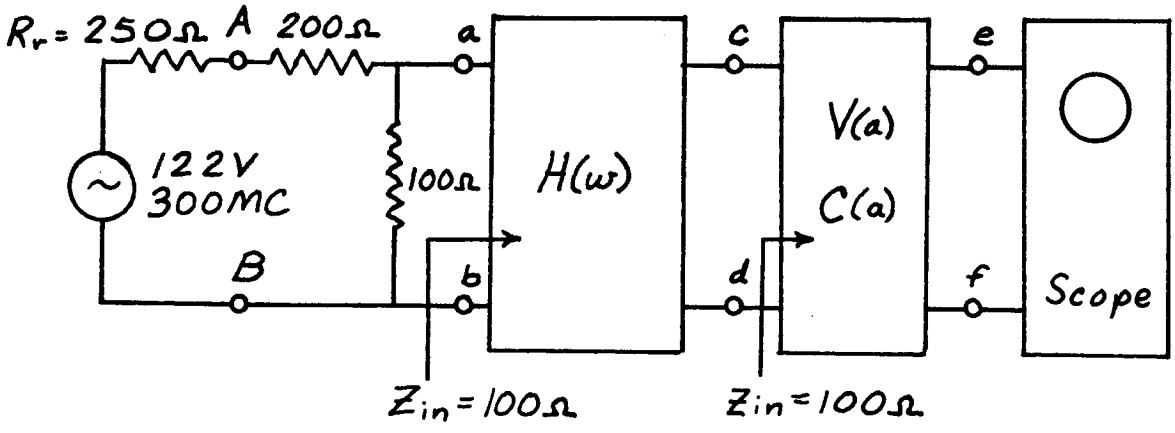

For "worst case" conditions, the voltage coupled into the circuit is

$$V = |\vec{E}|\, h = \left(\sqrt{P\, Z_w}\right) h = \left(\sqrt{(10)(377)}\right)(2) = 122 \text{ volts}$$

The voltage at the terminals AB will be

$$V_{AB} = (122)\left(\frac{1}{2}\right) = 61V$$

Let it be assumed that $H(2\pi\ 300\ M_c) = \frac{1}{2}$ and that the sensitivity and saturation points of the circuit are such that, at terminals cd, only voltages in the range, $4 \leq V \leq 20$ volts, and currents in the range, $.04 \leq I \leq .2$ amperes, can be measured. Furthermore, let it be assumed that the oscilloscope is responsive only to voltage (1 volt/volt) and that there is an ideal observer.

$$V(a) = [0_0 0_1 0_2 0_3 1_4 1_5 1_6 \cdots 1_{19} 1_{20} 0_{21} 0_{22} 0_{23} \cdots]$$

$$C(a) = \frac{1}{100}[0_0 0_1 0_2 0_3 1_4 1_5 1_6 \cdots 1_{19} 1_{20} 0_{21} 0_{22} 0_{23} \cdots]$$

$$[\alpha\beta] = [\infty\ 0]$$

such that

$$\alpha\beta = 1 \quad \text{and} \quad \begin{cases} K\alpha = 1 \text{ volt/volt} \\ K\beta = 0 \end{cases}$$

The remaining analysis will now be performed to determine if the circuit is susceptible.

$$V_{ab} = V_{AB}\left(\frac{50}{250}\right) = 12.2V$$

$$V_{cd} = V_{ab}\ [H\ (2\pi\ 300\ Mc)] = (12.2)\left(\frac{1}{2}\right) = 6.1V \approx 6V$$

$$I_{cd} = \frac{6.1}{100} = 0.061A \approx .06A$$

Since V_{cd} and I_{cd} are the voltage and current inputs to the load, INL_V and INL_I, respectively, the n-dimensional column matrices are now formulated where the n^{th} element represents n volts or n amperes.

$$INL_V = \begin{bmatrix} 0_0 \\ 0_1 \\ 0_3 \\ 0_4 \\ 0_5 \\ 6_6 \\ 0_7 \\ 0_8 \\ 0_9 \\ . \\ . \\ . \end{bmatrix} \qquad INL_I = \frac{1}{100} \begin{bmatrix} 0_0 \\ 0_1 \\ 0_2 \\ 0_3 \\ 0_4 \\ 0_5 \\ 6_6 \\ 0_7 \\ 0_8 \\ . \\ . \\ . \end{bmatrix}$$

$$V_{ef} = OUL_V = INL_V \times V(a) = 6 \text{ volts}$$

$$I_{ef} = OUL_I = INL_I \times C(a) = 0.06 \text{ amperes}$$

The transduced response is $\begin{bmatrix} 6 \\ .06 \end{bmatrix} K \left[\alpha\beta\right] = 6$ volts and the observed response is 6 volts. Therefore, the circuit is susceptible to both current and voltage although it was monitored only for voltage susceptibility. If I_{cd} had been greater than 0.2 amperes while V_{cd} was in the range, $4 \leq V_{cd} \leq 20$ volts, then the circuit would have been susceptible to voltage but not current due to a built-in current overload sensing mechanism, i.e., $I_{ef} = 0$. Similar problems may be solved and correlated with experimental results. It might happen that some of the parameters involved can be found most easily by doing experimental work such as irradiating a test circuit and determining susceptibility thresholds among other circuit responses.

9.3 RF Overstress. RF overstress may be interpreted as damage to a circuit caused by lack of heat dissipation, voltage or current levels which exceed the ratings of the circuit, or change in the electrical characteristics of the matter comprising the circuit. In general, the changes in the circuit caused by RF overstress can be structural, chemical or material. An example of structural damage is the melting and

running off solder due to lack of heat dissipation. An example of chemical change would be an increase in corrosive chemical activity due to high temperatures associated with lack of heat dissipation. An example of material damage is the change in the properties of a metal, dielectric or semiconductor due to voltage or current levels present that are great enough to interact with the bound electrons of the molecules of the material thus changing its electronic characteristics. Normally, electronics implies only conduction band electron activity which results in currents and voltages. However, an RF overstress involves change in circuit characteristics due to heat and/or interaction of circuit energy with bound electrons.

The mechanisms whereby RF energy is coupled from a field into an electronic circuit are the following:

1. Interaction with free electrons.
2. Interaction with bound electrons.

Type (1) is the normal method of coupling to an antenna used in communications. It does not necessarily involve RF overstress; in fact, RF overstress only occurs when the coupled energy is so great that circuit ratings are exceeded. The cause of the overstress is the movement of the electrons, and the cause of the movement is the RF field. Thus, the RF field is an indirect cause of overstressing. Type (2) provides a direct overstress caused by the RF field since any interaction with bound electrons will change the electronic properties of the circuit. Type (1) will usually result in a susceptibility in addition to circuit damage unless an overload mechanism is built into the circuit. Type (1) is readily identifiable by monitoring voltage and current levels in the circuit. Type (2) is more difficult to identify since a failure to operate normally is usually the only means of identification. It will be shown that the effects of Type (1) are the only cause of concern in an RF radiated test and that Type (2) can be neglected.

Type (1) will be considered first. Problems involving heat dissipation can be worked out. An example is the following. With the methods developed previously for the quantitative calculation of susceptibility, it is determined that a particular copper conductor will have a current of 20 amperes (DC) flowing in it. This copper conductor is AWG 18

gauge. Reference to charts of current carrying capacity[31] show there will be a 140° temperature rise in the conductor. The value of temperature rise plus ambient must not exceed the temperature rating of the conductor's insulation. Similarly, voltage breakdown and current ratings of circuit components can be used to determine if an RF overstress occurs.

In problems involving heat dissipation and breakdown, time is of the essence since these phenomena are usually determined by time-average quantities. For this reason it is possible to have very high peak power, or high voltages or currents for short periods of time and still have no problems so long as the average power, voltage or current is small enough. On the other hand electronic susceptibility is practically a non-time-dependent phenomenon since electronic circuits will generally respond almost instantaneously to a stimulus. The response time of an electronic circuit to a stimulus will now be considered. A circuit can be characterized by its impulse response function, which represents the output response versus time when an impulse is applied to the input. Borel's theorem states that[32] the response of a linear system to an arbitrary excitation (which is Laplace transformable) is the convolution of its impulse response function with the excitation or

$$g(t) = \int_{-\infty}^{+\infty} h(\zeta)\, f(t-\zeta)\, d\zeta \tag{56}$$

where

$f(t)$ = excitation or input function

$h(t)$ = impulse response function

$g(t)$ = response or output function

The nature of an electronic circuit is that it doesn't possess a memory longer than its impulse response function. Therefore, an electronic susceptibility is almost completely a threshold effect. If the excitation voltage or current exceeds a certain susceptibility level instantaneously, a susceptibility threshold will be reported by the observer. However, if the excitation approaches the threshold and remains near it for a long period of time, no susceptibility will occur unless the impulse response function is long enough

to sum up the excitations in adjacent time intervals. In analyzing a susceptibility we are interested in the maximum response in a circuit that can be produced at any instant of time. If this response exceeds the susceptibility threshold, a susceptibility has occurred. Let us consider Figure 37.

Figure 37A shows the case of a wideband excitation and a narrowband transfer function. The maximum output is dependent upon the amplitude and time duration of the input. Figures 37B and C show a wideband transfer function. The output is dependent on the amplitude of the input and whichever is the shorter, the excitation or impulse response time span. Figure 37D shows the "worst case" condition resulting in maximum output - narrowband excitation and narrowband impulse response function. If a susceptibility threshold is assumed, the situation depicted in 37D will be most likely to produce a level that reaches the threshold. The output level depends on the time span of the impulse response function and also the input level. It is assumed that the input time span is greater than or equal to the time span of the impulse response. If the maximum impulse response time span of any circuit in a particular environment is known, the minimum length of time that the circuit must be excited in order for any possible susceptibility to occur will, therefore, also be known. Using the expression found in Frederick Terman's book, "Electronic and Radio Engineering" on Page 289"

$$\text{rise time} = \frac{0.4}{B}$$

where

B = bandwidth

and assuming that the impulse response function rises and falls off at the same rate, the following relation holds:

time span of $h \approx 2$ (rise time)

The maximum time span of h will be found in the circuit with the narrowest bandwidth. Let it be assumed that the minimum intentional or unintentional bandwidth on a missile system is 100 cycles. Then the maximum time length of impulse response function of any circuit under consideration will be

$$\frac{2(.4)}{100} = 8 \text{ msec}$$

FIGURE 37

DIFFERENT COMBINATIONS OF INPUT AND TRANSFER FUNCTIONS AND CONSEQUENT MAXIMUM OUTPUTS

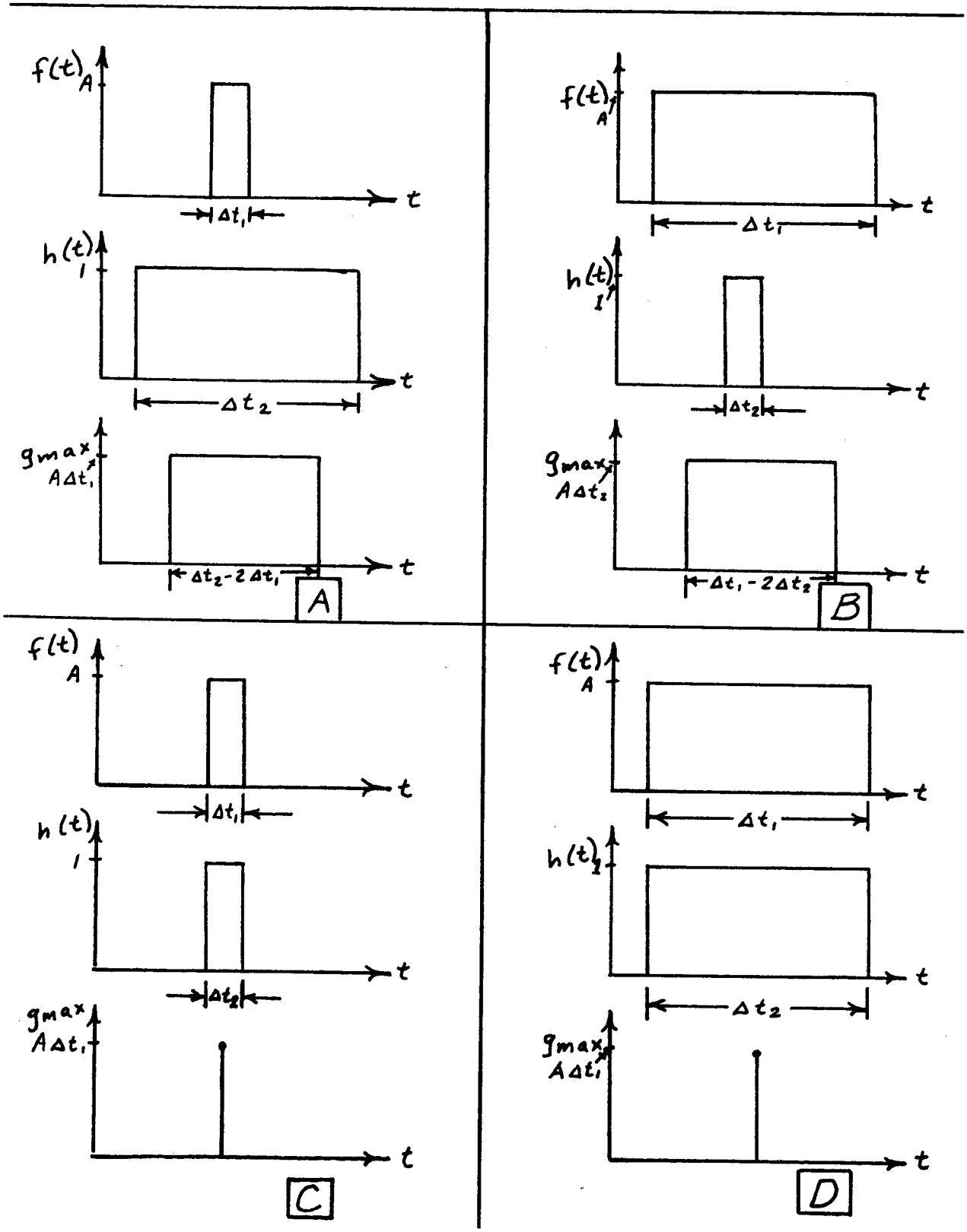

Therefore, it follows that every possible susceptibility will be discovered if a signal with the proper amplitude is applied for approximately 8 msec. For frequencies greater than 200 Mc, this time length is a few orders of magnitude greater than the time required to reach steady state so that transient effects can be neglected and it is assured that steady-state radiation occurs practically instantaneously. In an RF radiated susceptibility test, the maximum pulse length which the radiated signal must have is approximately 10 msec. There is no reason to perform the test for a longer period of time to find electronic susceptibilities. However, if the system's overall capability to withstand its environment is being tested, the system should be subjected to the RF radiation for a time equal to the "worst case" exposure time in actual environmental conditions. The additional failures of the system caused by increased time exposure are the result of RF overstressing of Type (1). In testing for RF overstressing of Type (1), circuits should be monitored for current, voltage and temperature.

In an attempt to dismiss RF overstressing of Type (2), the following discussion is presented. The direct interaction of electromagnetic fields with electronic circuits or matter in general is predicated on quantum mechanical principles. A well-known experiment which illustrates best the phenomena involved is the photoelectric effect[34]. The photoelectric effect is a process in which electromagnetic radiation is beamed at the "emitter" of a photocell. If the frequency of the radiation is higher than a certain threshold, electrons are observed to be emitted from the electrode. If the frequency of the radiation is lower than the threshold, no emitted electrons are observed no matter how high the incident power density is. Before the explanation of the photoelectric effect is stated, the concept of a "work function" of a metal is first developed. The following diagram depicts the energy relations at the surface of a metal.

There is a binding energy, $e\Phi$, of electrons to the metal. Φ is measured in volts and is called the "work function". $e\Phi$ is the additional energy that must be given to the most energetic electron in the metal in order to remove it and may be supplied by heat or electromagnetic radiation. The theory behind the photoelectric effect states that electromagnetic radiation can only eject an electron from the metal providing

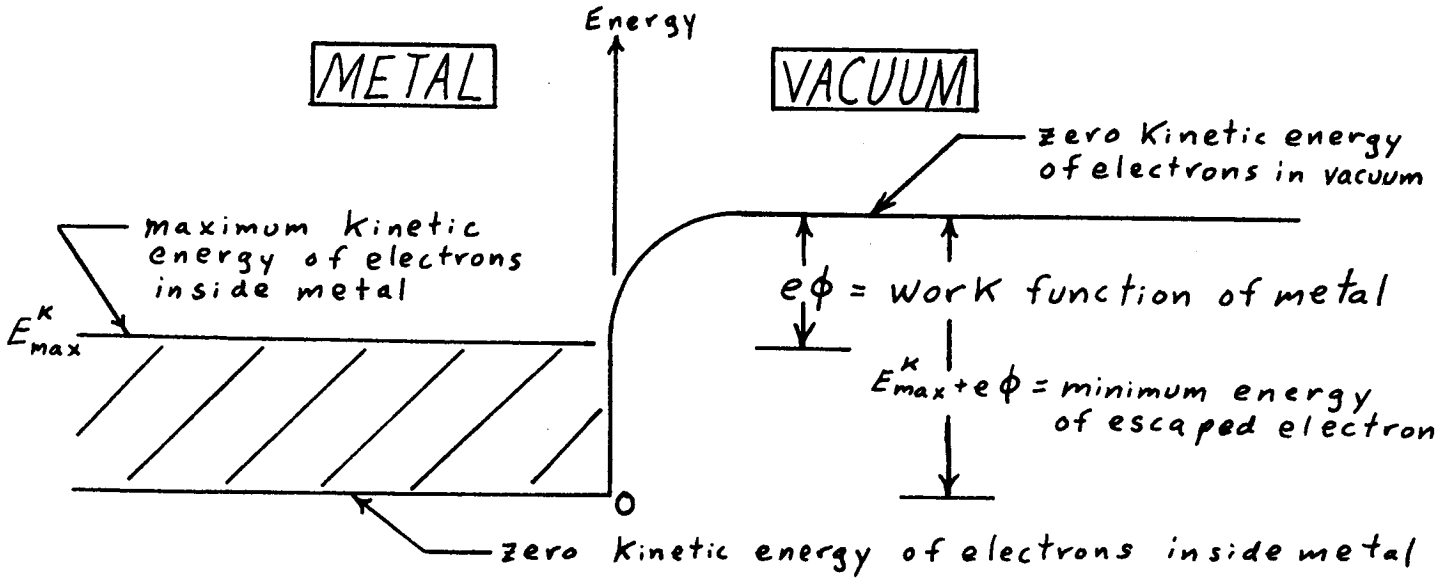

$$(hf)_{incident} > e\Phi$$

where

f = frequency

h = Planck's constant

Frequency not power density is the sole criterion for interaction of a field with a metal in a non-reversible manner.

An extension of these concepts is the band theory of solids which proposes that electrons exist in certain bands and can only change from one band to another if the frequency of incident electromagnetic energy is such that hf corresponds to the difference in energy of the two bands. Let us consider a metal, a dielectric and a semiconductor from the band theory point of view with regard to the following diagram.

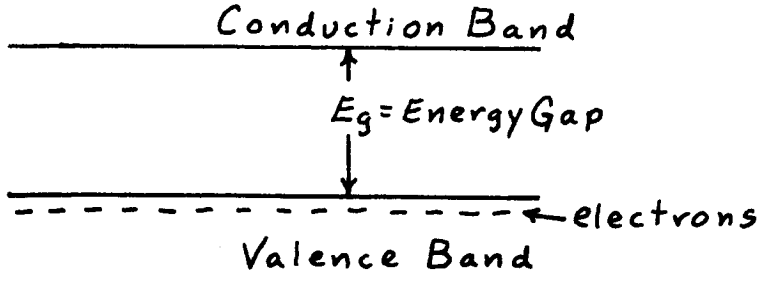

In a metal there are sufficient electrons to fill all the states in the valence band and partially fill the conduction band. Thus, there can be movement of electrons in the conduction band which account for most electronic phenomena. In a dielectric there are normally no electrons in the conduction band unless energy equal to the energy gap is supplied to an election in the valence band. This energy gap is usually quite large so that very high frequency radiation would be necessary to move electrons to the conduction band. In a semiconductor the situation is the same as exists in a dielectric except that the energy gap is smaller than in a dielectric and it is easier to supply the energy necessary to raise electrons to a conduction band. The frequency of radiation necessary to move electrons among energy bands or to overcome the surface barrier of a material is considerably higher than the RF range.

For example, the ionization potential of the least strongly bound electron of lithium, the most active metal, is 5.4 eV. The frequency of radiation necessary to free the most loosely bound electron would be found as follows:

$$hf = 5.4 \text{ eV} = (5.4)(1.6 \times 10^{-19}) \text{ joules}$$

$$f = \frac{(5.4)(1.6 \times 10^{-19})}{6.625 \times 10^{-34}} - 1.3 \times 10^{15} \text{ cps}$$

since

$$h = 6.625 \times 10^{-34} \text{ joule-sec}$$

This frequency is considerably above the RF range. Therefore, it can be concluded that no matter how large the power density of incident RF radiation, there will be no coupling between an RF field and a circuit due to a coupling mechanism of Type (2). However, RF radiation may couple into a circuit by a Type (1) mechanism and increase the heat in the circuit until there is enough heat energy available so that quantum mechanical effects may be observed.

9.4 Summary and Conclusions. Now that a detailed study has been made of the nature of susceptibility and RF overstress, a comparison can be made between them.

An RF susceptibility is a purely electronic phenomenon involving time invariance of the circuit elements. On the other hand, RF overstress is a physical phenomenon resulting in changes with time of the characteristics of the circuit. It is concluded that the effects of RF overstressing can only be produced indirectly by the coupling of energy to free electrons. Concerning the coupling of energy, it is important to distinguish between an RF field and an RF potential. A very high field may exist in a region of a circuit without high voltages or potentials existing concomitantly. If there are no free electrons present in the material, a high field intensity will not produce a high voltage and will not harm the circuit in any way providing the frequency is in the RF range. However, if there are electrons present, a high field intensity will produce movement of electrons. These electrons will move in such a way as to reach the region of lowest potential by the path of least resistance. If there are several paths in parallel, such as metal and dielectric in contact, even the highly resistive paths will experience some current and a voltage potential will exist across them. As the field increases, the current increases in the highly resistive paths and causes voltage breakdown.

In summary, RF overstressing is the result of voltage and current levels that exceed circuit ratings and that are produced by energy coupled from an RF field. RF overstress produces a change in the properties of a circuit which endures after the stimulus is removed. The situation can be detected by voltage, current and heat monitoring devices and can be ameliorated by short time or pulsed testing. Electronic susceptibility is caused by voltage or current levels that cause an inadvertant response because operation threshold levels are exceeded. However, once the stimulus is removed the circuit returns to its original state electronically and remains the same physically.

10. SUMMARY, CONCLUSIONS AND SUGGESTIONS FOR FUTURE WORK

The purpose of this study was to suggest improvements in the performance of an RF raidated susceptibility systems test involving

1) calculations of power density at a point caused by a finite number of radiators with known characteristics;

2) the extent to which modulation characteristics must be reproduced in the laboratory

3) the rationale behind an adequate test margin.

In accordance with the work statement, an analysis of the following three transmitter systems was undertaken:

1) Azusa Mark II ground transmitter

2) Launch vehicle telemetry transmitter

3) AN-FPS-16 radar transmitter

Spectra were plotted for each case to show the amplitude versus frequency characteristics of the analyzed systems. It was hypothesized that the amplitude versus frequency characteristics of all cases analyzed could be reproduced in the laboratory using relatively simple apparatus and pulsed - CW modulation. The pulse width and amplitude can be varied to give the desired peak power and roll-off characteristics. The pulse repetition frequency can be adjusted to give a relatively discrete or continuous spectrum. Examples were worked out showing how to calculate the required pulse parameters in order to simulate an arbitrary signal. The Gaussian noise quality of FM-FM telemetry systems was demonstrated. An adequate simulation in this case would be band-limited white noise. Future work should experimentally verify the adequacy of using pulsed CW to replace an arbitrary waveform for the puspose of inducing susceptibilities. Unfortunately, it was found that a supposedly FM-modulation susceptible circuit furnished by JPL was in fact susceptible to CW with average power level determining the

threshold. Although this particular circuit was fully analyzed with suggestions for eliminating the susceptibility incorporated in the report, it was not a sufficient test item for proving or disproving the fact that pulsed CW might be sufficient for susceptibility inducement. Hopefully, future work of an experimental nature in which demodulators of various types are subjected to radiated waveforms of various types and their responses measured, will demonstrate the usefulness of a pulsed-CW simulation. Future analytical work should also be undertaken in the useage of a white-noise source to simulate broadband radiators. Analysis of the spectral characteristics of white noise after it has undergone transformations such as band-limiting and modulation should be carried out and feasible experimental hook-ups, in which parameters of the simulating signal can be adjusted to create a spectrum corresponding to an environmental signal, studied. A list of equipment for use in creating simulating signals in the laboratory is included in the report.

A calculation of the power density level at a point resulting from the direct and ground-reflected waves of a known transmitter was performed. It was shown that a power density could be created at a point which was 6 db greater than the value that would have been calculated using the range equation which only applies in the absence of reflecting surfaces. Power densities caused by radiators on board a launch vehicle were considered, and it was concluded that, for frequencies greater than 200 MC, far field conditions would obtain in most cases for radiation in the vicinity of the payload. The power densities due to on-board radiators can then be analyzed similarly to off-board radiators.

A device for measuring power density was developed and calibrated for use in determining power density levels in the simulating environment of the laboratory. It was concluded that the useage of this device would allow a more accurate setting of power density levels in the vicinity of the test item without lengthy calculations involving the shape of reflectors in the testing room. A procedure for conducting a radiated susceptibility systems test was presented, an integral part of which was the usage of the power density detector.

An analysis of test margins was undertaken. Since in this particular case test margins are used to make up for the uncertainties arising from the redistribution of power densities caused by reflecting surfaces among other things, an experiment was devised in which a reflecting surface was used to create a "worst case" concentration of power density in a small region. It was concluded that random reflecting surfaces might cause as much as a 6 db increase in power density at a particular location.

The laboratory environment's effect upon the redistribution of power density was considered. It was shown that by proper procedures, such as keeping large objects out of the immediate vicinity of the test item, the effect of random reflections could be minimized. Quantitative criteria were presented involving distance from the test item and size of a reflecting surface.

The proposed test margin levels of 10 db and 6 db for proof test model spacecraft tests and flight spacecraft tests, respectively, were mentioned. Based upon information contained in this report, a 10 db test margin level is recommended for all tests. This level might possibly have to be increased to 15 db if there is a complex displacement of reflecting surfaces near a spacecraft that might provide energy concentration.

The role of statistics in establishing test margins was considered. It was suggested future work might be carried out involving the calculation of a "mean" gain between a transmitter and a volume of interest. Major reflecting surfaces would be taken into account, and the net effects averaged over the volume of interest would determine the expected value or mean gain. In this report the "worst case" criterion of maximum power density level within a volume of interest rather than mean level was used. The role of statistics in calibrating the power density detector and improving the quality of data was explained.

Finally, the natures of electronic susceptibility and RF overstress were considered. It was pointed out that whereas electronic susceptibility is a time-invariant phenomenon, RF overstress is a non-reversible process that changes the characteristics of a circuit. A possible technique for the analytical calculation and prediction of susceptibilities was presented. It was concluded that heat and high voltage or current levels

were the primary causes of RF overstress and that RF overstress was more likely to be a function of average applied power rather than peak quantities. It was concluded that in testing for susceptibilities, only relatively short duration pulses were needed. If a general environmental test is to be performed, critical parts of circuits should be monitored to see that heat dissipation, voltage and current ratings are not exceeded. Otherwise, exposure time of a test item to a simulation environment should be kept at a minimum.

Future work should be directed toward the coupling mechanisms responsible for extracting energy from an electromagnetic field which results in susceptibilities. An analysis of antenna to wire coupling mechanisms especially with regard to directional and polarization considerations would be valuable. Also the directional and polarization characteristics of near-field radiation should be investigated. In conclusion, a thorough knowledge of the susceptibility characteristics of the sub-systems yields important information for the analysis and prediction of susceptibilities in a systems test.

REFERENCES

1. S. Goldman; Frequency Analysis, Modulation and Noise; McGraw-Hill (1948); pp. 148-150
2. Jahnke and Emde, Tables of Functions; Dover (1945); pp. 156-179
3. Telemetry Standards, Document 106-65 (Revised July 1965); Para. 1.2.1.32
4. H.S. McGaughan; Performance Characteristics of Time and Frequency Multiplexed Telemetry Systems; 1956 National Telemetering Conference Report; pp. 1-5-1 to 1-5-16.
5. "Telemetry System Study," Aeronutronics; Volume II; p. II-5-8.
6. McGaughan, op. cit.
7. ibid
8. ibid
9. Report No. 55-03016A, Specification for Electromagnetic Interference Control, General Dynamics Convair, p. 31
10. "Telemetry System Study," op. cit; p. II-5-7.
11. J. Ormsby, PCM/FM Telemetry Signal Analysis and Bandwidth Effects; IRE Transactions on Space Electronics and Telemetry; Sept.-Dec. 1960, p. 130-8
12. "Telemetry System Study," op. cit.; Vol. I; P. I-2-84.
13. M. Nichols and L. Rauch, Radio Telemetry; Wiley (1956); p. 66
14. "Telemetry System Study," op. cit.; Vol. I; p. I-2-98.
15. M. Nichols and L. Rauch, op. cit.; p. 67
16. "Telemetry System Study," op. cit.; Vol. I; p. I-2-98.
17. Reed, H. R. and Russell, C. M., Ultra High Frequency Propagation; Wiley (1953); pp. 92-97.
18. Haber, E. and Jambor, L., Analytical Prediction of Transient Coupling; Eighth IEEE Symposium on Electromagnetic Compatibility
19. Oliver, B. M., Directional Electromagnetic Couplers; Proceedings of the IRE; 42:11; November 1954; pp. 1686-1692
20. "Study To Establish Electromagnetic Compatibility Speceifications," Report No. ZZK-65-027; 30 July 1965; pp. 189-208

21. Kraus, J. D., Antennas; McGraw-Hill (1950); p. 338.

22. Skolnik, M. T., Introduction To Radar Systems; McGraw-Hill, pp. 40-50.

23. Skolnik op, cit. p. 41

24. Reed and Russell, op. cit; p. 102

25. Reed and Russell, op. cit; p. 4

26. Skolnik, op. cit., p. 4

27. Carpenter, Desch and Tantum, Analytical Investigation of Electromagnetic Interference Measurements and Prediction of Radio Frequency Susceptibility of Digital Integrated Circuits; Technical Report AFAL-TR-66-117; Mar 1966; pp. 1-5.

28. A. H. Mills, Development of Probes and Measurement Techniques for Automated Interference Measurements (3 to 300 MHz) in Shielded Chambers; General Dynamics Report, GDC-AWV66-001, September 1966; pp. 75-82 and Appendices B and C

29. Study To Establish Electromagnetic Compatibility Specifications, op.cit. pp.163-168

30. Kraus, op.cit. pp. 41-56

31. Wire and Cable Reference Chart, Chilton Company (August 1966); "The Electronic Engineer," magazine; Vol. 25.

32. Cheug, D. K., Analysis of Linear Systems; Addison Wesley (1959); p. 233

33. Teiman, F. E., "Electronic and Radio Engineering," McGraw-Hill (1955) p. 289

34. Sproull, R. L., Modern Physics, Wiley (1956); pp. 73-109.

ADDITIONAL REFERENCES

King, R. W. P. and T. T. Wu, "The Scattering and Diffraction of Waves," Harvard University Press (1959)

Mentger, J. R., Scattering and Diffraction of Radio Waves, Pergamon Press (1955)

Telemetry System Study, Final Report; Volumes I and II; ASI Publications No. C-162, March 10, 1958

AD-260 221
MELPAR INC FALLS CHURCH VA
BROADBAND RADIATOR FOR RADIO INTERFERENCE GENERATOR SET AN/GRM-8 (XA-1) (U)
F
HIBBS,HERBERT H.;CZARNASKI,BENJAMIN P.;
MAY 61 MELPAR,FC
AF33 600 40839
ASD TR61 223
SCP 0 UNCLASSIFIED REPORT

DESCRIPTORS: *ELECTRONIC EQUIPMENT, *RADIO INTERFERENCE, *RADIOFREQUENCY GENERATORS, *TEST SETS, BROADBAND, COAXIAL CABLES, DESIGN, EFFECTIVENESS, ELECTROMAGNETIC FIELDS, INTERFERENCE, MEASUREMENT, NOISE GENERATORS, TEST EQUIPMENT (U)
IDENTIFIERS: AN/GRM-8 (U)

A BROADBAND RADIATOR WAS DEVELOPED WHICH PROVIDES A NEAR-UNIFORM RADIO INTERFERENCE FIELD FOR ELECTRONIC EQUIPMENT SUSCEPTIBILITY TESTS IN THE FREQUENCY RANGE OF 0.15 TO 1000 MC. THIS RADIATOR IS INTENDED FOR USE IN A SHIEL ED ENCLOSURE IN CONJUNCTION WITH THE AN/GRM-8 (XA-1) RADIO INTERFERENCE GENERATOR SET, WHICH GENERATES A NOISE SIGNAL WITH A CONTINUOUS PULSE SPECTRUM OVER THE FREQUENCY RANGE OF 0.10 TO 1000 MC. THE BROADBAND RADIATOR REQUIRES NO MANUAL CHANGE TO PROVIDE SIMULTANEOUS OPERATION AT ALL FREQUENCIES BETWEEN 0.15 AND 1000 MC, MEASUREMENTS IN THIS FREQUENCY RANGE WERE PREVIOUSLY CONDUCTED UTILIZING VARIOUS LOOP, STUB, AND DIPOLE RADIATORS REQUIRING NUMEROUS ADJUSTMENTS DURING A SINGLE QUALIFICATION TEST. DESIGN CON IDERATIONS, TECHNICAL ACHIEVEMENTS, AND EXPERIMENTAL RESULTS ARE PRESENTED. EIGHT BROADBAND RADIATORS WERE CONSTRUCTED. (AUTHOR) (U)

AD-260 892
ELECTRO-MECHANICS CO AUSTIN TEX
ADVANCED RECEIVER AND TRANSMITTER INTERFERENCE MEASUREMENT TECHNIQUES (U)
F
VARLASHKIN,P.;CRONENWETT,W.T.;
MAY 60 EL-MECH,A
AF30 602 1884
SCP 0 UNCLASSIFIED REPORT

DESCRIPTORS: *RADAR INTERFERENCE, *RADAR SIGNALS, *RADIO COMMUNICATION SYSTEMS, *RADIO INTERFERENCE, *RADIO RECEIVERS, *RADIO SIGNALS, *RADIO TRANSMITTERS, *RADIOFREQUENCY POWER, AIRBORNE, CALORIMETERS, COMMUNICATION SYSTEMS, EFFECTIVENESS, ELECTRICAL IMPEDANCE, ELECTROMAGNETIC FIELDS, ELECTROMAGNETIC WAVES, ELECTRON COUNTERS, ELECTRONIC EQUIPMENT, FOURIER ANALYSIS, HARMONIC ANALYSIS, INTERFERENCE, LOW-PASS FILTERS, MEASUREMENT, MODULATION, NOISE (RADIO), RADAR RECEIVERS, RADIO ALTIMETERS, RADIOFREQUENCY FILTERS, REDUCTION, SEMICONDUCTORS, SIGNAL GENERATORS, TESTS, VULNERABILITY (U)

SEMICONDUCTORS, RADAR RECEIVERS, *RADAR INTERFERENCE, *RADAR SIGNALS, EFFECTIVENESS.
SOME OF THE BASIC PARAMETERS TO BE MEASURED IN THE EVALUATION OF THE RADIO-FREQUENCY CHARACTERISTICS OF TRANSMITTERS AND RECEIVERS ARE DESCRIBED. AN ATTEMPT WAS MADE TO DEVELOP TECHNIQUES WHICH RESULT IN ABSOLUTE RATHER THAN RELATIVE DATA. EMPHASIS WAS PLACED ON MEASUREMENTS MADE AT THE EQUIPMENT ANTENNA TERMINALS. METHODS OF MEASURING RADIATED POWER ARE DESCRIBED AND PRELIMINARY TEST RESULTS ON SEVERAL PROPOSED TECHNIQUES ARE GIVEN. THE PROBLEMS INHERENT TO POWER-TYPE MEASUREMENTS ARE ANALYZED AND SEVERAL METHODS OF PERFORMING RADIATED POWER MEASUREMENTS ARE DESCRIBED. EXPERIMENTAL DATA IS GIVEN TO SHOW THE FEASIBILITY OF METHODS. A LIQUID-FLOW CALORIMETRIC POWER MEASUREMENT DEVICE FOR USE IN DETERMINING CALIBRATION ACCURACIES OF TEST EQUIPMENT AS WELL AS FOR MAKING POWER MEASUREMENTS DIRECTLY IS DESCRIBED. (AUTHOR) (U)

APPENDIX I

COMPUTER PROGRAM FOR CALCULATION OF BESSEL FUNCTIONS OF ARGUMENT 127.4

```
      DOUBLE PRECISION     AJ(250), AN, AJB
      PI = 3.14159265D00
      WRITE (6, 300)
300   FORMAT (29H        N            J(N)        )
      AJ(1) = DSQRT(2.0/(PI*127.4))*DCOS(127.4 - (PI/4.0))
      AJ(2) = DSQRT(2.0/(PI*127.4))*DCOS(127.4 - (3.0*PI/4.0))
      N = 2
 50   N = N+1
      NI = N-1
      NC = N-2
      AN = FLOAT ( NC)
      AJ(N) = ((2.0* AN /127.4)* AJ(N-1)) - AJ(N-2)
      AJB = DABS (AJ(N))
      WRITE (6, 310)  NI, AJ(N)
310   FORMAT ( 6H      . I3, D20.6)
100   IF (N - 200)   50, 50, 150
150   CONTINUE
      WRITE (6, 200)   NI
200   FORMAT ( 89H   THIS IS A LISTING OF BESSEL FUNCTIONS ,  J(I)(127.4) . .
     1FOR   I   FROM   0   TO   N   WHERE   N = , 13 /// )
      WRITE  (6, 206)  (AJ(I),  I = 1, N)
206   FORMAT   (5D20.6 )
      CALL EXIT
      END
```

NOTE: AJ(I) is symbol used for ith order Bessel function.

APPENDIX II

MEASURED FM-FM AND NOISE SPECTRA

(as shown in Reference 5)

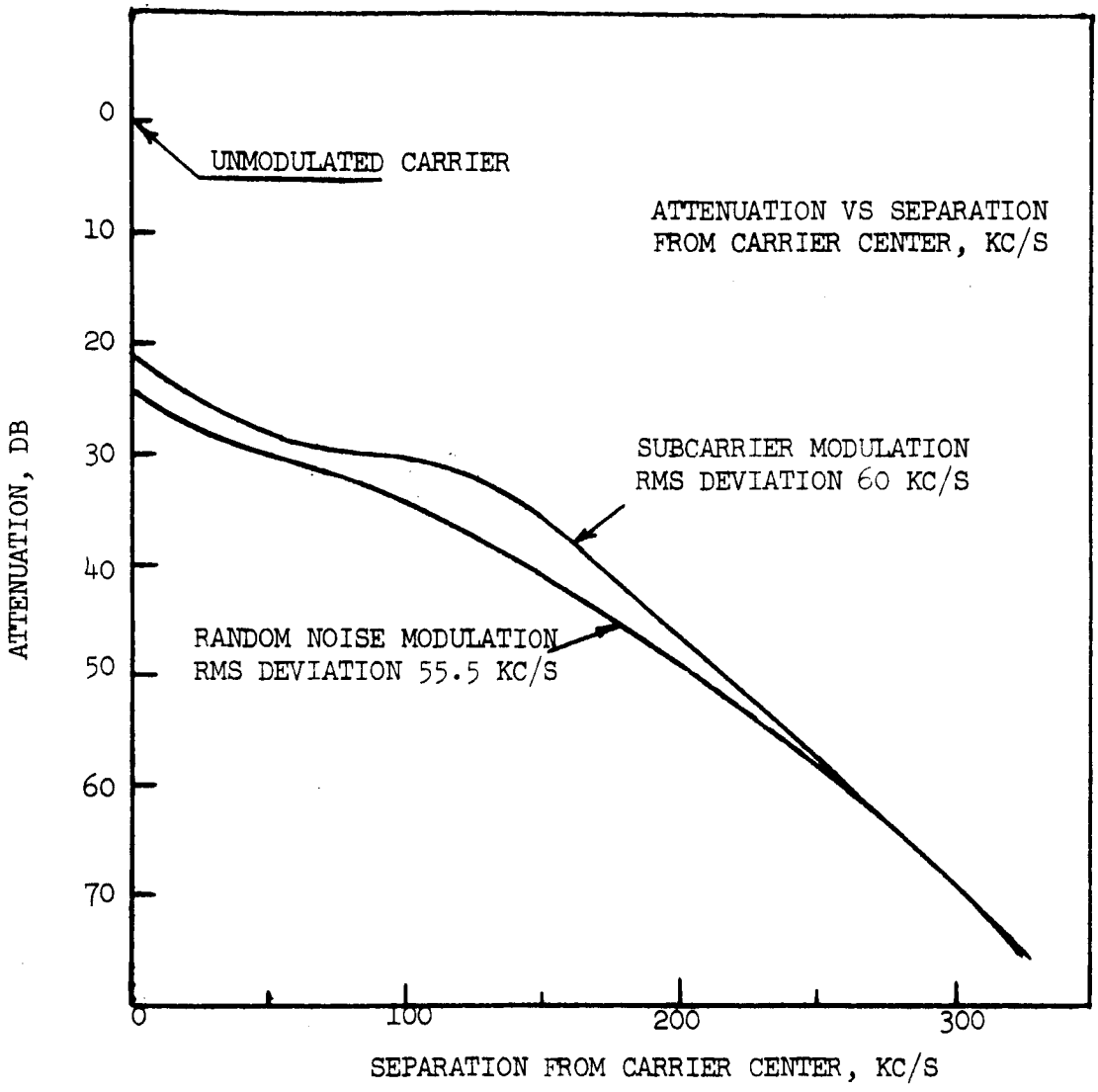

MEASURED FM-FM SPECTRUMS. TOTAL RMS CARRIER DEVIATION f_D = 60 KC/S, f_m = 70 KC/S, D = .86; AND SPECTRUM OF NOISE MODULATED FM CARRIER.

APPENDIX III
COMPUTER SOLUTION TO EQUATION 13

```
      DIMENSION U(20),FX(20)
      PI=3.14159265
      DO 10 I=1,6
      AI=FLOAT(I)
      D=2.*AI/10.
      A=3.*(D**2)
            DO 9 J=1,101
          AJ=FLOAT(J)-1.
          Y=AJ/10.
                DO 3 N=1,10
                AN=FLOAT(N)              -1.
                IF (Y-AN) 1,1,2
    1           U(N)=0.
                GO TO 3
    2           U(N)=1.
                GO TO 3
    3           CONTINUE
C
C
          FX(1)=PI*(1.-U(2))
          FX(2)=(PI/2.)*((Y+2.)-2.*Y*U(1)+(Y-2.)*U(3))
C
          FX(3)=(PI/8.)*(((Y+3.)**2)-3.*((Y+1.)**2)+3.*((Y-1.)**2)*U(2)
     1-((Y-3.)**2)*U(4))
          FX(4)=(PI/48.)*(((Y+4.)**3) -4.*((Y+2.)**3)+6.*(Y**3)*U(1)-4.
     1*((Y-2.)**3)*U(3)-((Y-4.)**3)*U(5))
C
          FX(5)=(PI/384.)*((Y+5.)**4-5.*((Y+3.)**4)+10.*(Y+1.)**4-10.*(
     1(Y-1.)**4)*U(2) +5.*((Y-3.)**4)*U(4)-((Y-5.)**4)*U(6))
C
        FX(6)=(PI/3840.)*((Y+6.)**5-6.*(Y+4.)**5+15.*(Y+2.)**5-20.*(Y**5
     1)*U(1)+15.*((Y-2.)**5)*U(3)-6.*((Y-4.)**5)*U(5)+((Y-6.)**5)*U(7))
C
          FX(7)=(PI/46080.)*((Y+7.)**6 -7.*(Y+5.)**6+21.*(Y+3.)**6-35.*
     1(Y+1.)**6+35.*((Y-1.)**6)*U(2)-21.*((Y-3.)**6)*U(4)+7.*((Y-5.)**6)
     2*U(6)-((Y-7.)**6)*U(8))
          FX(8)=(PI/645120.)*((Y+8.)**7-8.*(Y+6.)**7+28.*(Y+4.)**7-56.*
     1(Y+2.)**7+70.*(Y**7)*U(1)-56.*((Y-2.)**7)*U(3)+28.*((Y-4.)**7)*U(5
     2)-8.*((Y-6.)**7)*U(7)+((Y-8.)**7)*U(9))
C
          FX(9)=(PI/10321920.)*((Y+9.)**8-9.*(Y+7.)**8+36.*(Y+5.)**8-84
     1.*(Y+3.)**8+126.*(Y+1.)**8-126.*((Y-1.)**8)*U(2)+84.*((Y-3.)**8)*U
     2(4)-36.*((Y-5.)**8)*U(6)+9.*((Y-7.)**8)*U(8)-((Y-9.)**8)*U(10))
C
          SUM=0
                DO 6 L=1,9
                NN=1
                      DO 5 M=1,L
                      NN=M*NN
    5                 CONTINUE
          BN=FLOAT(NN)
          FS=((A**L)/BN)*FX(L)
                SUM=FS+SUM
    6           CONTINUE
```

```
C
      WSHY=(EXP(-A)/(2.0*PI))*SUM
    7 FORMAT(42H                D          Y              WSHY         ///)
                                                  WRITE(6,7)
    8 FORMAT(6H       ,2F10.2,F10.6)
      WRITE(6,8) D,Y,WSHY
    9 CONTINUE
   10 CONTINUE
   CALL EXIT
   END
   RETURN
```

Note:

D = deviation ratio

$$Y = \frac{f - fe}{f_m}$$

WSHY = $w_s H(y)$

APPENDIX IV
MEASURED FM-FM SPECTRUM, D = 1.1

(as shown in Reference 10)

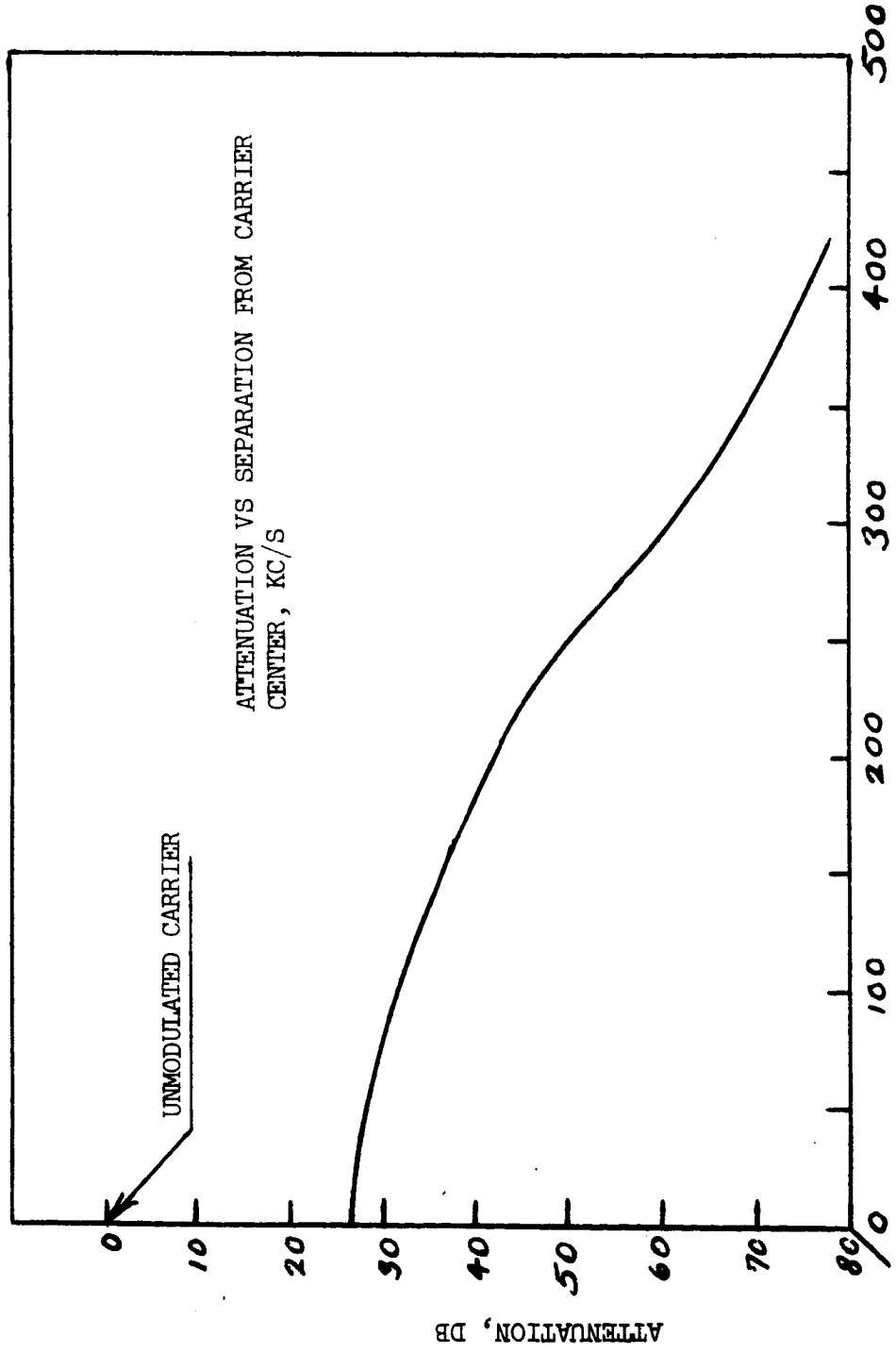

MEASURED FM-FM SPECTRUM. TOTAL RMS CARRIER DEVIATION, f_D = 75 KC/S, fm = 70 Kc, D = 1.1

APPENDIX V

SPECTRA FOR DIFFERENT FREQUENCY-MULTIPLEX MODULATION SCHEMES

(as shown in Reference 16)

ATTENUATION VS SEPARATION FROM CARRIER CENTER/INFORMATION BANDWIDTH

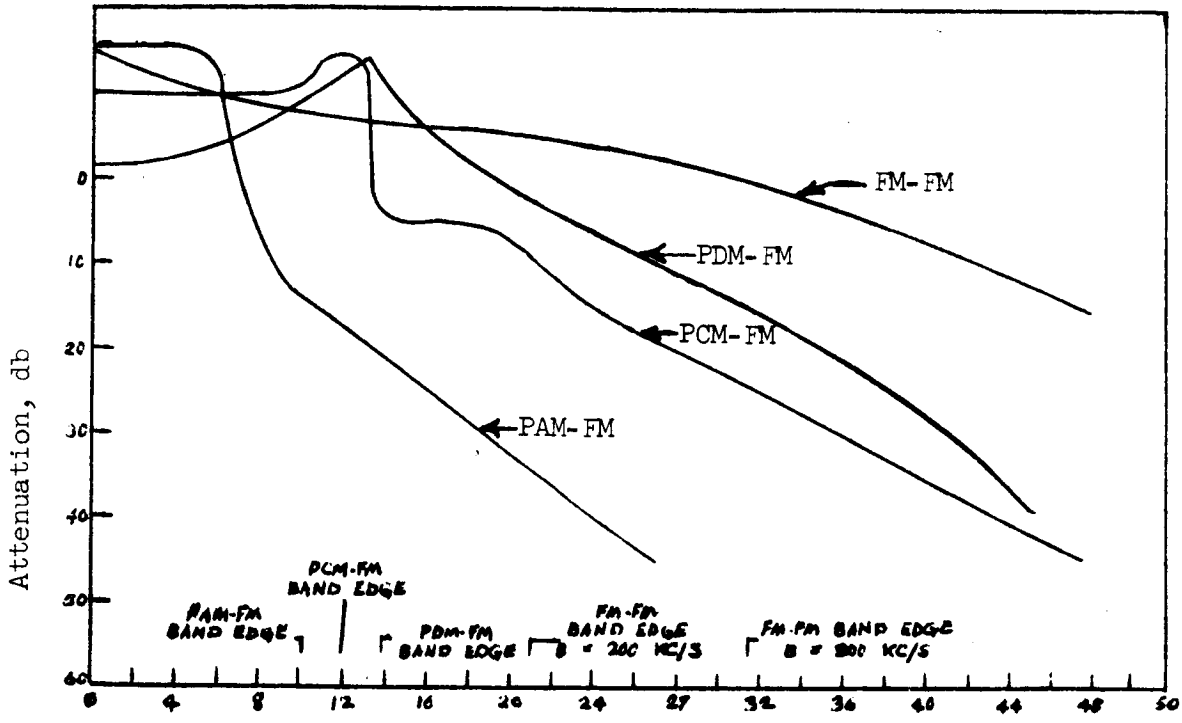

PAM-FM, PCM-FM, PDM-FM, and FM-FM spectra for equal information bandwidth and equal carrier power

APPENDIX VI

HIGH POWER SIGNAL SOURCES

LIST

MANUFACTURER	NOMEN-CLATURE	MODEL NUMBER	FREQUENCY RANGE	POWER
AIRBORNE INSTRUMENTS LABORATORY	Amplifier	Type 125	200 to 1000 MHz 1 to 2 GHz 2 to 3 GHz	50 watts 25 watts 5 watts
ALFRED ELECTRONICS	Amplifier	560 Series	1 to 12 GHz	1 watt
AMERICAN ELECTRONIC LABORATORY	Sweep Generator and Amplifier	Model R-360	100 kHz to 30 MHz	250 watts
APPLIED MICROWAVE LABORATORY	Amplifier	Model A-100	350 to 2000 MHz	3 watts
	Oscillators	Model C-201	150 to 6000 MHz	40 watts
		C-202	150 to 1000 MHz	100 watts
BORG-WARNER	Oscillator	Model 20	85 kHz to 40 MHz	10 watts
		Model 30A	40 to 400 MHz	5 watts
ENERGY SYSTEMS INC	Oscillator	Model 1310	1 to 10 GHz	150 watts
F X R	Oscillator	Model Z 790A	1 to 10 GHz	100 watts
HEWLETT PACKAGE	Amplifier	Model 230A	10 to 500 MHz	4 watts
HUGGINS LABORATORIES INC	Amplifier	400 Series	1 to 10 GHz	10 watts
INSTRUMENTS FOR INDUSTRY	Amplifiers	Several Models		Up to 100 watts
JANSKY AND BAILEY	Oscillator	Model C 5402	300 kHz to 50 MHz	10 amperes

MANUFACTURER	NOMEN-CLATURE	MODEL NUMBER	FREQUENCY RANGE	POWER
MICRODOT	Oscillator	Model 408 Model 410	200 to 500 MHz 500 to 1000 MHz	25 watts 50 watts
MICROWAVE CAVITY LABORATORY	Amplifier	Model 10039 Model 10221	200 to 400 MHz 400 to 800 MHz	125 watts 1000 watts
RHODE AND SCHWARZ		Type SMLR Type SMLM Type SLRD Type SLRC	100 kHz to 30 MHz 30 to 300 MHz 275 to 2750 MHz 2.3 to 7 GHz	
SERVO CORPORATION OF AMERICA	Amplifier	Series 970 - 979	1 to 18 GHz	20 watts
	Oscillators	Series 882 - 889	1 to 18 GHz	14 watts
SIERRA ELECTRONICS	Oscillators	215 Series 270 Series 470A Series	25 to 1000 MHz 25 to 1000 MHz 190 to 2500 MHz	50 watts 50 watts 35 watts min
TEXSCAN	Sweep Oscillator	PD 2, 3, 7, 8	20 to 1000 MHz	4 watts
TEXCAN	Sweep Oscillator	HS 70, 75, 80, 85	20 to 1000 MHz	4 watts
WATKINS-JOHNSON	Several Models TWT		Amplifiers	

APPENDIX VII

GRAPHS OF CALCULATED POWER DENSITY LEVELS FOR KNOWN TRANSMITTED POWER VERSUS INDICATED METER READING WITH POWER DENSITY DETECTOR AS PICKUP DEVICE (FOR FREQUENCIES BETWEEN 200 AND 300 MC)

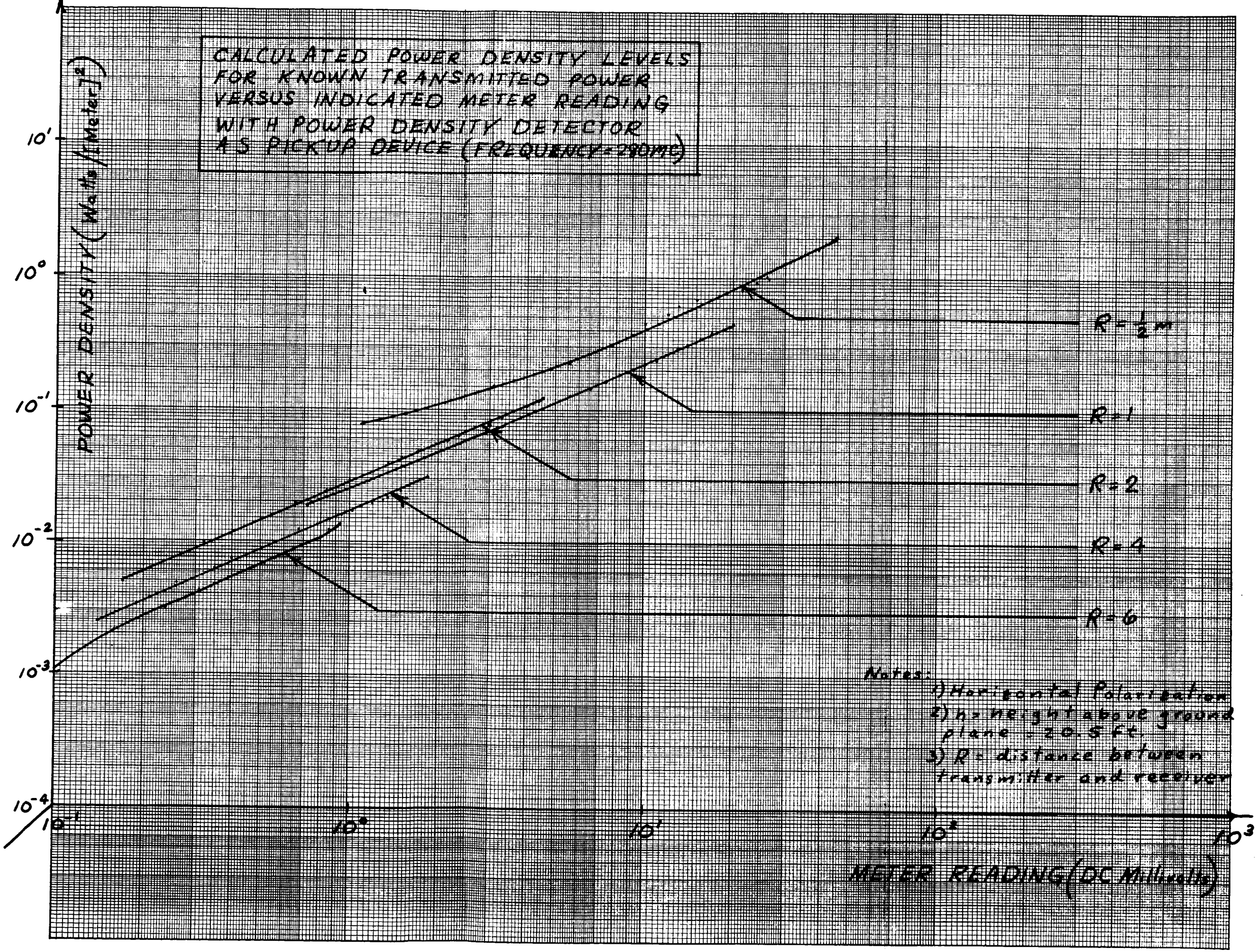

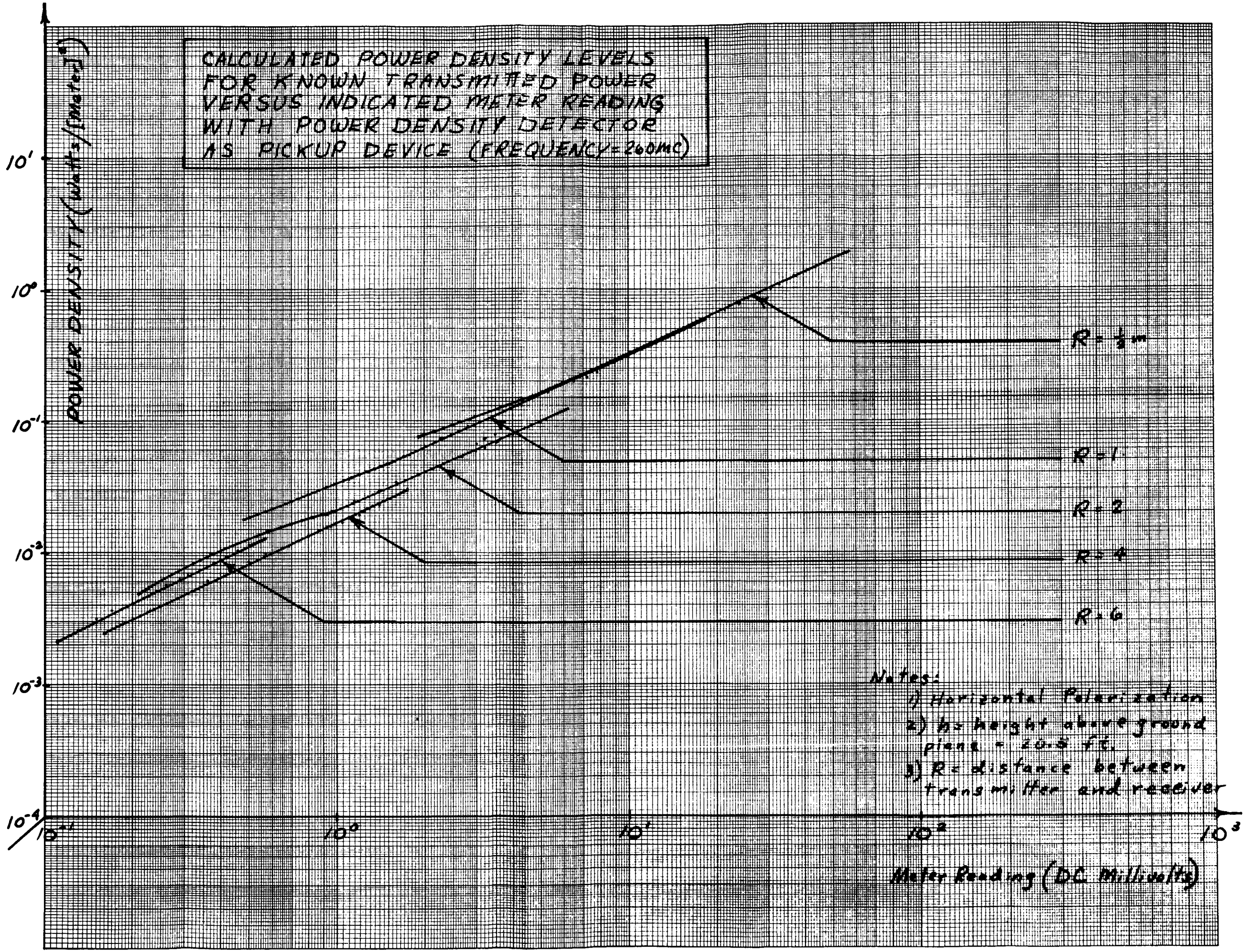
CALCULATED POWER DENSITY LEVELS
FOR KNOWN TRANSMITTED POWER
VERSUS INDICATED METER READING
WITH POWER DENSITY DETECTOR
AS PICKUP DEVICE (FREQUENCY=200MC)
POWER DENSITY (watts/(meter)²)
10¹
10⁰
10⁻¹
10⁻²
10⁻³
10⁻⁴
10⁻¹
10⁰
10¹
10²
10³
R = ½ m
R = 1
R = 2
R = 4
R = 6
Notes:
1) Horizontal Polarization
2) h = height above ground plane = 20.5 ft.
3) R = distance between transmitter and receiver
Meter Reading (D.C. Millivolts)

VII-4-2

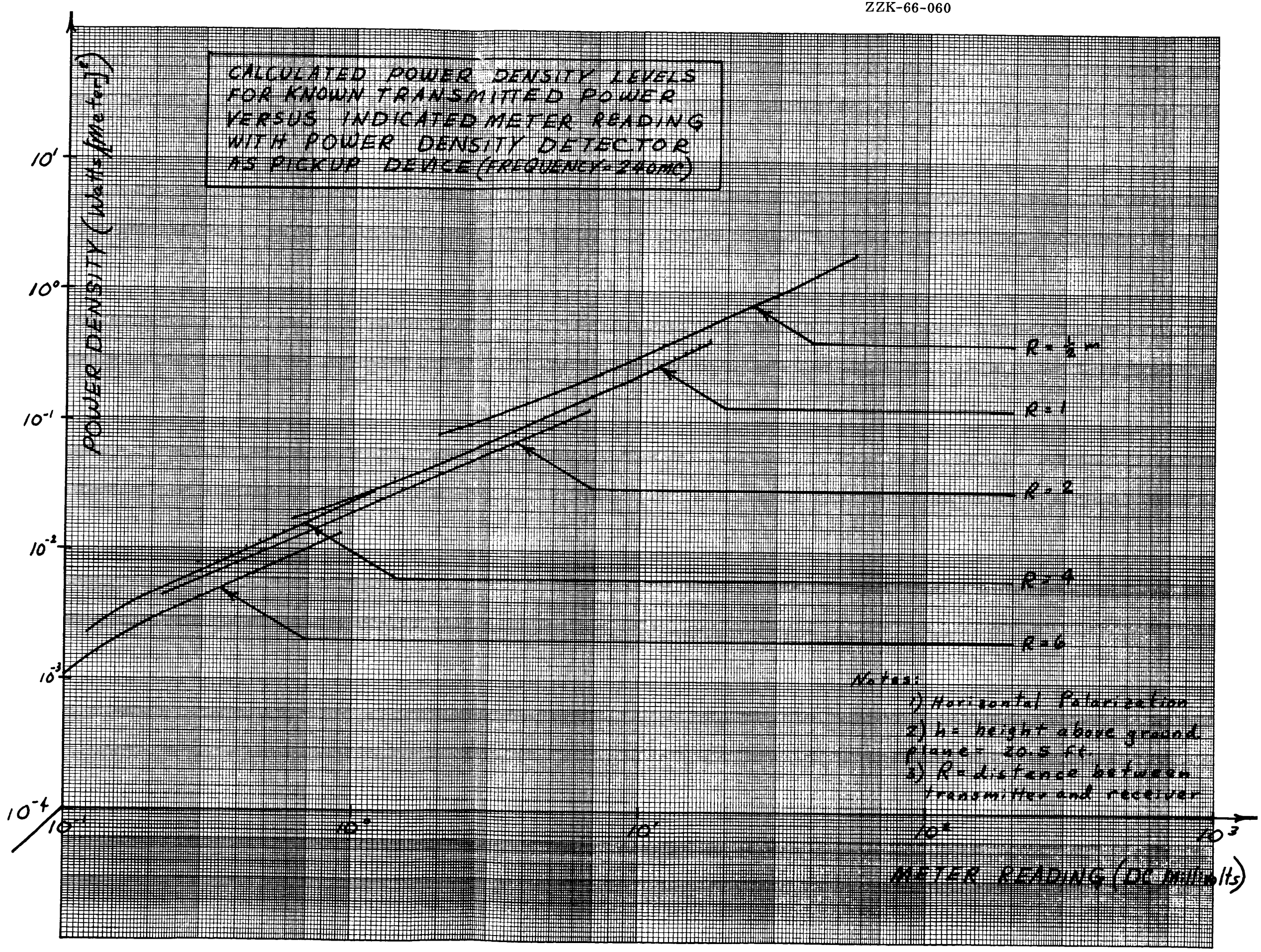
CALCULATED POWER DENSITY LEVELS FOR KNOWN TRANSMITTED POWER VERSUS INDICATED METER READING WITH POWER DENSITY DETECTOR AS PICKUP DEVICE (FREQUENCY = 240MC)
POWER DENSITY (Watts/M²)
10¹
10⁰
10⁻¹
10⁻²
10⁻³
10⁻⁴
R = ½ M
R = 1
R = 2
R = 4
R = 6
Notes:
1) Horizontal Polarization
2) h = height above ground plane = 20.5 ft.
3) R = distance between transmitter and receiver
10⁻¹
10⁰
10¹
10²
10³
METER READING (DC Millivolts)

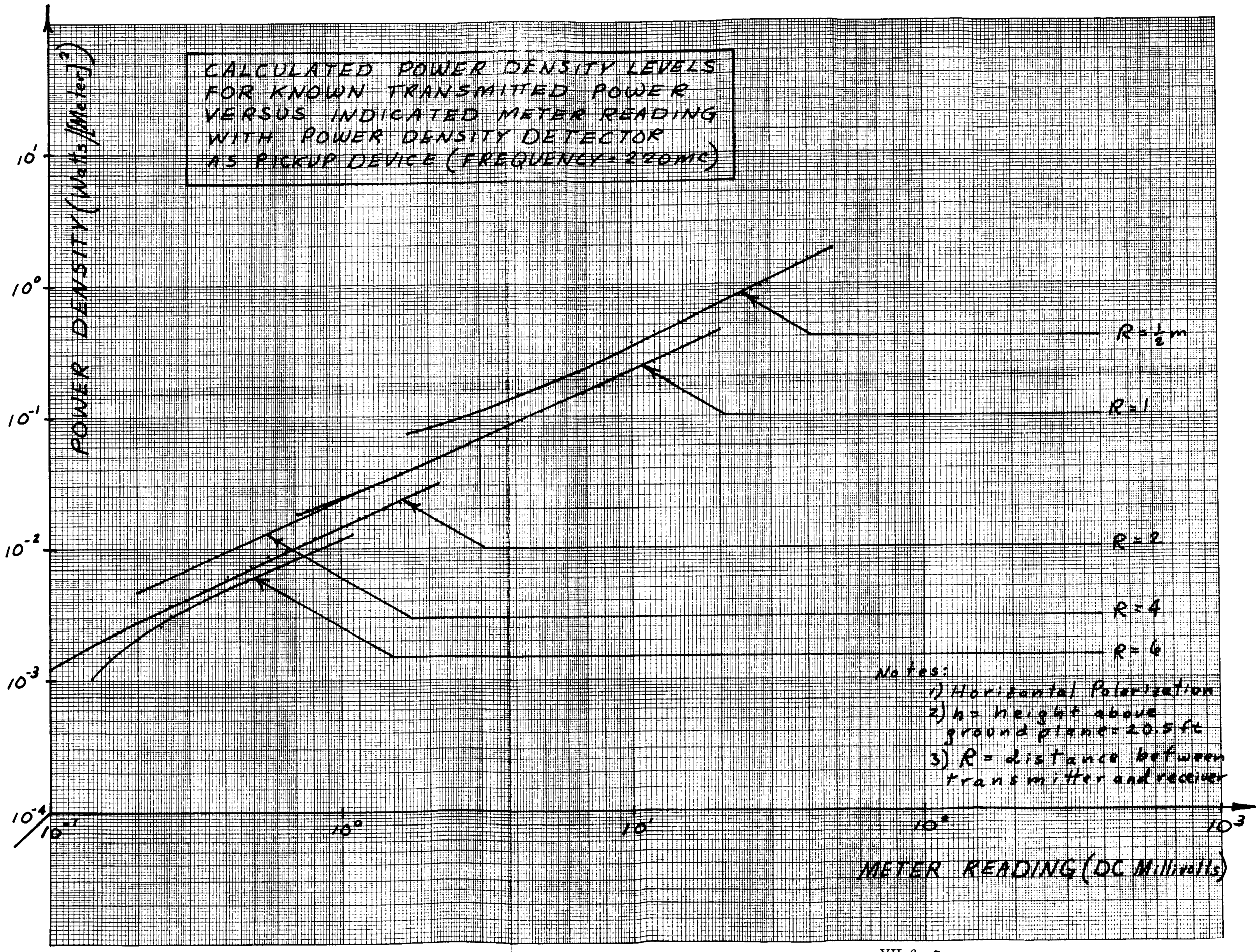
CALCULATED POWER DENSITY LEVELS FOR KNOWN TRANSMITTED POWER VERSUS INDICATED METER READING WITH POWER DENSITY DETECTOR AS PICKUP DEVICE (FREQUENCY = 220MC)
POWER DENSITY (Watts/Meter²)
10¹
10⁰
10⁻¹
10⁻²
10⁻³
10⁻⁴
R = ½ m
R = 1
R = 2
R = 4
R = 6
Notes:
1) Horizontal Polarization
2) h = height above ground plane = 20.5 ft
3) R = distance between transmitter and receiver
10⁻¹
10⁰
10¹
10²
10³
METER READING (DC Millivolts)

CALCULATED POWER DENSITY LEVELS FOR KNOWN TRANSMITTED POWER VERSUS INDICATED METER READING WITH POWER DENSITY DETECTOR AS PICKUP DEVICE (FREQUENCY=200mc)

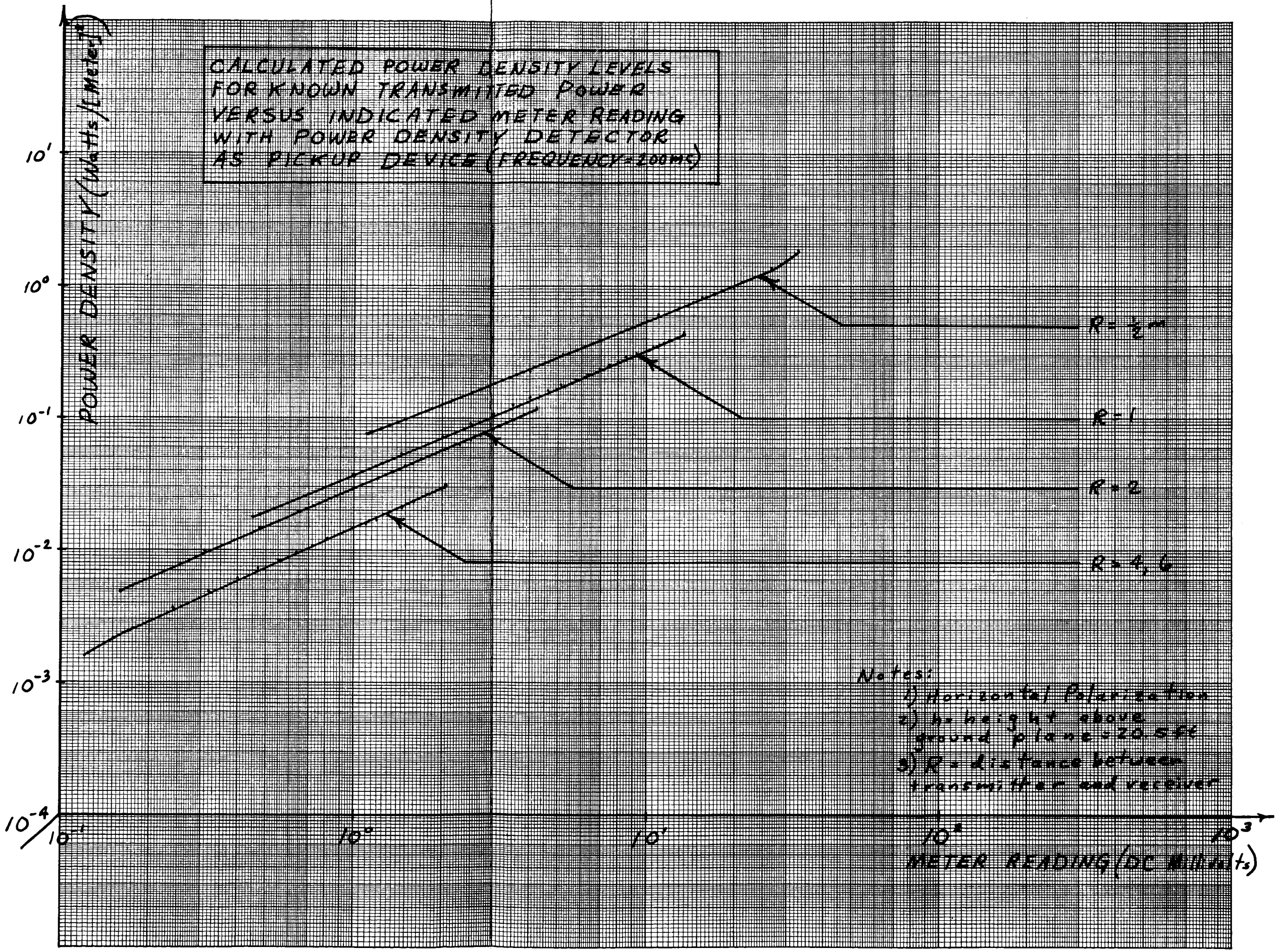

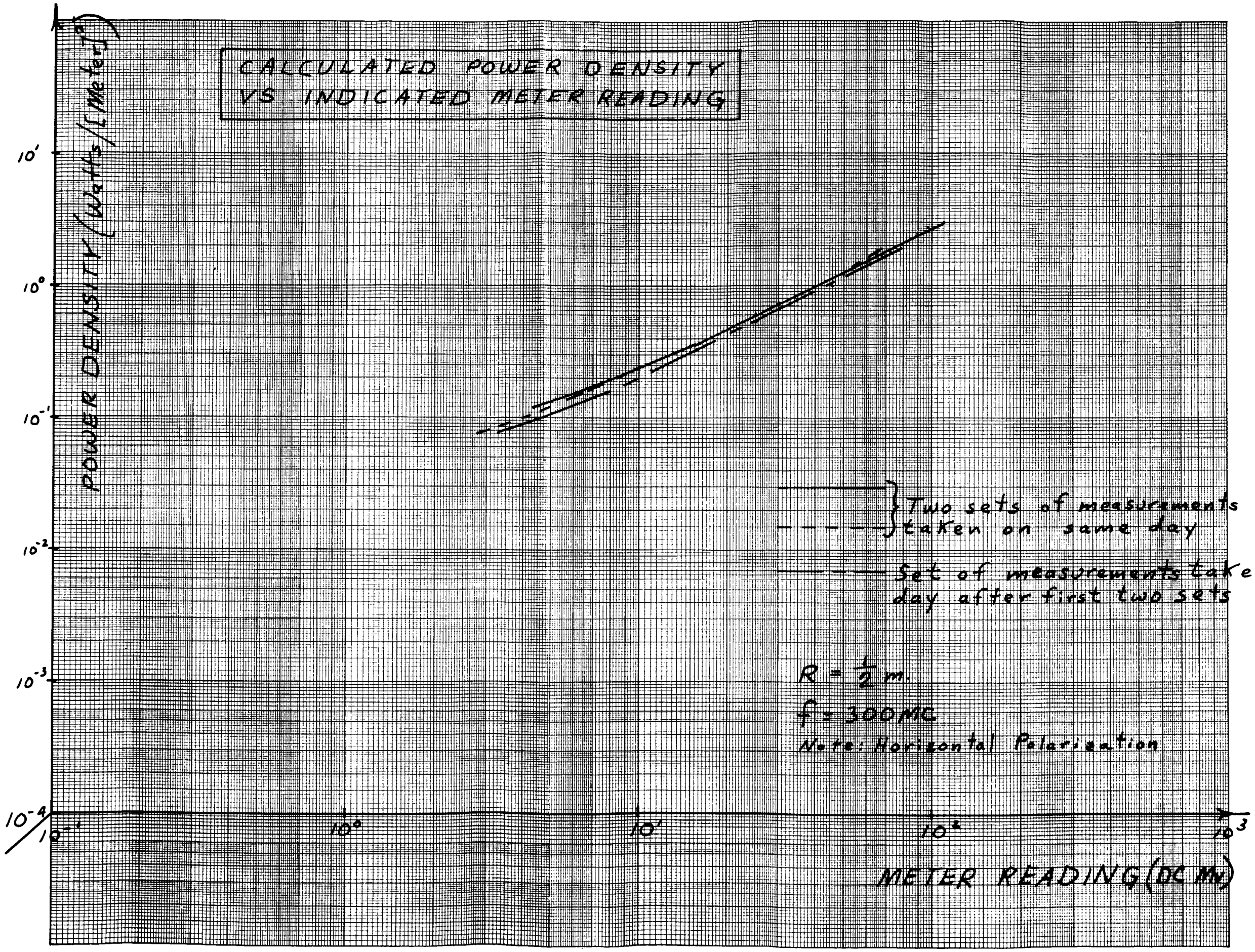
CALCULATED POWER DENSITY VS INDICATED METER READING
POWER DENSITY (Watts/Meter²)
10¹
10⁰
10⁻¹
10⁻²
10⁻³
10⁻⁴
10⁻¹
10⁰
10¹
10²
10³
METER READING (DC MV)
Two sets of measurements taken on same day
Set of measurements taken day after first two sets
R = 1/2 m.
f = 300MC
Note: Horizontal Polarization

APPENDIX VIII

COMPUTER PROGRAM FOR INTERMODULATION

A computer program is employed to determine potential intermodulation products that could occur with nonlinear mixing of intentional R.F. radiators.

The program reads in n frequencies and applies to the applicable intermodulation sum and difference equations. This particular version of the program uses the products

$$2A \pm B$$

$$3A \pm 2B$$

$$A + B \pm C$$

All values of A, B, and C (the n assigned R.F. frequencies) are used so that all combinations of the n frequencies are compared. A bandwidth tolerance is introduced so that the comparison between the possible products and the n frequencies may be made to any selected bandwidth. The program is general to the point that various frequencies and bandwidths can be applied in one run.

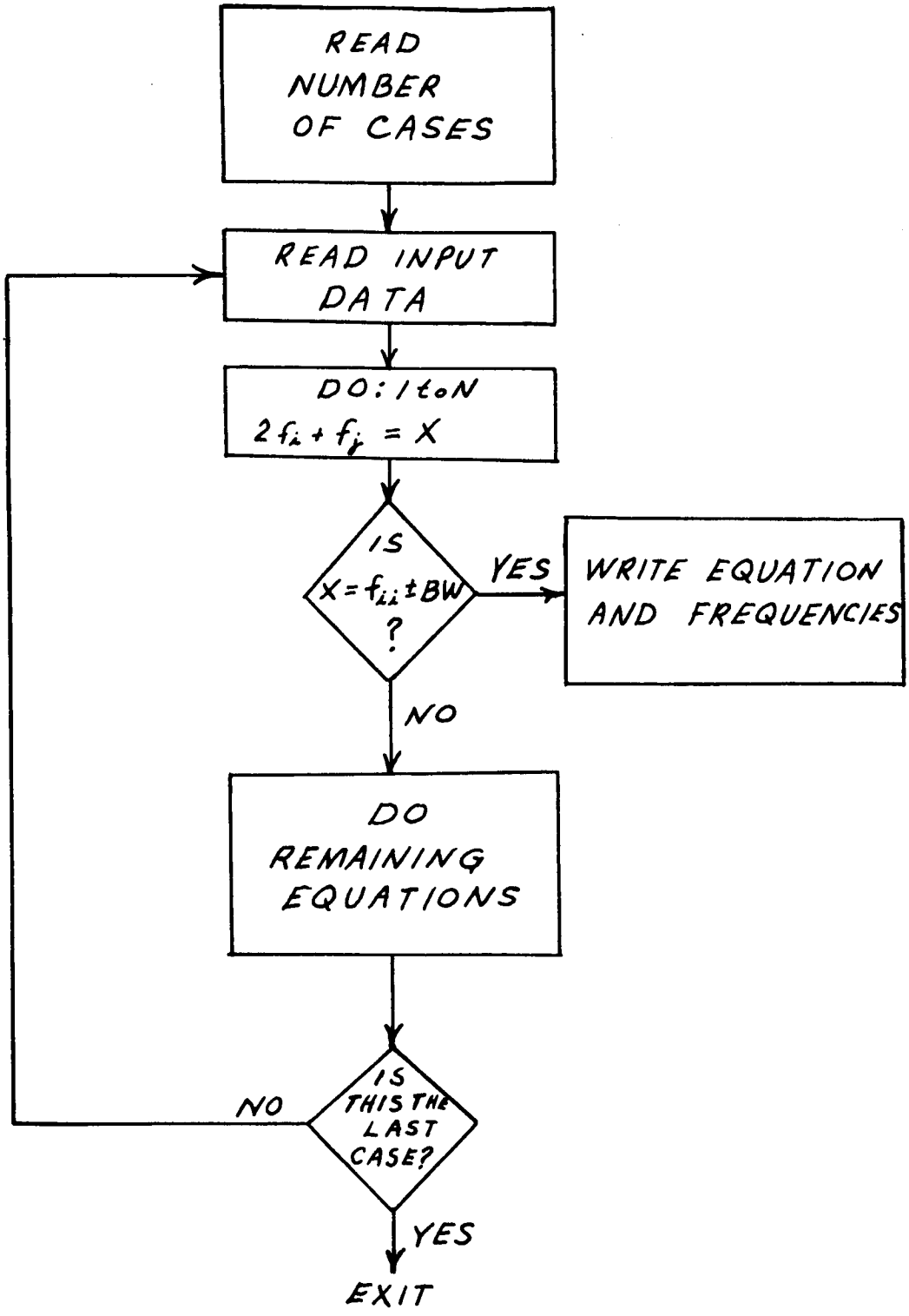

FLOW DIAGRAM: INTERMODULATION

```
$EXECUTE        IBJOB
$IBJOB          MAP
$IBFTC MAIN     LIST,REF
      DIMENSION      F(150)
      READ (5, 9)  (KASE)
    2 READ (5,10)  (N, SPRD)
      READ (5,20) (F(I),  I=1, N)
    9 FORMAT  (I3)
   10 FORMAT  (I3, F6.2)
   20 FORMAT  (8F9.2)
      WRITE  (6,11) (KASE, N, SPRD)
   11 FORMAT  (8H KASE = , I3, 7H   N = , I3, 10H    SPRD = , F6.2)
  100 DO  150  I=1, N
  101 DO  150  J=1, N
      X=(2.*F(I))-F(J)
      IF  (I-J)  102, 150, 102
  102 DO  145  II=1, N
      IF  (X-(F(II)+SPRD))  130, 130, 145
  130 IF  (X-(F(II)-SPRD))  145, 140, 140
  140 WRITE  (6, 160) (F(I), F(J), F(II), X)
  145 CONTINUE
  150 CONTINUE
  400 DO  450  I=1, N
  401 DO  450  J=1, N
      X=(2.*F(I))+F(J)
      IF  (I-J)  402, 450, 402
  402 DO  445  II-1, N
      IF(X-(F(II)+SPRD))  430, 430, 445
  430 IF(X-(F(II)-SPRD))  445, 440, 440
  440 WRITE  (6, 460) (F(I), F(J), F(II), X)
  445 CONTINUE
  450 CONTINUE
  460 FORMAT  (51H  INTERMODULATION PRODUCT FOR EQ. 2F(I)+F(J),  F(I)=,  F9
     1.2,  7H F(J)=  ,  F9.2,  9H F(II)  =  , F9.2, 7H  X =   , F9.2)
  160 FORMAT  (51H  INTERMODULATION PRODUCT FOR EQ. 2F(I)-F(J),  F(I)=,  F9
     1.2, 7H F(J)=  ,  F9.2,  9H F(II)  =  , F9.2, 7H  X  =  , F9.2)
  500 DO  550  I=1, N
  501 DO  550  J=1, N
      X=(3.*F(I))-(2.*F(J))
      IF  ( I - J )  502, 550, 502
  502 DO  545  II-1, N
      IF (X-(F(II)+SPRD))  530, 530, 545
  530 IF (X-(F(II)-SPRD))  545, 540, 540
  540 WRITE  (6, 560) (F(I), F(J), F(II), X)
  545 CONTINUE
  550 CONTINUE
```

```
560   FORMAT (47H INTERMOD. PRODUCT FOR EQ. 3F(I)-2F(J), F(I) = , F9.2,
     17H F(J) = , F9.2, 8H F(II) = , F9.2,5H  X=  , F9.2)
600   DO 650 I=1,N
601   DO 650 J=1,N
      X=(3.*F(I))+(2.*F(J))
      IF (I-J) 602,650,602
602   DO 645 II=1,N
      IF(X-(F(II)+SPRD)) 630,630,645
630   IF(X-(F(II)-SPRD)) 645,640,640
640   WRITE (6,660)(F(I),F(J),F(II),X)
645   CONTINUE
650   CONTINUE
660   FORMAT (47H INTERMOD. PRODUCT FOR EQ. 3F(I)+2F(J), F(I) = , F9.2,
     17H F(J) = , F9.2, 8H F(II) = , F9.2,5H  X= , F9.2)
700   DO 750 I=1,N
701   DO 750 J=1,N
      DO 750 K=1,N
      X= F(I)+F(J)-F(K)
      IF ( I - J ) 702,750,702
702   IF ( J - K) 703,750,703
703   DO 745 II = 1,N
      IF (X-(F(II)+SPRD)) 730,730,745
730   IF (X-(F(II)-SPRD)) 745,740,740
740   WRITE (6,760) (F(I),F(J),F(K),F(II),X)
745   CONTINUE
750   CONTINUE
760   FORMAT (50H INTERMOD. PRODUCT FOR EQ. F(I)+F(J)-F(K), F(I)= , F9.
     12, 8H F(J) = , F9.2, 9H  F(K) = ,F9.2, 9H F(II) = ,F9.2, 4H X= , 2F9.2)
800   DO 850 I=1,N
801   DO 850 J=1,N
      DO 850 K=1,N
      X= F(I)+F(J)+F(K)
      IF (I-J) 802,850,802
802   IF (J-K) 803,850,803
803   DO 845 II=1,N
      IF (X-(F(II)+SPRD)) 830,830,845
830   IF (X-(F(II)-SPRD)) 845,840,840
840   WRITE 96,860)(F(I),F(J),F(K),F(II),X)
845   CONTINUE
850   CONTINUE
860   FORMAT (50H INTERMOD. PRODUCT FOR EQ. F(I)+F(J)+F(K), F(I)= , F9.
     12, 8H F(J) = , F9.2, 9H  F(K) = ,F9.2, 9H F(II) = ,F9.2,  4H X= , 2F9.2)
      WRITE (6,98)
      WRITE (6,99) (F(I),I=1,N)
 98   FORMAT (18H FREQ. EVAL. WERE )
```

```
  99   FORMAT ( 10F9.2)
       kase = KASE - 1
       IF (KASE-1) 481,2,2
 481   CONTINUE
       CALL EXIT
       END
$DATA
```

APPENDIX IX

POWER DENSITY MEASUREMENT TECHNIQUE FOR INCIDENT RADIATION OF ARBITRARY DIRECTION AND POLARIZATION

The general problem is to measure total $\vec{E}$ vector at a point with a beam-width limited, polarized device. The power density detector has the following properties

1) 90° beamwidth.
2) linear polarization.

Consider the following coordinate system

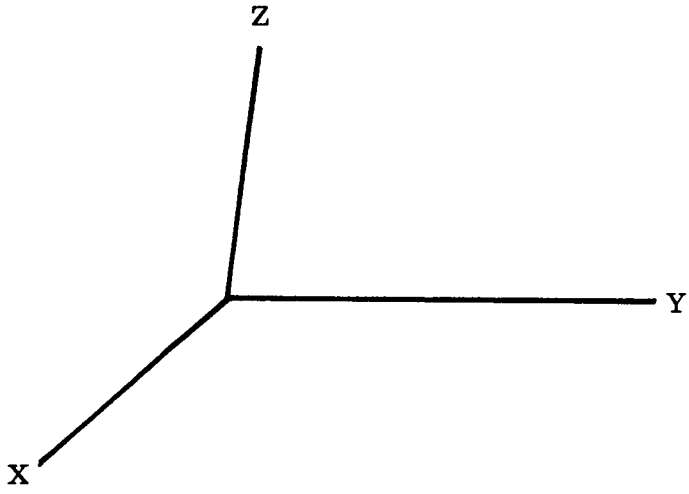

The question is now asked, how many measurements have to be made to determine the total $\vec{E}$ vector. Let us choose three independent components of the $\vec{E}$ vector: E_X, E_Y and E_Z. Let a propagation vector, $\vec{K}$, be associated with each incident wave. Since we will consider only plane waves, the $\vec{E}$ vector must be in a plane perpendicular to the $\vec{K}$ vector. Let us consider just the X-Y plane.

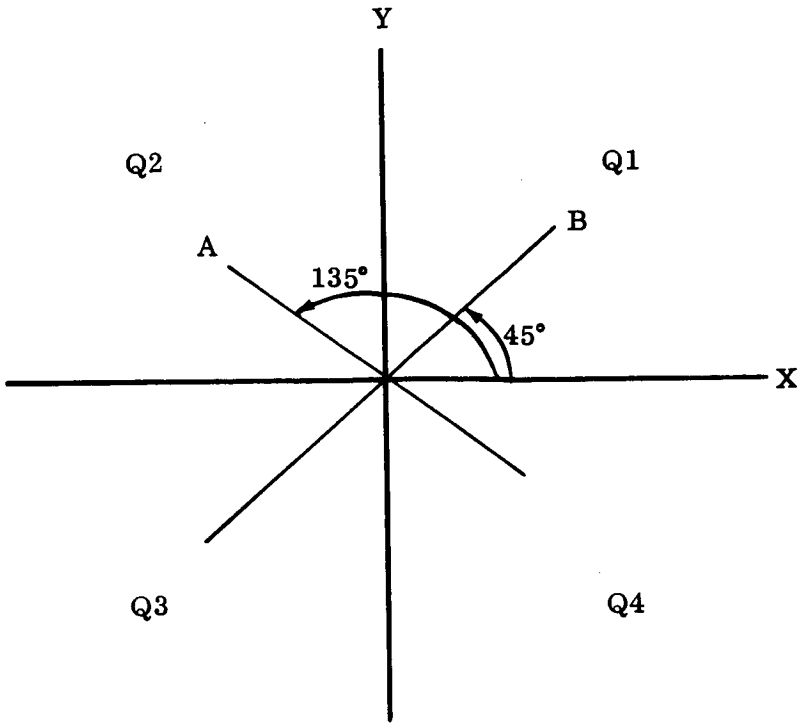

If the linear element of the antenna is placed in position A, it will be beamwidth sensitive to quadrants Q1 and Q3 and will measure

$$\left[\frac{1}{2}E_{X\,\text{total}} + \frac{1}{2}E_{Y\,\text{total}}\right]_{(Q1\text{ and }Q3)}$$

If a measurement is also made with the linear element in position B, $\vec{E}$ due to radiation incident in quadrants Q2 and Q4 will be measured. Again the total measurement will be

$$\left[\frac{1}{2}E_{X\,\text{total}} + \frac{1}{2}E_{Y\,\text{total}}\right]_{(Q2\text{ and }Q4)}$$

If the two measurements are added together the sum will be

$$\frac{1}{2}\left[E_X + E_Y\right]$$

and the E_X and E_Y components of waves with every possible $\vec{K}$ vector will have been measured. Similarly, if measurements are made in the X-Z and Y-Z planes,

$$\frac{1}{2}\left[E_X + E_Z\right]$$

and

$$\frac{1}{2}\left[E_Y + E_Z\right]$$

will be measured. If these three sets of measurements are summed, the result is

$$E_{total} = E_X + E_Y + E_Z$$

If the measuring device is calibrated in terms of power density, the total power density will be the sum of the power densities measured in the six measurements. In general it can be said that six measurements have to be made in three orthogonal planes with two orthogonal measurements in each plane.

APPENDIX X

BIBLIOGRAPHY ON RF OVERSTRESS

Anderson, G. P. and Erickson, R. A., "Failure Modes in Integrated and Partially Integrated Microelectronic Circuits," Univac Div., Sperry Rand Corp., Radc. Phys. of Failure in Electron., Vol. 2 (1963) p. 498-524 (N64-20967 14-09, N64-20997).

Aronowitz, L., "Rocket Engine Generated Voltage as a Source of Electromagnetic Interference and Electronic Component Damage on Interplanetary Vehicles," August 1965, 11p., refs. presented at the 1965 Electron. Symp., Miami, Fla., (2-4 November 1965).

Ballard, J. W. and Horn, E. F., "Investigation of RF Radiation as a Secondary Phenomenon for Use in Checkout," Systems Research Labs., Inc., AF Aero Propulsion Lab., Wright-Patterson AFB, Ohio (June 1965) 101p. (AF 33/615/ -1489, AFAPL-TR-65-46, AD-619899, N66-11459).

Ballard, J. W., "Detection and Prediction of Malfunctions of Electronic Components by Contact Thermography," National Aerospace Electronics Conference, Dayton, Ohio, proceedings, 11-13 May 1964, (A65-24101 13-09). Conference sponsored by the Professional Group on Aerospace and Navigational Electronics, Dayton section of the Institute of Electrical and Electronics Engineers, and American Institute of Aeronautics and Astronautics, Dayton Institute of Electrical and Electronics Engineers, (1964) p. 154-163, 7 refs. (A65-24118).

Bell, J. E., "Radiation Effects on Guided Missile Electronic Equipment," Final Technical Report, Hughes Aircraft Corp., 15 July 1963 - 15 January 1964, Rep. FR 64-17-41 (January 1964) 271p. (AD601457, A62170).

Bell, J. E. and Loveland, R. D., "Radiation Effects on Guided Missile Electronic Equipment IV," Final Report, Hughes Aircraft Co., 15 July 1964 - 15 June 1965 (U), Rep. FR65-10-45 (15 January 1965) v.p. (AD358967). Confidential Report

Bell., J. E., "Theoretical Study of Burst-Induced Transient Radiation Effects in Basic Electronic Circuits," Hughes Aircraft Co., (January 1963) 411p. (AD297484, AF SWC, Rep. TDR 62-118, A52211).

Beltran, A. A., "Radiation Effects on Electronic Circuits," Lockheed Aircraft Corp., Missiles and Space Div., Spec. Biblio. 60 - 4 (31 August 1960) 49p. (AD250955, A29920).

Bostak, R. J., "Nuclear Electromagnetic Pulse Simulation Studies in Support of the Nike X Electrical Power System Program," Final Technical Report, Army, Engineer Research and Development Labs., November 1964 - 31 October 1965 (U), (30 November 1965) 112p, (AD368109L). Secret Report

Bowman, R. E. and Kircher, J. F., "Effects of Radiation on Materials and Components," Reinhold Publishing Corp., New York, Chapman and Hall, Ltd., London, (1964) 690p. 1,082 (A64-21043).

Bowman, W. C. and Caldwell, R. S., "Transient Radiation Effects on Microelectronics," Final Report, Boeing Airplane Co., January - July 1965, Rep. D2 - 90696-1 (Dec 1965) 89p. (DASA, Rep. 5710, AF RADC, Rep. TR 65-355, AD476369L).

Brown, R. R., "Equivalence of Radiation Particles for Permanent Damage in Semi-Conductor Devices," IEEE-Transactions on Nuclear Science, NS-10, No. 5 (November 1963) p. 54-57.

Brown, W. L., "Semiconductor Radiation Damage in Space," American Rocket Society, paper 1755-61 (May 1961) 22p.

Brucker, G., et al., "High Energy Radiation Damage in Silicon Transistors," Radio Corporation of America, (July 1965) 3p., presented at IEEC Annual Conference on Nuclear and Space Radiation Effects, 12-15 July 1965, Ann Arbor, Michigan.

Brun, J. H., "Failure Modes in Naval Electronic Equipment," Naval Applied Science Lab., Brooklyn, N.Y., Radc. Phys. of Failure in Electron., Vol. 2 (1963) p. 535-549 (N64-20967 14-09, N65-20999).

Bush, T. L., Meyers, A. P., and Simonaitis, D. F., "Methods for Predicting Combined Electronic and Mechanical System Reliability," Final Report, 1 July 1962 - 30 September 1963, Technology Center, IIT Research Inst., Chicago, Ill. (1963) 134p., (DA-36-039-SC-90864, X64-14446).

Carter, E., et al., "Electromagnetic Pulse Tests on Titan II in a Simulated Flight Condition," Final Report, Martin Co., 1 January - 31 December 1965 (U), Rep. CR 65-71 (December 1965) 224p. (AF BSD, Rep. TR 65-201, AD368 188L). Secret - RD Report

Cary, H., et al., "Effect of Nuclear Radiation on Electronic Components," Battelle Memorial Institute, Rep. 8 (n.d.) 31p. (AD214695, A16319).

Chadderdon, G. and Hartman, T., "Infrared Testing of Electronic Components, Phase II," 8 July 1965 - 14 January 1966, Martin Co., (January 1966) 69p, (NAS8-20131, NASA-CR-71014 or -8031, CFSTI- HC $3.00/MR $0.75, N66-20139*).

Chapin, W. E., et al., "Space-Radiation Damage of Electronic Components and Materials," Battelle Memorial Institute, Rep. 32 (30 October 1963) 60p. (A52894).

Chinn, J. L., "Effects of Space Environment on Materials," North American Aviation Corp., Space and Information Systems Div., Rep. NP 15115 (1963) 47p.

Clark, F. M., "Insulating Materials for Design and Engineering Practice," Wiley (1962).

"Compilation of Nuclear, Pulsed, and Space Radiation Effects Projects (U)," Battelle Memorial Institute, Memo 11-C (15 April 1963) 85p. (A49571). Confidential Report

"Compilation of Nuclear, Pulsed, and Space Radiation Effects Projects (U)," Battelle Memorial Institute, Memo 13-C (15 April 1964) 112p. (A56275).

"Compilation of Nuclear, Pulsed, and Space Radiation Effects Projects," Battelle Memorial Institute, Memo 27 (15 October 1965) 102p. (A68692).

"Compilation of Nuclear, Pulsed and Space Radiation Effects Projects," Battelle Memorial Institute, Memo 29 (15 April 1966) 100p. (A72237).

Crain, C. M., et al., "Survey of the Electromagnetic Effects of High-Altitude Nuclear Detonations (U)," Rand Corp., Rep. RM-2302-ARPA (29 December 1958) 95p. (A22939). Secret - RD Report

"Designer's Guide Space Radiation Effects," Lockheed Aircraft Corp., Missiles and Space Div., Rep. 5-10-61-29, (n.d.) v.p. (AD288361, A55113).

Dinger, D. B., "Nuclear Electromagnetic Pulse Effects, Research and Development Studies in Support of the Nike-X Electrical Power System Program (U)," Army, Engineer Research and Development Labs. (12 July 1963) 43p. (AD362 962L). Secret Report

Dodge, H. S., "Failure Mechanisms in Semiconductors," Burroughs Labs., Burroughs Corp., Radc. Phys. of Failure in Electron., Vol. 2 (1963) p. 304-327 (64-20967 14-09, N64-20985.

Donaldson, B. J., "General Problems Associated with Operation of Electronic Systems in a Space Radiation Environment," Advance Electronics Dept., Douglas Aircraft Co., Inc., 12 July 1965, 19p., presented at IEEE Annual Conference on Nuclear and Space Radiation Effects, Michigan Univ., Ann Arbor, 1965, Douglas paper - 3606 (N66-21196.

Drennan, J. E. and Hamman, D. J., "Space-Radiation Damage to Electronic Components and Materials," Radiation Effects Information Center, Battelle Memorial Institute, (31 January 1966) 81p. (AF 33/615/-1124, REIC-39, AD-480010, X66-17798).

Drennan, J. E. and Hamman, D. J., "Space Radiation Damage to Electronic Components and Materials," Battelle Memorial Institute, Rep. 39, (31 January 1966) 65p. (A71697).

Egan, F., Mileaf, H., Theiss, E. C., "Handbook of Environmental Engineering," Technical Writing Service Div., McGraw-Hill Book Co., Inc., New York, Wright-Patterson AFB, Ohio, Environ. Div., (1961) 344p. (AF33/616/-6252, ASD-TR-61-363, AD-272272, N64-84926).

Eldin, J., "The Reliability of Electronic Materials - An Attempt at Classification Based on Users* Needs (Fiabilites des Materiels Electroniques - Essai de Classification Suivant les Besoins des Utilisateurs," Microelectronics and Reliability, Vol. 3, (December 1964) p. 263-269, in French.

Epstein, L., "Radiation Damage to Electrical Material and Components," Journal of Environmental Sciences, Vol. 7 (May 1964) p. 18-22.

Fischer, J. F., et al., "Proposal for the Study of Improved Techniques for Measurement of Electromagnetic Interference Susceptibility," GD/Convair, Rep. AE 60-0269 (24 March 1960) 39p. (A20437).

Gallacher, L. V., "Specific Effects of Radiation on Materials and Components, (U)," American Bosch Arma Corp., (April 1962) IDEP, (AD-292 370).

Gardner, L. B., "Reliability of Semiconductors," Litton Systems, Inc., IRE Third Annual Seminar - Reliability of Space Vehicles (1962) 10p. (N64-84050, N64-84054).

Goldberg, M. E., Horberg, A., and Levinson, D. W., "Comprehensive Failure Mechanism Theory - Metal Film Resistor Behavior," IIT Research Institute, Radc. Phys. of Failure in Electron., Vol. 2 (1963) p. 68-93 (N64-20967 14-09, AF 30/602/-2731, AF 30/602/-3054, N64-84054).

Goldberg, M. E. and Vaccaro, J., "Physics of Failure in Electronics," Vol. 2, Research and Technology Div., Rome Air Development Center, Griffiss AFB, (1963) 557p., reference proceedings of the Second Annual Symp. on the Phys. of Failure in Electron., Chicago, 25-26 September 1963.

Goodell, E. M., et al., "Electromagnetic Pulse Effects, (U)" Final Report, Aeronutronic Systems Corp., (June 1963) 173p. (AF SWC, Rep. TDR63-39, AD341331L, A60364). Secret - RD Report

Gordon, W., Massengill, E. B., Jr., and Morgan, P. L.,"Bibliography on the Vulnerability of Nuclear Weapons - Electromagnetic Radiation Environment," Vol. III, Naval Weapons Evaluation Facility, Albuquerque, N. Mex., (31 October 1964) 43p. (NAVWEPS-8300, Vol. III, AD-452877, X65-13051).

Hamman, D. J., "Effects of Radiation on Electronic Components," Battelle Technical Review, Vol. 15, (February 1966), p. 2-6 (A66-20969).

Hamman, D. J., "A Summary of Radiation Effects Thresholds," Battelle Memorial Institute, NASA Washington Second Symposium on Protection Against Radiations in Space (1965) p. 117-120 (N65-34575 22-29, GPO - $3.25, CFSTI - MF $2.50, N65-34587*).

Hamman, D. J., Hanks, C. L., and Wyler, E. N., "A Study of the Reliability of Electronic Components in a Nuclear-Radiation Environment Fifth Quarterly Report," Battelle Memorial Institute, 1 January - 31 March 1964, Jet Propulsion Lab., Calif. Inst. of Tech., Pasadena (1 April 1964) 20p., prepared for JPL (NAS7-100, JPL-950458, NASA-CR-60984, DTS- HC $1.00/MF $0.50, N65-17953*).

Henderson, W. D., Kikotas, B., and Graham, W. R., "Electromagnetic Susceptibility Testing of the 425L Group II System," Air Force Weapons Lab., Kirtland AFB, N. Mex., (February 1964) 110p. 8809 (WL TDR64 9, SCP 3, AD-348 469). Secret Report

Hollister, W. L., "Radiation Effects on Electronic Components: An Annotated Bibliography," Lockheed Aircraft Corp., Missile and Space Div., Spec. Biblio. 62-13 (April 1962) 99p.,(Rep. 3-88-62-2, AD277840, A43301).

"Investigation of Aerospace Vehicle Vulnerability to Coherent Radiation (U)," Bendix Corp., Rep. BSC 38921 (July 1963) 87p. (AF ASD, Rep. TDR 63-600, AD338735, A53547). Secret Report

"Institution of Electronic and Radio Engineers, and United Kingdom and Eire Section of the Institute of Electrical and Electronics Engineers," Conference on Components and Materials Used in Electronic Engineering, London, England, 17-20 May 1965, (IEE Conference Publication No. 12), Conference Sponsored by the Electronics Div. of the Institution of Electrical Engineers, (1965 228p.$5.60 (A65-26309).

Jones, D. C., "Tree (Transient Readiation Effects on Electronics) Handbook," Battelle Memorial Institute, (28 February 1964) 228p. (DASA-1420, AD-432213, X65-13086).

Jones, D. C., ed., "Tree (Transient Radiation Effects on Electronics) Handbook," Battelle Memorial Institute (28 February 1964) v.p. (DASA, Rep. 1420, AD432213, A62165).

Johnson, E. D., Kinoshita, G., and Kleiner, C. T., "Radiation-Induced Regeneration Through the P-N Junction Isolation in Monolithic I/C*S," Navigation Systems Div., Autonetics, (10 June 1965) 14p., references presented at the IEEE Annual Conference on Nuclear and Space Radiation Effects, Michigan Univ., Ann Arbor, 12-15 July 1965 (N66-17633.

Kaiser, Q. C., Meyer, O. L., and Scales, J. L., "Radiation Resistance Electronics," (U) Progress Report, Harry Diamond Labs., 8 August - 31 December 1961, (December 1961) 39p. (HDL PR61 12, AD-430 397).

Katona, J., "The Reliability of Communications Engineering Hardware," Foreign Technology Div., Air Force Systems Command, Wright-Patterson AFB, Ohio, (18 February 1963) 16p., translated into English from Nachrichtentechnik (East Berlin), No. 2, (1962) p. 68-71 (N64-23294).

Kimball, E. W., "The Real Cause of Electronic Equipment Failures," International Convention on Military Electronics, 8th, Washington, D.C., 14-16 September 1964, Conference proceedings. Conference sponsored by the Military Electronics Group of the Institute of Electrical and Electronics Engineers. Edited by B. J. Goldfarb, North Hollywoork, Western Periodicals Co., (1964) (A64-26790).

Klapp, S., "Empirical Parameter Variation Analysis for Electronic Circuits," IEEE Transactions on Reliability, Vol. R-13, (March 1964) p. 34-40, 8 Refs., Research Supported by the Aeronautical Div., Minneapolis-Honeywell Regulator Co. (A64-18386).

Lee, R. W. H., "Effects of Van Allen Radiation Belts on Electronic Materials, An Introductory Bibliography," National Research Council, Prevention of Deterioration Center, PDC 63-003 (18 January 1963) 7p. (AD601298).

Longhurst, E. C., "Confidence Limits and Their Significance in Reliability Studies," American Society for Quality Control, Annual Convention, 18th, Buffalo, N.Y., 4-6 May 1964, transactions, Edited by Irving W. Burr, Milwaukee, American Society for Quality Control, Inc., (1964) p. 81-90 (A64-23649).

Loveland, R. D., "Radiation Effects on Guided Missile Electronic Equipment V (U), Midterm Technical Report," January - 15 July 1965, Ground Systems Group, Hughes Aircraft Co., (15 July 1965) 50p. (NOW-65-0221-D, FR-65-10-169, AD-365311, X66-12813).

Miller, H. N., "Nondestructive High Potential Testing," Hayden (1964).

"Proposal to Investigate Electromagnetic - Induced Damage Mechanisms in Materials," GD/Convair, Rep. AE62-0122 (2 February 1962) 68p. (P.I.N. 62-070, A35411). Secret Report.

"Radiation - Effects State of the Art, 1965," Battelle Memorial Institute, Rep. 38 (30 June 1965) v.p. (A68810).

"Radiation - Electrical and Nuclear, (U)," Autonetics, (July 1964) 6p. (IDEP 347.10 .00.00-C1-09, AD-459 711).

Randle, W. R., "Infrared Testing of Electronic Components, Phase I," 5 April - 29 June 1965, Martin Co., (June 1965) 70p. (NAS8-20131, NASA-CR-71013, or -6610, CFSTI- HC $3.00/MR $0.75, N66-20138*).

"Reliability, Stress and Failure Rate for Electronic Equipment," MIL-HDBK-217, (8 August 1962).

Rohrback, E. J. and Goldstein, H. S., "Radiation vs. Electronic Components," Machine Design, Vol. 35 (January 1963) p. 101-105.

Scheffler, H. S., "Reliability Analysis of Electronic Circuits," Autonetics, (1964) 405p. (N64-24372.

Sharp, L. W. D., "Electronic Component Reliability - The Role of Environmental Testing," British Communications and Electronics, Vol. 12 (June 1965) p.354-356 (A65-25851).

Soltau, R., "Failure Modes and Mechanisms in Microelectronic Devices," Reliability in Space Vehicles, Seminar, 5th, 2 April 1965, proceedings. Seminar sponsored by the Los Angeles Section, Component Parts and Reliability Groups of the Inst. of Electrical and Electronics Engineers. Edited by C. E. Roth, Jr., Engineering Publishers, (1965) p. 91-107 (A66-15823 05-31, A66-15830).

Sullivan, J. M., Jr. and McLinn, J. F., "Examination of EMP Damage Effects and Simulation Feasibility, (U)," Tempo General Electric Co., (February 1966) 62 p. (AD-370 199).

Sullivan, J. M., Jr. and McLinn, J. F., "Examination of EMP Damage Effects and Simulation Feasibility (U)," General Electric Co., Rep. 65 TMP-51 (February 1966) 62p. (AD370199). Secret - RD Report

"Symposium on EMP Effects on Military Systems - Proceedings (U)," AF Electronic Systems Div., Rep. TDR 64-602 (January 1965) 2 Vols. (Vol. 1: AD357702L, Vol. 2: AD357703L, AF WL, Rep. TR 64-87). Secret - RD Report

Tarnay, K., "Degradation Failures of Electronic Devices (Degradationsausfaelle der Elektronischen Geraete)," Reliability in Electronics (Zuverlaessigkeit in der Elektronik), proceedings of the Wissenschaftlicher Verein Fuer Nachrichtentechnik, Ungarische Akademie der Wissenschaften, Abeilung Fuer Technische

Wissenschaften, and Regierungsamt Fuer Technische Entwicklung, Symposium, Budapest, Hungary, 27-29 October 1964, Vol. II, Section B. Budapest, Haus der Technik, (1964) 10p., in German (A65-23287 13-09).

Vaccaro, J., "Reliability Physcis at RADC," Rome Air Development Center, Griffiss AFB, N.Y., RADC Phys. of Failure in Electron., Vol. 3 (April 1965) p. 452-480 (N65-30300 19-09, N65-30329).

Vidoni, C. M., "Reliability and Failure of Electronic Equipment, Systems, and Mathematical Models - A Bibliography," California Univ., Livermore, Lawrence Radiation Lab., Maryland Univ., College Park (October 1964) 62p. (W-7405-ENG-48, UCRL-12040, N65-15065).

Wagnon, W., "Components Failure Physcis Analysis Document," National Aeronautics and Space Administration, Marshall Space Flight Center, Huntsville, Ala., (15 May 1963) 189p. (NASA-TM-X-54905, X65-10811*).

Wilcox, B., "Manufacturers' Reliability Data," Boeing Co., (7 October 1963) 70p. (D2-22571, N64-21376).